A Study of Heterogeneous Nucleation and Electrostatic Charge in Steam Flows

By

John Richard Buckley

M.Eng.

Thesis submitted for the degree of Doctor of Philosophy

School of Mechanical and Manufacturing Engineering

The University of Birmingham

November 2003

Synopsis

This thesis describes two experimental investigations concerned with condensing flows of steam in a cascade of turbine blading. The first considers the effect of heterogeneous nucleation on the flow of condensing steam. The second is concerned with the measurement of electrostatic charges generated on first nucleation in steam.

The facility is a blow-down steam tunnel constructed for the study of two-phase flows and has been available from earlier work. To carry out the first part of the investigation, substantial modifications have been introduced to generate a supply of ultra-pure steam for admission into the blade cascade. This has allowed a base line set of surface pressure measurements to be recorded in the absence of impurities. Next the steam has been dosed with known quantities of aqueous ammonia to investigate the influence of chemical impurities on the condensation process.

To investigate the electrostatic effects a Langmuir probe for operation in steam has been developed.

The introduction to the thesis provides a brief overview and background to the work. This is followed by the literature survey which covers early investigations of condensing flows of steam, the development of homogeneous nucleation theory and droplet growth laws. This is then followed by a discussion of heterogeneous nucleation, with regard to chemical impurities and electrostatic charge. Investigations concerning the measurement of electrostatic charge in the wet stages of steam turbines are also reviewed.

A description of the experimental facility, the test section, the instrumentation and the improvements introduced to it is given next. This is followed by a description of the arrangements and instrumentation for measuring the electrostatic charges as well as the control circuits and data acquisition employed.

The experimental results comprise three sections; 1. Pressure measurements using ultra-pure steam. 2. Pressure measurements using steam dosed with known quantities of aqueous ammonia. 3. Electrostatic measurements in both ultra-pure steam and steam dosed with aqueous ammonia.

Comparisons are carried out between the base line measurements using ultra-pure steam and the measurements using dosed steam. Both sets of results are compared with those of previous investigators. The electrostatic measurements are compared with similar measurements recorded by investigators working in LP steam turbines. The results are discussed and conclusions drawn.

To my wife, Alice

Whose constant love and support have encouraged me throughout

Original Work

The research work described in this thesis was undertaken at the School of Manufacturing and Mechanical Engineering at the University of Birmingham under the supervision of Prof. F. Bakhtar. The programme of work was funded by the Electrical Power Research Institute. The author was a research associate on this project. In the investigation of the effect of heterogeneous nucleation on the flow of condensing steam Dr. R. H. Winterton was the Principal Investigator. In the investigation of electrostatic effects associated with first nucleation in steam the measurements were carried out by Dr. H. A. Mashmoushy. The author has been personally responsible for:

1. The numerical solutions of flow with secondary nucleation in the venturi.
2. The design, supervision of the installation and commissioning of modifications introduced to feed the test section with ultra pure steam and steam dosed with ammonia and cater for its monitoring.
3. Preparations and performance of the experimental investigation into the effect of heterogeneous nucleation on condensing flows of steam, including all measurements.
4. Assistance in the design and testing of the Langmuir probe and associated equipment used for the electrostatic measurements.
5. Writing the data acquisition software used in the electrostatic measurements.
6. Assistance with procedures and preparation of further data logging software necessary for the electrostatic measurements.

Acknowledgements

The investigation was carried out at the University of Birmingham and was funded by EPRI.

The author wishes to express his gratitude to his supervisor, Prof . F. Bakhtar, for his patience, support, encouragement and guidance throughout these investigations and also during the writing of this thesis.

The author would like to thank Dr. R. H. S. Winterton for his help and guidance during the investigation into the effect of chemical impurities on the steam condensation process.

The author also wishes to thank Dr. R. B. Dooley of EPRI and Mr. M. Ball for providing guidance and advice during the investigations.

Many thanks are also due to the technicians of the University of Birmingham who have supported this project. In particular the author would like to thank Mr. M. Chapman, Mr. W. Hewitt, Mr. R. Humphreys, Mr. A. Loat and Mr. S. Rowan.

Contents

Nomenclature

The following is a list of the main symbols appearing frequently throughout the work. Minor quantities such as the constants in equations which appear only once, have not been tabulated. A certain symbol may represent more than one quantity, but unless the meaning is obvious, the variable to which this symbol applies is defined in the text.

Symbol	Meaning
C_g	Rate of condensation of size g clusters
E_g	Rate of evaporation of size g clusters
f_g	Non-equilibrium concentration of size g clusters
G	Gibbs free energy
h	Specific enthalpy
I	Current
J	Rate of formation of critical nuclei per unit mass per unit time
k	Boltzmann's constant
kg	Kilogram
K	Degrees Kelvin
L	Latent heat ($h_G - h_L$)
m	Mass
m_r	Mass of droplet or radius r
M	Molar mass
M_m	Molecular mass
Ma	Mach number
n_m	Number of molecules per unit mass
n_g	Number of g size clusters per unit mass
p	Static pressure

p_0	Stagnation pressure
$p_s(T_G)$	Saturation pressure at temperature T_G
P	Expansion rate
q	Condensation coefficient
r	Radius
R	Gas constant
s	Specific entropy
S	Supersaturation ratio ($p/p_s(T_G)$)
t	Time
T	Temperature
ΔT	Supercooling
$T_s(p)$	Saturation temperature at pressure p
u	Internal energy
v	Specific volume
V	Voltage

Greek Symbols:

Symbol	Meaning
α	Heat transfer coefficient
Δ	Incremental step
ε_0	Permittivity of free space
ε_r	Dielectric constant
μ	Chemical potential
ρ	Density
σ	Surface tension

Subscripts:

Symbol	Meaning
g	Number of molecules per cluster
G	Vapour phase
L	Liquid phase
0	Stagnation conditions
r	Droplet of radius *r*
s	Saturation conditions

Chapter 1 :
Introduction

At the dawn of the 21st century it is still the case that the majority of the world's electricity generators are driven by steam turbines. Despite the central position of the steam turbine in power generation and the large number of studies investigating flow in the dry stages of the turbine, relatively little attention has been devoted to the study of wetness problems associated with its operation and design.

During the course of the expansion of steam in the later turbine stages, the flow first supercools and then nucleates thus generating a large number of very small droplets to form a two-phase mixture (*Gyarmathy [1962]*). The formation and subsequent behaviour of the liquid phase causes problems, leading to losses of output, which are collectively called wetness losses (*Moore and Sieverding [1976]*, *Bakhtar et. al. [1997a-c]* and *Dooley, Bursik and Staudt [1999]*). In conventional power plants the wetness levels in the last few stages of the low-pressure turbine can be as high as 10-12%. In PWR nuclear plants, which have to operate with saturated steam, wetness problems are also experienced in the high-pressure stages and exhaust wetness may reach as high as 18%.

The present work forms part of a long term research programme into the effects of nucleation and droplet growth in steam at the University of Birmingham, which has been in progress for some years. The programme began with a theoretical study of condensation in converging-diverging nozzles by *Campbell and Bakhtar [1970]*. This led to the development by *Bakhtar et. al. [1975]* of a number of computer programs which predict the behaviour of one-dimensional nucleating and wet steam flows with reasonable accuracy. The treatment has since been extended for inviscid two-dimensional blade to blade flows, first by *Tochai [1978]*, *So [1984]*, then by *Abbas [1987]* and *Mahpeykar [1991]*, who included boundary layer terms and later by *Rodriguez [1992]* and by *Zamri [1997]*, who revised the basic structure to include second order terms based on Jameson's scheme and also included viscid dissipation terms. Early on the need to verify the predictions of these simulations with experimental results became clear. This led to the design and construction of a steam blow-down facility at Birmingham in the

late 1980s, initially by *Bakhtar, Webb, Shojaee-Fard and Siraj [1991]*. This facility enables the nucleating and wet steam flow conditions found in steam turbines to be reproduced and studied in a short duration cascade tunnel. In the investigations completed so far on this equipment various blade configurations have been tested under superheated, nucleating and wet steam conditions (e.g. *Bakhtar, Ebrahimi and Webb [1995]* and *Bakhtar, Mashmoushy and Jadayel [1997b]*). The present investigation follows from the above work and is concerned with two separate aspects.

The first part of the work is an investigation into the effect of heterogeneous nucleation on the flow of condensing steam. In the majority of previous investigations the presence of impurities in the steam has been ignored or simply considered to be a complicating factor. More recently there has been renewed interest in the role of impurities in the steam condensation process (e.g. *Petr et. al. [1995]* and *Stastny, Sejna and Jonas [1997]*). Before measurements with steam containing impurities can be made, measurements with ultra-pure steam are required to establish a baseline. To this end the existing blow-down facility has been modified to provide a supply of ultra-pure steam to the test section. Experimental data has been obtained for pure steam containing no impurities. Furthermore a facility for dosing a volatile chemical into the steam supply has been added and measurements made under these conditions to investigate the effect of heterogeneous nucleation on the flow.

The second part of the work comprises an investigation into the distribution of electrostatic charge on the first nucleation of steam. It has long been know that electro-static charge is present in wet steam (e.g. *Armstrong [1840]*) and builds up on the casing of steam turbines, which must be earthed to avoid a static discharge. Recently there has been renewed interest in the presence and distribution of electrostatic charge in the wet stages of steam turbines (e.g. *Tarelin, Skliarov et. al. [1996]* and *Hesler and Maurer [1998]*). In the current project instrumentation has been developed to measure electro-static charge on the first nucleation of steam in the blow-down test facility.

These two investigations are the subject of the thesis.

Chapter 2:
Condensation in flowing steam

2.1 Early Investigations

Commenting on investigations into gas and liquid states by *Andrews [1869]*, *J.J. Thomson [1871]* wrote in the Proceedings of the Royal Society:

> *"...it appears probable that, although there is a practical breach of continuity in crossing the line of boiling-points from liquid to gas or from gas to liquid, there may exist, in the nature of things, a theoretical continuity across this breach having some real and true significance. This theoretical continuity, from the ordinary fluid state to the ordinary gaseous state, must be supposed to be in unstable equilibrium, while passing through the intermediate conditions..."*

This is one of the earliest references suggesting that a substance may depart from thermodynamic equilibrium as its thermodynamic path crosses a line of state.

W. Thomson [1870] (later Lord Kelvin) made the first theoretical study recognising the existence of supersaturation in steam. In seeking to explain the rise of liquid in a capillary tube he developed an expression relating the curvature of a liquid surface to the vapour pressure above the surface. He discovered that the equilibrium vapour pressure above a convex surface is higher than that above a flat surface. Thus, for a small droplet to exist without evaporating, a supersaturated vapour must surround it.

Working independently in the early 1880's *Helmholtz [1886]* and *Gibbs [1888]* developed equations governing the equilibrium of thermodynamic systems. Kelvin's earlier equation may be derived from these relationships which are widely known as the Kelvin-Helmholtz or Gibbs-Thomson equations, describing the critical droplet radius for given vapour conditions.

In 1881 while expanding saturated steam into glass vessels, one containing filtered air and the other unfiltered air, *Aitken [1881]* noted that the unfiltered air produced a dense fog while the filtered air remained clear. This was due to heterogeneous nucleation in which the dust particles in the unfiltered air had acted as centres of condensation.

The first example of spontaneous, homogeneous nucleation, in the absence of foreign particles or ions, was seen during experiments by *Helmholtz [1887]*. He noted that saturated steam passed into clean, filtered air produced a dense fog some distance downstream of the steam inlet. *Helmholtz* also noticed that an electric discharge in the jet of steam caused an increase in the density of the fog.

It was ten years later when *Wilson [1897]* undertook the first detailed study of supersaturation in his cloud chamber experiments. He expanded particle free air[1] laden with moisture vapour using a piston and cylinder system. For a very fast expansion he noticed that condensation was delayed. To quantify this departure from thermodynamic equilibrium he formulated the supersaturation ratio as the ratio of the vapour pressure p to the saturation pressure p_s corresponding to the local vapour temperature T_G:

$$S = \frac{p}{p_s(T_G)} \tag{2.1}$$

Supercooling is defined as:

$$\Delta T = T_s(p) - T_G \tag{2.2}$$

where T_s is the saturation temperature at pressure p.

Wilson discovered that the largest supersaturation ratio he could obtain was 7.9, beyond this point the water vapour condensed forming a heavy cloud. *Wilson* used this vapour in his classic work visualising the paths of ionised particles as trails of condensation were formed around them.

It was not until the early 1900's that the relevance of supersaturation in steam to engineering problems began to be realised. Initial investigations began with studies of the expansion of steam through convergent-divergent *de Laval* nozzles by *Rateau [1905]*, *Bendemann [1907]*, *Loschge [1913]* and *Henderson [1913]*. The accepted theory at this time was that steam remained in equilibrium throughout such expansions. It was found that calculations to predict mass flow rate using *Zeuner's [1907]* isentropic index, which

[1] Using heterogeneous nucleation in successive expansions to remove foreign particles and ions.

assumed thermodynamic equilibrium, consistently underestimated the measured mass flow rates by 2% to 4%, even when the effects of friction were neglected in the theory. *Henderson [1913]* also reported that the discharge of steam in nozzles expanding in the wet region of the *Mollier* chart was 5% greater than the value expected from equilibrium calculations.

In discussion of *Henderson's* work *Stodola [1915]* cited *Bendemann's [1907]* work. This demonstrated that even initially dry saturated and completely dry steam showed similar tendencies. *Stodola* attributed this discrepancy in mass flow to the supersaturation of the steam undergoing rapid expansion in the nozzle.

Martin [1913] realised that the failure of steam to condense due to supersaturation could have some significance for the design of steam turbines. He worked on some simple calculations in an attempt to estimate the loss in a five-stage velocity compound turbine.

Further experiments using nozzles by *Callender [1915]* and *Stodola [1915]* confirmed the previous findings. In addition they used the Kelvin-Helmhotlz equation to estimate the size of droplets produced on nucleation of the steam. *Martin [1918 and 1923]*, using Wilson's data, calculated the limiting supersaturation ratios at other pressures by assuming that the droplet sizes remained constant for all conditions. He plotted his results on the *Mollier* diagram naming the result the *Wilson* line.

More detailed pressure measurements in convergent-divergent nozzles were performed by *Yellot [1934]* and *Yellot and Holland [1937]*. They located the position of the onset of condensation more precisely and found the *Wilson* line to be located on the 4.5% moisture line on the *Mollier* chart.

Rettaliata [1938] performed experiments using rough and smooth nozzles in which he also altered the rate of expansion. He discovered that low expansion rates in rough nozzles resulted in the *Wilson* line lying closer to the saturation line than was obtained with the smooth nozzle and higher expansion rates. He concluded that the limiting supersaturation ratio was not unique and proposed that the *Wilson* line be replaced by a *Wilson* zone.

Shortly afterwards *Binnie and Woods [1938]* carried out a series of careful and reliable measurements in *de Laval* nozzles. In particular they investigated the sharp rise in pressure in the supersonic zone downstream of the throat caused by the release of latent

heat during condensation. *Binnie and Green [1943]* continued the work by developing an electrical device to detect the onset of condensation in flowing steam. They also noticed that the position of limiting supersaturation was dependant on the initial conditions of the steam. The condensation shock investigated by *Binnie and Woods* was concurrently the subject of investigations by aerodynamicists such as *Prandtl [1935]* and *Hermann [1942]*.

2.2 Evolution of Nucleation Theory

In the same period as the investigations mentioned above a theory to describe the nucleation of droplets was being developed. *Volmer and Weber [1926]* were the first to take a significant step in the development of this theory. They suggested that in vapours the distribution of molecular clusters could be calculated using Boltzmann's distribution law.

$$n_g = n_1 \exp\left(-\frac{\Delta G}{kT_G}\right) \tag{2.3}$$

They obtained an expression for the droplet nucleation rate by considering the rate of molecular collisions with the droplet surface whilst assuming that the growth and decay of droplets had equal probabilities.

One year later *Farkas (and Slizard) [1927]* considered the kinetics of molecular interactions, treating nucleation as a quasi-steady process. They obtained an expression for nucleation rate that was consistent with *Volmer and Weber's* result. Based on this kinetic theory, many other workers, notably *Becker and Doring [1935]*, *Zeldovich [1942]* and *Frenkel [1946]*, continued the work, the result became known as 'classical' nucleation theory.

A fundamental problem with the use of a quasi-steady state theory for understanding nucleation is that if the time taken to reach the steady state is not small compared to the characteristic time for the nucleation process then the result will be unrealistic. This problem has been studied by various investigators including *Zeldovich [1942]*, *Kantowitz [1951]*, *Probstein [1951]*, *Farley [1952]*, *Wakeshima [1954]* and *Courtney [1961]*. An exact, analytical solution of the time dependant nucleation equations was obtained by *Kashchiev [1969]*. Sample calculations using his result

indicate that the time taken for nucleation to reach a steady state value is negligible in comparison with the time taken to traverse incremental distances adopted in the treatment of typical nucleating flows.

However the classical theory of nucleation is undermined by a number of other uncertainties. Most notable are its use of bulk liquid properties, such as surface tension and condensation coefficient, to describe those of small molecular clusters. In an effort to avoid these uncertainties a treatment using the statistical mechanical method was started e.g. see *Bijl [1938]*, *Band [1939]*, and *Frenkel [1946]*. This method analyses the nucleation process by applying theories of statistical mechanics at the molecular level. Other work in the same area includes that of *Kuhrt [1952]*, *Dunning [1965]*, *Feder [1966]* and *Wegener [1969]*. The complexities of this method will not be discussed in this thesis, but a comprehensive treatment of the subject is given by *Dunning [1969]*.

Later *Lothe and Pound [1962]* argued that the translational and rotational free energies of the droplets had been ignored in the derivation of the nucleation activation barrier. The inclusion of these free energy terms in the expression for the free energy of formation of a molecular cluster leads to a much higher predicted nucleation rate, of the order of 10^{17} times greater. This means that spontaneous nucleation is predicted to occur at much lower supersaturation ratios than predicted by classical theories and the agreement with experimental measurements is not good. *Lothe and Pound's* treatment was refuted by *Dunning [1965]*, *Reiss and Katz [1967]* and *Wegener and Wu [1976]*.

In the present work theoretical estimates of nucleation rate have been calculated using the classical nucleation theory together with corrections due to *Kantrowitz [1951]* and *Courtney [1961]*. Both these corrections reduce the overall nucleation rate predicted by the classical theory. Their combined effect is to decrease the nucleation rate by a factor of 20 to 30 over the whole pressure range. A brief derivation of classical nucleation theory and further details of these corrections are given in Chapter 3.

2.3 Condensation in One-Dimensional Flows

Many of the engineering investigations into the effect of condensation in flowing steam have been carried out using convergent-divergent nozzles because of the simplicity of the essentially one-dimensional flow within them. They have also proved useful for validating nucleation and droplet growth theories. Nozzle experiments are performed under steady state conditions and the whole history of the condensation process is conveniently displayed spatially along the length of the nozzle.

2.3.1 A Typical Expansion of Steam

A typical expansion of steam in a convergent-divergent nozzle is shown in Figure 2.1. The state path is shown on the *Mollier* diagram in Figure 2.2. Superheated steam enters the nozzle at (1) and then expands to the throat (2), where it reaches sonic condition. The state path crosses the saturation line at (3) and steam begins to nucleate. However the rate of nucleation is infinitesimally small at the beginning and the steam continues to expand in a meta-stable state. As it expands the supercooling, and with it the nucleation rate, increases until eventually nucleation becomes noticeable at around (4) where the rate increases dramatically. The supercooling continues to increase until the limiting supersaturation is reached at (5), this point also corresponds with the peak in the nucleation rate. The region between (4) and (5) is known as the nucleation zone and is terminated by the Wilson point. Downstream of (5) the population of droplets remains constant but the droplets grow rapidly in size to restore the steam to equilibrium conditions. The bulk of the latent heat, released as molecules condense on the droplets, is transferred back to the vapour by conduction. Here, in the rapid condensation zone just downstream of the Wilson point, the heat transfer rate is high. The release of latent heat decelerates the supersonic flow, causing the pressure to rise and is accompanied by a corresponding rise in enthalpy and entropy. The loss associated with this process is referred to as *thermodynamic nucleation loss*. Further expansion between points (6) and (7) takes place close to equilibrium.

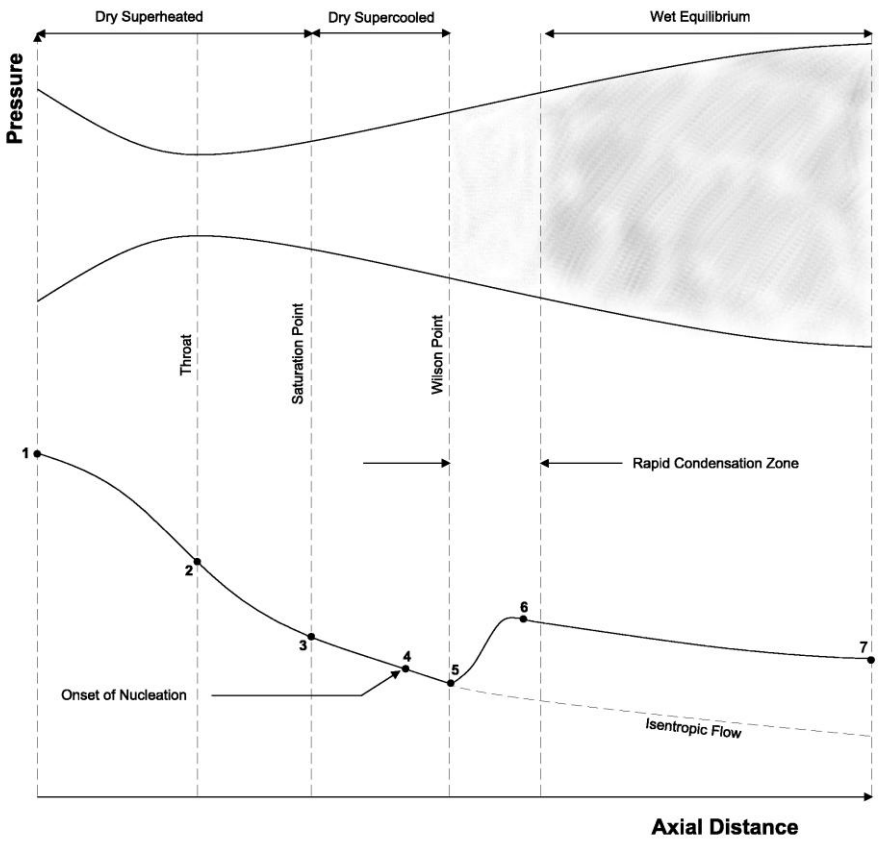

Figure 2.1: Axial Pressure distribution in a nozzle with spontaneous condensation

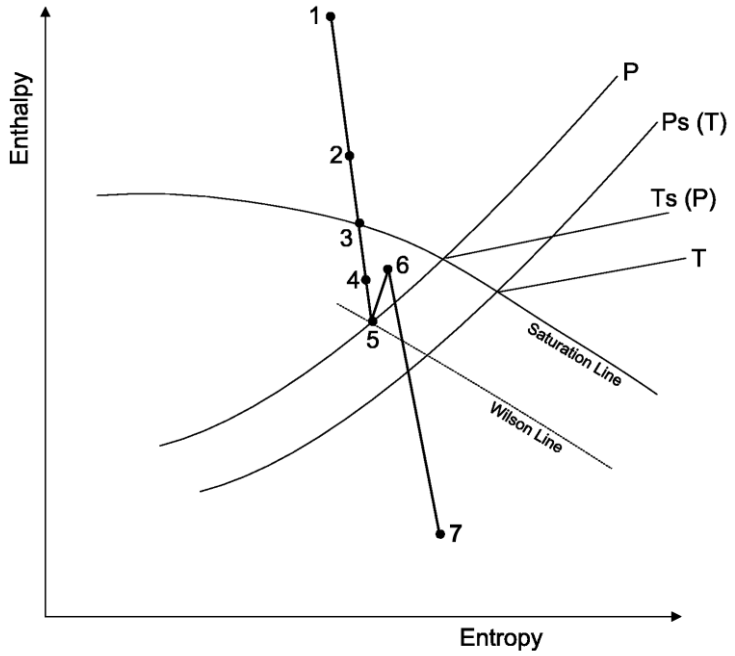

Figure 2.2: State Line for expanding steam with spontaneous condensation

2.3.2 Theoretical Developments

Oswatitsch [1942] made the first successful attempt to combine nucleation and droplet growth theories with the gas dynamic equations. His laborious hand calculations of the pressure distributions along the nozzle axis agreed well with his own experimental measurements using humid air and with those of *Yellot [1934]* and *Binnie and Woods [1938]* who used steam.

In the 1960's and 1970's, following *Oswatitsch's* success, other workers refined this theoretical treatment, again using comparisons with experimental measurements in convergent-divergent nozzles to validate their refinements to the theory. For example see *Gyarmathy [1962]*, *Hill et. al. [1963]*, *Gyarmathy and Meyer [1965]*, *Pouring [1965]*, *Campbell and Bakhtar [1970]*, *Deich et. al. [1972]* and *Filippov et. al. [1973]*.

At the same time another branch of work, driven by the need to understand erosion in turbine blades, led to the development of optical techniques to measure droplet sizes. *Gyarmathy and Meyer [1965]* and subsequently *Gyarmathy and Lesch [1969]*, *Petr [1969]*, *Krol [1971]*, *Walters [1973]*, *Ederhof and Dibelius [1976]*, and *Moses and Stein [1978]* were among the first to develop and use these techniques. The droplet data served as further basis for the validation of nucleation and droplet growth theories.

2.3.3 One-Dimensional Treatment of Two-Phase Flows

A one-dimensional, theoretical treatment of condensing two-phase flows was developed at the University of Birmingham by *Campbell and Bakhtar [1970]*. It has since been refined and developed by others but the basic treatment has remained the same. This section briefly describes this treatment and its further development.

A condensing flow of steam can be regarded as a special case of compressible flow with heat addition. For the purposes of analysis the fluid, in this case steam, is taken to consist of liquid droplets, of specified sizes, uniformly distributed in the vapour which fills the space between them. Slip between the two phases is regarded as negligible and is neglected. Condensation is by a combination of the nucleation of new droplets and by the growth of any existing droplets in the flow. The equation for nucleation rate, derived from classical theory, is reviewed in Chapter 3 and employs the refinements of *Kantrowitz [1951]* and *Courtney [1961]*. The growth of existing droplets is determined by solving the equations describing mass and heat transfer processes between the liquid and vapour phases. Both sets of equations are combined with the one-dimensional gas dynamic

equations in differential form and then integrated using a standard fourth order Runge-Kutta method. Beginning with superheated steam at inlet, the path of the fluid is followed step by step through supercooling, nucleation and droplet growth until the fluid returns to thermodynamic equilibrium and subsequently behaves as wet vapour.

Campbell and Bakhtar's [1970] theoretical treatment was used to investigate the sensitivity of the solution to the values adopted for friction factor, condensation coefficient and surface tension. Friction factor could be measured and had been well reported in the literature but there was some debate over the models adopted for the other two parameters. The solution for nucleation rate is very sensitive to both the value of surface tension for small water clusters and the value of condensation coefficient.

Studies by *Kirkwood and Buff [1949]*, *Tolman [1949]* and *Benson and Shutleworth [1951]* all independently came to the conclusion that the value used for surface tension should be smaller than that of the bulk liquid. However later *Oriani and Sundquist [1963]* suggested that the surface tension of very small clusters should be taken as higher than that of bulk liquids. *Abraham [1974]*, using *Lothe and Pound's* expression for the nucleation rate, had to choose a higher value of surface tension to bring his calculations into agreement with experimental results. This supported *Oriani and Sundquist's* prediction. Work by *Plummer and Hale [1972]* contradicted both these previous theories and suggested that the value of surface tension for small clusters should, after all, be close to that of the bulk liquid.

The value for condensation coefficient has also been subject to debate. For water *Alty and Mackay [1935]* and *Preneger [1940]* suggested that the coefficient lies in the range 0.02 to 0.04. Later *Hickman [1954]*, *Mills and Seban [1967]* and *Maa [1970]* proposed a value of unity. *Jamieson [1965]* suggested a value of 0.4.

Because of the uncertainty relating to these values it is possible to use different combinations to bring calculations into close agreement with experimental results. In making comparisons with the axial pressure measurements of *Binnie and Wood [1938]*, *Cambell and Bakhtar [1970]* were able to obtain good agreement using two combinations. Firstly, after *Plummer and Hale*, they took the surface tension of small clusters to be the same as that for bulk water and used a condensation coefficient of unity. Secondly they adopted *Benson and Shuttleworth's [1951]* model for the variations of surface tension, predicting values below the bulk value, combined with a condensation

coefficient much smaller than unity. From this, and later, studies it was found that best all round agreement is obtained by using the first method, i.e. taking the surface tension of small clusters to be the same as the bulk value combined with a condensation coefficient of unity.

Cambell and Bakhtar's 1970 study had considered the steam vapour as a perfect gas and was therefore only valid for relatively low pressures. Further work by *Young [1973]* and *Bakhtar et. al. [1975]* included the second virial coefficient in the equation of state for steam to extend the range of the theoretical treatment.

Later in the 1970's *Piran [1975]* and *Bakhtar and Piran [1979]* suggested that the virial equation of state due to *Vukalovich [1958]*, employing five virial coefficients, was the most suitable for extrapolation into the meta-stable state. *Zidi [1981]* and *Bakhtar and Zidi [1989, 1990]* employed this refinement along with a new semi-empirical self-diffusion coefficient and obtained good agreement with experimental results.

2.3.4 One-Dimensional Treatment of Two-Phase Turbine Flows

Gyarmathy [1962] made the first theoretical study of two-phase flow in steam turbines. He applied his own simplified one-dimensional two-phase flow analysis, originally developed to predict the *Wilson* points in *de Laval* nozzles, to two hypothetical steam turbines.

In the 1970's and early 1980's, following the successful application of a one-dimensional theory to flow in nozzles, *Bakhtar and co-workers* performed a number of studies applying this theory to the flow of steam in turbines. The turbine stages were modelled by constructing one-dimensional equivalents and the aerodynamic losses were accounted for by the use of friction factors. These studies include those of G*honeim [1975]*, *Bakhtar, Ghoneim and Young [1976]*, *Ghassemi [1977]*, *Heaton [1978]*, *Bakhtar and Ghassemi [1979]*, and *Bakhtar and Heaton [1981, 1988]*. The theoretical results obtained were compared with the results of *Smith [1965 and 1976]* who made measurements of pressure, temperature, mass flow rate and overall efficiency on scale models of real steam turbines. One conclusion of the studies was that the thermodynamic component formed a significant part of the total wetness loss.

2.4 Condensation and Wetness in Turbines

As the use of the steam turbine in power generation developed so did the need to maximise the efficiency. Initially the inlet temperature was increased improving the overall efficiency of the turbine, but soon metallurgical limits imposed by the blade materials were reached. It was then found that raising the inlet pressure also achieved a gain in efficiency. However this had the disadvantage of increasing the wetness fraction at the end of the expansion causing new problems for designers. The efficiency of the turbine operating in this wet region was considerably lower than that of the dry stages. *Baumann [1912]* made the first study of this problem and suggested that for every 1% of water present, the stage efficiency would be reduced by 1%. Although purely empirical, *Baumann's* rule was widely adopted and, due to its simplicity, is still used today (although others have attempted to improve on it e.g. *Laali [1991]*).

2.4.1 Blade Erosion and Corrosion

In the 1920's a further problem, erosion of the blades in the latter stages of low-pressure turbines, was noticed. *Honneger [1924]* made one of the first investigations into this problem. He recognised that erosion was caused mainly by droplets impacting on the blades and carried out simulated tests on various materials with water jets. *Von Freuderich [1927]* developed a mechanical theory for erosion while *Honneger [1927]* and *Gardner [1932]* carried out tests using rotating rigs showing that hardening the affected surfaces could reduce erosion. Drainage devices were also developed to combat erosion but, at the time, proved mostly unsuccessful.

As the demand for electric power increased through the 1930's the need to balance efficiency and losses became more acute. In the absence of superheaters a trade off between improving the efficiency via increases in inlet pressure and managing wetness loses led to an arbitrary limit of approximately 14% to be imposed on the wetness fraction at the outlet from the turbine.

In the post war years developments in materials allowed the turbine inlet temperatures and boiler pressures to be increased. These factors and the introduction of reheat cycles brought temporary relief from wetness problems. However as demand increased once again in the 1960's increases in plant size led to higher blade speeds, hence higher droplet impact speeds and consequently wetness and erosion once again

became an issue. At the same time development of the water-cooled nuclear reactor, with associated low fuel element temperatures, produced steam with little or no superheat and resulted in wetness problems being experienced in the high-pressure stages. These problems were partly overcome by using combined water separators and re-heaters at the high pressure end of the expansion.

Many investigations into the chain of events leading to the erosion of blades have been undertaken. The interest was particularly intense in the 1960's and 1970's and a wealth of results covering many aspects of erosion were reported, e.g. *Golvin and Putnam [1962]*, *Gardner [1963]*, *Krzeczkowski [1968]*, *Valha [1970]*, *Ryley and Parker [1967]*, *Ryley et al. [1970]*, *Filippov et al. [1973]*, *Stastny [1976]*, and *Hamitt et al. [1976]*.

Interest was again high in the late 1980s and into the 1990s when LP steam turbines again grew in size, increasing erosion problems due to the higher blade tip velocities. Such studies include those of *Thornton [1988]*, *Tomarov [1989]*, *Amelyushkin [1989]*, who studied erosion at the leading edge of moving blades, *Araki, Ryoichiro et. al. [1990]* who studied erosion phenomena with titanium blading and *Boroenstein, Kelly and Boone [1990]* who studied blade coatings.

One solution to erosion problems, mentioned above, is to introduce drainage slots into the turbine casing to remove as much coarse water as possible from the flow. Studies into such drainage slots include those by *Tanuma and Sakamoto [1991]*, who saw a 40% drop in coarse water droplets with the introduction of suction slots, and *Sakamoto, Nagao and Tanuma [1992]*.

A related problem to erosion is corrosion of blades and other metal parts in the LP turbine. Corrosion occurs as a consequence of chemical species being deposited on the metal when liquid films collect on the turbine surfaces. Factors influencing corrosion are the chemical composition of the nucleated droplets, the size of the droplets, the thickness of liquid films found on blades, the type of deposits and the pressure and temperature of the steam and blades. Research into this problem has also been ongoing, e.g. *Komarov and Yurkov [1991]*, who investigated corrosion damage to the blading and discs in condensing steam flows, and *Dooley, Feldburg et. al. [1997]*, which suggested that water treatment with phosphate or all-volatile chemicals produces the highest levels of corrosion and that the addition of impurities, such as chlorides and sulphates, increases the deposition rates. A further problem, which may lead to increased corrosion damage, is

that small amounts of condensate containing a high level of impurities has been observed upstream of the saturation line, e.g. *Steltz et al [1981]* and *Jonas [1998]*. These studies suggest that heterogeneous nucleation occurs locally where there are high concentrations of impurities even though the bulk of the fluid has not yet reached the saturation line. Since the number of droplets nucleating in this way is small (*Steltz* measured 0.5% wetness with 2.5×10^{-6} m diameter droplets) they are unlikely to significantly influence the nucleation process downstream of the saturation line. However the high concentrations of impurities are thought to increase corrosion levels in the wet turbine stages.

2.4.2 Sources of Loss due to Wetness

The presence of wetness in turbines has consequences other than erosion and corrosion. These fall into the three main categories of mechanical, thermodynamic and aerodynamic.

Mechanical losses consist of the drag of the small droplets in the main body of the flow and the deposition of water droplets on the stator and rotor blades. Drag losses occur because the population of small water droplets suspended in the flow may be moving at a slightly different speed from the vapour, resulting in drag between the phases. However since the droplets are very small this loss is usually an order of magnitude less than the thermodynamic loss. Secondly deposition occurs when these small water droplets impact the stator blades, thus giving up their kinetic energy and potential for doing work. Films and rivulets of water are formed and are driven to the trailing edge of the blades by the drag of the steam. This water is then re-entrained into the flow in the form of large droplets with a low absolute velocity. They impinge on the next row of rotor blades with large relative velocities and high negative incidence exerting a braking effect and eroding the leading edge. Strong centrifugal forces drive the water to the tip of the blades where it is flung off in a radial direction. Theses droplets can be caught in conveniently placed belts or drainage slots and have no further effect on turbine performance.

The thermodynamic component forms the dominant part of the total loss. These result from irreversible heat transfer across finite temperature differences. The latent heat of condensation is released to the liquid and then transferred back from the droplet surface to the parent vapour across a finite temperature difference and causes a rise in entropy.

Aerodynamic losses arise as repercussions of the release of latent heat into the flow. Some problems associated with this are the effect of the pressure rise due to condensation, instability as a result of super-critical heat addition[2] and choking (see *Zamri [1997]*). It has been suggested that unsteady flow due to super-critical heat addition may be responsible for increased loss due to boundary layer separation and may even be responsible for blade failures. Those investigating this instability include *Skillings [1987]*, *Whirlow et al. [1984]* and *Deich et al. [1987]*. However little evidence is available and it is not known whether this phenomenon occurs in two and three-dimensional flows.

2.4.3 Further Studies of Condensing Flows in Turbines

One major uncertainty in condensing flows in steam turbines is the size and distribution of the small droplets nucleated around the point of limiting supersaturation. The most popular technique for measuring the size of these droplets in operational turbines is that of light scattering. *Walters [1973]* and *Walters and Skingley [1979]* have done much to develop the technique but it is still an inherently inaccurate method of measuring the size of such small droplets. Research into droplet measurement techniques in wet steam turbines has been ongoing, for example *Walters [1985]*, *Umeda and Tatsumo [1988]*, *Kleitz and Laali and Courant [1988]*, *Walters [1988]*, *Cai, Wang and Wei [1994]*, *Bohn and Holzenthal [1997]*, *Petr and Kolovratnik [1997]* and *Wang et al [1998]*.

The quantity of moisture present in the form of coarse water is more easily measured, especially in turbines with suctions slots used for its removal, and is usually taken as a measure of deposition rates.

Over the previous decade or so there has been renewed interest in explaining the processes and effects of many aspects of condensation in low-pressure turbines. As discussed above condensation and subsequent growth of droplets has a major influence on thermal efficiency and on problems such as stress corrosion cracking, corrosion fatigue, and water droplet erosion. Studies have focussed on many aspects, including steam chemistry, deposition and evaporation of liquid films on turbine surfaces, heterogeneous nucleation and also electrostatic effects.

[2] It can be shown that addition of heat to a supersonic flow causes it to retard. The limiting case occurs when the flow Mach number is reduced to unity. Any further heat addition cannot be sustained and the flow becomes unstable.

Interest in heterogeneous nucleation, the nucleation of droplets on impurities or particles contained in the steam, has arisen mainly because of its relation to the corrosion processes in LP turbines. It is thought that heterogeneous nucleation occurring around the saturation line may lead to high concentrations of impurities in the condensate and that these impurities, finding their way to turbine surfaces may lead to increased levels of corrosion. Any possibility of controlling the impurity levels in the condensate by a fuller understanding of heterogeneous nucleation would help investigators control corrosion. However many investigations in this area have focussed on measurements related to the chemistry of steam before and after first nucleation, e.g. *Svoboda et al [1992]*, *Jonas [1998]* and *Dooley, Bursik and Staudt [1999]*, rather than the process of heterogeneous nucleation itself. *Petr et. al. [1995]* have measured the effect of steam chemistry on the size and number of droplets formed by heterogeneous nucleation. They found that chemicals with high-volatility would tend to reduce the size of droplets, while low-volatile chemicals would increase the droplet size. Others have attempted to model heterogeneous nucleation, e.g. *Servida et al [1992]* and *Sigon [1993]*, *Bakhtar et al [1997a]*, *Stastny et al [1997]* and *Petr and Kolovratnik [2003]*. However these models remain incomplete, because of the complexity of the problem and also because of uncertainties in experimental observations and conditions such as the state of chemical species in the steam.

Related to these investigations have been studies of the liquid films that form as a result of droplets finding their way to turbine surfaces. Liquid films have been observed even before the saturation line, as a consequence of the limited nucleation in the 'salt zone' e.g. *Filippov and Povarov [1980]* and *Semenov [1985]*. The thickness of the liquid films and their chemical composition has also been of interest, e.g. *Dooley, Bursik and Staudt [1999]* and *EPRI TR-113090 [1999]*.

Understanding heterogeneous nucleation also has implications for turbine performance (e.g. *Petr and Kolovratnik [1997]*). However of potentially more significance in this area is the effect of electrostatic charge on the condensation of steam in the LP turbine. Studies have focussed on the measurement of charge in the later stages of the LP turbine, e.g. *Hesler and Maurer [1998]*, *Tarelin and Skliarov [1999]* and *Hesler and Herzog [2000]* and also on the effects of electrostatic charge on the nucleation process e.g. *Rieger [1999]* and *Reiger and Dooley [2001]*. In addition researchers have been investigating the possibility of improving turbine and condenser performance by

introducing electric fields into the turbine itself, e.g. *Tarelin, Skliarov et. al. [1996]*. Results so far suggest that performance improvements may be possible, but are inconclusive.

Heterogeneous nucleation and electrostatic effects will be reviewed in more detail in chapter 3 of this thesis.

2.5 Two-dimensional investigations

The following sections summarise the theoretical and experimental research effort into condensation in two-dimensional flows in cascades of turbine blades.

2.5.1 Theoretical Treatment

Following the successful theoretical treatment of one-dimensional two-phase flows there was a drive to develop a similar treatment in two-dimensions. *Tochai [1978]* and *Bakhtar and Tochai [1980]* were the first to develop such a successful two-dimensional model of the two-phase flow of steam in a turbine cascade. They based their numerical method on *Denton's [1975]* finite-volume, time marching scheme making extensive modifications to couple the Euler and two-phase flow equations, allowing for nucleation and droplet growth. They obtained results for flows in *Krol's [1971]* convergent-divergent nozzles and a cascade of fifty percent reaction turbine blades. Many important differences between nucleating and dry steam flows in the cascade were highlighted by their solutions, including the shift of the sonic line downstream of the throat and the change in flow angles downstream of the trailing edge. However the results could not be validated since there were no suitable experimental results available at the time.

Later, when some measurements on a supersonic tip section became available, *Alubaidy [1982]* and *Bakhtar and Alubaidy [1984]* applied the treatment developed by *Tochai* to the conditions of the tests. Static pressures were predicted with reasonable accuracy, however the solutions were affected by shock smearing and accumulated numerical errors. The flow around leading edge was a particular source of error since the flow properties change rapidly here. The solution was also affected by internal inconsistencies in the time marching method. The errors are convected downstream affecting the rest of the flow. Of particular importance in two-phase flows is the effect these errors have on the local fluid temperature. This is crucial to predict correctly

because of it's influence on the position of limiting supersaturation and nucleation, the pressure rise that accompanies it, as well as heat and mass transfer rates between the phases.

A new scheme developed by *Denton [1983]* was adopted by *So [1984]* and *Bakhtar and So [1991]* in an attempt to overcome some of the above problems. *So [1984]* developed a technique for embedding a finer mesh into selected regions of the computational grid. With this he was able to produce a more accurate description of the flow in these regions, however his predicted thermodynamic losses were lower than those measured by experimental observers. In the absence of any allowance for viscous effects in the solution part of the disagreement between experimental and theoretical losses was attributed to the possible effect of condensation on boundary layer behaviour.

At around this time an experimental blow down facility was being brought into service (see section 2.5.2). So with the prospect of more data becoming available for comparison, work on the computational modelling continued. *Abbas [1987]* developed a boundary layer subroutine, using the integral method, which he included into the main treatment and made comparisons with the experimental data. Further comparisons with experimental results were carried out by *Savage [1989]*.

Following *Abbas* and *Savage*, *Mahpeykar [1991]* applied the treatment to the flow conditions studied experimentally. Based on So's experience he used an embedded fine mesh on the suction surface to improve the solution in the condensation zone. However, combination of an embedded mesh on the suction surface with the treatment of the trailing edge flow proved to be too complicated. He decided that using a quasi-orthogonal grid system could produce a more accurate solution. The solution around the trailing edge was also improved by the use of a base pressure model. *Mahpeykar* reported lower numerical errors and improved agreement with experimental observations on both the nozzle profile and rotor tip sections.

Henson [1995] extended the capability of the scheme by including additional terms to describe cases where the steam is wet at inlet. This allowed for the modelling of an existing population of droplets at entry to the cascade in addition to treating those formed by secondary nucleation further downstream. He compared his solutions with the *Mashmoushy's [1994]* experimental measurements and found good agreement.

Denton's scheme has the disadvantage that it is essentially of first order accuracy and requires the grid and the numerical factors to be selected carefully in order to yield satisfactory solutions. In an effort to avoid this *Rodriguez [1992]* developed a treatment based on the more robust four stage, Runge-Kutta, finite-volume, time-marching scheme of *Jameson*, *Schmidt and Turkel [1981]* and *Jameson [1982]*. This scheme is formally of second order accuracy and has been used to successfully predict the flow over aircraft wings and fuselages. The accuracy and improved shock capturing properties of this treatment led *Rodriguez [1992]* to believe that it had great potential for modelling two-phase flows. However his solutions did not agree with experimental observations as closely as those of *Mahpeykar [1991]*.

Zamri [1997] went on to improve the treatment based on *Rodriguez's [1992]* earlier efforts. He refined the technique, reducing the numerical errors and increasing the efficiency of the solver, while also extending the capability to include the treatment of viscous flows. He obtained very good agreement with experimental observations.

Others have worked on two-dimensional treatments for two-phase flows including *Snoeck [1983]* who developed a treatment based on the time marching scheme of *McDonald [1971]*, and *Moheban and Young [1984]* who, like *Bakhtar and Tochai [1980]*, used a scheme based on that of *Denton*. The prediction of unsteady phenomena due to super critical heat addition has also received some interest, e.g. *Guha and Young [1991 and 1994]* and *Zamri [1997]*. *Schnerr* and colleagues have used an implicit code, which includes turbulent terms and wetness terms. Much of their work has focussed on the investigation of unsteady, oscillating condensing flows, e.g. *Schnurr [1989]*, *Schnurr and Dohrmann [1990]*, *Adam and Schnurr [1997]* and *Winkler and Schnurr [2001]*. *Sejna and Lain [1994]* attempted to improve accuracy by introducing an unstructured triangular mesh, whilst *Singh et. al. [1999]* used a Eulerian method, as apposed to the more common Lagrangian approach, to predict two-dimensional nucleation and droplet growth. As already mentioned, there have also been some attempts to model the influence of chemical impurities on the condensation process, e.g. *Servida et al [1992]* and *Sigon [1993]*, *Bakhtar et al [1997a]*, *Stastny et al [1997]* and *Petr and Kolovratnik [2003]*. These studies will be discussed in more detail in chapter 3.

With the real flows in steam turbines three-dimensional there has been need to extend the treatment to three-dimensional fields. *Yeoh and Young [1982, 1984]* used a streamline curvature method to calculate the quasi three-dimensional through-flow of

steam in turbine stages. However *Bamkole [1987]* and *Bakhtar and Bamkole [1989]*, using a similar through-flow technique to simulate a quasi three-dimensional flow, found time-marching to be more suitable for this application. The scheme was based on *Denton's* so the quality of the solution was dependant on the selection of numerical coefficients and no comparisons with experimental results were made. Later, *Mohsin [1999]*, further developed the through-flow technique by refining *Bamkole's [1987]* treatment. He made comparisons with experimental data and obtained reasonable estimates of the condensation characteristics. A fully three-dimensional, time-marching, two-phase treatment has been developed by *Kosolapov and Liberson [1997]* and also by *Singh [1999]* who developed a three-dimensional, multistage treatment using a semi-viscous Euler solver coupled to the wet steam equations. Other implicit time-marching treatments, incorporating viscous and turbulence models, have been developed by *Liberson et al. [1998]* and *Liberson and McCloskey [1999]* and also by *Gerber and Knill [1999]* and *Gerber [2002]*.

2.5.2 Experimental Investigations

The replication and study of turbine wet flow conditions is difficult to achieve under laboratory conditions chiefly because of the problems of achieving the high degree of supercooling necessary for the steam to nucleate. In real turbines the flow is generally subsonic, and because of the work extracted by the moving blades, the flow can supercool sufficiently to nucleate without attaining the speed of sound. In contrast, in a steady state tunnel the flow must be accelerated to supersonic speeds in order to attain a similar level of supercooling. However it is possible to achieve a supply of supercooled steam, at subsonic speeds, using blow-down conditions and such a facility was constructed at the University of Birmingham during the 1980's.

The blow-down technique has the advantage of generating a supply of supercooled steam without the need to give kinetic energy to the steam. Saturated steam, contained in a large pressurised receiver, is expanded in much the same way as a cloud chamber, producing a reservoir of supercooled steam. This can then be passed to the test section and over a cascade of turbine blades. Pressure or optical measurements may then be made as the steam passes through the cascade. More details of the experimental set up and operation are given in Chapter 4 of this work.

Shojaee-Fard [1987] and *Siraj [1987]* studied the characteristics of the first blade profiles in nucleating flows. They recorded extensive sets of static pressure measurements, Scheiren and Mach Zehnder photographs and measurements of droplet size. Later *Ebrahimi [1991]* carried out wake traverses on the cascade of stator blades and investigated the characteristics of a set of rotor blades in superheated and nucleating flows. Typical blade surface pressure distributions for both superheated and nucleating flows can be seen in Figures 2.3 and 2.4 respectively. It can be seen that there is no difference between the pressure distributions over the pressure surface of the blade. However there is a departure between the two distributions on the suction surface. There is generally an inflection in the distribution at approximately 0.4 axial chord in the superheated test which is caused by a change in the radius of curvature of the surface just downstream of the throat. In the nucleating tests this interacts with the zone of rapid condensation resulting in a pressure rise.

In the case of the measurements carried out on the stator blades, the nucleating tests with subsonic outlet showed evidence of increased aerodynamic losses. It was thus thought possible that the performance of the blade could be improved by modifying its profile.

Mashmoushy [1994] extended the work by recording pressure profiles and flow traverses downstream of the cascade using the same rotor blades but under wet steam conditions. A venturi slightly upstream of the cascade was used to generate a supply of wet steam to the blades. When supercooled vapour was admitted to the venturi, expansion in its converging section triggered the nucleation process and, if the subsequent diffusion in the diverging section was carried out efficiently, the water droplets could be retained.

In tests where the outlet flow from the cascade was supersonic the characteristic of the blade differed under superheated, nucleating and wet inlet conditions. With steam wet at inlet, the magnitude of the pressure rise observed on the suction surface just downstream of the throat was less than that obtained when steam was supercooled at inlet and decreased as the inlet wetness increased. By contrast the results for tests with subsonic outlet were very similar under superheated, nucleating and wet conditions. It was concluded that the loss of efficiency due to thermodynamic irreversibility is lower when the steam is already wet at inlet.

Rassam [1995] continued the investigations into the performance of the rotor blades in wet steam. He conducted droplet size measurements using the light extinction method and flow visualisations, which consisted of Mach-Zhender interferometry and shadowgraphy.

In the last study carried out before the current work *Mamat [1996]* undertook an investigation of the nucleating characteristics of a second profile designed as a result of experience gained from the original.

In the investigations completed on this equipment so far the characteristics of three separate blade profiles, two nozzle blades and a rotor tip-section blade have been studied with steam superheated and supercooled at inlet; see *Shojaee-Fard [1987]*, *Siraj [1987]*, *Savage [1989]*, *Ebrahimi [1991]*, and *Mamat [1996]*. In addition, the characteristics of the rotor-tip section have been studied, with wet steam at inlet, by *Mashmoushy [1994]* and *Rassam [1995]*.

In the experiments discussed above it had been assumed that the primary cause of condensation was homogeneous nucleation, i.e. the spontaneous formation of very small water droplets at the molecular level. The effect of impurities on the condensation process was regarded as small. The current work has been undertaken to gain some understanding of the effect of chemical impurities on the condensation process downstream of the saturation line in flows of steam. In addition the distribution of electrostatic charge, on the first nucleation of water droplets, has also been investigated. The following chapter introduces homogeneous and heterogeneous nucleation theory and discusses the effect of chemical impurities and of electro-static effects in relation to the steam condensation process.

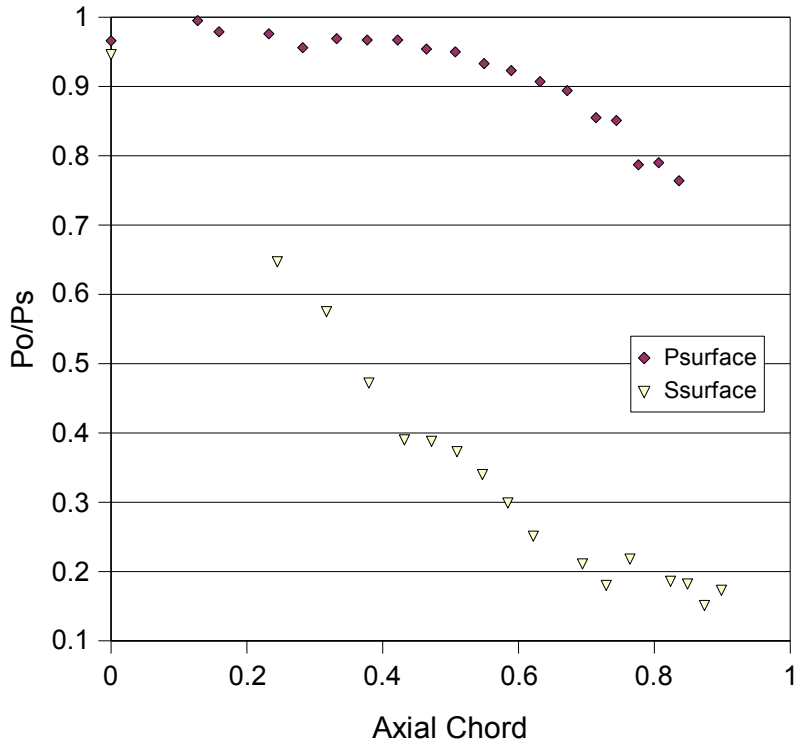

Figure 2.3: Stator blade superheated pressure profile, P_o = 1.019, ΔT = 35 K, P/P_o = 3.52

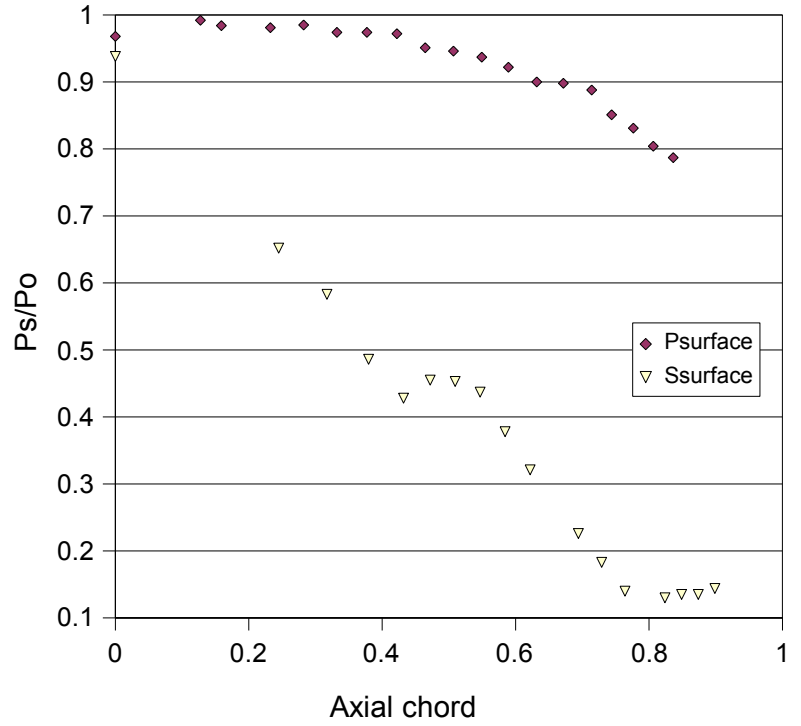

Figure 2.4: Stator blade nucleating pressure profile, P_o = 1.012, ΔT = -2.3 K, P_0/P_S = 3.54

Chapter 3:
Nucleation in Flowing Steam

3.1 Introduction

In the majority of theoretical and experimental investigations concerned with condensing flows of steam in nozzles and turbines, the main interest historically has concentrated on the behaviour of the pure fluid. The possible influence of chemical impurities or of electro-static charge on the nucleation process has received less attention. This is because of the assumption that homogeneous nucleation dominates the condensation process and that the small number of droplets forming on impurities are simply a complicating factor.

In recent years a continued need to understand the problems experienced in the LP steam turbine, from just before the saturation line to downstream of the Wilson line (a region collectively known as the Phase Transition Zone), has led to increased interest in the effect of chemical impurities and electro-static charge (e.g. *Rieger and Dooley [1997]*).

This chapter first reviews homogeneous nucleation theory and goes on to discuss binary nucleation theory in a two-component system. Studies concerned with the effect of impurities on the condensation process are reviewed. Lastly the theory, role and influence of electro-static charge on steam flows are discussed.

3.2 Homogenous Nucleation in a Pure Vapour

As the development of the theory of binary nucleation in a two-component system has followed that of homogeneous nucleation, before considering nucleation in a two-component system, it will be useful to consider homogeneous nucleation of a pure substance first.

In a fluid containing no impurities, or foreign particles, nucleation of liquid droplets from the vapour phase occurs by the fortuitous formation and subsequent growth of nuclei. This process is known as homogeneous nucleation. The development of a

theory to describe this process has followed two separate paths, the kinetic and statistical mechanical approaches, as discussed in chapter 2. The former, known as *classical* theory, is the model presented below.

3.2.1 Thermodynamic Aspects

Any thermodynamic system will attempt to attain equilibrium by reducing its *Gibbs* free energy. In a single component system the *Gibbs* free energy is defined as,

$$G = h - Ts \tag{3.1}$$

or in differential form,

$$dG = vdP - sdT \tag{3.2}$$

Where v and s are the specific volume and specific entropy of the system respectively. The *Gibbs* free energy is constant for a system in equilibrium, at constant pressure and temperature.

The change in *Gibbs* free energy for vapour at pressure p and temperature T_G condensing to a liquid droplet of radius r and mass m_r, may be written as;

$$\Delta G = m_r\left(G_L - G_G\right) + 4\pi r^2\sigma_r \tag{3.3}$$

The first term refers to the change in free energy as the fluid condenses from vapour to bulk liquid. This change in free energy is obtained by integrating equation 3.2. Because of the appearance of absolute entropy in the equation, it is integrated along a constant temperature path in three steps, i.e. expansion of the vapour from p to $p_s(T)$; condensation of the vapour to liquid at constant pressure and temperature; compression of the bulk liquid at constant temperature from $p_s(T)$ back to p. The second term on the right hand side of equation 3.3 refers to the change in free energy resulting from the creation of surface as the liquid droplet forms.

If the vapour can be assumed to behave as a perfect gas;

$$m_r\left(G_L - G_G\right) = -\frac{4}{3}\pi r^3\rho_L RT_G \ln\left[p / p_s(T_G)\right] \tag{3.4}$$

The variations of ΔG with droplet radius r, are shown in Figure 3.1. It can be seen that for a given supersaturation ratio (supercooling) ΔG has a maximum ΔG^* found at the critical radius r^*. Substituting equation 3.4 into 3.3 and then differentiating gives the equation for r^*;

$$r^* = \frac{2\sigma}{\rho_L R T_G \ln\left[p / p_S(T_G)\right]} \tag{3.5}$$

Equation 3.5 is the Kelvin-Helmholtz relation, relating the vapour pressure above a curved surface to that for a flat surface. It can be seen that for a given temperature the size of the droplet and the logarithmic supersaturation ratio are inversely related. For a given supersaturation ratio, droplets with a radius r^* will be just in equilibrium, droplets with a larger radius, which need a lower supersaturation ratio for equilibrium, will tend to grow, while those with a smaller radius will find the surrounding supersaturation ratio insufficient and tend to evaporate.

Substituting equation 3.5 into the equation for ΔG gives the free energy activation barrier at the critical radius r^*;

$$\Delta G^* = \frac{4}{3}\pi r^{*2}\sigma \tag{3.6}$$

It is this barrier that causes the vapour to supercool when its path crosses the saturation line. The breakdown of supersaturation in a homogeneous vapour is via chance collisions of water molecules within the vapour itself. This is considered in the following section.

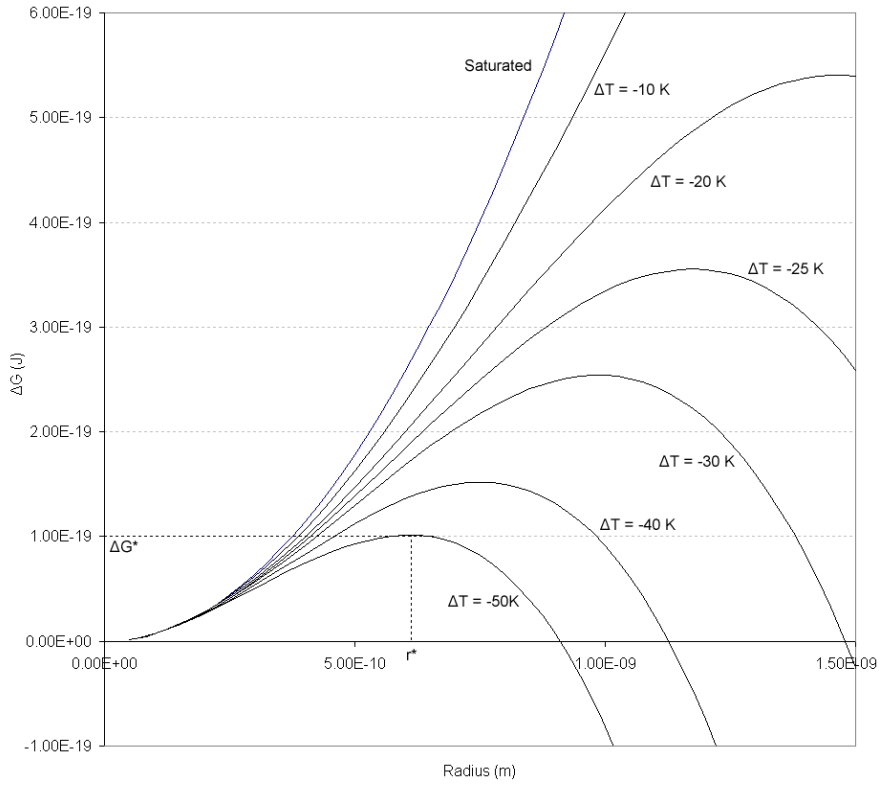

Figure 3.1: Variation of ΔG with droplet radius r

3.2.2 Kinetic Aspects

Volmer and Weber [1926] suggested that the distribution of molecular clusters in the vapour could be calculated using Boltzmann's law:

$$n_g = n_1 \exp\left(-\frac{\Delta G}{kT_G}\right) \tag{3.7}$$

Where n_1 is the total number of molecules per unit mass and n_g is the number of clusters of size g molecules per unit mass. ΔG is the change in free energy associated with the formation of g size clusters and k is the Boltzmann constant.

At equilibrium conditions $p = p_s$ and from equation 3.6 $r^* = \infty$. This means that for a pure vapour, despite there being a population of small water clusters formed by random collisions none of them will grow, because the likelihood of one of them reaching r^* and surmounting the activation barrier is extremely low. However as the supercooled steam expands the supersaturation ratio increases and this picture changes dramatically. Now the number of small clusters, formed by random collisions, reaching r^* increases by orders of magnitude. When a cluster reaches r^* it is able to grow. Eventually a large enough number of droplets will have reached r^* and begun to grow, releasing latent heat to the vapour and thus returning the system to thermodynamic equilibrium.

3.2.3 Nucleation Rate

In a saturated or super-heated vapour the rate of condensation of a cluster of size g to size g+1, denoted by C_g, and the rate of evaporation of the cluster size g to g-1, denoted by E_g, is balanced:

$$C_g n_g = E_{g+1} n_{g+1} \tag{3.8}$$

In a supersaturated vapour the condensation and evaporation rates will no longer be balanced because some clusters will reach the critical radius, r^* and continue to grow. Hence there will be a net rate at which clusters of size g grow into clusters of size g+1, denoted by J_g, the embryo current per unit mass. This is given by,

$$J_g = C_g f_g - E_{g+1} f_{g+1} \tag{3.9}$$

where to signify the difference a new symbol f_g is used to denote the concentration of clusters of size g in a supersaturated vapour i.e. not in equilibrium.

The rate of condensation of clusters, C_g, may be calculated from the kinetic theory of gases as,

$$C_g = \frac{4\pi r_g{}^2 qp}{\sqrt{2\pi m_1 k T_G}} \tag{3.10}$$

where q is the condensation coefficient, defined as the fraction of molecules colliding with the surface that result in condensation and m_1 is the mass of an individual molecule.

The rate of evaporation, E_g is calculated by assuming that if the clusters were moved to an environment in which they could maintain thermodynamic equilibrium then the rate of evaporation would equal the rate of condensation. Substituting equation 3.8 into equation 3.9 and rearranging yields:

$$\begin{aligned} \frac{J_g}{C_g n_g} &= \frac{f_g}{n_g} - \frac{f_{g+1}}{n_{g+1}} \\ &= -\frac{\partial}{\partial g}\left(\frac{f_g}{n_g}\right) \end{aligned} \tag{3.11}$$

A cluster of size g may be formed by either condensation of a molecule on a cluster size g-1, or by evaporation of a molecule from a cluster size g+1. Similarly the same cluster may be destroyed by either loss of a molecule, thus becoming a cluster size g-1, or by gaining a molecule, thus becoming a cluster size g+1. So the rate of change of cluster concentration, f_g may be written as,

$$\begin{aligned} \frac{\partial f_g}{\partial t} &= \left(C_{g-1} f_{g-1} + E_{g+1} f_{g+1}\right) - \left(C_g f_g + E_g f_g\right) \\ &= J_{g-1} - J_g \approx -\frac{\partial J_g}{\partial g} \end{aligned} \tag{3.12}$$

Substituting J_g from equation 3.11 gives:

$$\frac{\partial f_g}{\partial t} = \frac{\partial}{\partial g}\left\{C_g n_g \frac{\partial}{\partial g}\left(\frac{f_g}{n_g}\right)\right\} \tag{3.13}$$

Equation 3.13 is known as the *Becker-Doring* equation (see *Becker and Doring [1935]*) and is a general equation describing the nucleation process. Its solution gives the embryo current, J_g as a function of time.

3.2.4 Steady State Nucleation Rate

The solution of equation 3.13 is studied under two sets of conditions. Firstly there is a transient stage during which the population of clusters is unsteady and the nucleation rate varies both with g and with time. The second is a fictitious steady state stage in which supercritical clusters are continuously removed and new supercooled vapour is added such that the system remains steady.

Kantrowitz [1951], *Probstein [1951]*, *Wakeshima [1954]* and others have studied the transient stage prior to pseudo steady state nucleation. *Kaschiev [1969]* produced an exact analytical solution to equation 3.13 involving a time constant τ. He showed that the transient time before J reaches 99% of its steady state value is approximately 5τ. *Young [1973]* made some specimen calculations by substituting typical numbers for the time constant. He concluded that at both low and high pressures the transient time before steady state nucleation is reached is negligibly small compared with the time taken for steam to traverse typical increments employed in the analysis of condensing flows. Hence the pseudo steady state nucleation rate is representative of the actual nucleation rate with little loss of accuracy.

For the condition of steady state nucleation, equation 3.12 becomes,

$$\frac{\partial f_g}{\partial t} = J_{g-1} - J_g = 0 \tag{3.14}$$

Hence,

$$J_{g-1} = J_g = J_{st} = J_{g*} \tag{3.15}$$

where J_{st} is the steady state nucleation and J_{g*} is the net rate of formation of critical clusters, i.e. those having the critical radius r^*.

The expression for steady state nucleation is obtained by writing equation 3.11 for each of the range of clusters $1 < g < g^+$, where g^+ is large in comparison with g^*. Taking the sum yields,

$$\sum_{g=1}^{g=g^+} \frac{J_{st}}{C_g n_g} = \frac{f_1}{n_1} - \frac{f_{g^+}}{n_{g^+}} \tag{3.16}$$

At small values of g both the concentration n_g and f_g are large, so that to a good approximation the ratio $\frac{f_g}{n_g}$ approaches 1,

$$\lim_{g\to 1}\left(\frac{f_g}{n_g}\right)=1 \tag{3.17}$$

Also the ratio $\frac{f_g}{n_g}$ diminishes with increasing g so that,

$$\frac{f_g}{n_g}\to 0 \; for \; g=g^+ \tag{3.18}$$

Hence equation 3.16 becomes,

$$J_{st}\sum_{g=1}^{g=g^+}\frac{1}{C_g n_g}=1 \tag{3.19}$$

Replacing the summation with an integral,

$$J_{st}=\frac{1}{\int_{g=1}^{g=g^+}\frac{dg}{C_g n_g}} \tag{3.20}$$

Substituting the distribution for clusters defined in equation 3.7 into 3.20,

$$J_{st}=\frac{1}{\int_{g=1}^{g=g^+}\frac{dg}{C_g n_1 \exp\left(-\Delta G/kT_G\right)}} \tag{3.21}$$

From equation 3.10 it can be seen that C_g is proportional to r^2 and thus to $g^{2/3}$. It is therefore a slowly varying function of g and can be taken out of the integral with little loss of accuracy.

ΔG can be expanded as a power series about g^* to give:

$$\Delta G=\Delta G^*+\left(\frac{\partial \Delta G}{\partial g}\right)_{g^*}\left(g-g^*\right)+\frac{1}{2}\left(\frac{\partial^2 \Delta G}{\partial g^2}\right)_{g^*}\left(g-g^*\right)^2+\ldots \tag{3.22}$$

The second term on the right hand side is zero by definition. Truncating the series at the second order term and substituting into equation 3.21 allows the integral to be evaluated,

$$J_{st} = \frac{C_{g*} n_{g*}}{\sqrt{\frac{2\pi k T_G}{Q}}} \tag{3.23}$$

where,

$$Q = \left(\frac{\partial^2 \Delta G}{\partial g^2} \right)_{g*} \tag{3.24}$$

C_g can be substituted from equation 3.10 and the term Q evaluated from equation 3.5. After some re-arrangement the final expression is (*MacDonald [1962]*):

$$J_{st} = Z \exp\left[-\Delta G^* / (kT) \right] \tag{3.25}$$

where the term Z contains the kinetic terms and evaluates to,

$$Z = q \sqrt{\frac{2\sigma_r}{\pi m^3}} \frac{\rho_G}{\rho_L} \tag{3.26}$$

Equation 3.25 is the expression for steady state nucleation according to the *classical* theory.

3.2.5 Refinements of the Classical Theory

As discussed in chapter 2 the *classical* nucleation theory has been studied and reviewed by numerous authors over the years. However the refinements proposed by *Courtney [1961]* and *Kantrowitz [1951]* have been adopted in this work and will be briefly summarised.

Courtney suggested that the distribution of clusters, defined in equation 3.7 is only applicable to equilibrium conditions. He proposed that the partial pressure of the clusters should be taken into account when the vapour is supercooled. Thus equation 3.7 should be re-written as,

$$n_g = n_1 \frac{p_s(T_G)}{p} \exp\left(-\frac{\Delta G}{k T_G} \right) \tag{3.27}$$

This reduces the nucleation rate by the supersaturation ratio.

Kantrowitz considers that the water clusters are at temperature θ above their surrounding vapour. This allows for the transfer of latent heat from the cluster to the

vapour. Equation 3.9, describing the embryo current for a supersaturated vapour, is re-written as,

$$J_g = C_g(T_G) f_g - E_{g+1}(T_G + \theta) f_{g+1} \tag{3.28}$$

This leads to a correction,

$$J_g = \frac{1}{1+v}\left(C_g f_g - E_{g+1} f_{g+1}\right) \tag{3.29}$$

where,

$$v = q\frac{\rho_G}{\alpha}\sqrt{\frac{RT_G}{2\pi}}\left(\frac{L^2}{RT_G{}^2} - \frac{L}{2T_G}\right) \tag{3.30}$$

and α is the heat transfer coefficient and L is the latent heat associated with condensation ($h_G - h_L$).

These two corrections combined modify the pre-exponential Z in the equation for steady state nucleation (equation 3.25) such that,

$$Z = \frac{1}{1+v} q \sqrt{\frac{2\sigma_r}{\pi m^3}} \frac{\rho_s(T_G)}{\rho_L} \tag{3.31}$$

where $\rho_s(T_G)$ is the density of the vapour corresponding to T_G and $p_s(T_G)$.

Both corrections have the effect of reducing the steady state nucleation rate, by a factor of between 20 and 30, over the whole of the pressure range.

The variation of the steady state nucleation rate with supercooling, calculated using equation 3.25 with the refinements in equation 3.31, at a series of constant pressures are shown in Figure 3.2. The exponential increase in nucleation rate with increased supercooling can clearly be seen. For example, at a pressure of 1 bar the nucleation rate is 10^{10} droplets per kg per second at 22 K of supercooling, but this rises to 10^{20} droplets per kg per second at 33 K of supercooling. This corresponds to the reduction in the free energy barrier as supercooling increases as seen in Figure 3.1.

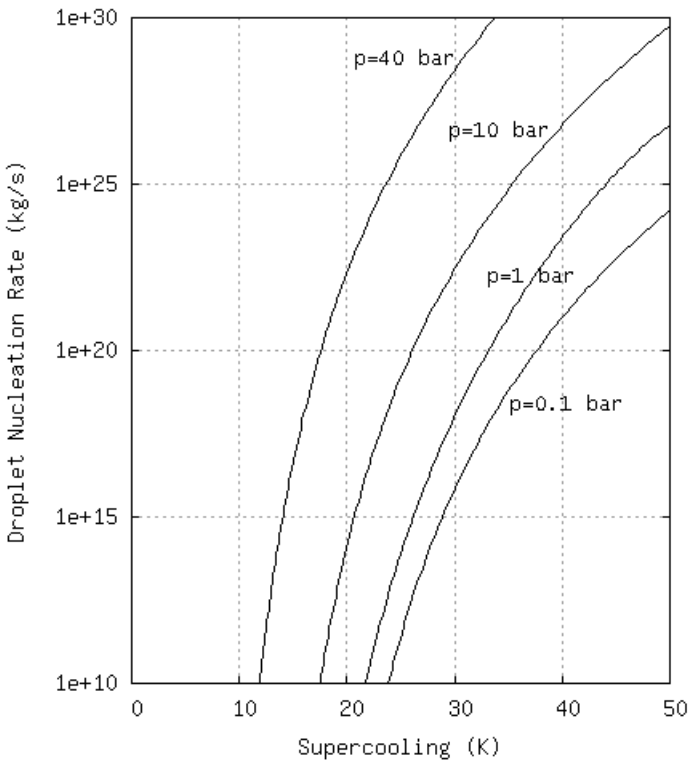

Figure 3.2: Steady state nucleation rate vs. pressure

In the above discussion it is assumed that the steam is pure, containing no impurities. However, in the case of steam in mixture with impurities, this assumption may no longer be valid. The influence of impurities on the nucleation process is discussed in the following sections.

3.3 Heterogeneous Nucleation in Binary Systems

A binary system contains two distinct chemical species. In such a two-component system the free energy is defined in terms of chemical potential μ. In a single component system chemical potential can be defined as,

$$\mu = u + pv - Ts \tag{3.32}$$

where u is internal energy.

For a pure, single component system this is exactly equivalent to the definition of Gibbs free energy (see equation 3.1). However for a multi-component system the chemical potential for each individual component is defined as,

$$\mu_i = \left(\frac{\partial G}{\partial n_i} \right)_{T,p} \tag{3.33}$$

where the subscript *i* refers to the individual component and *n* is the number of molecules.

Thus the total free energy for a two-component system becomes,

$$\Delta G = \left(\frac{\partial G}{\partial n_1} \right)_{T,p} dn_1 \quad + \quad \left(\frac{\partial G}{\partial n_2} \right)_{T,p} dn_2 \tag{3.34}$$

or alternatively,

$$\Delta G = \mu_1 dn_1 + \mu_2 dn_2 \tag{3.35}$$

For a vapour containing two species, 1 and 2, condensing to form embryos consisting of n_1 molecules of 1 and n_2 molecules of 2, the change in free energy can be formulated as,

$$\Delta G = n_1 \left(\mu_{1,L} - \mu_{1,G} \right) + n_2 \left(\mu_{2,L} - \mu_{2,G} \right) + 4\pi r^2 \sigma \tag{3.36}$$

Where *n* is the number of each species in the cluster and the subscripts *L* and *G* represent the liquid and gas phases respectively. The third term is the contribution due to surface tension of the cluster. In a cluster of water and a second component, the influence of the second component will change the chemistry and thermodynamics of the cluster. Whether the changes tend to have a positive effect on the condensation process depends on various factors.

- The surface tension, σ, of the cluster may differ from the bulk value of either of the two components. If the resulting surface tension is lower than that for a pure water cluster, then ΔG will be reduced and spontaneous nucleation will occur at a lower supersaturation ratio.
- The hydration energies involved may be large and may therefore influence the thermodynamics of the cluster and its parent vapour.
- There may be differences in the specific volume of the mixture compared to the value of either of the two components
- Hydrates may form in the vapour phase bringing additional complications.

Also of importance are the equilibrium compositions of the liquid and vapour phases, which may differ. Figure 3.3 shows a typical composition/temperature diagram for a simple two-component system where both components are completely miscible in both phases. The percentage of B in A in the gaseous phase at point (1) is not the same as the percentage in the liquid phase at point (2). The exact percentage found in the liquid phase will depend on the dilute component's affinity for water. If this is large then the concentration of the dilute component in the water cluster may be large also. The concentration of the dilute component in the cluster will determine the properties of the cluster.

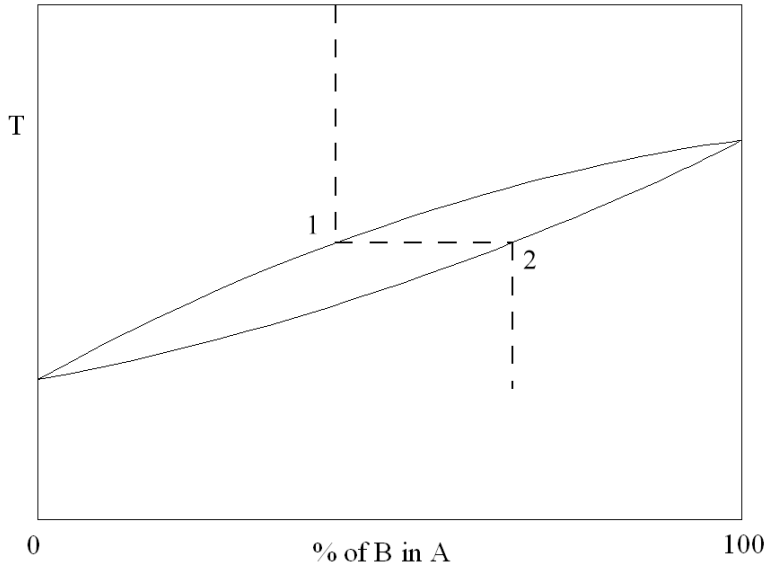

Figure 3.3: Composition diagram for a two component system

3.3.1 Free Energy Surface for Phase Change

Due to the complexities of a binary system it is un-surprising that the free energy surface for phase change differs from that in a single component system. *Reiss [1950]*, *Stauffer [1976]* and others have shown that the free energy surface for the phase change of a binary system turns out to contain a saddle point (see Figure 3.4), rather than the single maxima seen in single component systems. Thus for a droplet to grow in such a binary system it must pass through the saddle point.

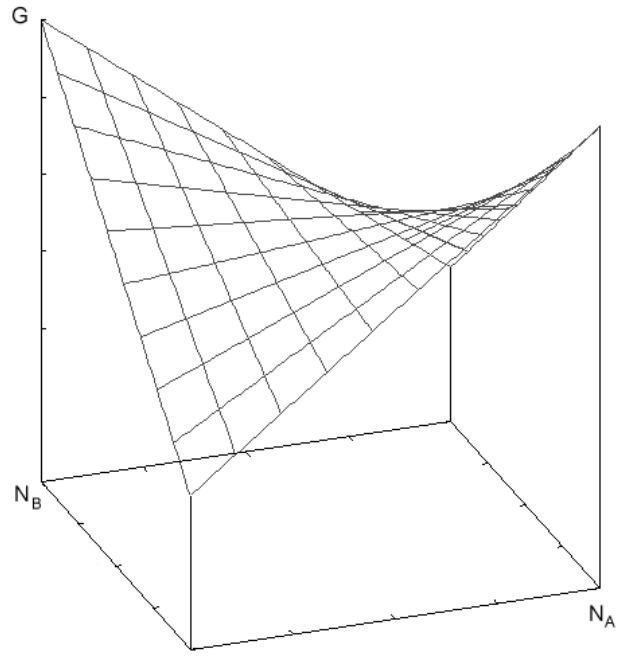

Figure 3.4: Schematic representation of a free energy surface near the saddle point

3.3.2 Binary Nucleation Rate

Flood was the first to study binary nucleation in 1934. However it was not until *Reiss [1950]* that a full theoretical treatment was published. *Reiss* based his analysis on the kinetic theory of *Becker and Doring* and *Zeldovich*. However his derivation of the nucleation rate for a binary system diverges from the earlier work on homogeneous nucleation because of the introduction of the second component. He starts by considering the possible reactions that an embryo, containing *a* molecules of species A and *b* molecules of species B, can undergo. Because of the low probability of collisions between embryos *Reiss* considered only the possibility of growth via addition of one molecule of either species A or B, or decay via loss of one molecule of either species A or B. This process is represented schematically in Figure 3.5.

$$
\begin{array}{c}
(a,b+1) \\
\Updownarrow \\
B \\
+ \\
(a-1,b)+A \Leftrightarrow (a,b)+A \Leftrightarrow (a+1,b) \\
\Updownarrow \\
B \\
+ \\
(a,b-1)
\end{array}
$$

Figure 3.5: Possible reactions for a binary embryo

Reiss then went on to represent all the possible combinations of embryo composition on a two-dimensional lattice (see Figure 3.6). An embryo of composition (*a*, *b*) is represented by a single point on the lattice with co-ordinates *a* and *b*. The possible reactions are represented by lines connecting each point on the lattice. For each line there will be a *net* rate (the difference in the rates of growth and decay) at which embryos traverse the connecting line and become embryos corresponding to the other lattice point. Thus a net rate can be calculated for the horizontal and vertical directions. By making a number of assumptions, including using the bulk value of surface tension in the region of an embryo, *Reiss* combined his analysis of the embryo growth rates with analysis of the free energy surface to arrive at an equation for nucleation rate. He considered the path of an embryo as it grows towards the point where it can become a stable fragment of the new phase. The analysis is complicated, and takes into account the variation of free energy surface with embryo composition. He assumes that because of the steep sides of the saddle point, the flow of molecules will only occur along the axis of the saddle point pass. The net flow in the direction perpendicular to this is considered to be zero. His solution for nucleation rate is of the form:

$$J = C \exp\left[-\Delta G^* / (kT)\right] \tag{3.37}$$

where the term *C* evaluates to,

$$C = \frac{\beta_a \beta_b \left[1 + (b^2/a^2)\right] S(a',b') F}{\beta_b + \beta_a (b^2/a^2)} \left(\frac{P}{Q}\right)^{\frac{1}{2}} \tag{3.38}$$

β – rate at which molecules strike unit area of the embryo surface

F – the total number of molecules present

S – surface area of an embryo at (a', b')

P – the negative curvature of the saddle along the path the embryo grows

Q – the positive curvature perpendicular to the path the embryo grows

a, b – number of molecules of species A and B respectively (i.e. the co-ordinates of the lattice in Figure 3.6)

a', b' – the lattice "co-ordinates" transformed such that they are parallel and perpendicular to the path the embryo grows along

The form of C is interesting. When Q is large, this means that the positive curvature at either side of the saddle is high and the pass is narrow, with very steep sides. It follows in this case that the flow of embryos through the pass would decrease. On the other hand if P, the negative curvature leading up to the saddle, is large then the barrier will be flattened and therefore easier to overcome. In this case the flow of embryos would increase.

If the solution of one component is very dilute in the other (as would most likely be the case in a steam turbine) then b/a will be very small and the expression for C can be approximated as,

$$C = \beta_a S(a', b') F \left(\frac{P}{Q} \right)^{\frac{1}{2}} \tag{3.39}$$

It follows from equation 3.39 that;

1. An increase in the rate of impact of species A will increase J
2. As the embryo surface area increases J increases – therefore if the second component were a large molecule nucleation rate may be increased.
3. Using a second component that reduces Q or increases P would also cause J to increase. This would depend on the chemistry of the second component.

However it must be remembered that C is just a factor to an exponential component in equation 3.37. It may therefore play a role in determining the onset of nucleation, but will probably have little impact on the equilibrium nucleation rate, which is largely determined by the exponential factor. The influence of the second component on the activation barrier ΔG^* will probably have a greater effect on the nucleation rate.

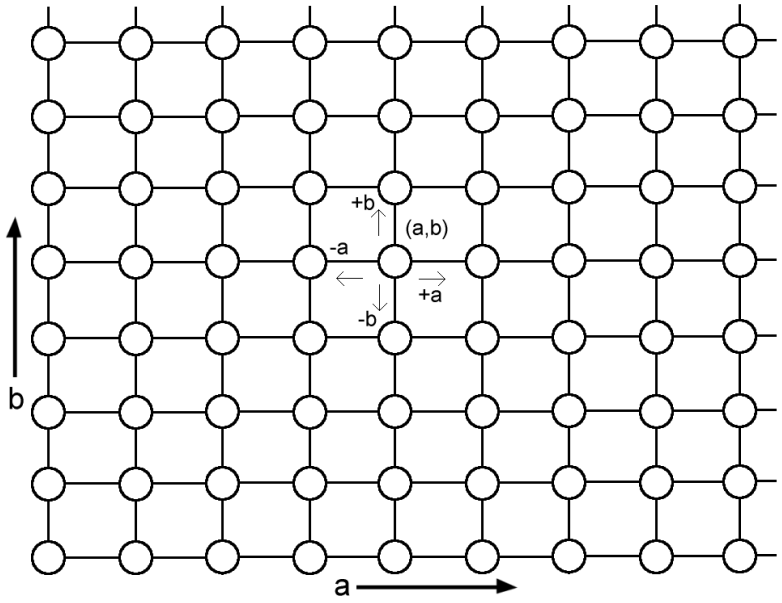

Figure 3.6: Two-dimensional lattice of molecules of species A and B

3.3.3 Examples of Further Studies

Since the development of the above 'classical' binary nucleation theory it has been applied mainly in relation to studies of binary nucleation in the atmosphere, in cloud chambers and aerosols. There have also been some refinements made to the theory (e.g. *Wilemski [1984]*). The theory has also been adapted due to inadequate predictions when applied to very small clusters (e.g. *Oxtoby and Kashchiev [1994]*). Modifications have also been made in an attempt to include the hydration energies in the equation for the Gibbs free energy of formation (e.g. *Noppel [1998]*). Studies specifically involving the nucleation of ammonia appear to be scarce. However recently, ternary nucleation models for water, sulphuric acid and ammonia systems have been developed (e.g. Napari et. al. [2002]). These models seem to suggest that adding ammonia to a water – sulphuric acid system greatly reduces the concentration of sulphuric acid required for a given nucleation

rate. This finding has implications for the study of aerosol formation in the atmosphere where earlier binary nucleation models could not explain the formation of atmospheric aerosols at the concentrations of sulphuric acid typically found in the atmosphere.

Examples of calculations made using *Reiss's* original theory are shown in Figures 3.7 and 3.8 taken from *Mirabel and Katz [1974]*. The activity of the acid in Figure 3.7 refers to the concentration of the acid relative to its saturation value. It can be seen that quite low concentrations of acid result in considerable nucleation rates. Figure 3.8 shows the activity of sulphuric acid and nitric acid required to achieve a nucleation rate of 1 $cm^{-3}s^{-1}$. This illustrates that acid rain is formed primarily by the action of sulphur oxides in the atmosphere.

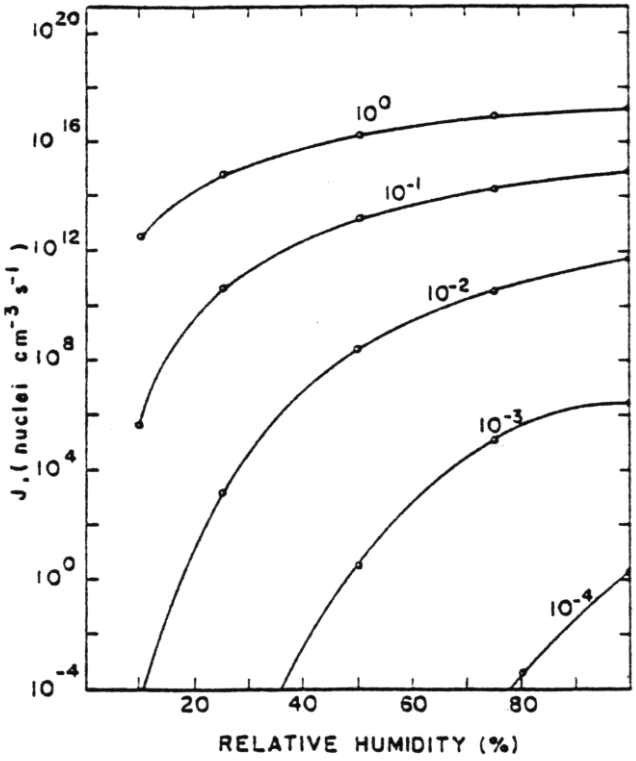

Figure 3.7: Calculated nucleation rates in $H_2SO_4 - H_2O$ system at 25°C
Numbers on the curves refer to the concentration of acid relative to its saturation value

Wilemski [1987] made a comparison between theoretical and experimental data for nucleation in a water-ethanol system in a shock tube. Figure 3.9 shows the theoretical and experimental activities of water and ethanol needed to achieve a nucleation rate of 10^{10} $cm^{-3}s^{-1}$. It can be seen that the addition of ethanol substantially lowers the level of activity required in the water-ethanol mixture to achieve a given nucleation rate.

Studies examining binary nucleation in sulphuric acid/water vapour, e.g. *Sopuch [1996]*, have reported that the associated time lags are large and the droplet growth rates low. Other studies have concentrated on binary nucleation in the atmosphere and in aerosols. Studies relating to the LP steam turbine will be discussed in section 3.4.

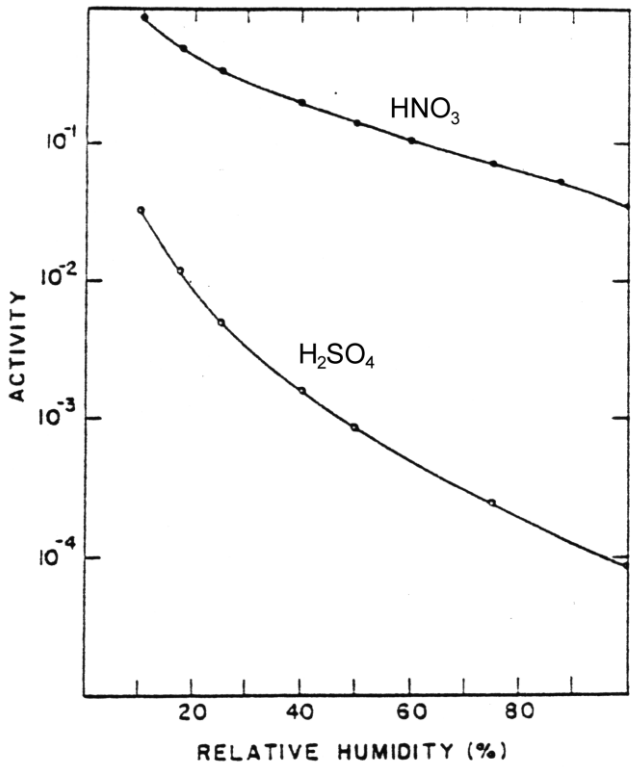

Figure 3.8: Activity of acid required to achieve a nucleation rate of 1 cm^{-3} s^{-1} as a function of relative humidity in the atmosphere

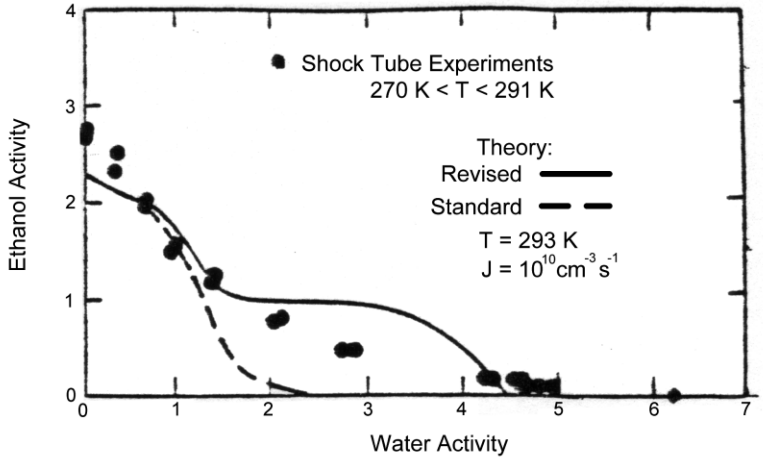

Figure 3.9: Theoretical and experimental conditions for a nucleation rate of 10^{10} $cm^{-3}s^{-1}$ in a water-ethanol system (from *Wilemski [1987]*)

3.3.4 Surface Tension

As discussed above the value of the surface tension of the binary cluster has a significant effect on the *Gibbs* free energy and therefore on the nucleation rate. The surface tension of pure water clusters is relatively high and thus a second component whose properties reduced the surface tension of the two-component cluster would be highly desirable. This is generally the case for solutions of organic substances in water. For example the variation of surface tension with concentration of ethanol in an ethanol-water cluster is shown in Figure 3.10, the numbers on the curves refer to the number of molecules in the cluster (see caption). The reduction is less for smaller water clusters at a given concentration. This is probably because it is thought that in very small clusters the concentration of the additive will differ between the mean and the surface of the cluster.

The organic substance, octadecylamine (ODA), has been known to influence the steam condensation process in turbines and even to improve turbine performance when added to the feed water (*Dooley, Feldburg, et al [1997]*). These effects are probably due to ODA's influence on the surface tension of water droplets. However it is not suitable for use in an operating turbine since once introduced to the plant it is almost impossible to remove from surfaces.

Petr and Kolovratnik [1995] in their investigation into the effect of steam chemistry on droplet nucleation observed slightly smaller droplet sizes for steam dosed with highly volatile chemicals, such as ammonia, and suggest that these chemicals may reduce the surface tension slightly.

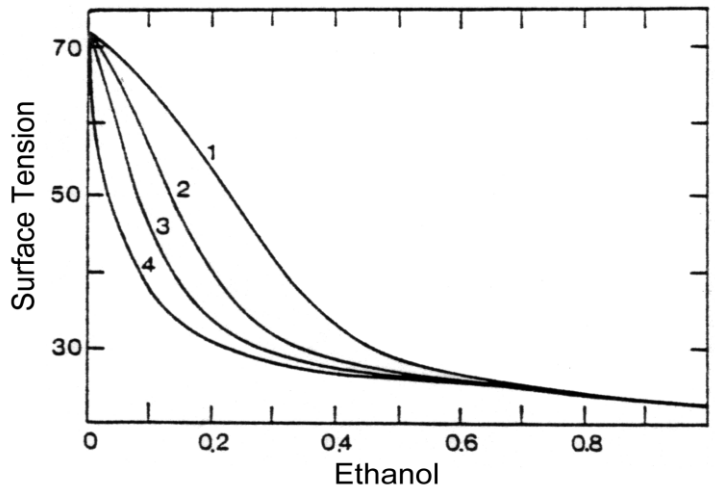

Figure 3.10: Variation of surface tension with the size of water-ethanol cluster at 293 K
No. molecules: 10^2 for curve 1, 10^3 for 2, 10^4 for 3. Flat surface for curve 4.
(from *Flageollet-Daniel et. al. [1983]*)

3.3.5 Ideal Cases for Binary Nucleation in Steam Turbines

a) *Substances that are volatile and mix completely with steam vapour and also dissolve completely in water*.

Such a substance would be easy to introduce into either the boiler feed-water, or directly into the steam. As the steam begins to cool and approaches the saturation line binary clusters containing the substance dissolved in water form. If the characteristics of the substance were carefully picked and the nucleation rates high then the limiting supersaturation of the flow might be reduced, preventing or substantially reducing homogeneous nucleation. If the number of binary droplets formed is too small then the effect might only be to increase the amount of wetness in the flow, potentially also increasing damage by erosion and/or corrosion without having any significant effect on the overall nucleation process.

As discussed above such a substance would ideally reduce the surface tension of the water clusters. It might also have properties that fortuitously alter the shape of the saddle point as discussed in section 3.3.1.

b) *Substances with high boiling/melting points that are soluble in water*.

Such a substance (e.g. a salt) could be added to the feed water. When the water is boiled the substance will be carried into the steam in the carry over droplets. In the super-heater these droplets evaporate leaving clusters of the substance in the steam. As the steam cools they can form clusters of solid or liquid while the steam is still superheated. As the steam approaches the saturation line these clusters act as sites for nucleation. As in case (a) the number of nucleation sites would need to be very high if the limiting supersaturation is to be reduced.

3.4 Studies of Nucleating Flows and Impurities

The engineering literature contains relatively few references to investigations of binary nucleation in conditions representative of steam turbines. *Steltz et. al. [1981]* have studied impurities in low pressure turbines but they do not consider binary nucleation. *Steltz's* results are interesting however because he suggests that salts soluble in water appear in solution above the steam saturation line. His measurements, in a selection of low-pressure turbines from fossil fuel stations and a nuclear unit, indicated the presence

just above the saturation line of a small numbers of droplets containing relatively high levels of salt contaminants in solution. These droplets are referred to as 'early condensate' and the region around the saturation line where they form as the 'salt zone'. In the single case where wetness was measured *Steltz* estimated moisture content of 0.5% with droplets of 2.5 μm in diameter. In comparison the theoretically predicted moisture content at the same conditions is 0.1%. It is suggested that these salts in concentrated solution have a large part to play in blade corrosion in the LP turbine (e.g. *Jonas et al [1998]*). Their effect on nucleation downstream of the saturation line was not studied.

Studies initiated by EPRI (see *Dooley, Bursik and Staudt [1999]* have also measured the concentration of impurities in the early condensate around the saturation line. Investigators have found (e.g. *Dooley, Feldburg et. al [1997]*) that very small droplets (radius 0.1 μm) exist near to turbine surfaces as early as the 1% moisture line, with slightly larger droplets (radius 5 μm) existing at the 2% moisture line in the bulk of the flow. These early condensate droplets have a much higher concentration of sodium, sulphates and chlorides that found in the superheated steam, from 2 – 150 times more. Also the early condensate was found to be more acidic. The consequences for the formation of liquid films and for corrosion have been considered by these studies, but not the effect on homogeneous nucleation later on in the expansion into the wet region. It is possible, if large numbers of small droplets form by heterogeneous nucleation around the saturation line, that supercooling below the saturation line may be reduced.

Servida, Morbidelli and Sigon [1992] and later *Sigon [1993]* evaluated models for assessing the behaviour of chemical species in steam nucleation. However these models are not complete because of the complexity of the problem and the lack of experimental data and are still subject to a number of uncertainties. In particular the state of chemical impurities (molecular, hydrated or ionic) near the saturation line in the 'salt zone' is still open to speculation (*Petr and Kolovratnik [2003]*).

Although not representative of turbine conditions, *Petr, Kolovratnik et al [1995]* studied the effect of steam chemistry on droplet nucleation in a convergent-divergent nozzle. They dosed steam with a number of different chemicals, including volatile and non-volatile chemicals, and measured the resulting droplet size and wetness fraction after nucleation using a light extinction technique. An increase in droplet size, compared to measurements in pure steam, was observed for low-volatile chemicals, e.g. sodium chloride, and a slight decrease observed in droplet size for high-volatile chemicals, e.g

ammonia (although due to uncertainty in the light extinction measurements any influence of volatile chemicals was found much less probable). The effect of the chemical additive was reduced for higher expansion rates and the tests were also performed at equilibrium conditions, rather than the non-equilibrium conditions representative of supercooled flows in turbines.

Stastny, Sejna and Jonas [1997] (see also *Stastny and Sejna [2001]*) modelled the flow of steam containing sodium chloride (NaCl). The heterogeneous nucleation of water and sodium chloride was not modelled, but estimates of the number and size of droplets nucleated upstream of the saturation line were calculated and then used to provide an initial population of droplets for the homogeneous solver. The effect of heterogeneous nucleation downstream of the saturation line was evaluated by modelling both this population of droplets and also any droplets subsequently forming via homogeneous nucleation. A similar approach has been taken by the author (see *Bakhtar, Mashmoushy and Buckley [1997a]* and section 3.5.2). *Stastny* reported that for higher concentrations of NaCl (0.23×10^{17} molecules per kg) the homogeneous nucleation rate and maximum supercooling were reduced. However they assumed that 100% of NaCl molecules acted as heterogeneous nucleation sites upstream of the saturation line. A smaller concentration of NaCl (10^{15} molecules per kg) did not affect the homogeneous nucleation rate. They were also able to predict concentrations of NaCl downstream of the saturation line as well as determining steam parameters on the blade surface, aiding the assessment of areas particularly at risk to corrosion.

Petr and Kolovratnik [1997] performed droplet measurements downstream of the last set of rotor blades in a 200 MW steam turbine. They observed a bi-modal system of droplets and suggested that this was due to a "complex mixed homogeneous-heterogeneous nucleation process". Such a bi-modal system of droplets was also observed by *Mashmoushy [1994]* whilst measuring droplet sizes downstream of a venturi used as a wet steam generator. The larger droplets were attributed to heterogeneous nucleation on impurities upstream of the venturi (see section 3.5.2).

In addition to their experimental investigations *Petr and Kolovratnik* have also assessed computational models of heterogeneous nucleation (*Petr and Kolovratnik [1999], [2001]* and *[2003]*). In *Petr and Kolovratnik [2003]* experimental measurements of droplet sizes from both a 200 MW fossil plant and a 1000 MW nuclear plant were used to assess the accuracy of three nucleation models. The first model was based on classic

unary homogeneous nucleation, the second modelled only heterogeneous nucleation and the third was a coupled hetero-homogeneous model similar to the scheme used by *Stastny et. al. [1997]*. All three models required additional parameters to be specified to achieve agreement with the experimental data. Despite reasonable agreement with the light intensity measurements only the homogenous and coupled hetero-homogenous models gave good agreement with the droplet size data. Thus *Petr and Kolovratnik* concluded that, given the current state of knowledge, classic homogeneous models still provide the best picture of nucleation in turbine flows.

3.5 Studies At Birmingham University

In all the previous experimental studies of nucleating steam at the University of Birmingham, mains water treated with an alkaline corrosion inhibitor was used as the boiler feed water. Thus the feed water and steam contained an unknown level of impurities. At the time the effect of these impurities was unknown and they were considered to be simply a complicating factor (particularly in the case of optical measurements). One of the main aims of the current project is to produce a baseline set of measurements using ultra-pure steam that will be unaffected by the presence of impurities. These pure-steam measurements will allow the effect of impurities in the previous studies at Birmingham to be assessed. A further aim of the current project is to introduce a known level of an impurity chemical into the steam and observe the effect on the nucleation process, again using the pure-steam measurements as a point of comparison.

3.5.1 Previous Experimental Results

The experimental studies relevant to the current work are those of *Ebrahimi [1991]* and *Mashmoushy [1994]*. Although major modifications have been made to the steam blow-down facility for the current project[1], the GEC rotor blade profile under investigation and the inlet and outlet steam conditions have remained unchanged between studies. A full summary of *Ebrahimi's and Mashmoushy's* results can be found in Appendix F.

[1] For more information on the current experimental facility see chapter 4.

Ebrahimi [1991] studied the behaviour of superheated and nucleating steam flows through the GEC rotor tip cascade for dry inlet conditions. In the turbine blading studied there is a high expansion rate in the throat region. This results in the steam supercooling during the fast expansion and in the case of the tests with supersonic outlets this supercooling is sufficient to cause the flow to nucleate just downstream of the blade throat – known as the zone of rapid condensation. The release of latent heat resulting from condensation returns the system to thermodynamic equilibrium and is associated with a pressure rise on the blade suction surface appearing in the zone of rapid condensation. Ebrahimi also found that in tests with steam supercooled at inlet the pressure distributions were insensitive to the level of inlet supercooling.

Mashmoushy [1994] studied pressure distributions for steam wet at inlet to the blade cascade. Wet steam was generated by passing supercooled steam through a venturi placed upstream of the blade cascade. Two such venturi were used, a 'standard' venturi and a 'fast' venturi, which had a higher expansion rate and generated smaller droplets. In tests with steam wet at inlet the droplets provided some surface for condensation and in tests with a supersonic outlet the supercooling was reduced. In the case of the droplets generated using the 'standard' venturi the droplet surface was not enough to lower the supercooling sufficiently and the steam nucleated again in the zone of rapid condensation just downstream of the blade throat. This secondary nucleation was accompanied by a pressure rise on the suction surface and was similar to the changes observed by Ebrahimi. However in *Mashmoushy's* case the magnitude of the pressure rise was reduced as the level of inlet wetness was increased. In the case of the smaller droplets generated by the 'fast' venturi, secondary nucleation was suppressed and the pressure distributions were similar to those for superheated steam.

In *Mashmoushy's* investigation the droplets at inlet to the cascade were generated by homogeneous nucleation in the venturi. However his results indicate the form of pressure distributions that would be expected in the blade cascade if an equivalent number of small droplets were formed upstream of the cascade by heterogeneous nucleation due to the presence of impurities in the steam.

3.5.2 Nucleation in a Venturi

As mentioned above *Mashmoushy [1994]* generated a supply of wet steam at inlet to the blade cascade by first expanding supercooled steam through a venturi. Since the steam was already supercooled at inlet to the venturi expansion through the converging section caused the flow to further supercool leading to nucleation of water droplets. If the diffusion in the diverging section was carefully controlled the nucleated droplets could be retained.

The initial design of the venturi assumed that the steam supply was pure. However, as discussed above, this was not the case. The impurities present acted as sites for heterogeneous nucleation early on in the expansion. As the supercooling in the venturi increased further then a second population of droplets nucleated spontaneously via homogeneous nucleation. Since the droplets formed by heterogeneous nucleation on impurities formed earlier they grew to a larger size. This was supported by extinction measurements at the exit of the venturi that indicated a group of droplets of 0.4 – 0.5 μm radius. The existence of these droplets masked the smaller ones and made the determination of their size very difficult.

To provide a more accurate picture of the distribution of droplets at exit of the venturi a one-dimensional numerical simulation of two-phase flow through a convergent-divergent nozzle was used by the current author (see *Bakhtar, Mashmoushy and Buckley [1997a]*). This simulation is able to treat two-phase venturi steam flow to a good degree of accuracy. It is based on the development of two-phase flow simulations that has been on-going at University of Birmingham for a number of years (e.g. see *Bakhtar and Zidi [1990]*). The simulation models the presence of impurities at inlet to the venturi using a group of water droplets. This assumes that the impurities would behave exactly like water droplets in their growth. The simulation also models the spontaneous nucleation of a second group of water droplets by homogeneous nucleation downstream of the inlet.

In addition to measuring droplet sizes at outlet from the venturi *Mashmoushy* measured the change in total pressure across the venturi. This information was used in the theoretical calculations to estimate the droplet size at inlet to the venturi that produced the correct outlet droplet size and wetness fraction and also matched the drop in total pressure.

Figure 3.11 shows a typical comparison between the measured and theoretical pressure distribution for the standard venturi. At inlet to the venturi the steam has a stagnation pressure of 1 bar and is 16 K supercooled. The theoretical solutions have been run for an inlet wetness of 0.00% (no impurities) and 0.01% (with impurities). The experimental conditions are dry at inlet, but contain real impurities. Given the one-dimensional model used in the theoretical simulation, there is reasonable agreement between the experimental data and the theoretical solutions. It can be seen that the two theoretical solutions, with and without impurities, are identical.

The variation of supercooling for both theoretical solutions is shown in Figure 3.12. In the presence of impurities the position at which the fluid attains its maximum supercooling has sifted very slightly downstream. The maximum supercooling of 30.16 K without impurities has changed to 29.98 K with them.

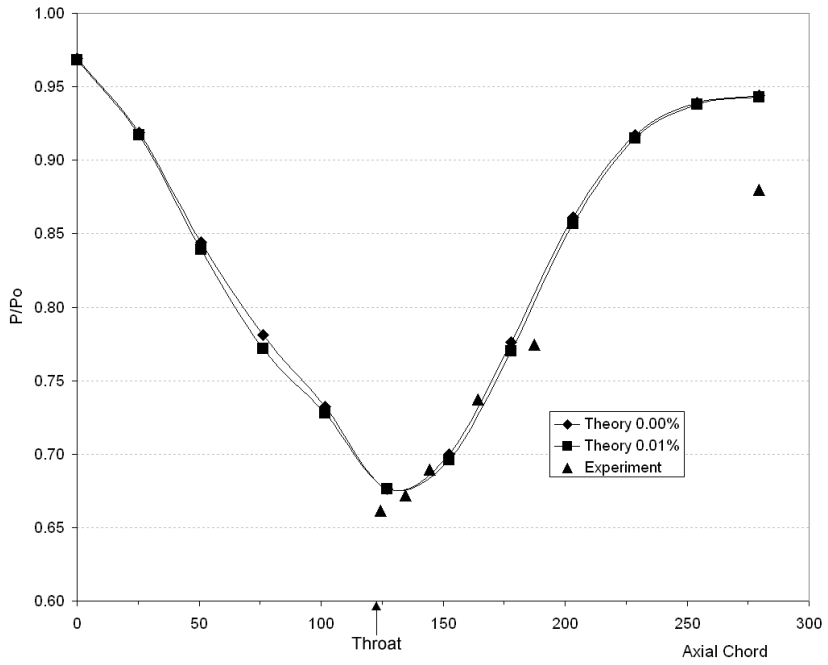

Figure 3.11: Standard venturi – Comparison of theoretical and experimental pressure distribution.

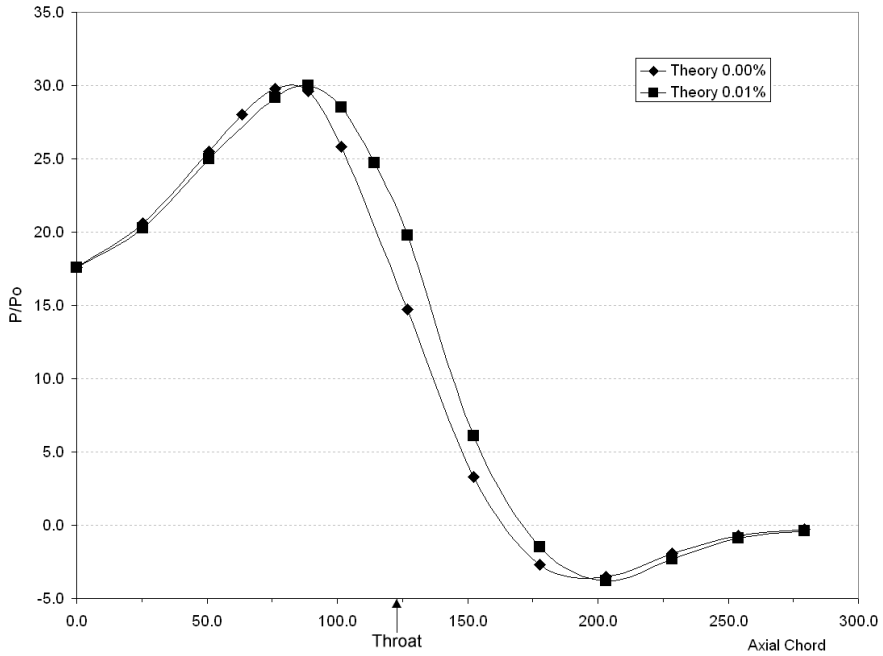

Figure 3.12: Standard venturi – Theoretical supercooling values.

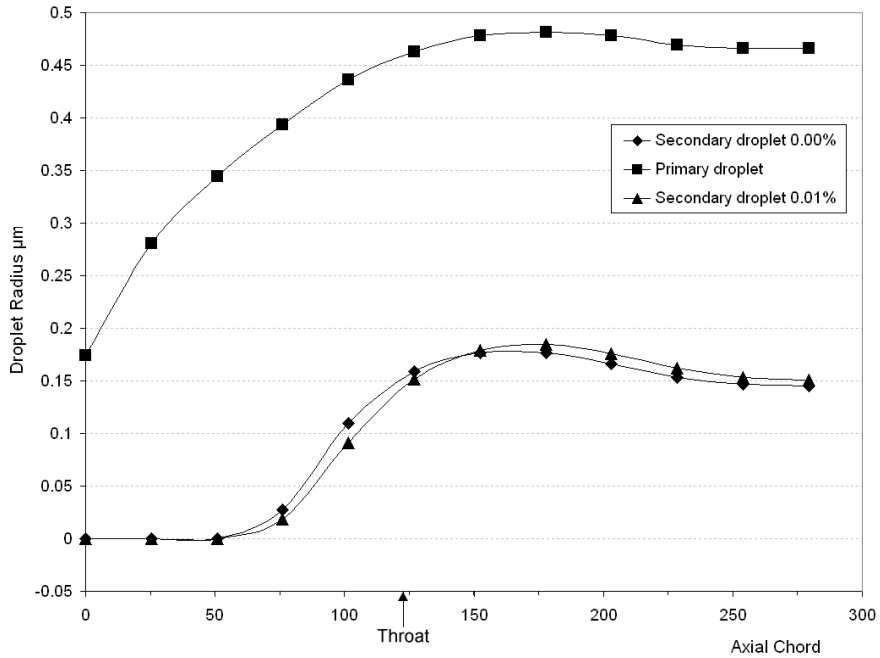

Figure 3.13: Standard venturi – Theoretical droplet sizes.

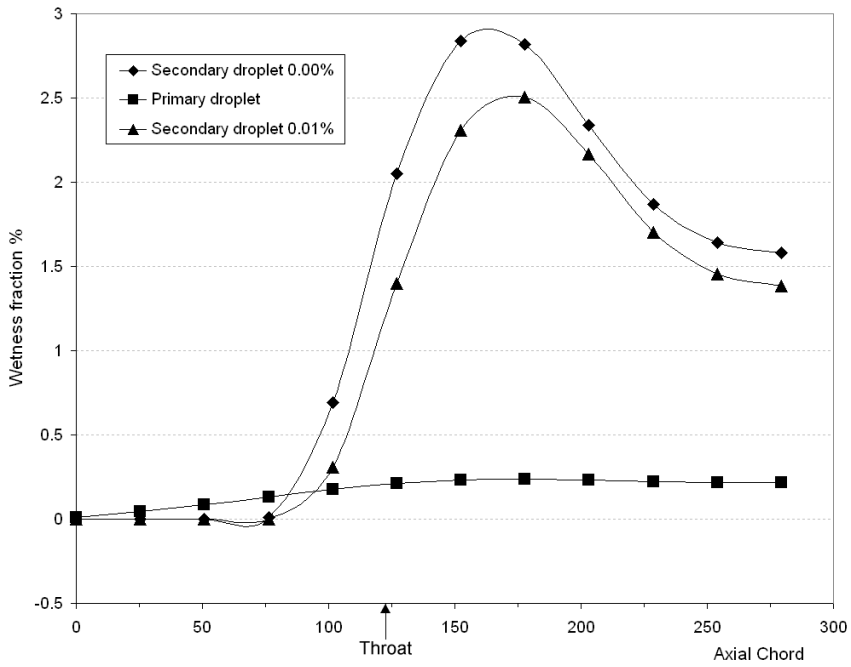

Figure 3.14: Standard venturi – Theoretical wetness values.

The theoretical variation of droplet size is shown in Figure 3.13. The mean radius of droplets formed by homogeneous nucleation, in the absence of impurities, is indicated by diamonds. The mean radius of droplets for the two populations modelled with impurities present are indicated by squares for the impurity droplets and by triangles for droplets formed by secondary homogeneous nucleation. The initial size of the impurity droplets was selected by trial and error to give outlet values corresponding to extinction measurements. It can be seen that the presence of impurities has no effect on either the onset of homogenous nucleation, nor on the size of the nucleated droplets.

The theoretical wetness fraction is shown in Figure 3.14. The symbols correspond to the same droplet groups as in Figure 3.13. In the solution with impurities present the wetness fraction of the droplets formed by homogeneous nucleation is less than the wetness fraction of these droplets with no impurities present. However the overall wetness fraction remains unchanged between the two solutions.

The solutions for the fast venturi are not presented here, but follow very similar trends.

Since a total pressure loss is associated with the irreversible release of latent heat to the flow during nucleation the “wetness fraction” used to model the impurities was

estimated by comparing the loss of total pressure between the theoretical calculations and experimental measurements. Despite the fact that the theoretical solutions tended to underestimate the measured losses it was concluded that the best overall agreement between theoretical solutions and experimental measurements was obtained by considering the impurities to be equivalent to a wetness fraction of 0.01% contained in droplets of 0.15 μm radius at inlet to the venturi. This corresponds to 2.4×10^{12} impurity nucleation sites per kg of steam, in comparison with 1.1×10^{15} droplets per kg formed by homogeneous nucleation. Overall the theoretical measurements tend to indicate that the presence of impurities in the steam did not alter the limiting supersaturation, the onset of homogeneous nucleation or the overall amount of wetness in the venturi flow.

3.5.3 Nucleation in the Turbine Cascade

In order to estimate the effect of impurities on flow behaviour in LP turbine blading *Bakhtar and Henson [1999]* ran two-dimensional theoretical solutions for the flow over the rotor tip section used in the above studies. They idealised the impurities using the estimates generated by *Bakhtar, Mashmoushy and Buckley* i.e. droplets of 0.15 μm radius and a wetness fraction of 0.01% at inlet to the blade cascade. They ran solutions for pure saturated steam and steam containing impurities with inlet stagnation conditions of 1 bar and an outlet static pressure of 0.43 bar. Similar to the venturi simulation the solutions for pressure distribution, supercooling, droplet size and wetness fraction are almost identical for both pure steam and steam containing impurities. The same conclusion, that in this case the presence of impurities has little effect on the limiting supersaturation, onset of homogeneous nucleation or overall amount of wetness can be drawn.

Bakhtar and Henson go on to suggest that to completely suppress homogeneous nucleation would require of the order of 2×10^{17} impurity particles per kg of steam with a radius of approximately 0.002 μm.

3.6 Electro-Static Charge and Heterogeneous Nucleation

The first recorded example of electro-static charge produced by condensing steam was reported by *Lord Armstrong [1840]* in a letter to Faraday. *Lord Armstrong* was recounting an episode at Seghill, Newcastle upon Tyne, where boiler steam leaked out through a crack in cement around a safety valve. A workman, who had one hand on a metal lever, placed his hand in the steam and received an electric shock. *Faraday* wrote back to *Lord Armstrong* saying that he had investigated the incident and using an electrometer found that the steam was positively charged. He had also determined that the mine water used in the boiler was acidic because of the sulphate of lime deposit found on the boiler wall. However steam found in another boiler using rainwater was found not to be charged.

Faraday [1865] went on to investigate the generation of charge in steam expanding through a nozzle. He was satisfied that the source of charge was not evaporation or condensation, based on the observation that the charge of the steam would vary by changing the material of the metal nozzle, while the evaporation remained the same. *Faraday* confirmed *Lord Armstrong's* findings that dry steam produced no electricity, but when the steam was wet charge was measured. He also noticed that acidity and alkalinity had some effect on the charge, but few pH measurements were reported.

Later in 1887 *Helmholtz* noticed in his experiments investigating steam flow in nozzles, that introduction of charge to the steam increased the condensation rate. *Wilson [1897]*, during his famous cloud chamber experiments, having already established that in air water mixtures cleared of impurities condensation was delayed, went on to show that the supercooled vapour thus produced could show up the path of ions because it would condense on them.

Since *Wilson's* time much work has been done to investigate the effect of electrostatic charge on liquids and the mechanisms by which liquid acquires charge. A theoretical solution for the nucleation of droplets on ions was first proposed by *Tomfor and Volmer [1938]*. *Pauthenier and Moreau-Hanot [1932]* studied the development of electric charge on a particle by field distortion. Later *Haydon [1974]* and *Felici [1984]* investigated double layer charging of liquid films. The break up of large droplets in an intense electric field was first studied by *Raleigh [1882]* and later by *Wilson and Taylor [1925]*, *Schweizer and Hanson [1971]* and *Taylor [1964]*. It has also been noted that heat

transfer rates can be improved by the application of an electric field. For example investigators using plate condensers have noted that heat transfer coefficients were substantially improved (by up to 300%) when an electrode grid producing a corona discharge is placed close by the condenser, see *Velkof [1962]*, *Velkof and Miller [1964]* and *Choi [1967]*. Cloud physics is another area where the effect of electric charge on liquid droplets has been of interest; see for example *Dufour and Defay [1963]* and *Byers [1965]*.

More recently research has been undertaken by various authors to investigate the nature and distribution of electrostatic charge in the steam flow of turbines (e.g. *Hesler and Maurer [1998] and Rieger [1999]*). There have, at the same time, been efforts to understand how the addition of electrostatic charge to the steam flow could improve the condensation rate and efficiency of the wet stages and of the condenser (e.g. *Tarelin, Skliarov et. al. [1996]*, *Hesler and Herzog [2000]*). The following sections discuss the possible mechanisms involved in the creation of charge in steam flows and summarise the theory of heterogeneous nucleation on charged particles. Some of the results seen so far, from attempts to measure and control charge in the LP turbine and condenser entrance, are also mentioned.

3.6.1 Sources of Charge in Steam Flow

The results of a number of authors confirm *Faraday's* observation that there is very little charge present in dry steam (e.g. *Tarelin and Skliarov [1999]*). Significant charge only appears once the steam has nucleated and become wet. There is still much discussion regarding the source of this charge, but the following mechanisms may be responsible:

1. Molecules will acquire some charge from random collisions with other molecules, ions and electrons.
2. Disassociation of electrons from water molecules in the boiler and/or super-heater.
3. The flow may acquire induced charges from charged components.
4. Double layer charging of condensed water flows across blade and diaphragm surfaces may produce charged drops.

5. Shattering of water streaming from the trailing edges of blades and diaphragms may produce charges on the resulting droplets.
6. Chemical pH from feed-water additives may contribute towards charged ions.
7. Surface charges may develop at the liquid-gas interface between droplets and the parent vapour/bubbles in the droplet.

Only the first three cases apply to the steam before it reaches the phase transition zone. As mentioned above dry steam vapour appears to have little or no charged ions present, so it is safe to assume that these mechanisms produce almost no net charge in the dry steam.

Mechanisms 4-7 apply to the steam after it has nucleated and water droplets have formed.

Double-layer charging is described by *Cross [1987]* and has a literature of its own e.g. *Felici [1984]* and *Haydon [1974]*. It is possible that molecules in the liquid films found on the metal surfaces of turbine casing and blades are stripped off by the passing flow. The charge arises because the molecules in the liquid films arrange themselves with molecules of one polarity on the outside and molecules of the opposite polarity on the inside. The outer molecules are stripped off by the passing flow. The effect of the charging increases with the resistivity of the fluid (and depends on several other parameters). Consequently it is only highly insulative fluids (resistivity > 10^7 Ωm) that charge by flowing over electric double layers and this would appear to exclude water and steam from charging via this mechanism.

Shattering of water droplets occurs at the blade trailing edge and on other sharp edges on the turbine casing where water collects. This mechanism is known to produce positive charge on the coarse water drops and negative charge on the fine drops and is discussed by *Cross [1987]*. Shattering of water droplets in steam turbines has been has been studied by various authors including *Gardner [1963]* and *Heymann [1970]*. *Gardner* and *Heymann*, have observed that the coarse water droplets formed by shattering are between 10μm and 100μm in diameter, with a typical size of 40μm. Shattering of water droplets is one explanation for the charged droplets observed in waterfalls. In waterfalls the coarse droplets tend to have a positive charge and the finer droplets, forming a mist around the waterfall, have a negative charge.

The influence of chemical pH on charge in water and steam is not discussed by *Cross*. However results from various investigators (e.g. *Hesler and Maurer [1998]*) have highlighted a link between pH and the polarity and magnitude of charge in wet steam. As discussed above *Faraday* also observed a link between pH and the charge of steam flowing from a nozzle.

Liquid-gas interface charging is thought to occur by some authors. Charging occurs because ions collect around the liquid gas interface leading to a net charge at the surface and producing an opposite charge below the surface. When the interface breaks up (e.g. when a bubble or droplet bursts) then the charge becomes separated leaving a net charge on the droplets produced.

3.6.2 Distribution of Charge in the Steam Flow

Studies of charge distribution in a steam turbine are scarce. *Tarelin and Skliarov [1999]* performed limited charge measurements using a 5mm diameter cylindrical probe. This was insulated from earth and the probe to earth current measured using an ammeter. Negligible charge was measured in the steam with no wetness present. However in condensing steam a current of 1.4mA was recorded. The lack of charge in dry steam and presence of charge in wet steam is consistent with the results of all other investigators.

More comprehensive tests were performed by *Hesler and Maurer [1998]* on an 800MW unit in Navajo, U.S.A. They preformed radial traverses downstream of the L-1R and L-0R blades using a cylindrical charge probe, a wetness probe and a pressure probe. They also investigated the influence of pH levels on the charge distribution and magnitude. A selection of their results can be seen in Figures 3.15 – 3.17. Charge was measured using a 5mm diameter stainless steel probe, insulated from, and held in, a stainless steel tube. The probe to earth voltage and current were measured by connecting the probe, via an ammeter and voltmeter, to earth outside the turbine casing. Wetness measurements were taken using an EPRI designed wetness probe. Total and static pressure traverse measurements were also recorded.

The radial variation of wetness fraction and probe to earth current (in μA) downstream of both the L-1R and L-0R stages are shown in Figure 3.15. There is no direct correlation between wetness fraction and charge along the axis of the blades. However the charge is negative over the majority of the blade axis from the blade root outwards - here the water droplets are mostly small. Only near the blade tip, where larger

drops exist, formed by coarse water from the liquid films and break-up from the blade trailing edge, was a positive charge measured. This is in agreement with the mechanisms suggested above which indicate that large droplets, e.g. formed by droplet shattering, generally carry a positive charge.

The radial variation of charge for a feed-water pH of 8.2 and 9.3 are shown in Figure 3.16. There appears to be an increase of positive charge associated with an increase in pH level.

Finally the radial variation of velocity and charge are shown in Figure 3.17. In this case there appears to be no correlation between velocity and charge.

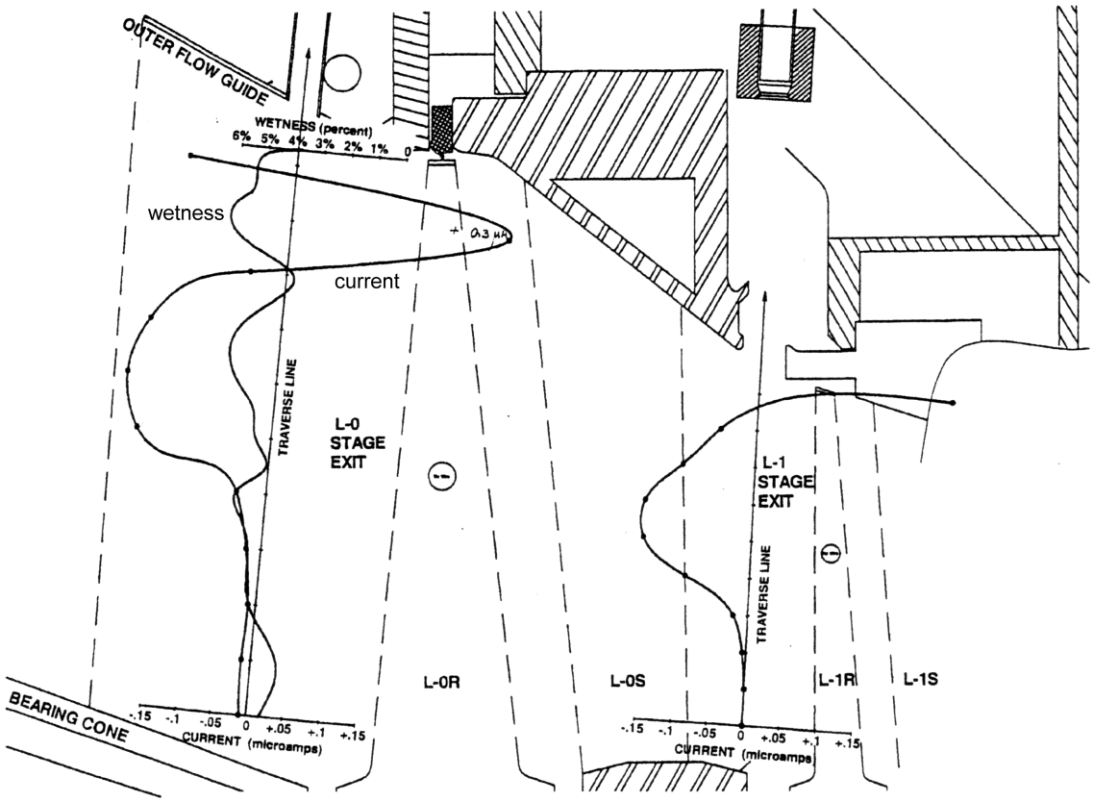

Figure 3.15: Radial variation of wetness fraction and charge distribution, Navajo 1998

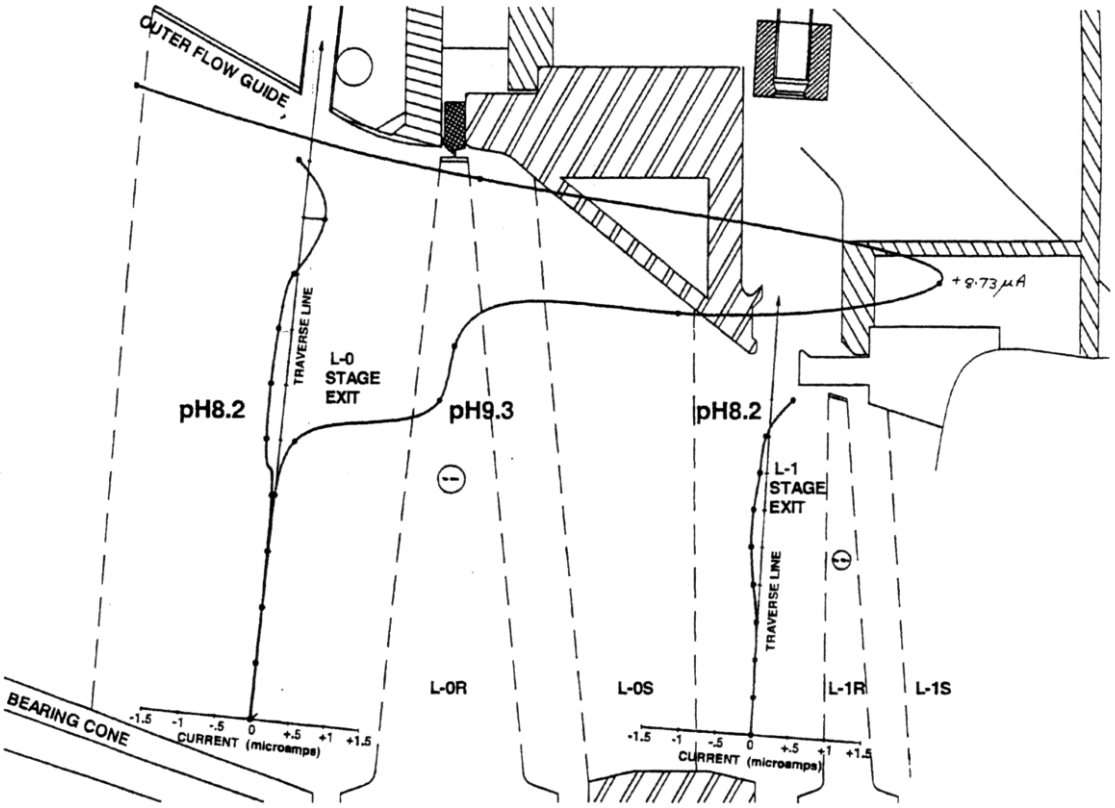

Figure 3.16: Radial variation of charge distribution for pH=8.2 and pH=9.3, Navajo 1998

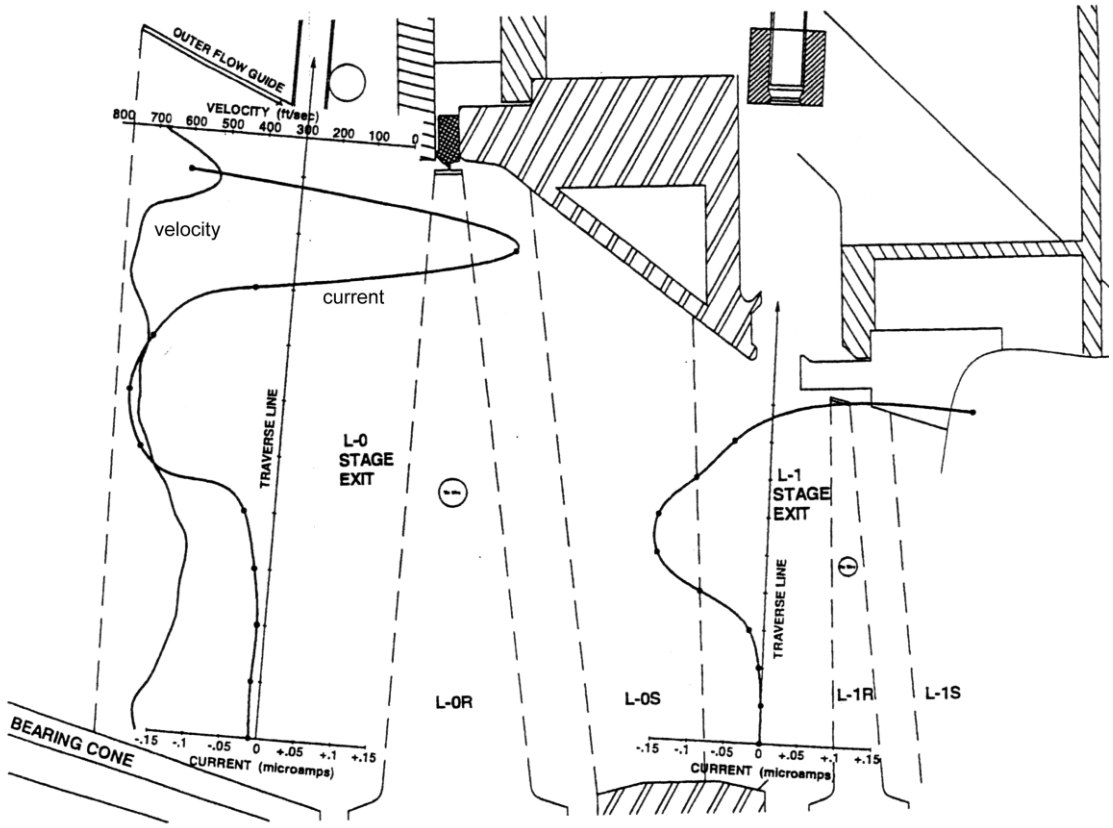

Figure 3.17: Radial variation of velocity and charge distribution, Navajo 1998

Measurements were also made at the exit from the exhaust hood, at the condenser neck. Readings from a fixed charge probe and a traversing charge probe were taken and measurements were made at various pH levels. As indicated by the measurements in the last two turbine stages there was a correlation between pH level and charge. Although the charge in the condenser neck was negative over the complete traverse, increasing the pH led to a significant reduction in negative charge. This is consistent with the results in the last two LP turbine stages where an increase in pH was associated with an increase in the level of positive charge. The investigators also noted there was some evidence of an inverse trend between velocity and charge in the condenser neck. Lower steam velocity was observed to correlate with greater values of negative charge.

Further charge and velocity distributions were recorded by *Hesler and Herzog [2000]* at the Conesville Station, U.S.A. These tests were intended to provide more information about the charge distribution in the turbine discharge, at the diffuser exit, midway down the exhaust hood and above the condenser tube bundles. There are some inconsistencies between *Rieger and Dooley's [2001]* summary of the Conesville results and the earlier report from Navajo. For example *Rieger and Dooley* cite low velocities in regions of large negative charge at Navajo, while at Conesville "high velocities were found in regions of high negative charge close to the diffuser wall, whereas velocity was low in the central regions of the diffuser and hood, where charge was low or zero". They also note that positive steam polarity was found in the lower exhaust at Navajo in comparison with a negative polarity found in the same region at Conesville. Further studies are clearly needed to determine exactly which factors influence the polarity and magnitude of the charge distributions found downstream of the turbine discharge.

Petr and Kolovratnik [2003] measured the charge present downstream of the L-0 rotor blades in the LP steam turbine of a 1000 MW PWR nuclear plant. They used a cylindrical charge probe to collect charged droplets and measured the resulting probe to earth current. Because of the different flow angles of the fine and coarse droplets past the L-0 rotor blades it was possible to separate measurements of charge for these two populations of droplets. Their results show that the fine droplets were negatively charged, with a space charge of approximately -2×10^{-3} C/kg and an estimated 3-6 electron charges per droplet. The magnitude of the charge increased slightly from the blade root to the tip. In contrast the coarse droplets had a positive charge, with a space charge of approximately $+2\times10^{-3}$ C/kg. The charge was almost zero at the blade root (where there

would be very few coarse droplets) and was at a maximum near the blade tip. *Petr and Kolovratnik* also performed some theoretical analysis of the flow using a nucleation model of water molecules nucleating on negatively charged ions. They concluded that the negatively charged ions probably had only a minor effect on the nucleation process, which was dominated by homogeneous nucleation.

3.6.3 Addition of Charge to Steam Flows

As described above charge exists naturally in flowing wet steam. However it has been suggested e.g. *Tarelin [1996]* and *Rieger [2001]* amongst others, that the addition of charge to steam could improve the turbine/condenser efficiency.

In all the studies so far charge has been imparted to the steam via a corona discharge, produced when a very high voltage is applied to an electrode in the flow. The physics of these coronas is discussed in section 3.6.4. The influence of electro-static charge on nucleation is discussed in section 3.6.5.

Only a few investigators have studied the introduction of high voltage electric fields downstream of the PTZ. There are some indications that a negative or positive electric field, introduced downstream of the PTZ can increase the efficiency of the wet stages and of the condenser. For example *Tarelin et. al. [1996]* obtained an approx. 1.1% increase in power output by introducing a high voltage electric field at the condenser neck of a 50MW single-flow condensing turbine in Eshkar, Ukraine. However certain combinations of charge polarity and electrode position also caused a reduction in power output. Effective combinations of electrode position and polarity are still under investigation with no firm conclusions having yet being drawn. The reasons for any power increase are currently also unknown. It was suggested by *Tarelin et. al.* that the increase in power output is due to condensation being enhanced by the splitting of large drops into smaller drops as they pass through the electric field. This is a known phenomena first studied by *Raleigh [1882]*. As drops pass through a strong electric field they will first elongate and then shed smaller droplets from their ends. *Schweizer and Hanson [1971]*, using n-octanol, found that although only approximately 5% of the mass of the droplet mass is lost to the smaller droplets they carry up to 23% of the overall charge. The *Raleigh* charge, q_R, required to break up a droplet is given by the equation:

$$q_R = \left[8\pi^2 \varepsilon_o \sigma r^3\right]^{\frac{1}{2}} \tag{3.40}$$

Further tests were performed on the same turbine by *Tarelin and Skliarov [1999]*. The position of electrodes was different to the earlier tests. This time two sets of electrodes were introduced to the flow downstream of the L-0R stage. A third group of electrodes was installed just above the condenser neck in the diffuser section of the exhaust hood. The electrodes were formed by stainless steel wires strung across the turbine or exhaust hood wall. The wires were insulated from the wall and positioned so that structural items close by would serve as "counter electrodes". A typical electrode design is shown in Figure 3.18.

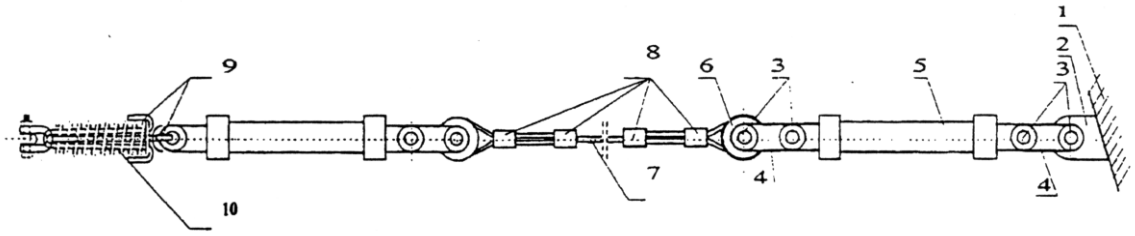

Figure 3.18: Typical electrode design, Eshkar 1998
1 – Wall of exhaust hood; 2 – Cramp; 3 – Bolt; 4 – Steel lath; 5 – Silicone rubber covered suspension insulator; 6 – Eyelet; 7 – Stainless steel cable; 8 – Cable clamps; 9 – Cramp; 10 – Safety spring attached to opposite wall (not shown)

The results obtained by *Tarelin and Skliarov* are summarised in Table 3.1. These are the results recorded under stable operating conditions. In the first table row a negative voltage of -10 kV was applied to the electrodes downstream of L-0R (electrodes 1, 2 and 10) with no voltage applied to the condenser electrodes. This resulted in a power increase of 400 kW (+1.37%). A positive charge of 10 kV applied to electrodes 1, 2 and 10 along with a negative voltage of -13.5 kV applied to the condenser electrodes resulted in a power decrease of 400 kW. Also a negative voltage of -7.2 kV applied to the 1, 2 and 10 electrodes gave a power increase of 300 kW (+1.0%).

The next series of tests applied a positive voltage of between +19 kV and +25 kV to the condenser electrodes. This resulted in a power decrease of 622 kW (-2.1%). However removal of the voltage from these electrodes caused the power output to recover and then *increase* by 500 kW (+1.65%).

In the third set of tests the turbine exhaust electrodes were set at -13.5 kV and condenser electrodes 8 and 9 set to +35 kV. This caused a power increase of 300 kW (+1.0%).

Table 3.1: Test Conditions and Power Changes Observed, Eshkar 1999

Turbine Electrodes (kV)	Condenser Electrodes	Flow (tons/hr)	Pressure (psi)	Temp (ºC)	Pressure Cond. (psi)	Power (MW)	Power Change (kW, %)
-10 (1,2,10) +10 (1,2,10) -7.2 (1,2,10)	0 -13.5 (3,4) 0	207	1207	457	2.44	29.3	+400, 1.37 <400, <1.37 +300, +1.0
0 (1,2,10) 0 (1,2,10)	+19 to +25 (3,4,5,7,8,9) 0 (3,4)	220	1180	450	1.81 – 2.14	31.1	-622, -2.1 +500, +1.65
-13.5 (1,2)	0 (3,4) +35 (8,9)	220	1180	450	1.81 – 2.14	31.1	+300, +1.0
0 (1,2,10) -16 (1,2) -16 (1,2)	0 (3-9) -23.5 (8,9) +30 (3,4)	200	1300	472	1.23 – 1.31	39.4	+300, +1.0 +600, +1.4 <600, <1.4
-11 (1,2) -11 (1,2)	-22.5 (6) -25 (6) -22.5 (6), +34 (8,9)	197.5	1349	480 - 475	1.12	31.5	+420, +1.4 +500, +1.5 +540, +1.7

The other results indicate similar trends. Negative charge applied to the turbine exhaust electrodes (1, 2 and 10) appears to have led to an increase in power output - and positive charge to a decrease in power output. The picture is slightly more complex for the condenser electrodes. For those electrodes closest to the diffuser a negative voltage again appears to be related to a power increase and a positive voltage with power decrease. However in the case of the two electrodes closest to the condenser tubes (8 and 9) a positive voltage here appears to further increase the power output (e.g. see the last test in Table 3.1), but this is only in combination with negative voltages applied to other electrodes, specifically those either in, or closer to, the turbine exhaust.

Although *Tarelin and Skliarov* state that the power output was measured with great accuracy the operating conditions during the tests varied somewhat. The back-pressure achieved was 57.5mmHg. The inlet steam pressure varied from 8.8 to 9.2 Mpa at 450 – 500 °C and the condenser pressure range was 8.8 – 20.1 kPa with a steam flow of 173 to 203 tonnes/hr. The authors also go on to discuss the influence of the electrode voltage on the flow conditions. They suggest the following effects when the electrodes were active:

1. A “pressure reduction in the extraction zone” (possibly the exhaust hood), consistent with an increase in power output.

2. An increase in wetness fraction with power increase (consistent with a pressure and enthalpy decrease at the turbine exit).
3. Droplet size remained constant (however note that wetness fractions and droplets sizes were *calculated* rather than measured).
4. A "calming effect" i.e. reduction of pressure fluctuations and possibly turbulence downstream of the L-0R blades.

It does however remain unclear what the effects on flow conditions really are. And although *Tarelin and Skliarov's* work does suggest the possibility of increasing power output by addition of electric charge to the steam exhaust and condenser flow the combinations of electrode position, polarities and voltages remain uncertain.

3.6.4 Corona Discharge

In the tests discussed above charge was introduced into the steam flow via a corona discharge created when a very high voltage is applied to an electrode in the flow. A corona discharge is indicated by a visible glow forming around an electrode in a gas. To form a corona effectively the active electrode must be a sharp point or narrow wire, the second, passive, electrode having a larger area. In the work of *Tarelin et. al.* the active electrode, around which the corona formed, was a thin wire strung across the turbine or condenser while the passive electrode was formed by large structural items e.g. the turbine casing.

Normally when an electric field is applied across two electrodes in a gas little current flows because there are few ions and free electrons to carry the current. However when the voltage exceeds a certain threshold value the gas molecules around the sharp electrode begin to ionise. The ions and free electrodes formed around the active electrode then collide with other gas molecules causing further ionisation and producing an 'avalanche' effect. This ionisation produces the visible glow associated with a corona discharge. The current flow then increases as the ions and free electrons carry the current between the electrodes. For air of relative density δ, with a smooth wire of radius a inside a concentric cylinder of radius b the corona starting voltage (in kV) is given by:

$$V_0 = \left(30a\delta + 9\sqrt{a\delta}\right)\ln\left(b/a\right) \tag{3.41}$$

where the relative density is defined in terms of perfect gas behaviour,

$$\delta = \frac{T_0}{T}\frac{P}{P_0} \tag{3.42}$$

In the case when the active electrode is negatively charged the electrons formed during ionisation are accelerated quickly away from the electrode. The high velocity they gain means that they will produce other ions and free electrons as they collide with gas molecules. The heavier positive ions travel at a much lower velocity towards the active electrode. When the active electrode is positive electrons travel towards the electrode, whilst the heavier ions are accelerated away. However because the velocity of ions is much lower they tend not to produce further ions and free electrons during collisions. In both cases ions are generated in the steam outside the corona and therefore charged particles are added to the flow.

Bakhtar, Mouhandes and Winterton [1982] studied negative corona discharges in steam for a range of pressures above and below atmospheric. Figure 3.19 shows a sample of their results for an electrode wire of 0.26mm radius, enclosed by cylinder of 12.5mm inner diameter acting as a passive electrode with steam at temperature 415 K. At low pressures where the steam was well above saturation, the corona starting voltage is clearly defined. However at pressures closer to saturation a significant leakage current can be observed before the onset of the corona discharge. The anomalous results are not what would be expected in a perfect gas such as air. This is firstly because steam cannot really be treated as a perfect gas near to the saturation line and secondly because when steam is saturated or approaching the saturation line it will condense on solid surfaces and the water films will conduct producing leakage currents. It is also possible that near the saturation line the increased numbers of $(H_2O)_n$ polymers become easier to ionise.

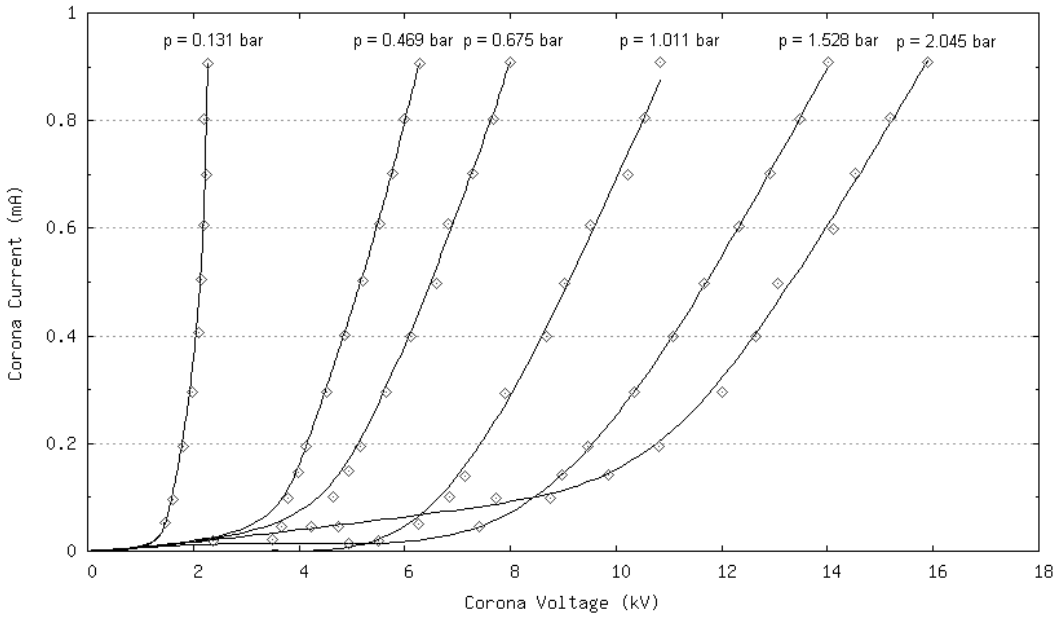

Figure 3.19: Corona current for small-radius wire at various pressures.
T = 415 K, wire radius 0.26 mm, cylinder radius 12.5 mm

3.6.5 Nucleation in an Electric Field

The influence of charge on the critical radius determining the onset of nucleation is discussed below.

The equation for the change in Gibb's free energy when a pure, uncharged water droplet with radius *r* spontaneously condenses is given by the equation;

$$\Delta G = -\frac{4}{3}\pi r^3 \rho_L R T_G \ln\left[\frac{p}{p_s(T_G)}\right] + 4\pi r^2 \sigma \tag{3.43}$$

The original revision of nucleation theory to include the effect of charge was by *Tohmfor and Volmer [1938]*. According to *Byers [1965]*, when the droplet nucleates on a particle with *q* Coulombs charge and radius r_0 equation 3.43 becomes:

$$\Delta G = -\frac{4}{3}\pi r^3 \rho_L R T_G \ln\left[\frac{p}{p_s(T_G)}\right] + 4\pi r^2 \sigma + \frac{q^2}{8\pi\varepsilon_0}\left[1-\frac{1}{\varepsilon_r}\right]\left[\frac{1}{r}-\frac{1}{r_0}\right] \tag{3.44}$$

where ε_0 is the permittivity of free space, taken to be the same for steam, ε_r is the dielectric constant of water. The dielectric constant for water is affected by charge and is different for positive and negative charges.

In order to illustrate the effect of charge on the free energy surface the variation of ΔG with charged droplet radius is plotted in Figures 3.20 and 3.21. In Figure 3.20 the charge on the droplet is 1e, whilst in Figure 3.21 the charge is 2e (where e is the charge on one electron). In both figures the variation of ΔG is plotted for a number of supersaturation ratios. In addition the variation of ΔG for uncharged droplets is plotted using dashed lines, for comparison.

The figures show that the effect of charge on the droplet is to create an energy well for small droplet sizes. The free energy activation barrier is therefore reduced, compared to the same supersaturation ratio for an uncharged droplet. Thus droplets with some charge will begin to nucleate at lower supersaturation ratios than uncharged droplets. Comparing the two figures at a given supersaturation ratio it can be seen that increasing the charge reduces the critical radius required for droplets to grow. Notice also that for higher values of supercooling the activation barrier disappears altogether. Hence if the supercooling is increased to this point, and there are ions present, droplets forming on these ions will grow without limit.

It can be concluded that, in theory at least, the addition of a small amount of charge to water clusters may increase the nucleation rate and reduce the limiting supersaturation reached in the last few stages of the LP turbine.

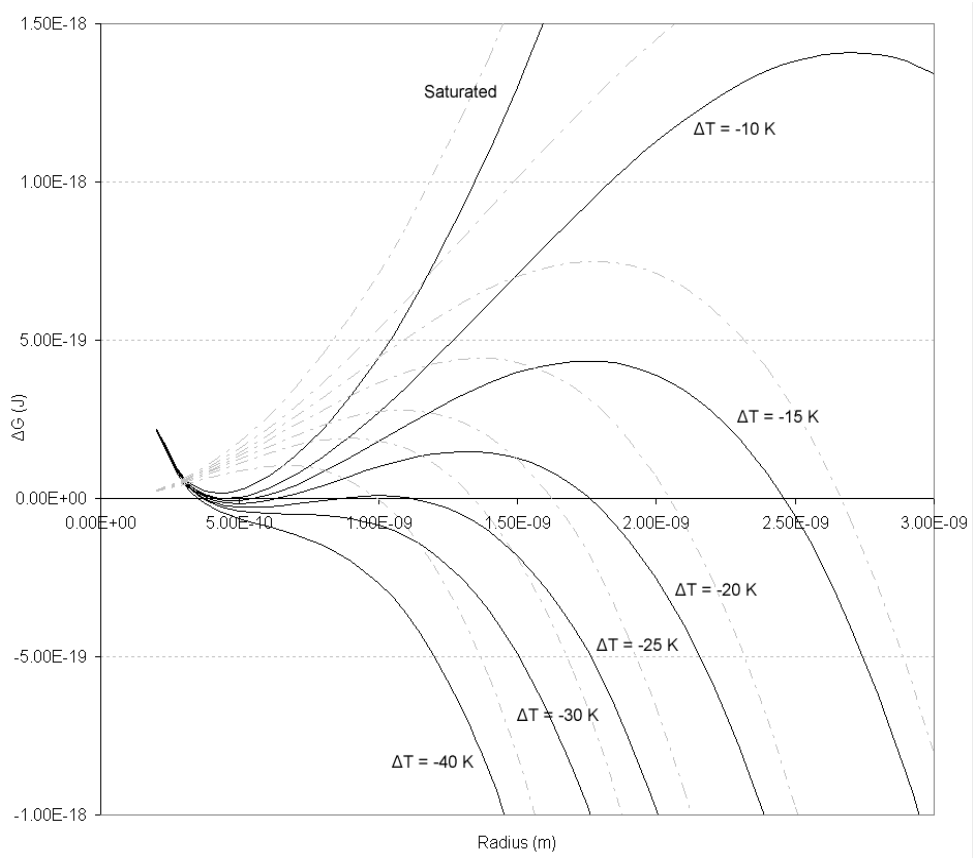

Figure 3.20: Variation of ΔG with radius for droplets with a charge of 1e

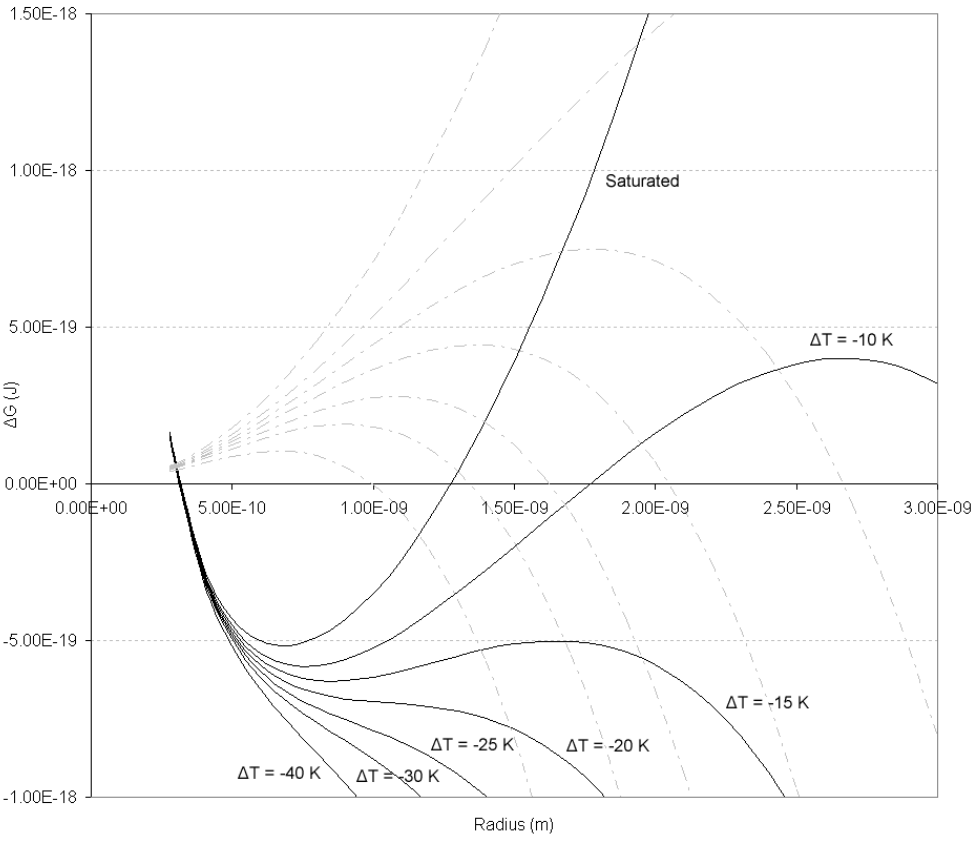

Figure 3.21: Variation of ΔG with radius for droplets with a charge of 2e

3.7 Conclusion

The effect of chemical impurities on the nucleation of flowing steam in turbines and the distribution and effect of electro-static charge in turbines are both complex and little understood at the present time. In comparison with homogeneous nucleation in steam the theory of heterogeneous nucleation in binary systems and on electrically charged ions in steam is less well developed. There have been relatively few experimental studies in these areas and a detailed knowledge of these processes and their implications for nucleation is currently incomplete.

The following chapters introduce experimental work that encompasses these two areas. Chapter 4 describes the general experimental arrangement and procedures. Chapter 5 introduces the experimental work, observations and results in the investigation concerned with the effect of impurities and heterogeneous nucleation. In chapter 6 an investigation into the nature and distribution of electro-static charge on the first nucleation of steam is presented.

Chapter 4:
General Experimental Arrangement and Procedures

4.1 General Arrangement

The general arrangement of the steam blow-down facility is shown in Figures 4.1 and 4.2. The facility is split into two sections; steam generation equipment, shown on the left hand side of Figure 4.1 and a test section, shown on the right hand side of Figure 4.1, and in more detail in Figure 4.2.

A reverse osmosis water treatment plant provides a supply of ultra-pure water for steam generation. The water is pumped into the hotwell, which supplies the steam boiler. The boiler generates saturated steam at 16 bar. Coarse water droplets carried from the boiler are removed by a steam separator and may be sent back to the hotwell or to drain. The steam is then passed, via a reducing valve, at 7 bar to the steam receiver, which acts as a reservoir of steam for the test section. It is possible to control the conditions in the steam receiver to supply superheated, saturated or supercooled steam to the test section.

The test section houses the blade cascade under investigation and the majority of the instrumentation. With reference to Figure 4.2, opening the quick acting valve (1) allows the steam to pass from the steam receiver into the test section. Measurements may then be taken during a short period where conditions in the test section are stable. Spent steam leaves the test section and enters a water-cooled condenser. The condensate is dumped to drain.

The facility is described in more detail in the following sections. Firstly the equipment existing before the current project began is described. This then followed by discussion of the modifications and additions made during the current project.

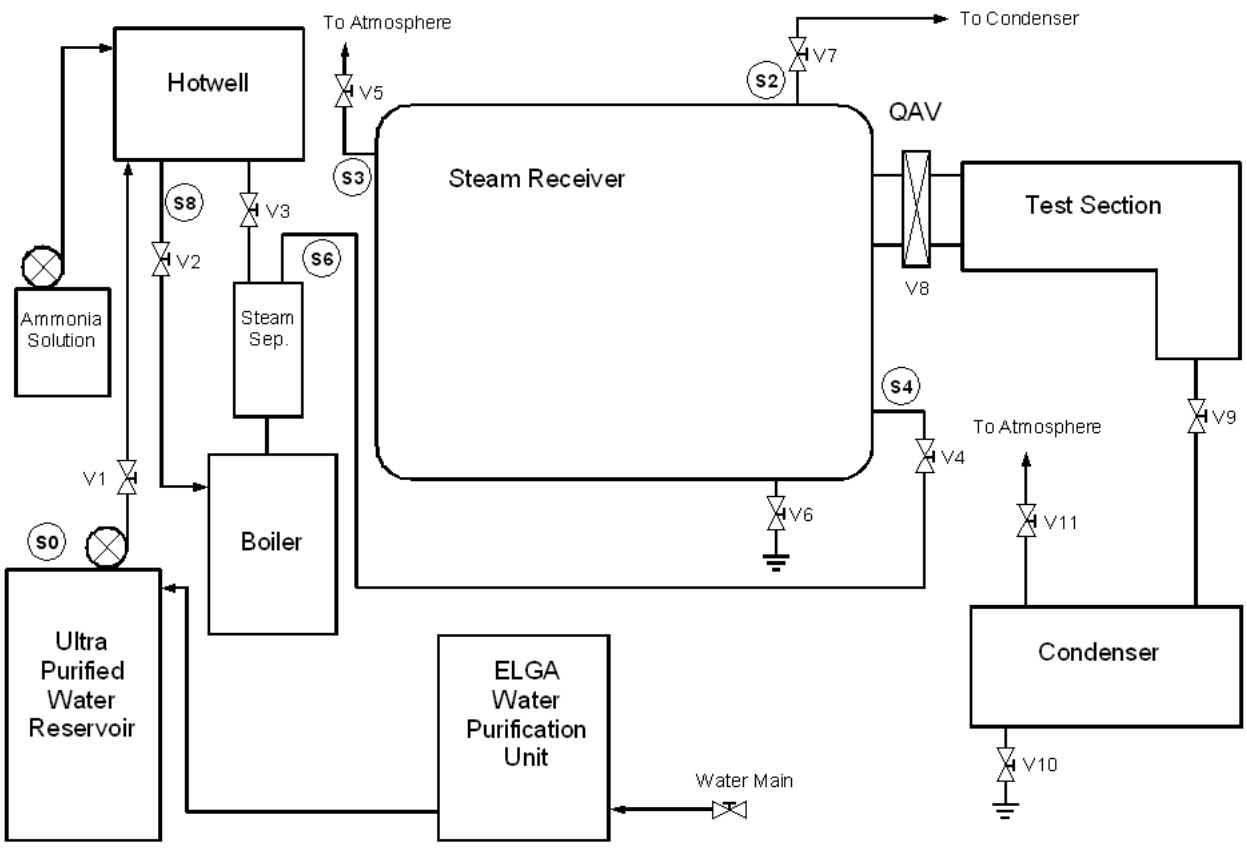

Figure 4.1: Schematic diagram of the blow-down facility. The numbers refer to sampling points where water/steam samples are taken for analysis.

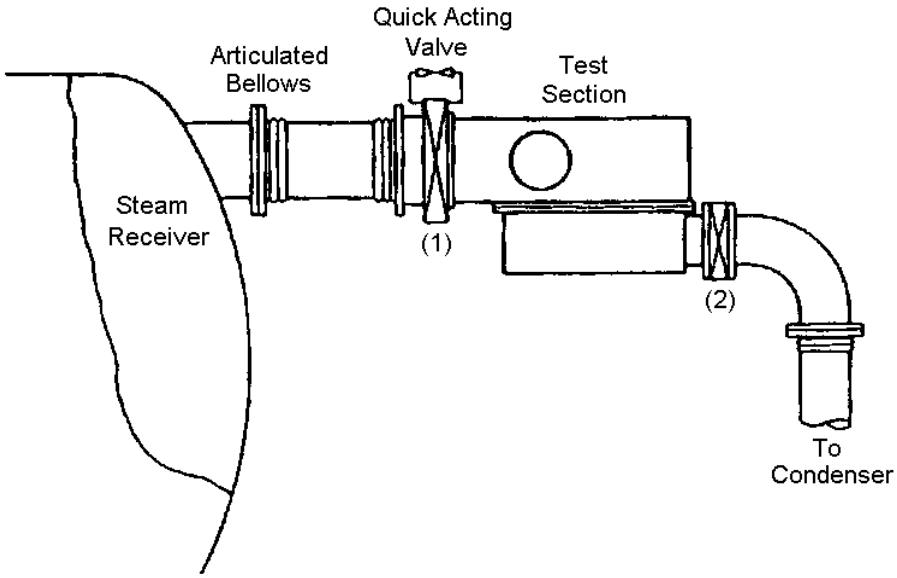

Figure 4.2: Details of the test section region. The quick acting valve opens in about 70ms. Measurements are taken after a transient that lasts about 0.7s.

4.2 Existing Equipment

4.2.1 The Boiler System

Steam is generated by a fully automated once through gas fired boiler which has a maximum capacity of 0.2 kg/s of steam at 16 bar with a moisture content of less than 1%. It is fed from the hotwell. This acts as a reservoir of warm, de-oxygenated feed water. In its original design the water in the hotwell was heated by feeding with hot water from the steam separator and a little steam from the boiler outlet back into the hotwell. Modifications to this system proved necessary and are discussed in section 4.3.

4.2.2 The Receiver

The receiver is a large mild steel vessel with an internal diameter of 3.04 m and a volume of 28 m^3. It acts as a reservoir of high pressure steam. Its volume is sufficient to maintain stagnation conditions steady during the short run time while measurements are taken. The vessel is designed for an internal working pressure of 7 bar gauge as well as full vacuum and a maximum temperature of 343^oC. A heat shield is mounted approximately 10 cm from the inner wall to lower thermal contact between the body of the receiver and the steam it contains.

4.2.3 Quick Acting Valve

Inlet to the test section from the receiver is controlled by valve 1 (Figure 4.2), also shown in cross-sectional view in Figure 4.3. This is a quick acting valve with a typical opening time of 70 ms. The valve body is designed as a shutter and when opened allows steam to pass from the receiver into the test section and then on to the condenser. When closed the shutter is pulled against seals in the valve housing. The shutter is actuated by a pneumatic impact cylinder and is arrested by means of an ACE oil damper that absorbs the kinetic energy of the shutter, protecting the housing and test section instrumentation. Transients in the flow, as a result of opening the quick acting valve, have been shown by *Shojaee-Fard [1987]* to decay in approximately 120 ms after which a pseudo steady state is maintained in the test section for over 1 sec. During this time measurements may be taken.

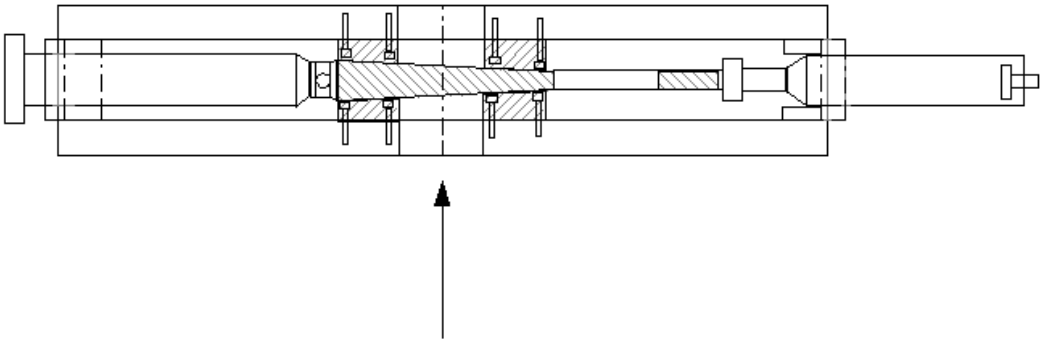

Figure 4.3: Cross-sectional view of the quick acting valve.

4.2.4 The Test Section

The test section itself is essentially a stainless steel structure that holds two large cover plates mounted 76 mm apart. A cross section of the test section is shown in Figure 4.4. The steam flows from left to right and is smoothed and guided by contraction liners as it passes from the quick acting valve into the blade cascade.

The blades forming the cascade are mounted on circular supporting plates (shown in Figure 4.5), which fit into the test section. The cascade consists of four blades and two half profiles machined into the spacer blocks, forming five passages. The central passage formed by the second and third blade is the focus of the instrumentation. To cater for different measurements the central two blades are mounted into a separate interchangeable unit. Two such units have been constructed; one for surface pressure measurements, the other for optical observations, but only the former unit has been used in the present investigation.

To traverse the flow downstream of the cascade one of the cascade supporting plates can be replaced with one machined with a slot to allow for probe access. This arrangement was used for the electrostatic measurements downstream of the blades. The probe was mounted in a holder supported by a traversing mechanism, which could be driven across the passage and its position could be measured using a linear displacement transducer. However, in the present investigation both the positioning and the measurement were carried out manually. To provide for sealing, the whole assembly was mounted in a steel drum bolted to the test section cover.

The tips of the two central blades are located in two slots machined into a matching plate mounted on the opposite side of the test section (see Figure 4.6). This plate has wall pressure tapping points machined into it for the measurement of static pressures upstream and downstream of the cascade and along the central mid-passage. Access for total pressure and electrostatic probes to be inserted upstream of the cascade is also provided.

Two tailboards are fitted to the trailing edges of the upper and lower half profiles and can be adjusted separately. These allow the flow at outlet from the cascade to be controlled. Valve 2 (Figure 4.2) is a butterfly valve and is set fully open during normal use of the equipment.

The blade profile used in all tests is the tip section of the penultimate rotor of an operating turbine. Details of the blade profile and the co-ordinates of the pressure tapping points are given in appendix A.

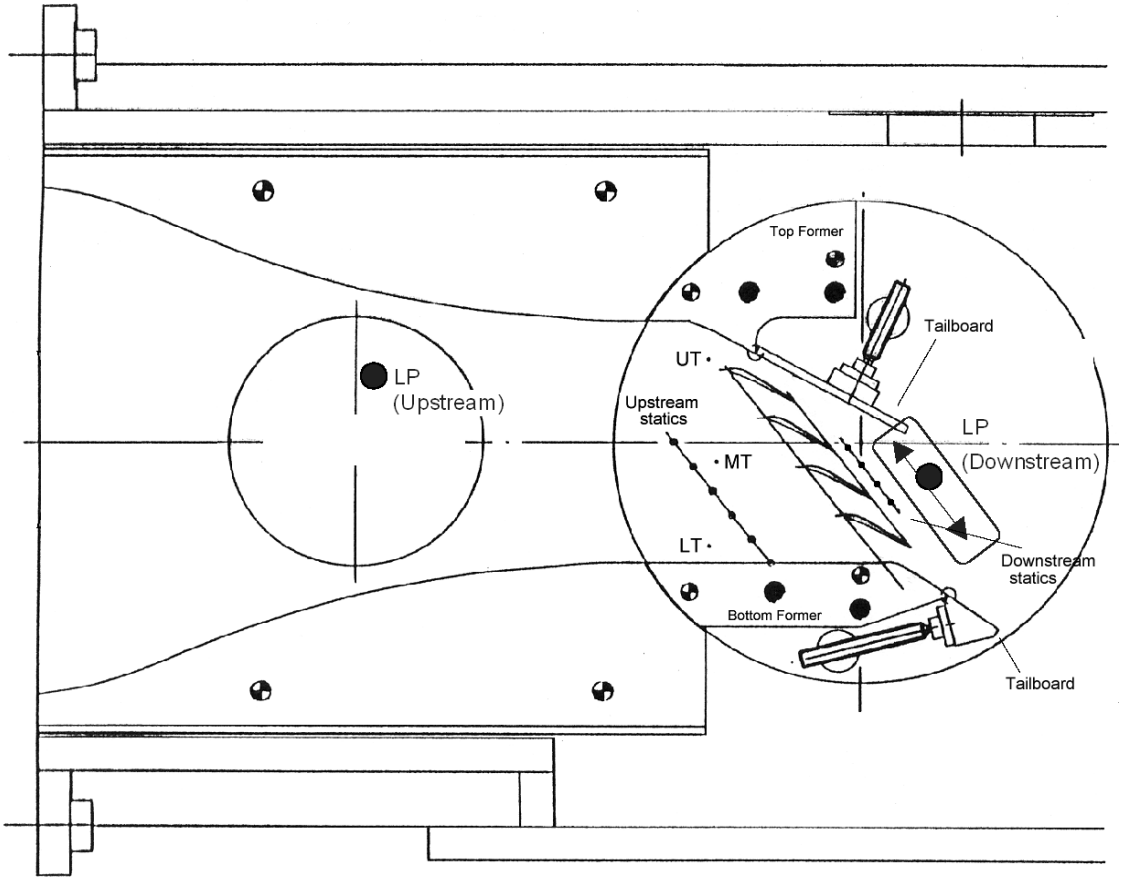

Figure 4.4: Flow passage through the test section showing the cascade of blades and the positions of upstream and downstream pressure tapping points, tailboards and position of electrostatic (Langmuir) probes.

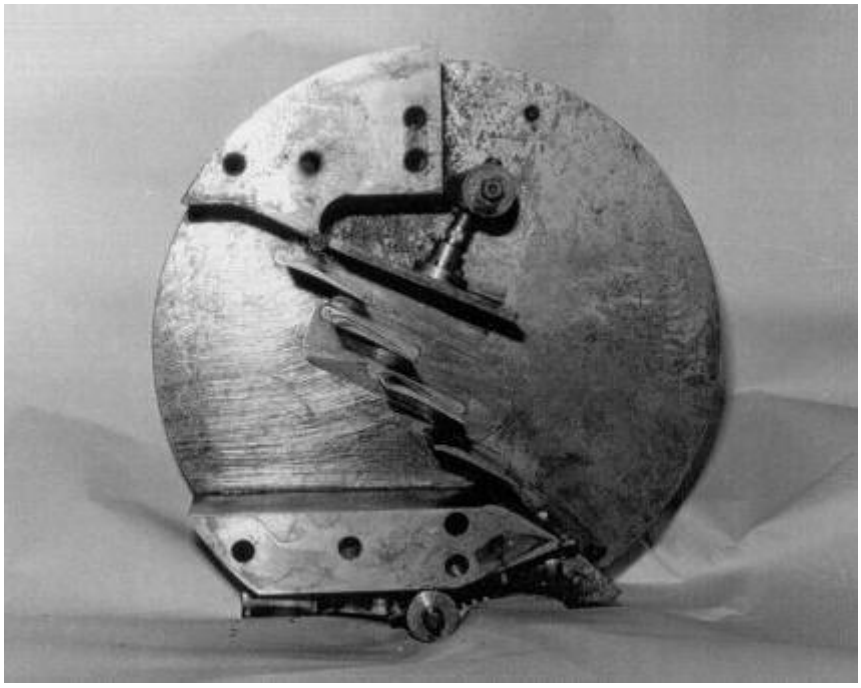

Figure 4.5: Photograph of the blade cascade assembly and tailboards. The removable plate holding the central two blades can just be made out.

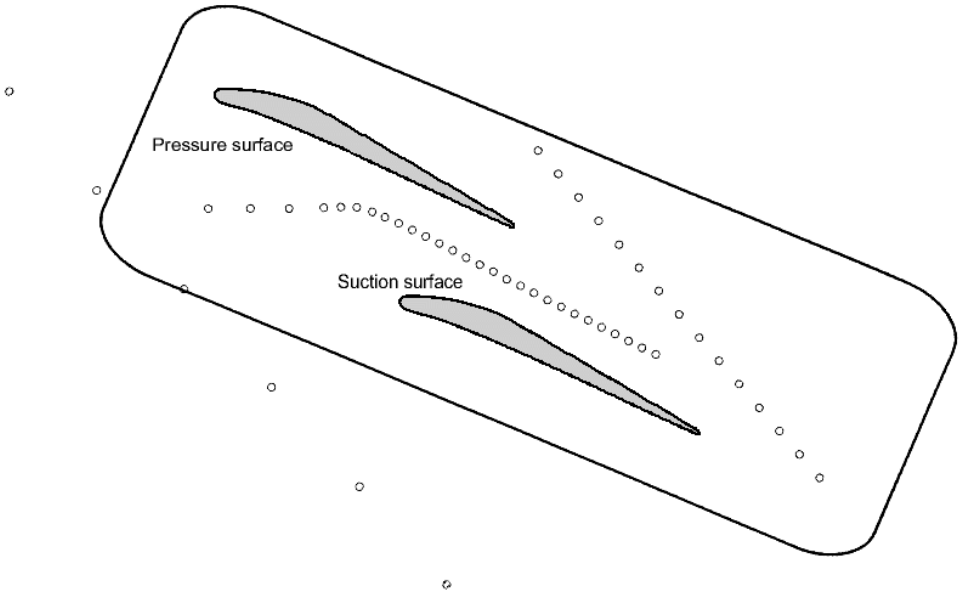

Figure 4.6: Position of the tip slots for the central blades and wall static pressure tapping points on the mounting plate.

4.2.5 Steam Condenser

The spent steam passes from the test section to a water-cooled condenser, which has a condensing surface area of 60 m^2 and a capacity of 9.46 MW and is designed to condense the mass flow rate through the test section on a continuous running basis. A large vacuum pump is used to evacuate the condenser and test section. The condenser vacuum controls the pressure downstream of the blades and is finely controlled by allowing a small leakage of air into the condenser.

4.3 Modifications to the Steam Plant

In its original form the water used in the blow-down facility was taken directly from the municipal water supply. The water was treated with an alkaline corrosion inhibitor, but was otherwise untreated. In addition to this the pipe work, fittings and larger components were constructed mainly of mild-steel. The level of impurities in the steam was never measured, but would likely have been relatively high (estimated at 2.4×10^{12} impurity particles per kg of steam using theoretical simulations as discussed in chapter 3 section 3.5.2).

A primary aim of the current project has been to provide a baseline of measurements in the absence of impurities. This required the supply of ultra-pure steam to the test section. Thus major modifications to the blow-down facility have been undertaken to provide a source of ultra-pure water and to avoid contamination of the water/steam as it passes through the pipe work and other components on its way to the test section.

A further aim of the current project has been to provide measurements using steam containing a known level of impurities. Thus it has been necessary to add equipment capable of dosing the steam with an aqueous, volatile chemical. These modifications are described in the following sections.

4.3.1 Pure Water Treatment Plant

To provide a supply of ultra-pure water an USF ELGA reverse osmosis water treatment plant has been installed. The plant generates ultra-pure water, up to 0.056 μSiemens/cm conductivity, at a rate of 2 litres/min. The pure water is stored in a 2 tonne

reservoir from which it is pumped, via a final polishing unit, to the boiler hotwell. This provides adequate capacity to run the steam blow-down facility once every two days; that is three times in a five-day week.

To avoid contaminating the boiler feed-water it was decided to no longer add the alkaline corrosion inhibitor. Although this will probably shorten the life of the boiler coil, this step was necessary to maintain the steam quality.

4.3.2 Replacement of the Mild Steam Items

As mentioned above the existing facility consisted mainly of mild steel pipe work and fittings. To minimise contamination of the ultra-pure steam much of this equipment has been replaced with stainless steel components. The major items that have been replaced in stainless steel are; the hotwell and all pipe work and fittings in the main steam line from the boiler to the receiver. A list of the main items in the system and whether they have been replaced is provided in Table 4.1. It was impractical to replace every item, the most noticeable exceptions being the boiler coil, the steam separator and the main body of the receiver, which are all constructed of mild steel. However, the heat shield fitted inside the receiver, originally constructed of aluminium sheet, has been replaced by stainless steel sheet. Before re-installing the heat shield the receiver wall was scrubbed to remove any loose materials that may have accumulated there. The test section itself was originally constructed from stainless steel. In addition stainless steel sampling points have been added at various locations throughout the facility, with positions indicated by the circled numbers in Figure 4.1. These sample points allow conductivity measurements to be made and samples to be taken for later chemical analysis of the water and steam in the system.

Table 4.1: List of items replaced in the steam rig.

Item	**Replaced?**	**Material**
Valves 39, 1, 2	Yes	Plastic/stainless steel
Hotwell	Yes	Stainless steel
Boiler system to separator	No	Mixed (boiler coil is mild steel)
Separator	No	Mild steel
Steam trap	Yes	Stainless Steel

Item	Replaced?	Material
Pipe work from steam separator to manifold block and valve 17	Yes	Stainless Steel
Manifold block	Yes	Stainless Steel
Return pipe work and valves from separator, steam trap and manifold block to the hotwell.	Yes	Stainless Steel
Pipe work from manifold block to the receiver	Yes	Stainless Steel
Valves 18, 20, 25, 26	Yes	Stainless Steel
Receiver	No	Mild steel
Receiver heat shield	Yes	Stainless Steel
Quick acting valve	No	Stainless Steel
Test section	No	Stainless Steel
Condenser	No	Mixed

4.3.3 Provision for Chemical Dosing

A further modification has been to introduce a dosing facility that can accurately dose an aqueous volatile chemical into the boiler feed water with the final concentration of the chemical in the steam at the ppm level. In comparison to dosing non-volatile aqueous solutions, or to dosing substances that are solid or gaseous directly into the steam, the above system has the advantage of being relatively easy to implement. Ammonia was chosen as the dosing chemical for the following reasons:

1. It is extremely soluble in both water and steam.
2. It is volatile and passes easily from aqueous solution to the vapour phase.
3. It gives pH values in steam representative of those found in operating turbines.
4. It is readily available and relatively easy to work with in the laboratory.
5. It is commonly added to the feedwater and steam of operating turbines.

The aqueous solution of ammonia is contained in a small reservoir and pumped directly into the hotwell where it mixes before passing to the boiler. Dosing at this point allows mixing to take place of the chemical in the feed water and boiler. Since the chemical is volatile it will therefore also be evenly dispersed throughout the steam. To pump the aqueous solution a small Watson Marlow peristaltic pump, model 101U/R, has been installed with a flow rate of approximately 34 ml/min at 1 bar head. The pump is

switched on and off via a solenoid, controlled by the same switch that operates the ELGA pure-water feed pump.

4.3.4 Nitrogen Blanket

In normal operation the hotwell, which provides warm water to the steam boiler, runs approximately half full. Originally atmospheric air took up the space above the water. The CO_2 content of the air was found to be a source of contamination. To eliminate this source of contamination and further improve the purity of water entering the steam boiler from the hotwell a modification was introduced to provide a blanket of Nitrogen gas in the hotwell.

4.3.5 Commissioning

On completion of the modifications described above, the system was run over a period of approximately six months before water and steam purity was considered satisfactory for taking measurements in the test section. In addition to the improvement in water and steam quality, this period of commissioning allowed problems in the system to be ironed out. The improvements in purity, and steps taken to achieve them, are described in more detail in the following section.

4.4 Pure Water and Steam Quality

4.4.1 Water and Steam Sampling Equipment

To obtain an idea of the purity of water and steam in the plant samples were taken at various locations around the system at positions indicated in Figure 4.1. A portable water-cooled condenser, manufactured by Lowe Engineering and constructed from 11m of small-bore stainless steel tubing, was used to cool and condense the sample to room temperature. The sample was then passed to a conductivity cell for measurement of direct conductivity and then through a resin and into a second conductivity cell for the measurement of cation conductivity. The conductivity meters actually measure resistivity in MΩ/cm. This can be converted easily to μSiemens/cm since one is the reciprocal of the other.

From time to time the samples were collected in plastic sample bottles for full chemical analysis at USF ELGA's laboratory.

4.4.2 Pure Water and Steam Quality

Figures 4.7 and 4.8 show a selection of results from the chemical analysis of water and steam taken from the system. The first set of samples (Figure 4.7) were taken shortly after commissioning of the refurbished system, while the second set were taken around 7 months later (Figure 4.8). Ion content is presented as parts per billion (ppb) and the location of sample points, S0 etc. are indicated on Figure 4.1. It should be noted that some of these values are maximum concentrations since the levels are at the limit of detection. Also note that the scale of Figure 4.8 is one-tenth that of Figure 4.7. Further more in Figure 4.7 the concentration of calcium ions (as Ca^{2+}) goes off the scale for S3, peaking at 150 ppb.

The improvement in feed water and steam quality in the system over the first six months or so of operation can be clearly seen. Figure 4.7 indicates relatively high levels of contamination. High chloride levels are present throughout the system, peaking at 20 ppb, while calcium ion levels are particularly high in the receiver (S3 and S2). High levels of chloride were expected since the anti-corrosion additive used in earlier work contained chloride. The high levels of calcium can only be attributed to a build up of scale on the receiver walls. Figure 4.8 reveals a dramatic improvement in quality throughout the system. Ion levels are down to 3 ppb or below, except for the steam in the receiver. Here there are unexpectedly high levels of ammonium, up to 10 ppb (this was before any dosing of ammonia took place). The overall improvement in quality can be attributed to three factors.

1. Prolonged flushing the system with ultra-pure feed water 'cleaned' the system.
2. The original boiler system had a feedback loop which returned hot water from the separator to the hotwell. It was discovered that this hot water leaving the steam separator contained particularly high levels of impurities and returning the water to the hotwell was causing a build up of contaminants. Disabling this feedback loop and discarding the water from the separator to drain immediately led to a dramatic improvement in water quality in the hotwell.
3. In normal operation the hotwell only half fills. The remaining volume is taken up by atmospheric air. This appeared to be causing CO_2 contamination

of the water. Introducing a blanket of high purity Nitrogen in the hotwell, expelling any air, also led to an improvement in water quality.

In Figure 4.9 conductivity measurements, taken at the five sampling points over a period of time, show a similar trend to the chemical analysis of Figures 4.7 and 4.8. The effect of removing the feedback of hot water from the separator to the hotwell is clearly shown by the drop in conductivity on 11.09.1998. The conductivity reading at S8 on 31.07.1998 and 03.08.1998 is actually off the scale at 25 μSeimens/cm. The addition of a nitrogen blanket to the hotwell in the early months of 1999 also improved the water quality, although the improvement is less dramatic. Finally the conductivity measurements also reveal the gradual improvement in steam quality in the receiver (S2 and S3) over this time period. A compete set of results from the detailed chemical analysis of the samples and the conductivity measurements are presented in appendix B.

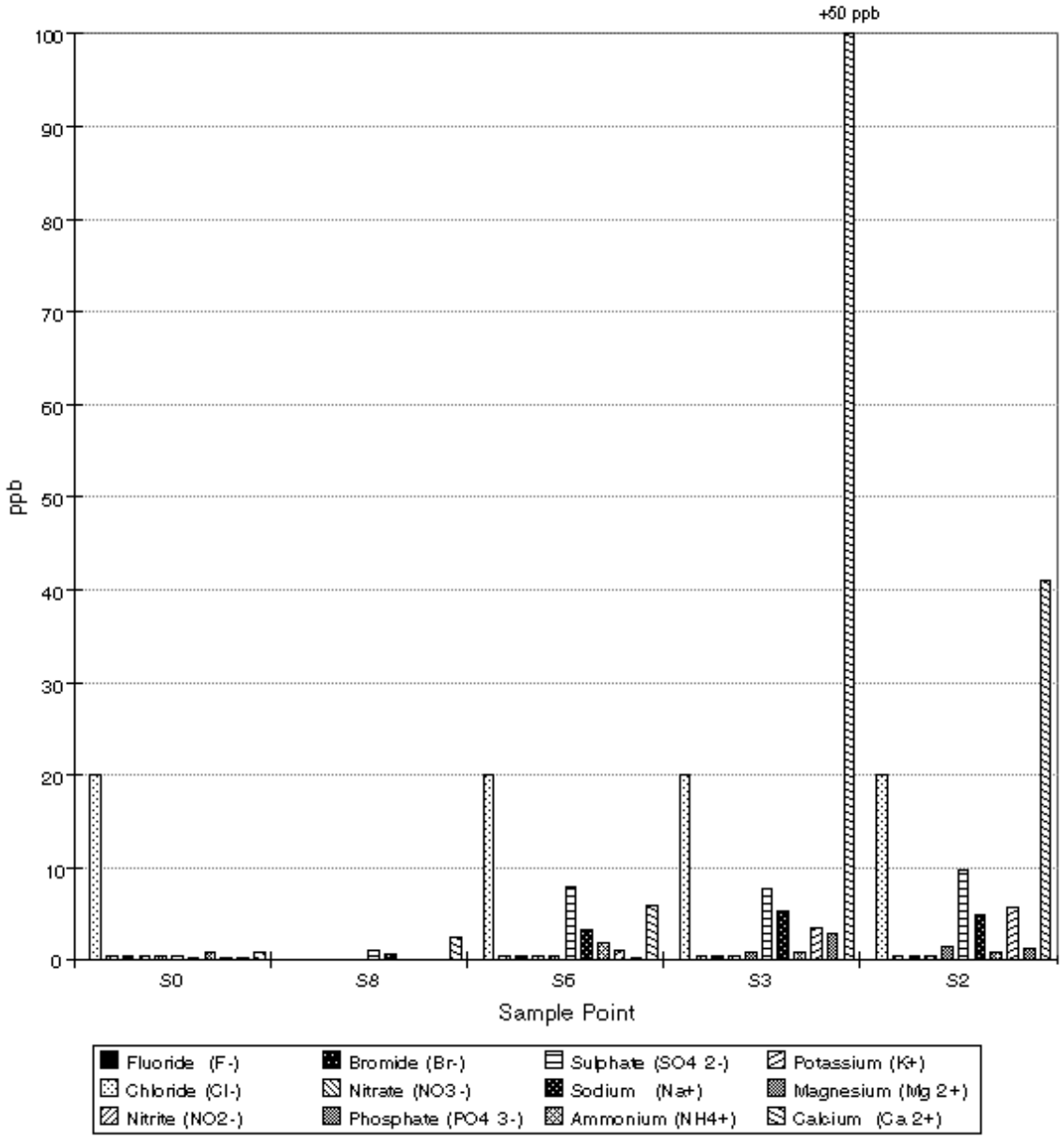

Figure 4.7: Comparison of ion concentrations measured at the various tapping points. Relates to an early stage, soon after connecting the pure water supply.

S0: ELGA system, S8: Boiler feedwater, S6: Receiver steam inlet, S3: Receiver steam, S2: Receiver steam

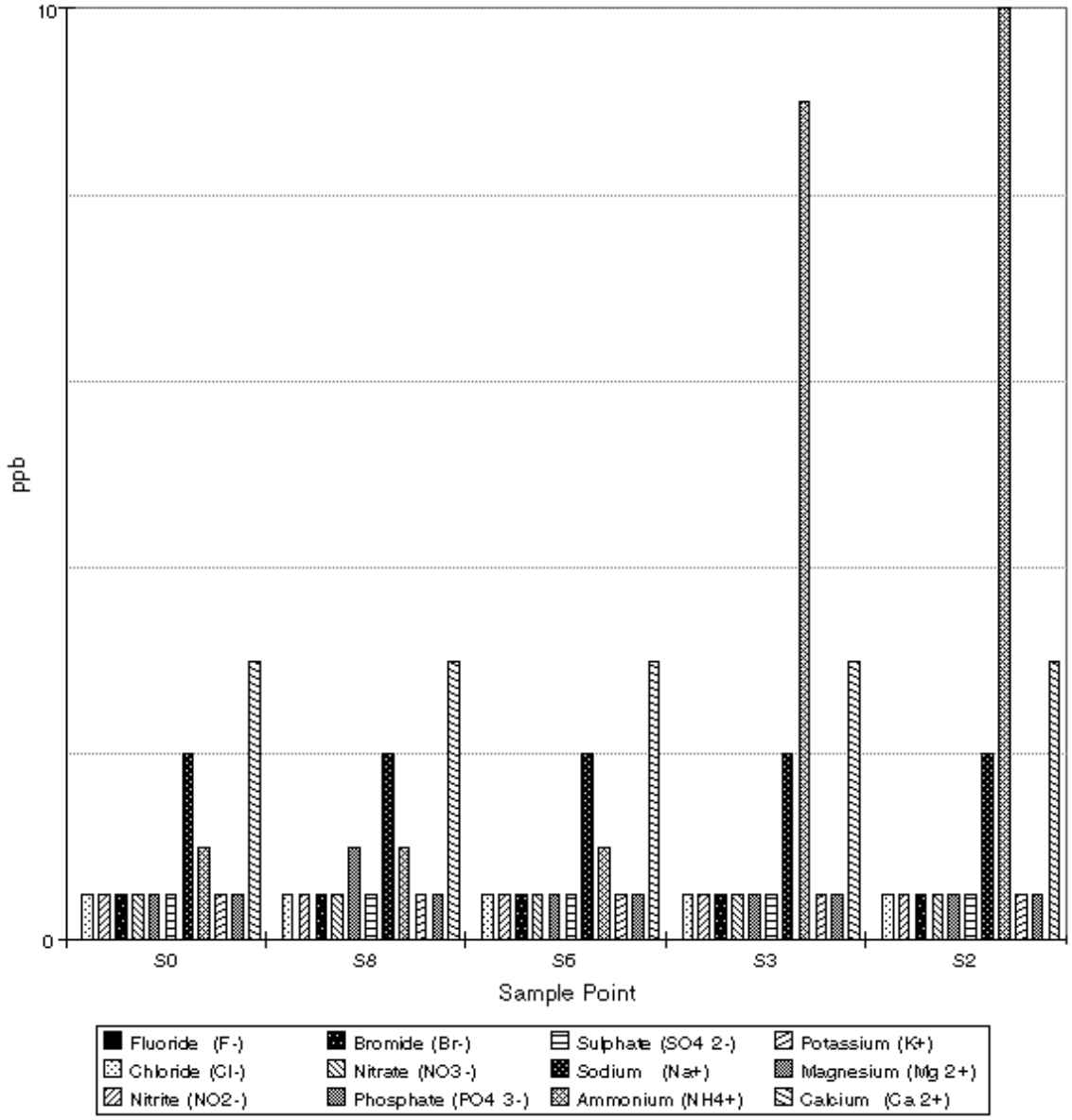

Figure 4.8: Comparison of ion concentrations measured at the various tapping points. Relates to a late stage when the main measurements were made, note the change of scale.

S0: ELGA system, S8: Boiler feedwater, S6: Receiver steam inlet, S3: Receiver steam, S2: Receiver steam

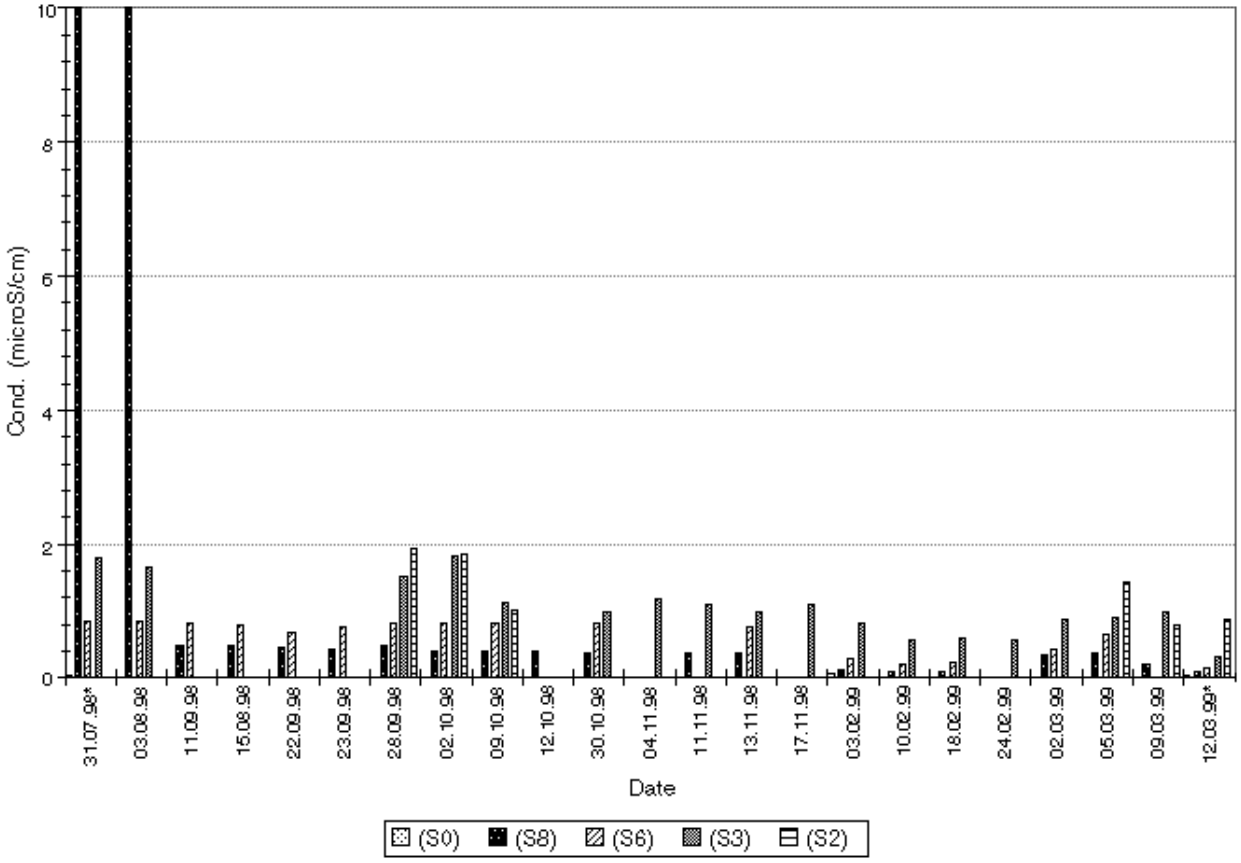

Figure 4.9: Improvement of conductivity over time with the pure water supply (note that the conductivity at S8 for 31.7.98 and 03.8.98 is off the scale at 25μScm^{-1})

4.5 Instrumentation and Data Acquisition

4.5.1 Pressure Measurement

To investigate the behaviour of the flow, as discussed in section 4.2.4, static pressures were measured through tapping points in the test section walls upstream and downstream of the blades and along the mid-passage as well as along the blade suction and pressure surfaces. With reference to Figure 4.4, total pressures were also measured upstream of the cascade at points UT and LT.

To record the pressure, each tapping point was connected via an oil filled hypodermic tube to a separate pressure transducer. The transducers were mounted into the bottom face of a cell machined in a Perspex manifold block, each block containing 10 cells (see Figure 4.10). The manifold blocks themselves were mounted in a steel frame in such a way that each block could be rotated allowing for the removal of air bubbles

trapped in the system. Each cell was connected via a small valve to a reservoir of oil fitted on top of the steel frame. An oil filed hypodermic tube connecting each transducer to its pressure tapping point, was connected to the side of the manifold with the transducer mounted on an adjacent side (Figure 4.10). From time to time air bubbles formed in the oil, leading to abnormalities in the pressure reading, and therefore it was important to regularly purge the lines with fresh degassed oil.

For the measurement of static pressures Sensor Technics type LX1604-GB backward gauge transducers were used. These are piezo-resistive devices, each built integral with its own amplifier. They have a range of ±1 bar gauge and a nominal accuracy of ±0.01 bar. The transducers operate on a supply of +15 V D.C. and produce an output of +2.5 V to +12.5 V. This was shifted down to 0 V to +10 V before reaching the data acquisition equipment. The transducers used for total pressure measurements were more sensitive Kulite type XT-190-30 transducers that operate with separate amplifiers. These have an operating range of ±1 bar gauge and a nominal accuracy of ±0.005 bar. They require a +10 V D.C. supply and produce an output of 0 - 100 mV which was fed directly into the data logger, where the signal was amplified. All the transducers were calibrated in situ using the voltages measured by the data acquisition system against pressures read from a mercury manometer.

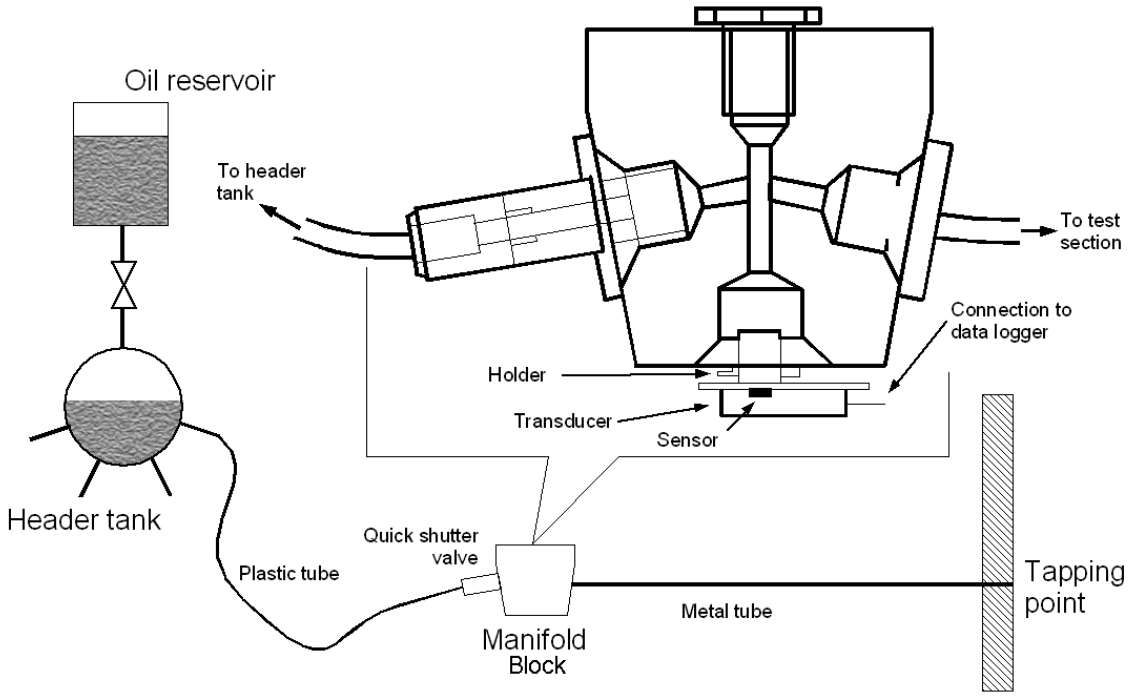

Figure 4.10: Schematic diagram of pressure transducer, connections and manifold block.

4.5.2 Temperature Measurement

The temperature of superheated and saturated steam in the receiver was measured by a radiation shielded thermocouple positioned approximately 1m inside the receiver wall. A second thermocouple was positioned in the wall to measure the receiver wall temperature. However, the temperature of supercooled steam cannot be measured directly by thermocouples. This is because steam condenses on the surface of the instrument, which will then indicate the saturation temperature. Instead the temperature of supercooled steam was deduced by establishing the condition law for the receiver during blow-down using the procedure described by *Bakhtar and Webb et. al. [1991]* and by *Mashmoushy [1994]*. This method assumes that the condition laws for similar superheated and supercooled expansions would be the same over the range of conditions used in the experiments. Thus by obtaining temperature ratios as a function of pressure ratios in a series of superheated expansions, the results can be used for expansion into the supercooled region. It is estimated that the deduced stagnation temperatures are accurate to within ±1 K. The condition law deduced and used for this work is plotted in Figure 4.11.

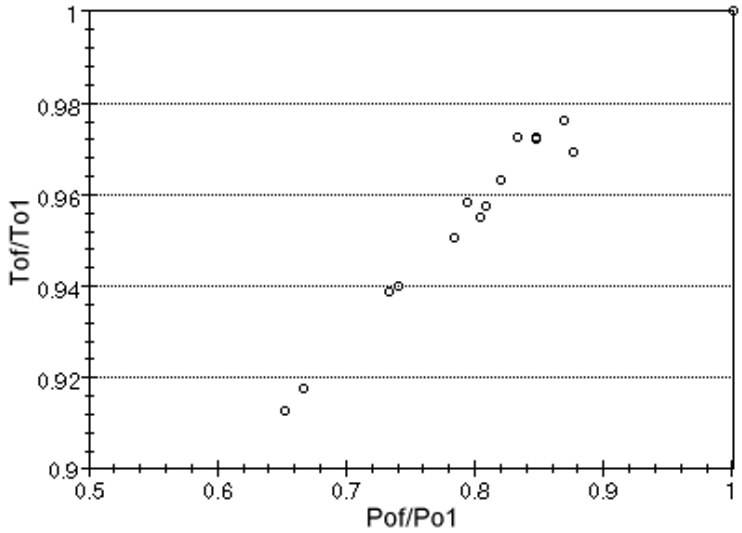

Figure 4.11: The receiver condition law for superheated expansion. Subscript 1 represents superheated conditions and subscript 'fog' represents conditions on the saturation line.

4.5.3 Data Acquisition Equipment

To record the transducer outputs a model MDAS-7000 data logger of 12 bit accuracy manufactured by Acurex Corporation was used. The data logger accepts up to sixteen, four channel, sample and hold cards, although only 11 such were in use. This meant a maximum of 44 transducers could be monitored. An interface box was used to allow switching between two sets of transducers doubling the total number that could be monitored to 88. The switching was controlled by a signal from the data logger. The time to record the voltage on a single channel was approximately 4 μs, thus a set of 88 readings could be recorded in 352 μs. For pressure readings an average of 100 samples per channel was adopted as the measurement at each tapping point. Therefore a full set of readings over all the channels could be obtained in approximately 35.2 ms. The data acquisition process was controlled by software running on a PC. Communication with the data logger took place over a standard IEEE-488 link. Before taking measurements the PC software uploads a complete set of commands to the data logger's memory. These commands are then executed locally on the data logger, independently of the PC, thus eliminating any need to synchronise the PC software with the data logger during data acquisition. After the data was acquired it was stored in the data logger memory and later transferred to the PC via the IEEE-488 link. The PC software allowed the results of each run to be saved to file and also plotted. Finally, using the software, it was also possible for the transducers to be calibrated interactively as described in section 4.5.1. A typical calibration curve for the pressure transducers is shown in Figure 4.12.

In addition to recording pressure data the data acquisition system was used to record electrostatic data. The instrumentation involved and modifications to the data acquisition system are described in section 4.5.5.

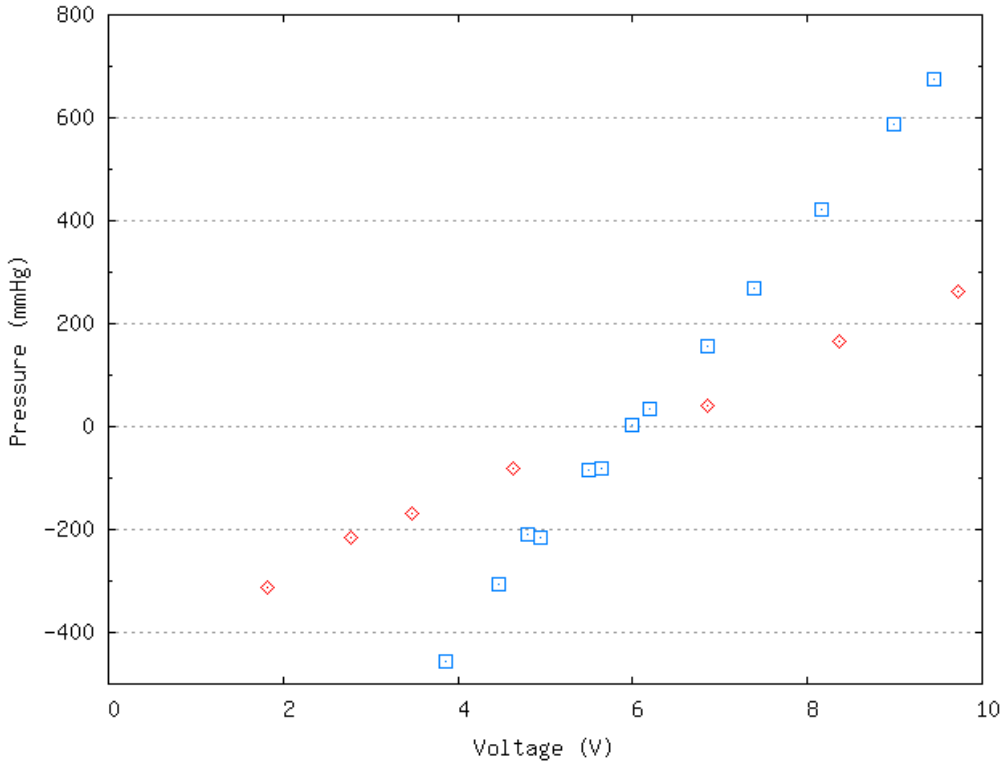

Figure 4.12: Typical calibration curve for pressure transducers.
Key: Squares represent gauge pressure transducer data
Diamonds represent total pressure transducer data

4.5.4 Data Acquisition Software

The data acquisition software used to record the first set of pressure measurements for pure steam and for steam dosed with ammonia was written by Marc Wiseman. It was a DOS program written in C++. This software enabled the data logger to perform the following functions:

1. Sample static and total pressure readings for all 88 channels of the data logger.
2. Retrieve data from the data logger memory.
3. Plot graphs of the retrieved data.
4. Save the raw sample data to a file.
5. Interactively calibrate the pressure channels.
6. Communicate with the Mdas data logger via a HP GPIB library.

The data acquisition requirements of the electrostatic instrumentation, particularly of the electrostatic probe (described in the following section), were significantly different from the requirements for pressure measurements so that writing new software became necessary. Although the source code of the original software was available it was decided that it was impractical to re-write the code because a) it was not written with an extendable architecture and b) the HP GPIB library was out of date and un-documented.

The new software is a Win32 GUI program written by the author in C++ using the wxWindows (www.wxWindows.org) toolkit. It can perform the following functions *in addition* to those of the original software:

1. Control the electrostatic probe voltage ramp.
2. Sample the electrostatic probe voltage and current.
3. Save the *averaged* data and/or raw sample data to a file.
4. Provide diagnostic output.
5. Communicates with the Mdas data acquisition logger via a NI GPIB library.

A full set of the source files can be found on removable media in Appendix E.

4.5.5 Electrostatic Probe and Circuits

The equipment used to obtain readings for electrostatic charge in the steam is described in the following sections.

4.5.5.1 Langmuir Probe

The Langmuir probe was named after I. Langmuir who was the first to use such a probe for the characterisation of gas plasmas (see *Mott-Smith and Langmuir [1926]*). The principle of operation of the Langmuir probe may be illustrated with reference to Figure 4.13. The probe electrode (1) should have a much smaller surface area than the reference electrode (2). A variable voltage is applied across the two electrodes. When this voltage is large and negative, with reference to electrode 2, the plasma electrons cannot reach the probe electrode (1) so any current flow is dominated by the flow of ions and a symmetrical ‘sheath’ of positive ions forms around the probe tip. When the voltage

applied across the electrodes is positive, with reference to electrode 2, the current flow is dominated by the high-velocity electrons reaching the probe electrode (1) and a similar symmetrical 'sheath' of electrons forms around the probe tip. In the sheath region the potential drops from the probe tip potential to effectively the space charge potential at the edge of the sheath.

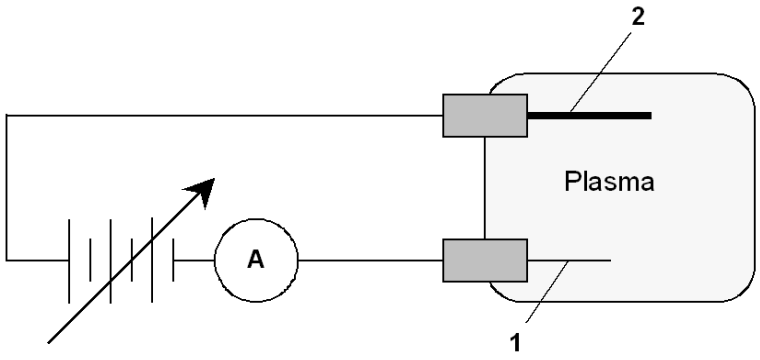

Figure 4.13: Schematic Illustration of Langmuir Probe.

A typical probe current-voltage characteristic from a gas plasma is shown in Figure 4.14. Positive values of current represent an electron current, negative values represent an ion current. In region A, where the electrode potential is negative, the probe current is dominated by ion current flow. As the electrode voltage increases, in region B, the higher energy electrons begin to overcome the negative potential and contribute towards the probe current. In region C the electrode voltage is positive and the probe current is dominated by the flow of electrons to the probe, and quickly reaches saturation. Under suitable conditions the current-voltage characteristic can be used to determine the electron concentration, temperature and energy spectrum and to estimate the ion temperature.

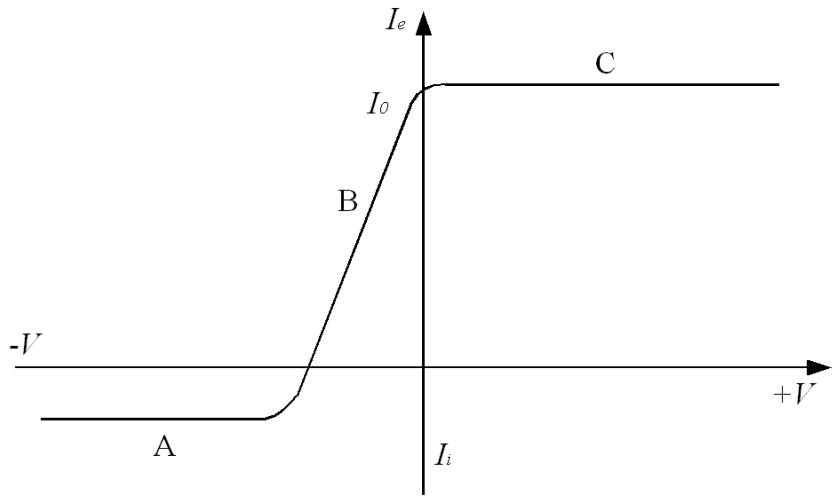

Figure 4.14: Typical Langmuir Probe Current-Voltage Characteristic.

The decision to use a Langmuir probe to measure electrostatic charge, rather than an earthed, single electrode probe used by other investigators (e.g. *Hesler and Maurer [1998]*), was taken because it was believed that the Langmuir probe might enable accurate measurement of the space potential and perhaps also provide useful information about the charge carriers in flowing steam. Although flowing steam differs greatly from the conditions typically found in low-pressure gas plasmas, for which the Langmuir probe was originally conceived, such probes have been used successfully to measure charge in collision dominated plasmas at atmospheric pressure. *Clements and Smy [1969]* developed a theory applicable to moving flame plasmas at high pressures, using probes with a high negative bias. Their theory has been applied to Langmuir probe measurement of temperature in arc welding plasmas (*Gick et. al. [1973]* and *Clements and Smy [1974]*). It has also been developed and improved upon (e.g. *Smy [1976]*, *Dawe, Rizvi and Smy [1993]*. Complications due to the interplay between convection and diffusion in the sheath surrounding the probe were illustrated by *Clements and Smy [1994]*. However the Langmuir probe has not been used in flowing steam and such conditions present further difficulties for the interpretation of probe data.

In addition to its operation as a Langmuir probe, the probe can also be configured to operate as a single electrode probe if desired, and the probe to earth currents measured directly (see section 4.5.5.5).

4.5.5.2 Probe Design

To construct a probe for use in the blow down steam tunnel a number of characteristics particular to the operating conditions employed had to be included in the design:

1. The measurements were to be carried out across the test section passage and it was likely that the conditions would vary with distance. Thus, it was desirable to insert the probe into the test section perpendicularly to the side walls and arrange the reference surface as a cylindrical surface coaxial with the probe tip.
2. To minimise disturbance of the flow it was desirable to make the probe as small as possible.
3. It was necessary to insulate the sensing element, the reference surface, the probe stem and any heating wires used, from each other completely and to ensure that the surfaces exposed to steam were kept completely dry to avoid leakage currents conducted through water films.
4. To ensure that the junctions between the various components were completely sealed to prevent ingress of water.

After considerable testing of materials and configurations the final design adopted is shown in Figure 4.15. The dimensions of the probe are shown in the figure. The probe electrode (1) is held and insulated by the quartz tube (2). To stabilise the probe electrode in the flow it was attached to a metal piece of slightly larger diameter. This was then fitted into the enlarged section of the quartz insulator to anchor the probe. The heater coil (3) was used to keep the temperature of the exposed probe surfaces above the steam dew point during operation of the test section. The coil was wrapped around the quartz insulator tube (2). To minimise any electromagnetic field produced by the heater coil affecting the measurements and at the same time reduce the problem of making electrical connection to the heater it was wound as a double coil. (4) is the reference electrode and was made of stainless steel. A quartz tube (5) insulates the heater coil from the reference tube. Stainless steel tube (6) forms the probe stem and was insulated from the reference surface by a further quartz tube (7).

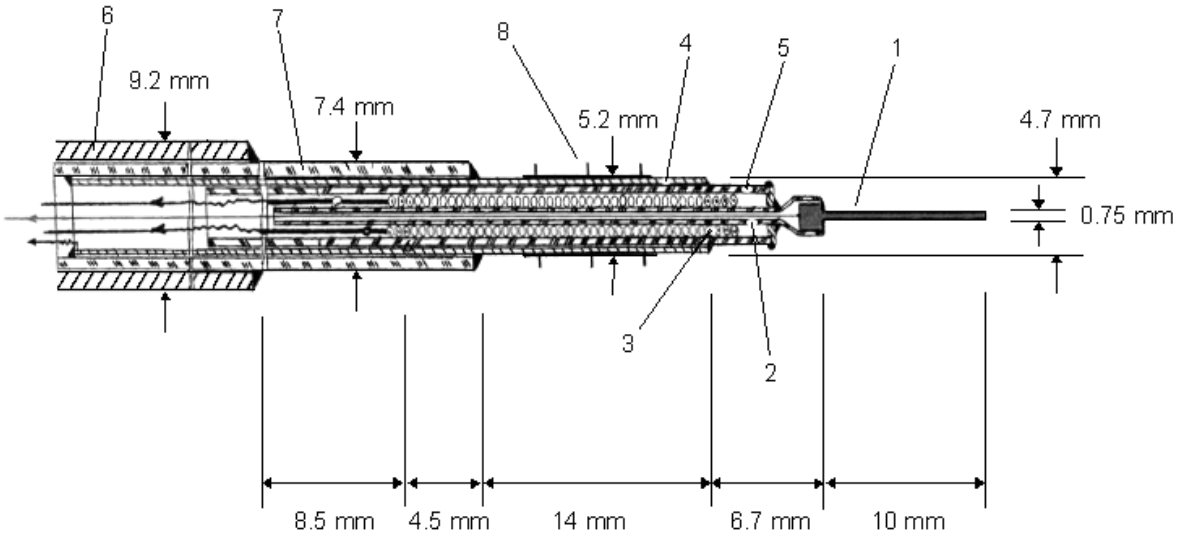

Figure 4.15: A Cross-Sectional View of the Langmuir Probe.
(Not drawn to scale)

Quartz was eventually chosen as a suitable electrical insulation material because of its reasonably high electrical resistivity (10^6 – 10^8 MΩ m at 20 ºC) along with a high (for a non-metal) thermal conductivity (~8 $Wm^{-1}K^{-1}$ at 0 ºC) and a coefficient of linear thermal expansion close to that of steel (~10^{-5} K^{-1}). In addition the electric resistivity does not break down until the material reaches very high temperatures. From a practical point of view it was also possible to produce small diameter quartz tubes, with a narrow wall thickness, suitable for use in the probe and which allowed a construction that minimised the overall diameter of the probe whilst maintaining good electrical insulation between its constituent parts.

To ensure that the insulator surfaces exposed to steam remained dry, under transient running conditions, the heater current was substantial. This caused considerable temperature differences between the surfaces, and temperature gradients from the heater wires to the outer surfaces of the insulators. To keep the temperature of the probe surfaces exposed to steam sufficiently above its dew point, it was estimated that the temperature of the insulation round the heater wire was about 800°C. The largest temperature drops in the probe were associated with the insulation round the heater wire and the two air gaps, which were approximately 0.12 mm radial distance in each case. To reduce these temperature differences the gaps needed to be reduced, but this necessitated unacceptable

tolerances on the dimensions of the components. Allowances also had to be made for the differential thermal expansion of the materials.

To avoid leakage of steam into the body of the probe the external junctions between the various components had to be sealed. The requirement of the sealing compound, in addition to withstanding high temperatures was that it should be a good electrical insulator as well as have some flexibility to accommodate differential thermal expansion.

For a given heater coil current it was important that the temperatures of the three affected areas (surfaces 4, 5 and 7 in Figure 4.15) did not differ greatly. This was necessary because while the temperature of the coolest part of the surface must be raised to a sufficiently high value, the temperature of the hottest part should not exceed the limiting temperature of the adjoining seal. Some latitude was gained by adjusting the closeness of the coils when winding the heater. The extent of the heater coils just under the quartz insulator section between the reference tube and the tip could be selected to adjust the temperature. Finally the temperature of the main part of the reference tube could be controlled by fitting it with cooling fins, shown as (8) in Figure 4.15.

A further problem in the use of the probe was the effect of the impulsive loads generated by the operation of the quick-acting valve on the quartz components of the probe, which caused them to crack. By using a softer material between the probe stem and the holder to provide some cushioning the problem was greatly reduced, although it was not completely eliminated. Consequently the probes were regarded as expendable items.

The measurements were constantly checked for signs of electrical break down during operation. At the end of each session the probes were examined thoroughly and repaired or replaced as necessary.

4.5.5.3 Probe Heater Power Supply

In the normal operation of the test section the time interval between the opening of the quick-acting valve, initiating the flow, and establishment of the required flow conditions was 1-2 seconds. Starting with a cold probe this time interval was totally insufficient to allow the probe's temperature to rise to a level high enough to ensure that the probe remained dry. Furthermore, the heat loss from the probe when placed in stationary air was considerably lower than the heat loss when placed in flowing steam

conditions. It was originally thought that the problem could be overcome by heating the probe to a temperature above its operating temperature before initiating the flow and then increasing the current to the heater as the quick-acting valve was opened. A power supply control circuit was constructed to fulfil this requirement. But when tested with a dummy probe using a reasonable amount of excess power it was not possible to raise the temperature of the outer surfaces of the probe to the desired values in the time available. This was because on being subjected to cooling by the flow after the opening of the quick-acting valve the probe surface temperature initially dipped and there was a considerable delay before it began to rise again. To achieve the desired probe surface temperatures it was necessary to include a third stage in the heater power supply. With this arrangement the probe was kept at a high steady temperature before the start of any run. Then for a few seconds just before the opening of the quick-acting valve the probe current was raised to its first boost value. Then, concurrently with the opening of the quick-acting valve, the heater current was switched to its full value; the boost current was automatically switched off on closing the quick-acting valve.

4.5.5.4 The Amplifier Circuit

Figure 4.16 shows the circuits used for generating the variable 'ramp' voltage for input to the probe and for the amplification of the probe output current. The probe was fed with a preset floating ramp voltage. The ramp was generated by a 12-stage counter (CD 4040); this drove a D/A converter (AD 558) that produced a stepped analogue output to the probe. The ramp voltage range was set at ±10 volts over 255 steps. The variation of the ramp output voltage with number of steps was linear. Over a cycle of the ramp the voltage changed from +10 volts to -10 volts in equal steps and was then reset back to +10 volts and the cycle repeated. The step speed was adjustable with a small potentiometer. The control part of the system consisted of a 555-timer chip (not shown in the figure) feeding another 12-stage counter that was in turn controlled by a logic circuit. The ramp was controlled and triggered by a pulse generated from the data logger upon a set-up command from the PC. Subsequently switching off the trigger stopped the ramp.

The probe output current was passed through one of the five resistors selectable via switch SW1. The current was then fed to the first stage amplifier A1. Amplifier A2 further amplified the resulting signal. The voltage of the circuit up to amplifier A1 was

floating. However at the output from A2 the voltage was relative to earth. The amplified signal from A2 was fed into an assigned channel on the data logger.

In the absence of any information about the magnitude of currents to be measured, in the original design the resistors were selected to enable probe currents of fractions of a nano-ampere to be detected. But in the course of the preliminary measurements this sensitivity was found to be excessive. As will be seen from the results, to be presented in Chapter 6, the actual currents were several tens of micro-amps. The correct characteristics of the circuit were found by progressively lowering the gains of the amplifier stages by changing the gain resistors as well as the selector resistors until a more appropriate output voltage was achieved.

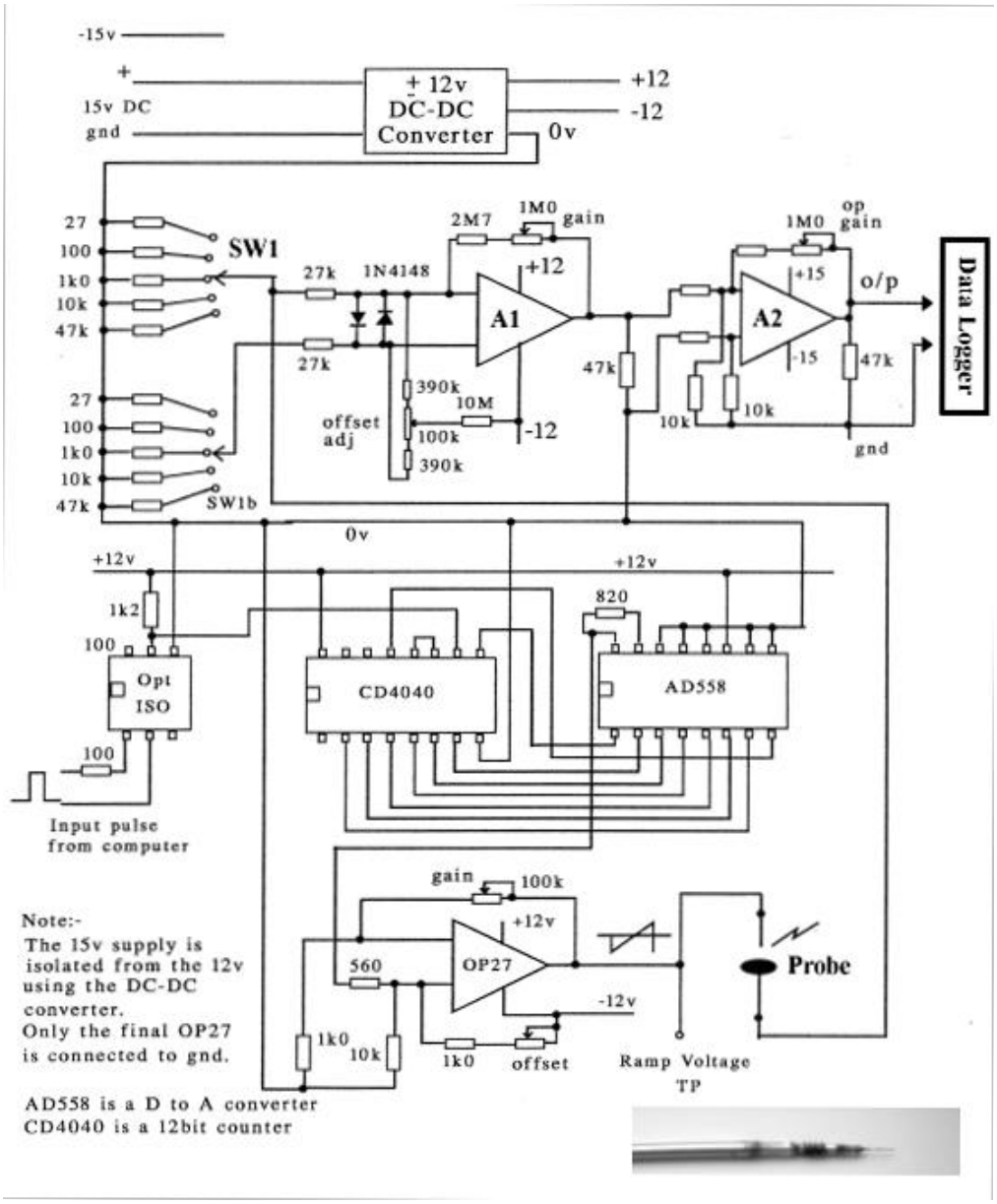

Figure 4.16: Schematic Diagram of the Electronic and Electric Circuits for Langmuir Probe.

4.5.5.5 Direct Potential Measurements

With both the probe tip and reference surface electrically insulated from the stem, it was possible to measure the potential difference between the tip or the reference surface and the test section casing directly. To achieve this, a simple potential divider illustrated in Figure 4.17 was built.

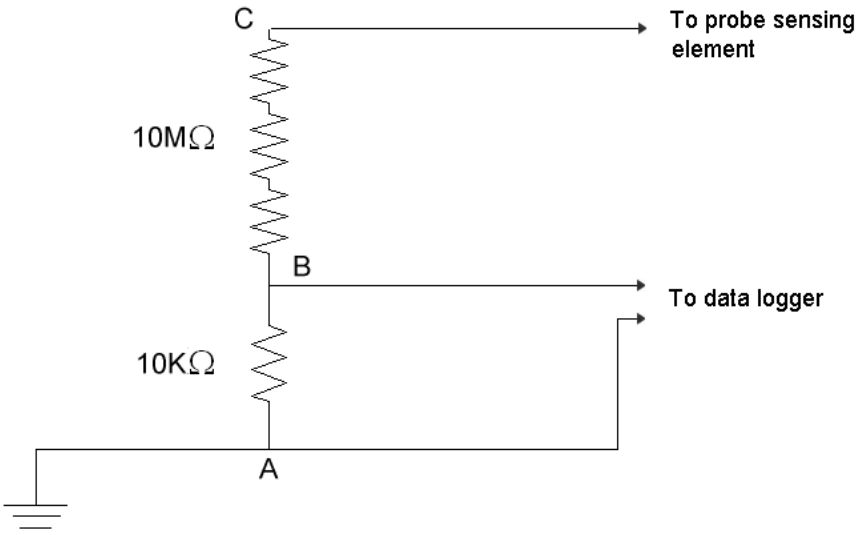

Figure 4.17: Schematic Diagram for Direct Potential Current Measurements.

The output from point B of the potential divider could be connected to the data logger directly. Thus, the potential difference between the probe tip or the reference surface and the test section casing could be measured.

4.5.5.6 Positioning of the Probe

It will be recalled that to allow for probe access one of the cascade supporting plates could be replaced with one machined with a slot. To take electrostatic measurements downstream of the cascade the Langmuir probe was mounted in a probe holder and traversing mechanism. Its traverse position was manually adjusted before each set of readings was taken. With this arrangement in place the only pressure measurements possible were through wall tapping points upstream and downstream of the blades as well as along the mid-passage. The Langmuir probe could also be mounted upstream of the cascade in a hole drilled in the test section wall for this purpose. Figure 4.4 shows the two possible locations of the probe.

Data acquisition was controlled by the Mdas data logger. The software described in section 4.5.4 controlled both the acquisition of the wall static pressure data, total pressure data and also electrostatic data. In addition, and concurrently with, the pressure measurements, a command was sent by the acquisition program via a TTL pin, connected to a card in the data logger. The TTL pin was connected to the Langmuir probe control circuit, which triggered the voltage ramp.

4.6 General Experimental Procedure

This section describes the general experimental procedures used for the measurements involving pressure distributions and the measurement of electrostatic charge.

4.6.1 Purging the Receiver

At the end of each working day the receiver drains were left open. This caused the receiver to fill with air. Before taking any measurements it was therefore necessary to purge the receiver for a period of two hours to guarantee the removal of this air. With the quick acting valve closed the steam inlet valve and the receiver vent valve were opened simultaneously allowing steam to purge the air. After this process was completed the steam in the receiver was suitable for using in experiments.

4.6.2 Setting the Initial Conditions

The upstream stagnation conditions for a test were set as follows for steam initially superheated, saturated or supercooled at inlet.

4.6.2.1 Superheated Steam

Superheated steam was generated by first filling the receiver with steam at a higher pressure than ultimately desired. Over a period of time this caused the receiver walls to heat up. It was usually found necessary to heat the walls to a temperature at least 10 K higher than the desired superheat temperature. Then the steam pressure was lowered to the desired stagnation pressure. After some time heat radiation from the receiver walls raised the steam to the target superheat. Often it was then necessary to re-adjust the stagnation pressure of the steam by letting small amounts of steam in or out of the receiver.

4.6.2.2 Saturated Steam

The receiver was filled to the desired upstream pressure with saturated steam. The pressure was set to a value slightly above the test stagnation pressure to allow for the small pressure drop in the receiver during the slight delay between opening the quick acting valve and starting the data acquisition. The corresponding drop in temperature was calculated using the receiver condition law (Figure 4.11).

4.6.2.3 Supercooled Steam

To generate supercooled steam, the receiver was first charged with saturated steam. The conditions of the saturated steam required to produce a given degree of supercooling were determined using the condition law. Steam was then vented to the condenser via the test section as well as through the bypass lines. This had the effect of expanding the steam remaining in the receiver to predetermined degrees of supercooling without the penalty of it gaining kinetic energy. When the desired upstream conditions were reached in the receiver the data acquisition system was triggered.

4.6.2.4 Setting the Pressure Ratio

To set the downstream pressure for flow supersonic at outlet the condenser pressure was set low and the tailboards adjusted until the desired pressure was achieved. With the outlet flow subsonic the condenser was set to a sufficiently low pressure, the tailboards opened and the mass flow rate through the test section controlled by using the butterfly valve at the exit of the test section (valve 9 in Figure 4.1). In both cases the receiver pressure determined the pressure upstream of the test section. It required some skill and experience to consistently obtain the desired pressure ratio across the test section for different steam and flow conditions. In addition to this the tailboards downstream of the cascade had to be adjusted to maintain a periodic flow across the blade cascade.

4.6.3 Blow-Down Test Procedure

4.6.3.1 Blade Static Pressure Measurements

The procedure for recording blade and wall static pressure measurements for a single set of upstream and downstream conditions was as follows:

1. The upstream conditions in the receiver were set as described above noting the initial pressure and temperature in the receiver.
2. The downstream pressure in the condenser and test section was set by making small changes to the air leakage into the condenser.
3. The quick acting valve was opened and shortly afterwards the data acquisition started using the PC software.

After completion of each test the quick acting valve was reset and the results viewed on the PC. If regarded as satisfactory they were saved to a file for further processing.

4.6.3.2 Electrostatic Measurements

The procedure used for recording electrostatic measurements for a single set of upstream and downstream conditions was as follows:

1. The Langmuir probe was pre-heated by switching the heater circuit to its first level.
2. The upstream conditions in the receiver were set as described above noting the initial pressure and temperature in the receiver.
3. The downstream pressure in the condenser and test section was set by making small changes to the air leakage into the condenser.
4. A few seconds before opening the quick-acting value the probe heater current was raised to its first boost value.
5. The quick acting valve was opened (which also triggered the probe's next heater level) and the data acquisition was started at the appropriate time via the PC software.

After completion of each test the quick acting valve (and heater circuit) were reset and the results viewed on the PC. If regarded as satisfactory they were saved to a file for further processing.

4.6.3.3 Steam Dosed with Ammonia

In addition to the above steps for either blade pressure or electrostatic measurements the following steps were necessary when taking measurements using steam dosed with ammonia:

1. An aqueous solution of ammonia was made up using ultra-pure water. The concentration of this solution was determined by the desired target concentration in the feed water and steam and by the flow rate of the peristaltic pump (see appendix C for details of these calculations).
2. The aqueous solution of ammonia was transferred to a reservoir from which it was pumped to the hotwell. In the hotwell it was allowed to mix with the boiler feed water.
3. The receiver was purged as usual using the dosed steam.
4. Samples were taken both of the feed water and of the steam at various positions throughout the system to determine the stable concentration of ammonia. The concentration in ppm and the pH were inferred using the relations between conductivity, ppm and pH (see Figure B.1).
5. When the receiver had been satisfactorily purged of air and the concentration of the ammonia was stable measurements could be taken as described previously.

Chapter 5:

Experimental Results – Effect of Impurities

5.1 Introduction

The present chapter is concerned with the investigation of the effect of impurities on nucleating flows of steam. It will be recalled that prior to the current investigation two separate sets of studies of the flows of steam over the same cascade of blades have been carried out. In the first set, carried out by *Ebrahimi [1991]*, the characteristics of the cascade were studied with steam superheated, saturated and supercooled at inlet to the cascade. The water supplied to the plant was taken from the normal Birmingham mains, which is known to be soft, and was dosed with corrosion inhibitors. Thus, it contained a number of impurities. In the second study *Mashmoushy [1994]* investigated the characteristics of the same cascade with steam wet at inlet to the blades. For this purpose the inlet passage to the cascade was arranged as a venturi. With steam supercooled at inlet to the venturi, expansion in its converging part caused the steam to nucleate. Careful diffusion of the flow in the diverging part allowed the droplets to be retained. To examine the influence of droplet size two separate venturi, designated as 'standard' and 'fast', were used in the investigation. It has been observed that when steam is wet at inlet, the water droplets present provide surface for condensation and depending on their number and size can reduce the supercooling attained by the fluid and suppress secondary, homogenous nucleation. The effect of the droplets on the heat release in the zone of rapid condensation can be seen by comparing the pressure distribution on the suction surface.

In the current work, prior to investigating the effect of impurities on the behaviour of nucleating steam flows, the steam has first been studied in the absence of chemical impurities. These observations using ultra-pure steam are intended to act as a baseline for comparison with other measurements in steam containing impurities. The next stage of the investigation has studied the same nucleating flows but for steam dosed with known levels of ammonia. In the same way that the effect of water droplets on the nucleation process in *Mashmoushy's* work was evident by the change in the suction surface pressure distribution, any effect of adding ammonia to the steam can be detected by comparing the

suction surface pressure distributions for ultra-pure steam with those for steam dosed with ammonia.

This chapter summarises the blade cascade surface and wall pressure measurements recorded over a range of flow conditions for ultra-pure steam and for steam dosed with ammonia at 4ppm and 12ppm. Additionally these measurements are compared with those recorded by *Ebrahimi* and *Mashmoushy*.

5.2 Range of Measurements

The experimental conditions used in the present study follow those used by previous investigators working on the blow-down rig at Birmingham University. In determining the flow conditions the most important factors to consider are the flow Reynolds number, outlet Mach number and, in the case of two phase flows, the condition of the steam at inlet to the cascade. Since the cascade is an exact geometrical model of an operating turbine stage, its Reynolds number based on blade opening and outlet isentropic conditions, was matched to that of a full scale machine by running the tests at correspondingly higher inlet stagnation pressures. Because of the uncertainty in the speed of sound in wet steam the overall inlet stagnation to downstream pressure ratio was used as a more readily quantifiable measure of the outlet Mach number. The pressure ratios correspond to those used in previous investigations, those adopted being 3.53, 2.33 and 1.83 all at 1.1 bar gauge inlet stagnation pressure. In superheated steam these pressure ratios correspond to outlet isentropic Mach numbers of approximately 1.5, 1.2 and 1.0 respectively. Previous investigators have also recorded measurements for the pressure ratios 1.49 and 1.26, for which the outlet Mach numbers are subsonic. However, at these pressure ratios the differences between the pressure distributions for superheated and nucleating flows are small. In order to focus on the conditions of primary interest to the current project these pressure ratios were not used.

For each pressure ratio blade surface and wall pressure measurements have been recorded at different inlet stagnation temperatures corresponding to superheated, saturated and supercooled steam. The steam was dry at inlet for all the tests. These conditions are summarised in Table 5.1 along with an example test number. The same conditions were used for tests with ultra-pure steam and for tests with pure steam dosed with ammonia at nominal 4 ppm and to a more limited extent, steam dosed with ammonia at nominal

12 ppm. A complete set of the experimental conditions covered, corresponding plots and tabulated data of the results are presented in appendix D.

Table 5.1: Summary of Experimental Conditions and Example Test Numbers with $P_{0, Inlet}$ = 1.1 bar

	To-Ts	**+33 K**	**0 K**	**-10 K**	**-13 K**	**-17 K**	**-21 K**
P. ratio	**Steam**						
1.83	Pure	2704e	0203h	0203m	0203t	2904ab	2904ad
	4 ppm NH_3	1904c	2903b	0104c	0104i	2303v	-
2.33	Pure	2704a	2904d	2904g	-	2904v	2904af
	4 ppm NH_3	1904b	2903f	2303q	2303m	2903o	1604d
	12 ppm NH_3	-	2104e	2104s	-	2104x	-
3.53	Pure	2704g	0903e	2904p	-	-	2904s
	4 ppm NH_3	1904f	2903i	2903f	2303l	2603q	1604a
	12 ppm NH_3	-	2104i	2104q	-	2104af	-

5.2.1 Experimental Uncertainty

In the case of static pressure readings the pressure transducers have an accuracy of ±0.01 bar. Thus the error at the low end of the recorded pressure range is approximately ±2.5% and ±1.0% at the high end. In the case of total pressure readings the transducers have an accuracy of ±0.005 bar. The error in total pressure readings is therefore approximately ±0.5%.

The error in temperature readings has been estimated at ±1 K, or approximately ±0.25% for typical stagnation temperatures. The error in non-dimensional distances has been estimated at ±0.5%.

5.3 Measurements with Ultra-Pure Steam

Surface pressure distributions for pure steam were recorded for upstream total to downstream static pressure ratios of 1.83, 2.33 and 3.53 and at the inlet temperatures listed in Table 5.1. The full results are provided in Appendix D. This section presents typical pressure distributions for steam superheated, saturated and supercooled by 10 K at inlet. Pressure is plotted as the ratio of local static pressure divided by inlet total pressure versus the axial distance along the blade normalised by the axial chord length. In the figures for pure steam, squares indicate the distribution on the blade pressure surface, while diamonds indicate the distribution on the suction surface. Distributions on the pressure surface are very similar for all inlet conditions and pressure ratios.

For each pressure ratio typical distributions of mid-passage and downstream wall static pressures are also shown. In both cases the pressure is normalised by inlet total pressure. For the mid-passage plots, pressure is plotted against axial distance normalised by the blade axial chord length. For the downstream wall pressure plots, pressure is plotted against tapping point position in mm.

Due to the nature of the equipment there is some slight variation in the pressure ratio and inlet stagnation temperature between tests nominally run at the same conditions. However, the effect of these variations on the resulting pressure distributions is small.

It should be noted that the results presented here are representative of the general trends measured and have been found to be repeatable over extended periods of operation.

5.3.1 Surface Pressure Distributions at a Pressure Ratio of 1.83

Figures 5.1a-d show the blade surface pressure distributions for a nominal pressure ratio of 1.83.

In Figure 5.1a the steam is superheated at inlet and the outlet flow Mach number approximately sonic. The pressure distribution on the blade pressure surface is smooth over the whole expansion and is typical of the pressure surface distribution for all pressure ratios and inlet conditions. On the suction surface initially the flow expands rapidly up to the blade passage throat. The throat is positioned at approximately 40% of the chord length. At this point the radius of curvature of the suction surface changes and this tends to influence the flow on the suction surface. In this case a normal shock-wave

forms just downstream of the throat. Downstream of the shock wave the flow expands smoothly to the cascade exit.

Figures 5.1b and 5.1c show the pressure distributions for flow initially saturated and supercooled by 10 K respectively. In both cases the pressure distributions are very similar and were found to be independent of inlet supercooling[1] (the pressure distribution for steam supercooled by 21 K at inlet is shown in Figure 5.1d to illustrate this). In these three cases the flow has supercooled and subsequently nucleated. Despite the same initial rapid expansion as for the superheated test, the nucleation of droplets changes the thermodynamics and aerodynamics of the flow as can be seen by the distributions on the suction surface, downstream of the throat. In these cases there is a much smaller pressure rise and the flow then diffuses to match the outlet pressure. As discussed by *Bakhtar, Mashmoushy and Jadayel [1997b]*, the outlet Mach number of wet steam differs from that for dry steam at the same pressure ratio. The outlet flow in the superheated test is sonic. However in the cases where the steam is saturated and supercooled at inlet, the steam nucleates during the expansion and as a result the flow is slightly subsonic at outlet.

Figure 5.2a shows a typical plot of the wall mid-passage pressure distribution at a pressure ratio of 1.83 for steam saturated at inlet. The flow expands smoothly throughout the mid-passage region, accelerating slightly downstream of the blade throat.

The wall pressure distributions in the traverse plane downstream of the cascade exit, covering the three central blades, are shown in Figure 5.2b. As expected the flow is periodic in this region.

[1] This is attributed to two reasons. Firstly the high expansion rate upstream of the throat tends to prevent nucleation. Secondly *Bakhtar and Young [1978]* showed that in a constant area duct, for steam with a Mach number in the range of 0.9 – 1.0 any heat release due to condensation tends to increase the supercooling. Thus even if the steam is substantially supercooled upstream of the throat on reaching Mach 0.9 any heat release due to condensation will increase the supercooling until the throat is reached.

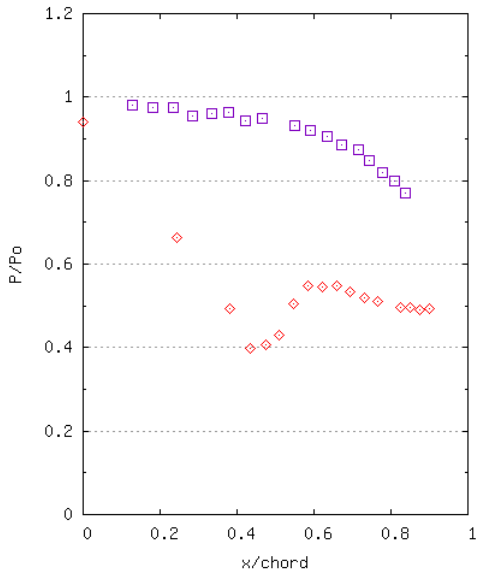

a) P_{ratio} = 1.85, ΔT = +33.0 K, P_0 = 1.11
(Test: 2704e)

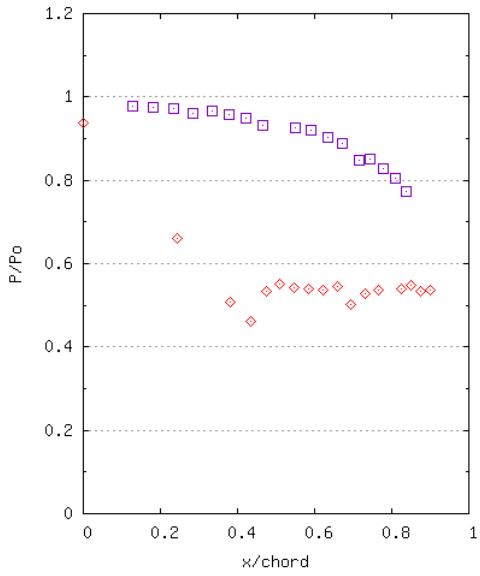

b) P_{ratio} = 1.82, ΔT = -1.98 K, P_0 = 1.06
(Test: 0203h)

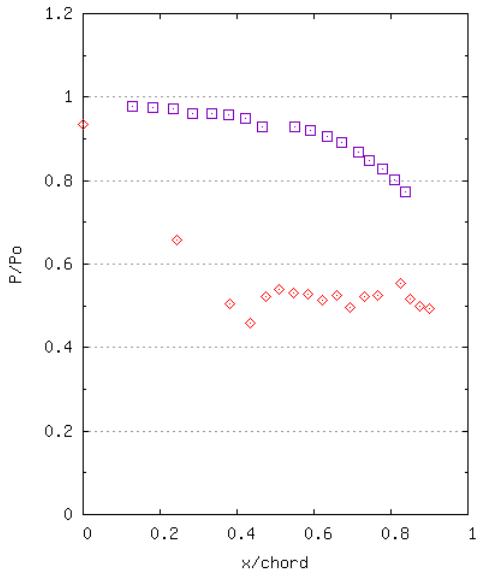

c) P_{ratio} = 1.89, ΔT = -11.4 K, P_0 = 1.06
(Test: 0203m)

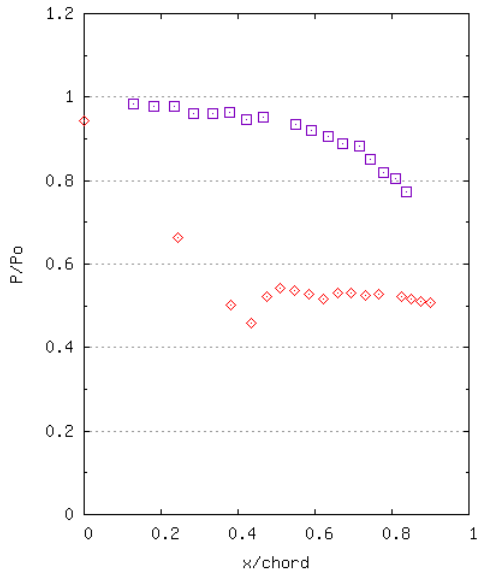

d) P_{ratio} = 1.83, ΔT = -21.2 K, P_0 = 1.11
(Test: 2904ad)

Figure 5.1: Blade surface pressure distributions for pure steam. Nominal $P_{ratio} \approx 1.83$

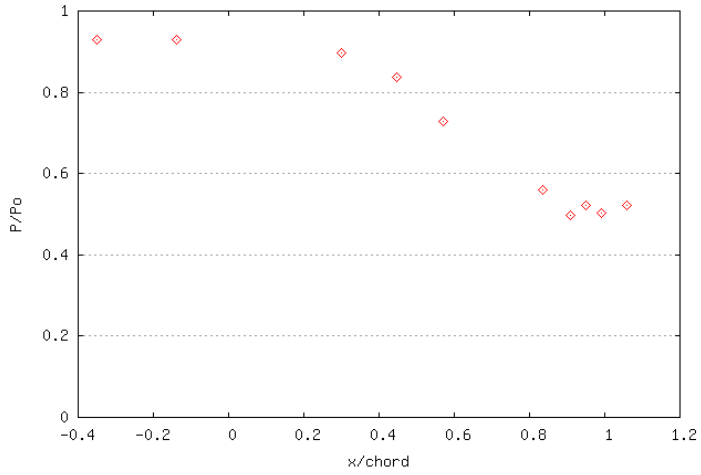

a) Mid-Passage

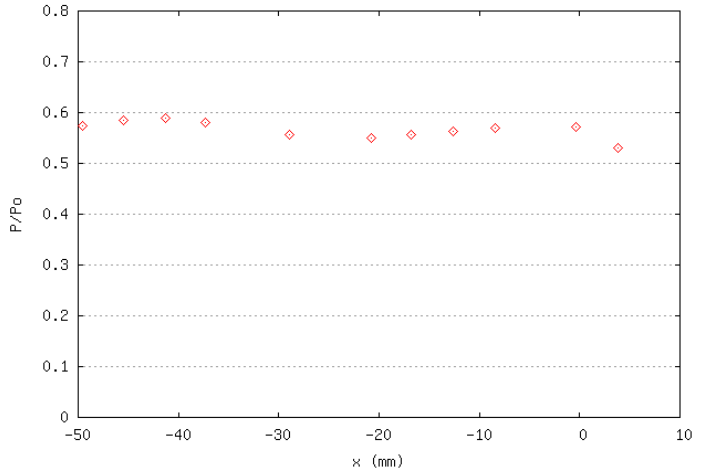

b) Downstream

Figure 5.2: Typical wall pressure distributions for pure steam. P_{ratio} = 1.83, ΔT = -1.98 K, P_0 = 1.06 (Test: 0203h)

5.3.2 Surface Pressure Distributions at a Pressure Ratio of 2.33

The distributions at a nominal pressure ratio of 2.33 are shown in Figures 5.3a-c. In Figure 5.3a the steam is superheated at inlet. On the suction surface the steam expands rapidly to the blade throat. Just downstream of the throat, at approximately 45% chord length, there is a small knee in the pressure profile. This corresponds to a change in the blade radius of curvature at this point. Until reaching 70% chord the steam has remained dry, however at this position a sharp pressure rise can be seen. Comparison with one-dimensional solutions indicates that at this pressure ratio, an inlet temperature of 27.2 K is insufficient to prevent the steam from supercooling downstream of the throat, and thus the pressure rise in this region is due to reversion of the steam. As droplets nucleate and grow

they release latent heat back to the parent vapour, which retards the supersonic flow leading to the pressure rise.

In Figures 5.3b and 5.3c the steam is saturated and supercooled by 10 K at inlet respectively. The suction surface pressure profiles for both these cases are very similar to each other, but both differ from the superheated pressure distribution. The steam expands rapidly to the blade throat, gaining a high degree of supercooling. In comparison to the flat 'knee' seen in the superheated profile, a pressure rise can be observed on the suction surface just downstream of the throat at approximately 45% chord. This pressure rise indicates the spontaneous homogeneous nucleation of water droplets and the region around it is known as the zone of rapid condensation. Latent heat is released as droplets nucleate and is returned to the parent vapour. Since the flow is supersonic in this region the flow is retarded and this leads to the pressure rise. The steam quickly recovers thermodynamic equilibrium and then continues to expand before diffusing to match the cascade outlet pressure.

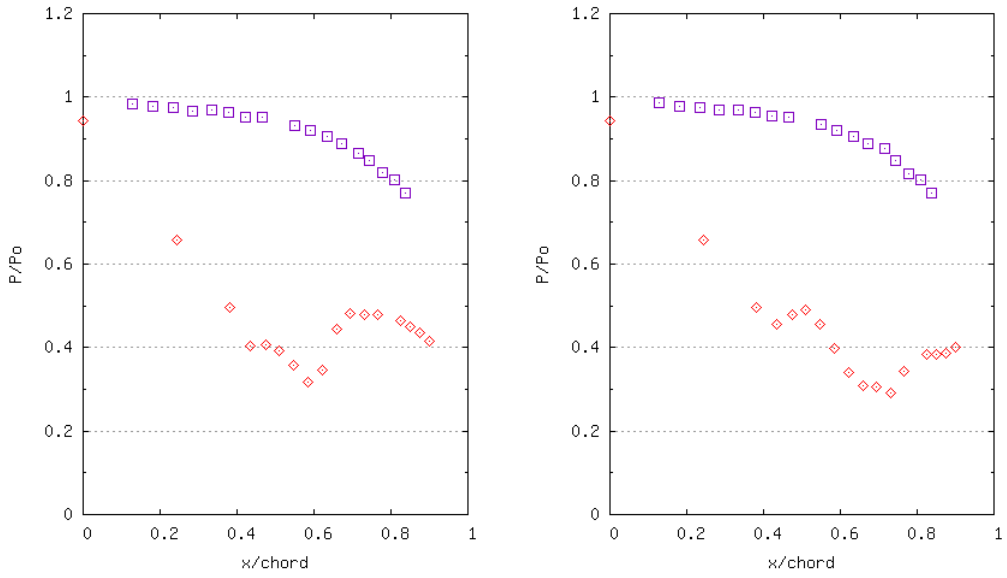

a) P_{ratio} = 2.30, ΔT = +27.2 K, P_0 = 1.14 (Test: 2704a)

b) P_{ratio} = 2.28, ΔT = -0.49 K, P_0 = 1.12 (Test: 2904d)

Figure 5.3a-b: Blade surface pressure distributions for pure steam. Nominal $P_{ratio} \approx 2.33$

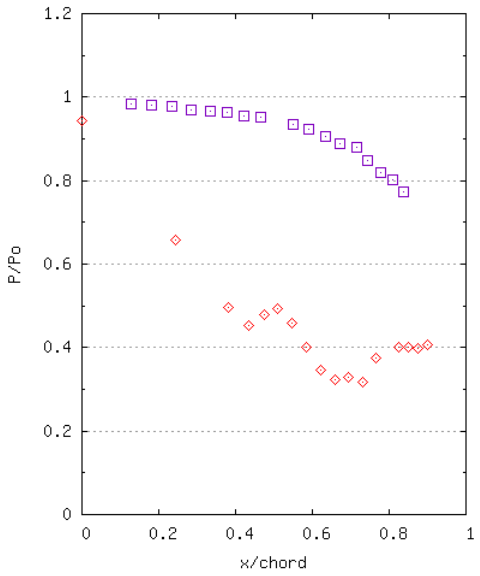

c) P_{ratio} = 2.32, ΔT = -10.6 K, P_0 = 1.13
(Test: 2904g)

Figure 5.3c: Blade surface pressure distributions for pure steam. Nominal $P_{ratio} \approx 2.33$

Typical wall pressure distributions for the blade mid-passage and in a transverse direction downstream of the blades are shown in Figures 5.4a and b respectively. The mid-passage distribution is very similar to that at a pressure ratio of 1.83. The downstream pressure distribution indicates that the flow was periodic over the central blade passages.

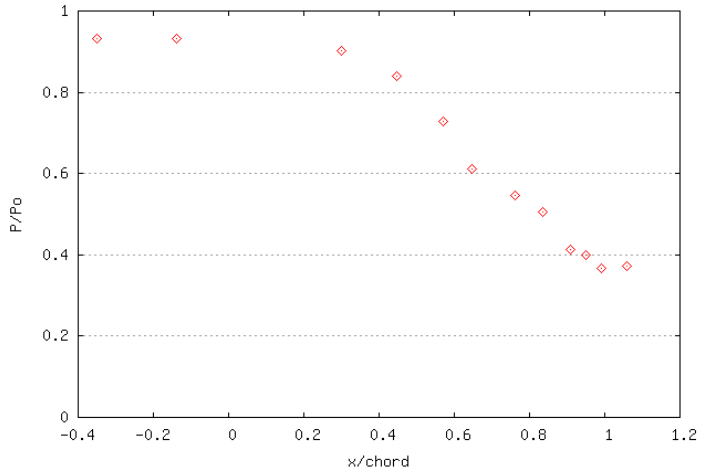

a) Mid-Passage

Figure 5.4a: Typical wall pressure distributions for pure steam. P_{ratio} = 2.35, ΔT = -0.99 K, P_0 = 1.11
(Test: 1002j)

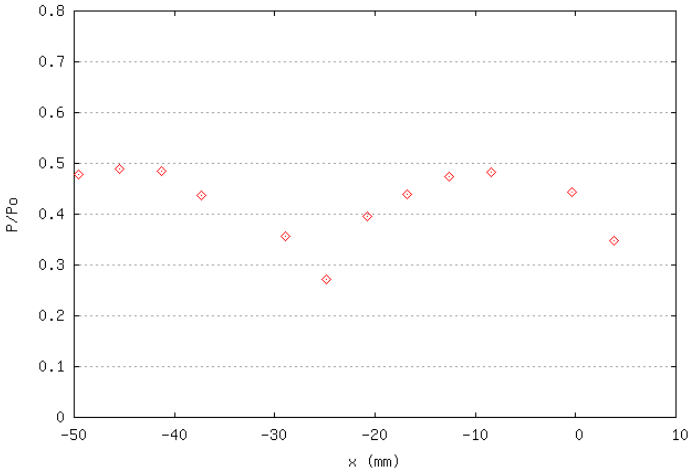

b) Downstream

Figure 5.4b: Typical wall pressure distributions for pure steam. P_{ratio} = 2.35, ΔT = -0.99 K, P_0 = 1.11 (Test: 1002j)

5.3.3 Surface Pressure Distributions at a Pressure Ratio of 3.53

The results for a nominal pressure ratio of 3.53 are shown in Figures 5.5a-c. It was considerably more difficult to set the pressure ratio correctly for these tests. The downstream pressure was extremely sensitive to small changes in the condenser pressure. Consequently the results presented here are not exactly at a pressure ratio of 3.53.

In the superheated test (Figure 5.5a) the flow expands to the throat, where there is a small knee as a result of the change in blade radius of curvature. The flow continues to expand smoothly until approximately 60% chord length. As is the case for the flow at a pressure ratio of 2.33, an inlet superheat of 32.4 K is not sufficient to prevent the flow from nucleating later in the expansion. At 60% chord there is evidence of condensation as the flow retards slightly and then diffuses to the cascade exit.

The saturated and supercooled profiles are shown in Figures 5.5b and 5.5c respectively. On the suction surface there is a fast expansion until the throat region is reached. At this point the steam has gained a high degree of supercooling. Here, as for the 2.33 pressure ratio, a small pressure rise indicates the location of spontaneous homogenous nucleation. The pressure rise is quite distinct when compared with the flat knee found in the same region for steam superheated at inlet. The flow remains supersonic downstream of the throat, it accelerates smoothly, before diffusing very slightly near the cascade exit.

Figure 5.6 shows typical wall pressure mid-passage and downstream pressure distributions. The expansion along the mid-passage is very similar to the previous two pressure ratios. The downstream pressure distribution is periodic.

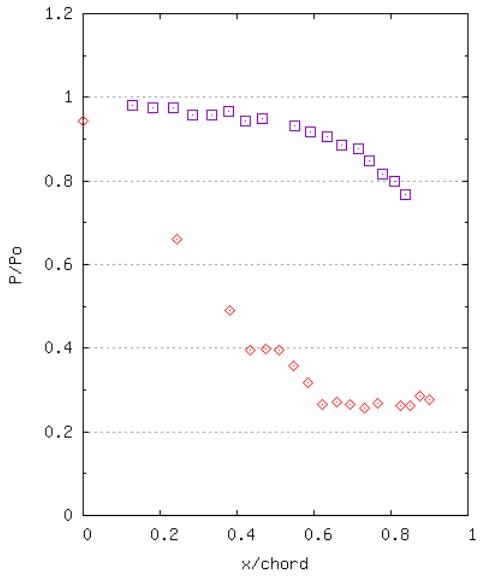

a) P_{ratio} = 3.05, ΔT = +32.4 K, P_0 = 1.12
(Test: 2704g)

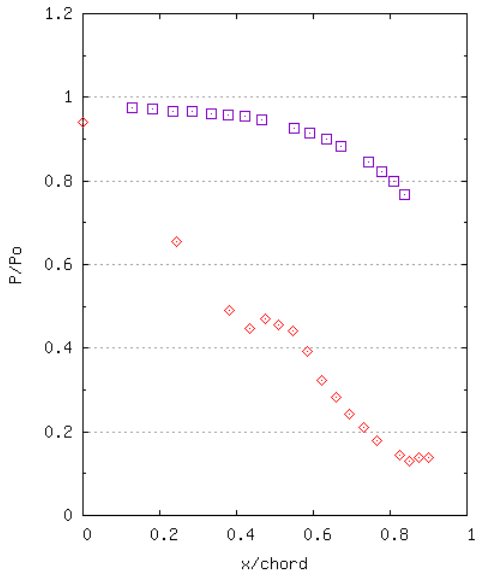

b) P_{ratio} = 3.47, ΔT = -1.78 K, P_0 = 1.09
(Test: 0903e)

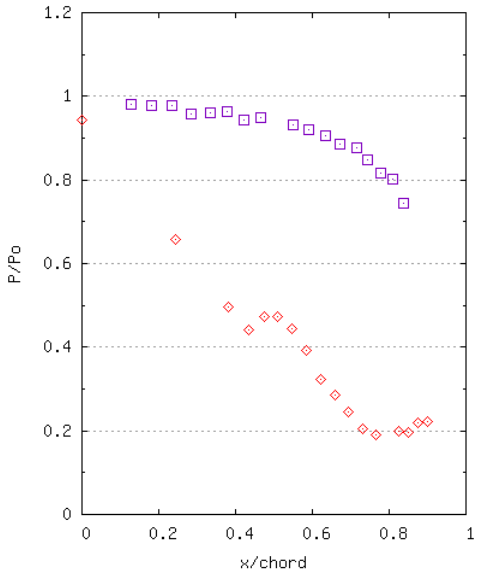

c) P_{ratio} = 3.65, ΔT = -10.5 K, P_0 = 1.11
(Test: 2904p)

Figure 5.5: Blade surface pressure distributions for pure steam. Nominal $P_{ratio} \approx 3.53$

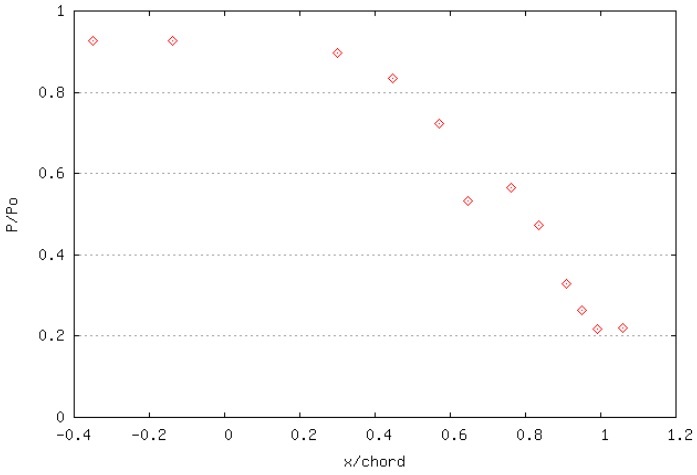

a) Mid-Passage

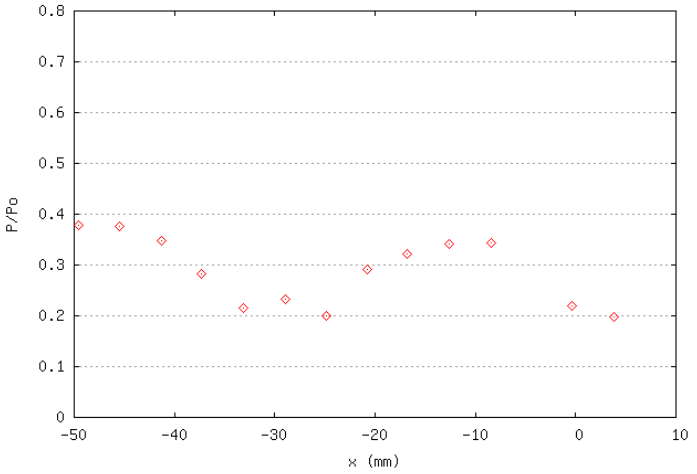

b) Downstream

Figure 5.6: Typical wall pressure distributions for pure steam. P_{ratio} = 3.47, ΔT = -1.78 K, P_0 = 1.09 (Test: 0903e)

5.4 Measurements with Steam Dosed with Ammonia

The tests with steam dosed with ammonia have been carried out at the same series of overall conditions as those used for the ultra-pure steam tests discussed above. Results are presented here for ammonia at nominal concentrations of 4 ppm and 12 ppm.

5.4.1 Ammonia Concentration

At the time the readings were taken the concentration of ammonia in the feed water and steam were estimated based on the water/steam conductivity measurements and then converted to ppm using the chart in Appendix B, Figure B.1. This estimate has since been corrected based on the results of detailed chemical analysis of the samples. An example of this chemical analysis is presented in Figure 5.7 as impurity concentration at the ppm level for each sample point in the system. Detailed results from this analysis are found in Appendix B. It can be seen from the figure that by the time the dosed steam has left the boiler (sample point S6) a stable concentration of ammonia has been achieved. Samples at S3 and S2 represent the concentration of ammonia in the steam receiver before entry into the test section.

Although a stable concentration of ammonia was reached for each test, obtaining a consistent concentration of ammonia in the steam over multiple tests has proved to be impossible with the current equipment. Consequently tests conducted on different days have varying ammonia concentrations in the steam. However the discrepancy is only in the order of 1 or 2 ppm compared to an underlying ion content at the ppb level. Therefore of all the impurity ions present, ammonium ions form by far the largest number.

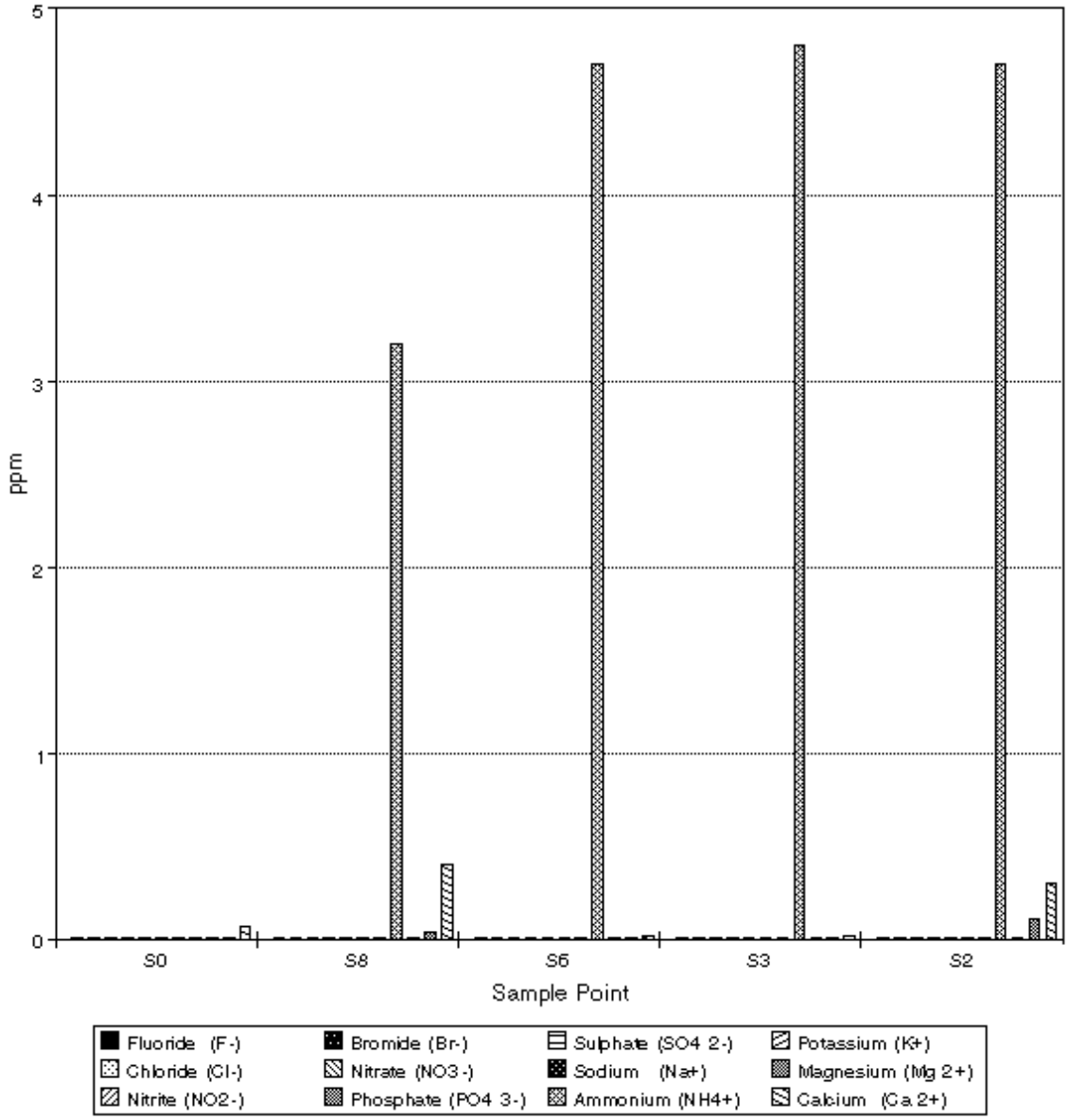

Figure 5.7: Analysis of the steam with 4ppm of ammonia

S0: ELGA system, S8: Boiler feedwater, S6: Receiver steam inlet, S3: Receiver steam, S2: Receiver steam

5.4.2 Surface Pressure Distributions with Ammonia at 4 ppm

Blade suction surface pressure distributions are presented in Figures 5.8, 5.9 and 5.10 for nominal pressure ratios 1.83, 2.33 and 3.53 respectively. The pressure surface pressure distributions are not plotted in these figures because, as has been shown above, they are very similar under all the conditions studied and because they are in all cases identical to the pressure surface pressure distributions recorded using pure steam.

For each pressure ratio Figures a-c represent conditions superheated, saturated and -10 K supercooled at inlet respectively. The ammonia concentration in the steam for each test is given in the figure caption. 'Plus' signs are used as the symbol for the suction surface pressure distribution for steam dosed with ammonia. For comparison the suction surface pressure distribution recorded using pure steam is also plotted on each figure, indicated by diamonds and offset in the y-direction. The y-axis used for each pressure distribution is indicated using a text label; they share a common x-axis.

The pressure distributions for the tests with ammonia dosed steam, superheated at inlet, are identical to the pressure distributions for ultra-pure steam at the same inlet conditions. This is the case even in the two tests at pressure ratios of 2.33 and 3.53 where the inlet temperature was insufficient to prevent the steam supercooling and there is evidence of homogeneous nucleation towards the cascade exit as discussed previously.

For conditions where steam is saturated or supercooled at inlet and homogeneous nucleation is observed downstream of the throat in the tests with ultra-pure steam, it was expected that there might be some evidence of binary nucleation in the steam containing ammonia. If the number of very small droplets forming on the impurities was large and the droplets nucleated upstream of the zone of rapid condensation then this would reduce the maximum supercooling attained by the steam during the rapid expansion upstream of the throat. Consequently the number of droplets formed by spontaneous homogeneous nucleation at the point of limiting supersaturation would be lower and the pressure rise, associated with the release of latent heat just downstream of the throat, smaller. If the pressure rise observed at 40% chord in the pressure distributions for steam containing ammonia was smaller, then it could be concluded that many small droplets had formed by binary nucleation and influenced the flow.

However this is not the case; in the throat region the suction surface pressure distributions for all three pressure ratios and inlet conditions are almost identical to the ultra-pure steam distributions. There is no indication of a reduction in the pressure rise in the zone of rapid condensation for the nucleating tests. It can therefore be concluded that binary ammonia/water nucleation has not occurred, or has not generated a large enough number of small droplets sufficient to inhibit homogeneous nucleation. For both the tests using ultra-pure steam and the tests using steam dosed with ammonia it appears that the steam condensation process is dominated by homogeneous nucleation.

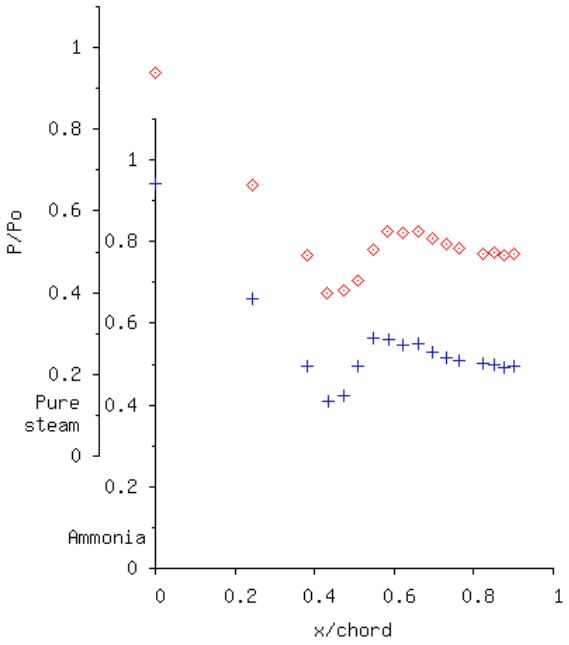

a) P_{ratio} = 1.78, ΔT = +34.0 K, P_0 = 1.10, 6.81 ppm NH_3 (Test: 1904c)

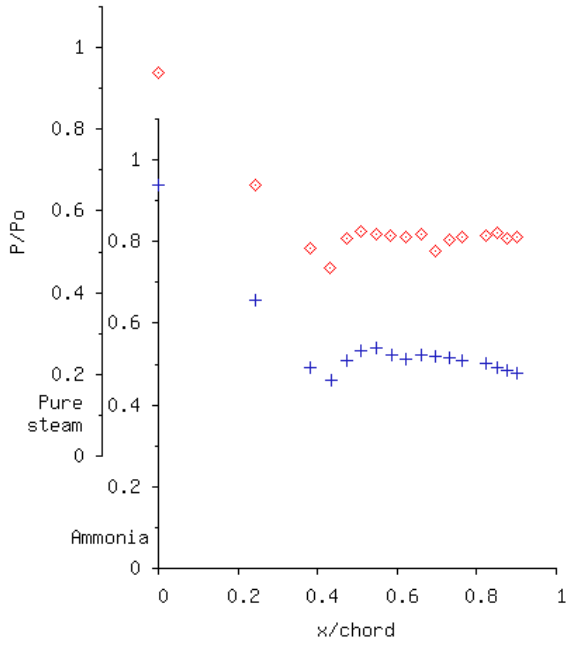

b) P_{ratio} = 1.83, ΔT = -1.78 K, P_0 = 1.08, 4.78 ppm NH_3 (Test: 2903b)

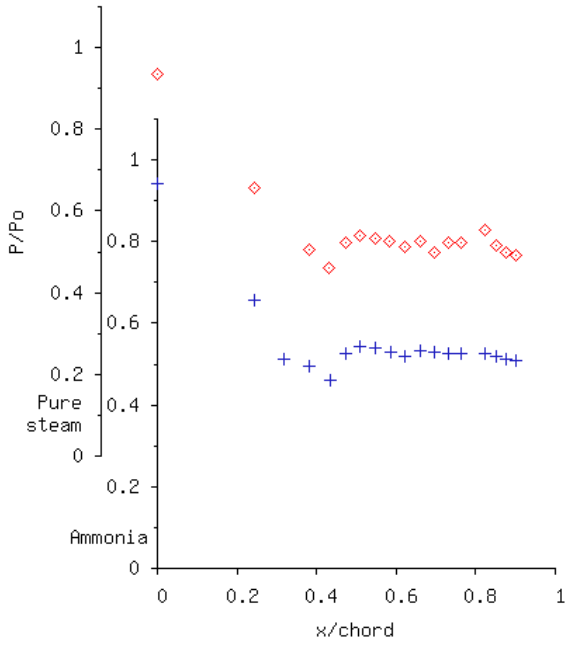

c) P_{ratio} = 1.82, ΔT = -10.8 K, P_0 = 1.10, 6.37 ppm NH_3 (Test: 0104c)

Figure 5.8: Blade suction surface pressure distribution for steam dosed with nominal 4 ppm ammonia. $P_{ratio} \approx 1.83$. The pure steam distribution is shown for comparison offset on the y-axis. Key: + indicate steam dosed with 4 ppm ammonia, ◊ indicate pure steam

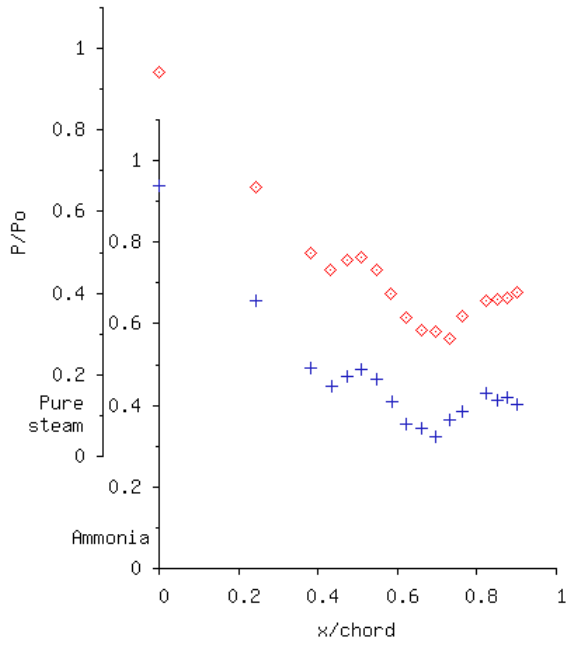

a) P_{ratio} = 2.29, ΔT = +32.6 K, P_0 = 1.11, 6.81 ppm NH_3 (Test: 1904b)

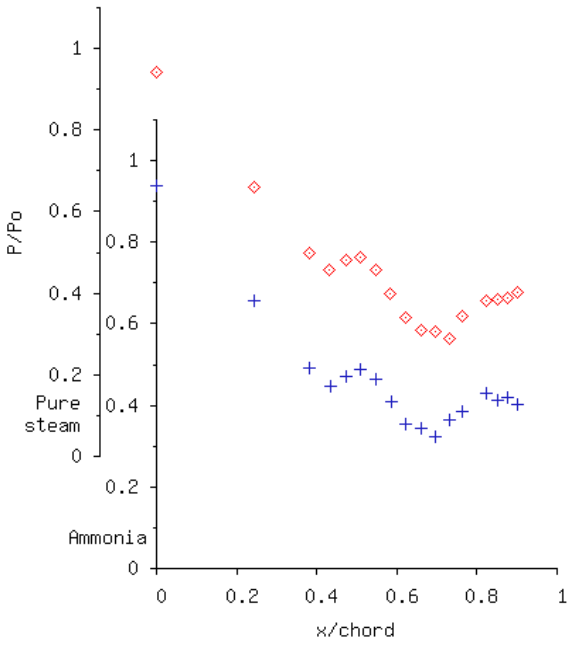

b) P_{ratio} = 2.33, ΔT = -1.18 K, P_0 = 1.09, 4.78 ppm NH_3 (Test: 2903f)

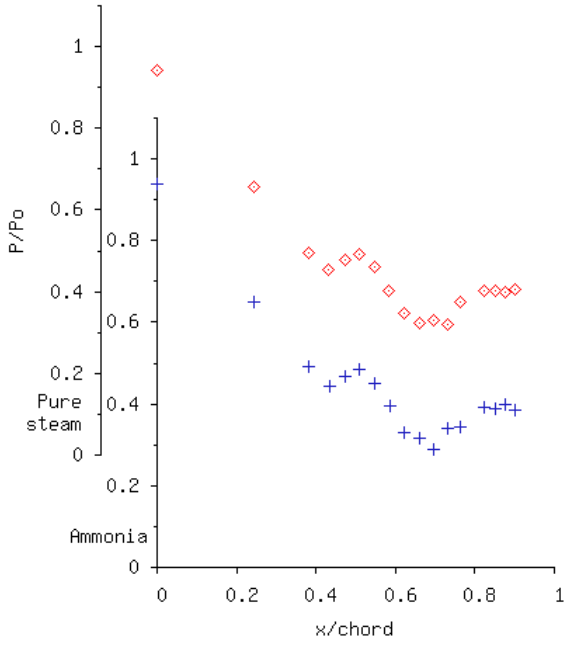

c) P_{ratio} = 2.30, ΔT = -12.8 K, P_0 = 1.08, 6.67 ppm NH_3 (Test: 2303q)

Figure 5.9: Blade suction surface pressure distribution for steam dosed with nominal 4 ppm ammonia. $P_{ratio} \approx 2.33$. The pure steam distribution is shown for comparison offset on the y-axis. Key: + indicate steam dosed with 4 ppm ammonia, ◊ indicate pure steam

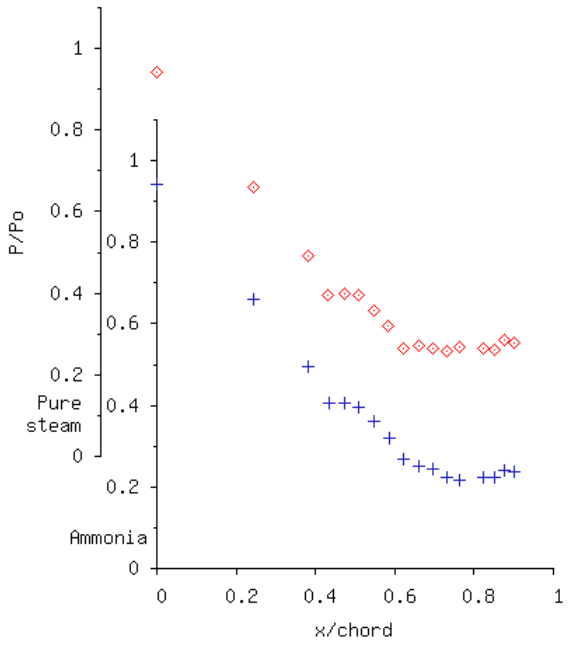

a) P_{ratio} = 3.06, ΔT = +33.9 K, P_0 = 1.10, 6.81 ppm NH_3 (Test: 1904f)

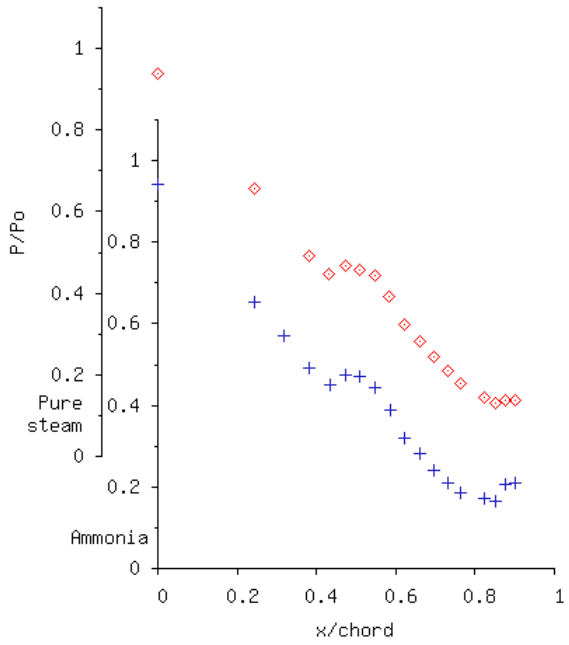

b) P_{ratio} = 3.28, ΔT = -1.68 K, P_0 = 1.09, 4.78 ppm NH_3 (Test: 2903i)

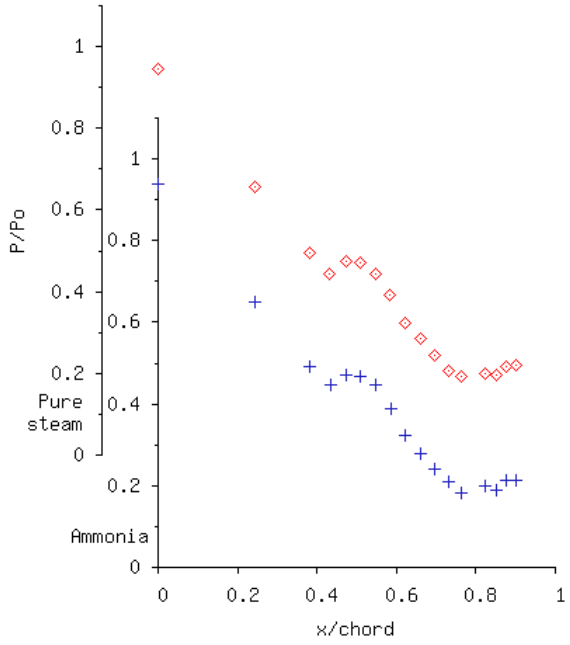

c) P_{ratio} = 3.54, ΔT = -8.6 K, P_0 = 1.08, 6.67 ppm NH_3 (Test: 2303f)

Figure 5.10: Blade suction surface pressure distribution for steam dosed with nominal 4 ppm ammonia. $P_{ratio} \approx 3.53$. The pure steam distribution is shown for comparison offset on the y-axis. Key: + indicate steam dosed with 4 ppm ammonia, ◊ indicate pure steam

5.4.3 Surface Pressure Distributions with Ammonia at 12 ppm

The tests for steam dosed with nominal 12 ppm ammonia were run over a more limited set of conditions. There are no results at a pressure ratio of 1.83, neither are there any results for steam superheated at inlet.

The results for pressure ratios of 2.33 and 3.53 are presented in Figures 5.11 and 5.12 respectively. The same symbols are used as for ammonia at 4 ppm. The pure steam suction surface pressure distributions are superimposed, offset on the y-axis. It could be expected that the higher concentration of ammonia in these tests might result in larger numbers of droplets forming by binary nucleation, indicated by a reduction in the pressure rise downstream of the throat as discussed above. However this is not the case; the pressure distributions are again almost identical to the distributions for ultra-pure steam and for steam dosed with 4 ppm ammonia.

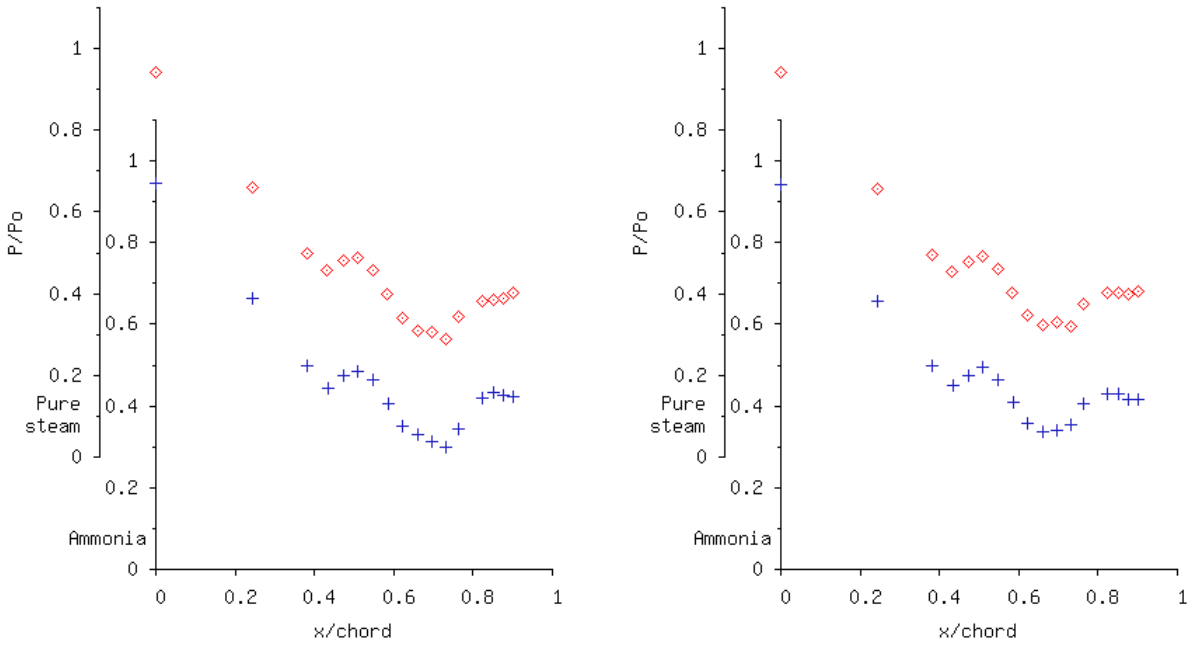

a) P_{ratio} = 2.31, ΔT = -3.10 K, P_0 = 1.09, 12.36 ppm NH_3 (Test: 2104e)

b) P_{ratio} = 2.35, ΔT = -11.50 K, P_0 = 1.08, 12.36 ppm NH_3 (Test: 2104s)

Figure 5.11: Blade suction surface pressure distribution for steam dosed with nominal 12 ppm ammonia. $P_{ratio} \approx 2.33$. The pure steam distribution is shown for comparison offset on the y-axis.
Key: + indicate steam dosed with 4 ppm ammonia, ◊ indicate pure steam

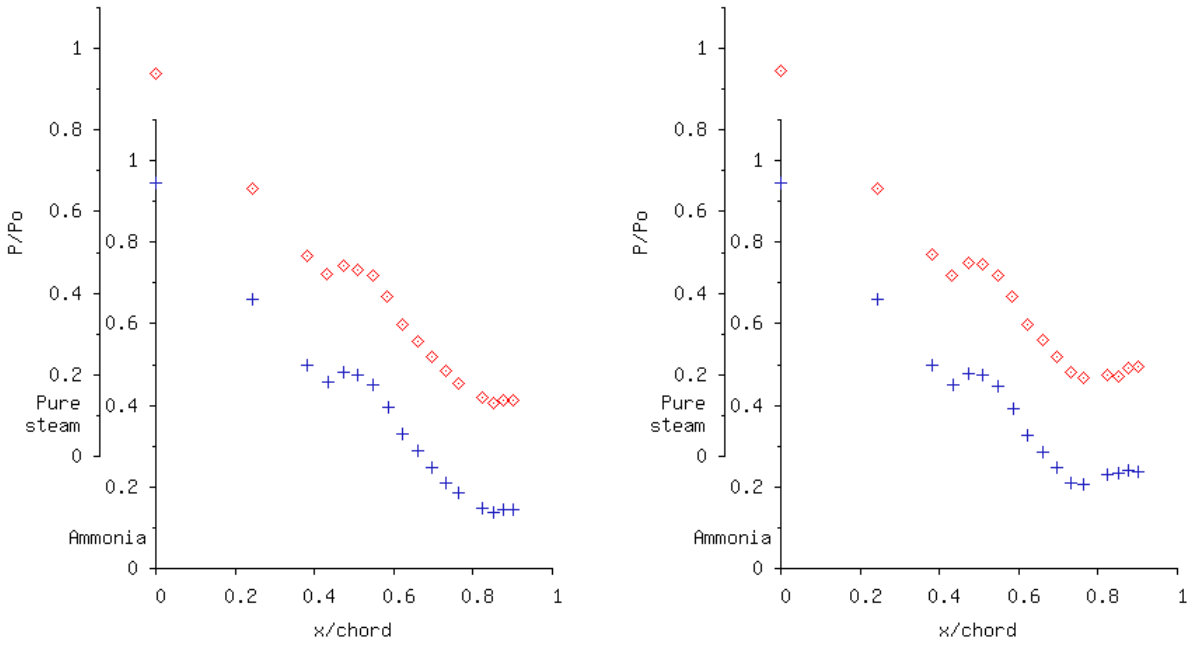

a) P_{ratio} = 3.67, ΔT = -3.69 K, P_0 = 1.10, 12.36 ppm NH_3 (Test: 2104j)

c) P_{ratio} = 3.48, ΔT = -10.74 K, P_0 = 1.08, 12.36 ppm NH_3 (Test: 2104q)

Figure 5.12: Blade suction surface pressure distribution for steam dosed with nominal 12 ppm ammonia. $P_{ratio} \approx 3.53$. The pure steam distribution is shown for comparison offset on the y-axis. Key: + indicate steam dosed with 4 ppm ammonia, ◊ indicate pure steam

5.5 Comparison of Results

A baseline of measurements using ultra-pure steam containing no impurities has been presented above. This allows a comparison to be made between the ultra-pure steam pressure distributions, the pressure distributions for steam containing ammonia and those previously recorded by *Ebrahimi [1991]* and *Mashmoushy [1994]*, who both used the same cascade of rotor blades. As described in Chapter 3 both *Ebrahimi* and *Mashmoushy* used mains water, dosed with anti-corrosion inhibitor, to generate the steam supply for the test section. Thus the steam contained an unknown level of chemical impurities. To gain an estimate of the base level of impurities present in the steam consider that the conductivity of steam in the receiver (sample point S3), shortly after flushing with ultra-pure steam began, was 1.8 μScm^{-1} (see Appendix B, Table B.4). Converted to an equivalent ammonia concentration this is approximately 225 ppb. Despite flushing having begun the level of impurities in the feed water in the hotwell was still very high (conductivity 25 μScm^{-1}). Also, in the receiver there were still high levels of calcium ions

(150ppb), chlorides (20ppb) and sulphates (10ppb) in the steam, so this estimate is probably a reasonable, if conservative, estimate of the impurities present.

As explained in Chapter 3 *Ebrahimi's* and *Mashmoushy's* measurements were recorded using exactly the same apparatus and blade configuration as has been used in the current work – with the exception that some of *Mashmoushy's* results used a venturi upstream of the blade cascade to generate a supply of wet steam for admission to the cascade section. In the following sections the suction surface pressure distributions for ultra-pure steam and for steam dosed with 4 ppm of ammonia are overlaid on the same figure as the corresponding pressure distribution from *Ebrahimi's* or *Mashmoushy's* work. The pressure distributions for dry steam, superheated and supercooled at inlet, are *Ebrahimi's*. The pressure distributions for dry steam, saturated at inlet, are *Mashmoushy's*. In addition, the current pressure distributions are also overlaid in a separate figure on to *Mashmoushy's* pressure distributions for steam wet at inlet. In the figures the symbols used for ultra-pure steam and for steam dosed with ammonia are the same as those used previously. For the older results a × indicates the distribution on the suction surface. As before, in each figure the suction surface pressure distributions are offset slightly from each other in the y-direction. The y-axis used for each pressure distribution is indicated using a text label; they share a common x-axis.

In the following comparisons there are small differences between the pressure distributions due to the slight variation in conditions used by each investigator at nominally the same overall condition e.g. slightly different inlet stagnation conditions, overall pressure ratio and tailboard settings. However, these differences are small and do not prevent useful comparisons being made, particularly in the area of interest, the zone of rapid condensation.

5.5.1 Comparisons of Results at a Pressure Ratio of 1.83

Comparisons of results for tests using dry steam at inlet are shown in Figures 5.13a-c. Overall the suction surface pressure distributions for dry steam are very similar for each set of inlet conditions.

In the case of steam superheated at inlet (Figure 5.13a) the position of the shock wave is the same in all three tests. In the case of the tests saturated at inlet (Figure 5.13b) the pressure profiles around the zone of rapid condensation are very similar, but in the measurements with ultra-pure steam, the expansion flattens out very slightly towards the

blade outlet. In the case where the steam is supercooled at inlet (Figure 5.13c) the pressure profiles around the zone of rapid condensation are also very similar. In both Figures 5.13b and c the pressure rise in this region appears to occur at a slightly lower pressure but the magnitude of the rise is identical. Further downstream, the steam then continues to expand, at a slightly higher rate in the case of *Ebrahimi's* work in Figure 5.13c.

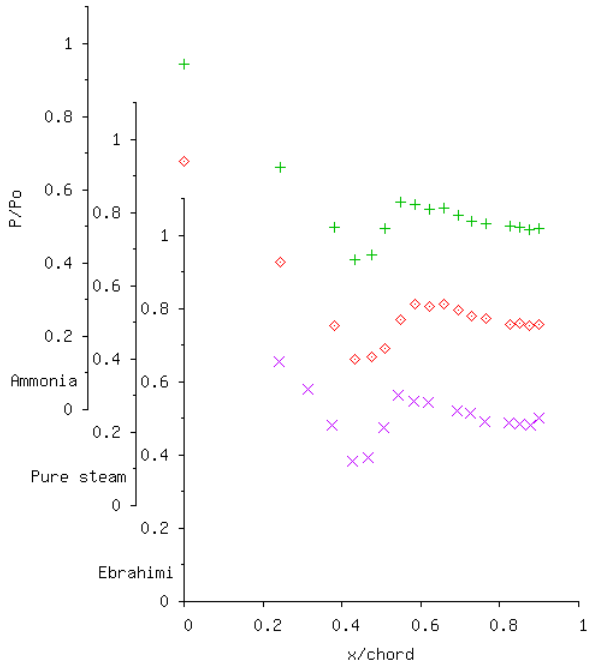

$P_{ratio} \approx 1.83$, Superheated

Figure 5.13a: Comparison of Ebrahimi/Mashmoushy pressure distributions with ultra-pure steam and steam dosed with 4 ppm ammonia

Key: × indicate results using steam with conventional water treatment
◊ indicate pure steam
+ indicate steam dosed with 4 ppm ammonia

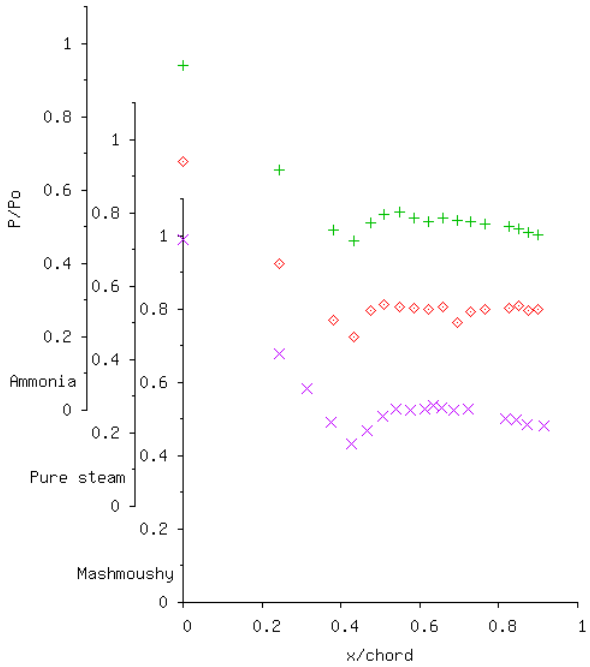

b) $P_{ratio} \approx 1.83$, Saturated

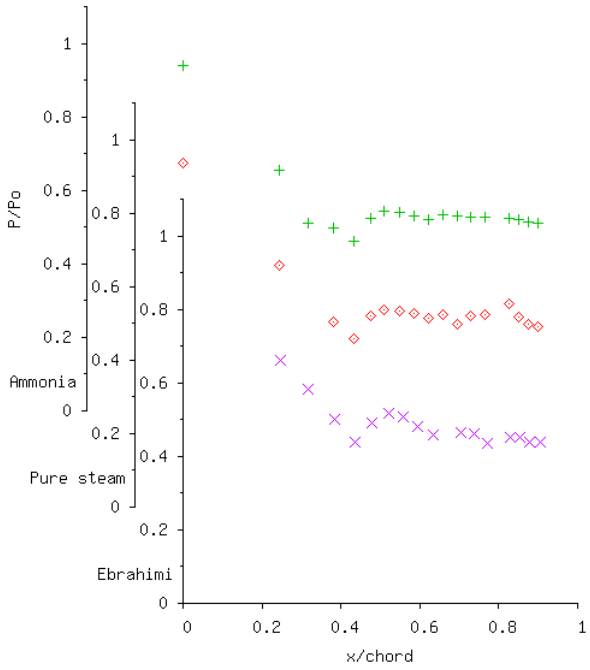

c) $P_{ratio} \approx 1.83$, -10 K Supercool

Figure 5.13b-c: Comparison of Ebrahimi/Mashmoushy pressure distributions with ultra-pure steam and steam dosed with 4 ppm ammonia
Key: × indicate results using steam with conventional water treatment
◊ indicate pure steam
+ indicate steam dosed with 4 ppm ammonia

5.5.1.1 Comparisons with Steam Wet at Inlet, P_{ratio} = 1.83

Figure 5.14 shows a comparison of *Mashmoushy's* results for steam wet at inlet with the corresponding results for ultra-pure steam and steam dosed with ammonia, still both dry at inlet. In *Mashmoushy's* test the steam had an inlet wetness fraction of 2.16% and the inlet droplet radius was estimated as 0.127 μm.

On the suction surface the pressure rise in the zone of rapid condensation occurs at a slightly lower pressure in *Mashmoushy's* work. However the magnitude of the pressure rise is identical for all three cases. The expansion further downstream is also similar for all three cases. *Mashmoushy [1994]* concluded that at this pressure ratio the droplets generated by the venturi had no effect on nucleation in the blade cascade and therefore on the pressure distribution in the throat region. This is supported by the current comparison.

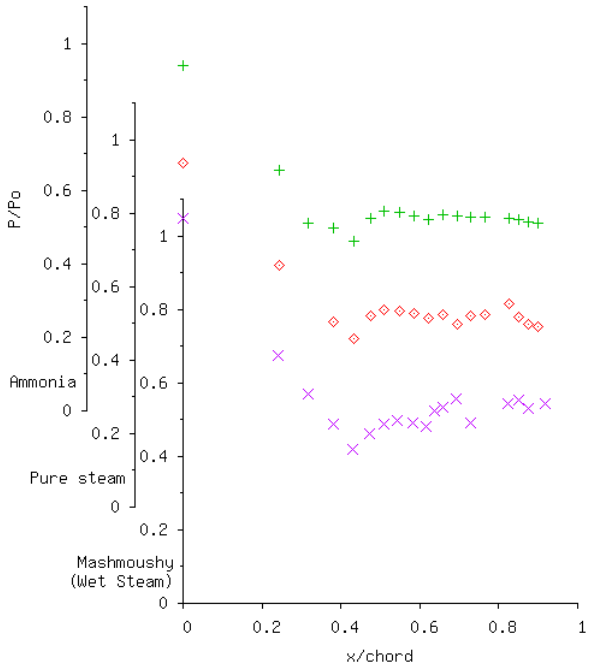

P_{ratio} ≈ 1.83, wetness = 2.16%, radius = 0.127μm

Figure 5.14: Comparison of Mashmoushy's results using wet steam at inlet with ultra-pure steam and steam dosed with 4 ppm ammonia

Key: × indicate results using steam wet at inlet with conventional water treatment

◊ indicate pure steam

+ indicate steam dosed with 4 ppm ammonia

5.5.2 Comparisons of Results at a Pressure Ratio of 2.33

Comparisons of results at a pressure ratio of 2.33 are shown in Figures 5.15a-c. The suction surface pressure distributions are very similar up to approximately 60% of the chord length. In the superheated test (Figure 5.15a) a pressure rise is visible at this position in the profiles from the current work. As explained earlier the inlet superheat used for these tests was not high enough to completely suppress nucleation throughout the expansion and the pressure rise is a result of supercooled steam nucleating and releasing latent heat to the flow. In the case of *Ebrahimi's* test he used a much higher inlet superheat of 45.6 K, which was large enough to almost completely suppress nucleation.

The suction surface pressure distribution for a slightly higher overall pressure ratio of 2.71, with an inlet superheat of 31.1 K, and using ultra-pure steam is shown in Figure 5.16 along with *Ebrahimi's* results for steam superheated at inlet. In this case the higher expansion rate coupled with the slightly higher inlet superheat appears to have mostly suppressed nucleation and the distribution on the suction surface is almost identical to *Ebrahimi's*.

Returning to Figure 5.15, for steam saturated and supercooled at inlet, in the region just downstream of the throat the agreement between all three sets of results is very good. The pressure rise in the zone of rapid condensation is almost exactly the same for all the tests, irrespective of whether the steam was pure, contained ammonia or contained impurities. This suggests that in all three cases the nucleation process was very similar and was dominated by homogeneous nucleation.

Further downstream there are slight differences between the current work and *Ebrahimi's/Mashmoushy's* results. The flow expands smoothly to the outlet in the older tests compared to a faster initial expansion downstream of the zone of rapid condensation followed by diffusion to the outlet in the current tests. These differences may be due to slight variations in inlet stagnation pressure, outlet condenser pressure and overall pressure ratio between the tests. The outlet flow is also sensitive to the position of the tailboards downstream of the blade cascade.

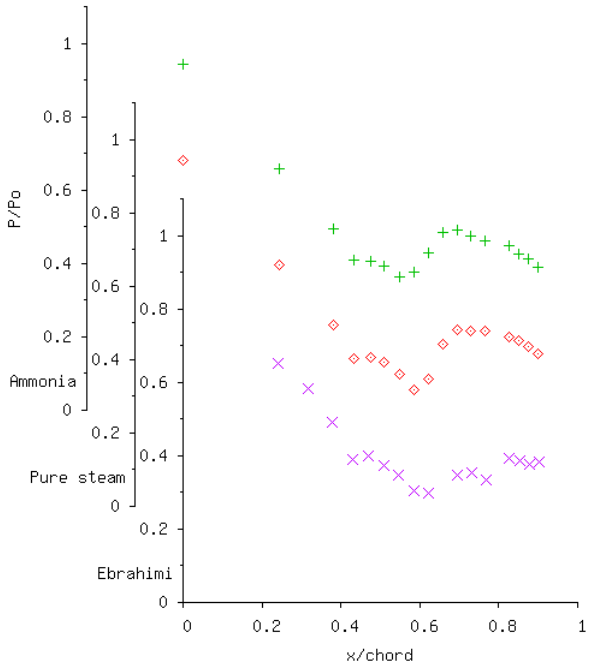

a) $P_{ratio} \approx 2.33$, Superheated

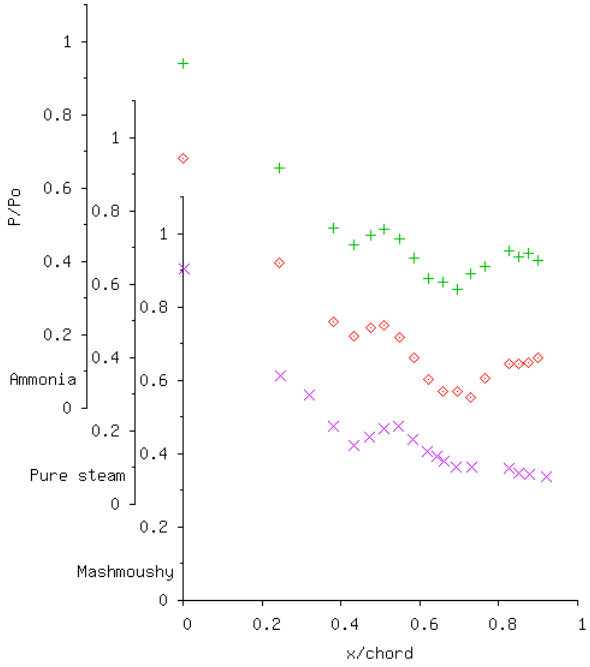

b) $P_{ratio} \approx 2.33$, Saturated

Figure 5.15a-b: Comparison of Ebrahimi/Mashmoushy pressure distributions with ultra-pure steam and steam dosed with 4 ppm ammonia
Key: × indicate results using steam with conventional water treatment
◊ indicate pure steam
+ indicate steam dosed with 4 ppm ammonia

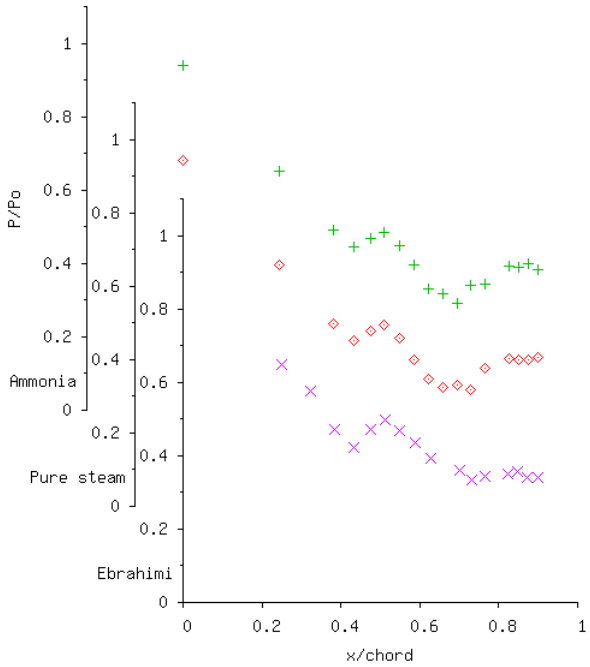

c) $P_{ratio} \approx 2.33$, -10 K Supercool

Figure 5.15c: Comparison of Ebrahimi/Mashmoushy pressure distributions with ultra-pure steam and steam dosed with 4 ppm ammonia
Key: × indicate results using steam with conventional water treatment
◊ indicate pure steam
+ indicate steam dosed with 4 ppm ammonia

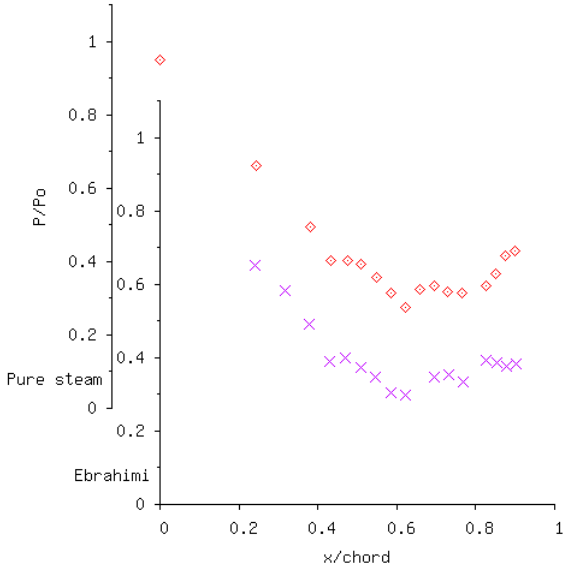

$P_{ratio} = 2.71$, Superheated ($\Delta T = 31.06$ K)

Figure 5.16: Pressure distribution for pure steam with a higher overall pressure ratio and inlet superheat compared with *Ebrahimi's* experimental results.
Key: × indicate *Ebrahimi's* results using steam with conventional water treatment
◊ indicate pure steam

5.5.2.1 Comparisons with Steam Wet at Inlet, P_{ratio} = 2.33

Figures 5.17a-b show comparisons between the suction surface pressure distributions for ultra-pure steam, steam dosed with 4 ppm of ammonia and with *Mashmoushy's* results for steam wet at inlet. In Figure 5.17a *Mashmoushy's* steam had a wetness fraction of 2.17% and contained droplets of approximately 0.123 µm radius. On the suction surface the pressure rise at 40% chord length is slightly smaller for *Mashmoushy's* test. It is flatter and appears to be more like the knee in the pressure profile at the same location for steam superheated at inlet (c.f. Figure 5.15a). For the steam wet at inlet the pressure rise at 40% chord is only 0.023 bar compared to around 0.040 bar in the current tests using pure and dosed steam. The same is true for the comparison in Figure 5.17b, where the wet steam had a similar wetness fraction of 2.09% but contained smaller droplets of 0.046 µm radius. In this case the pressure rise for the test with steam wet at inlet is also 0.023 bar. *Mashmoushy [1994]* attributed the reduction in the pressure rise in the zone of condensation to the influence of the small water droplets at inlet to the cascade. These droplets provide surface for condensation, reducing the limiting supersaturation reached by the flow and therefore inhibiting homogeneous nucleation in the throat region.

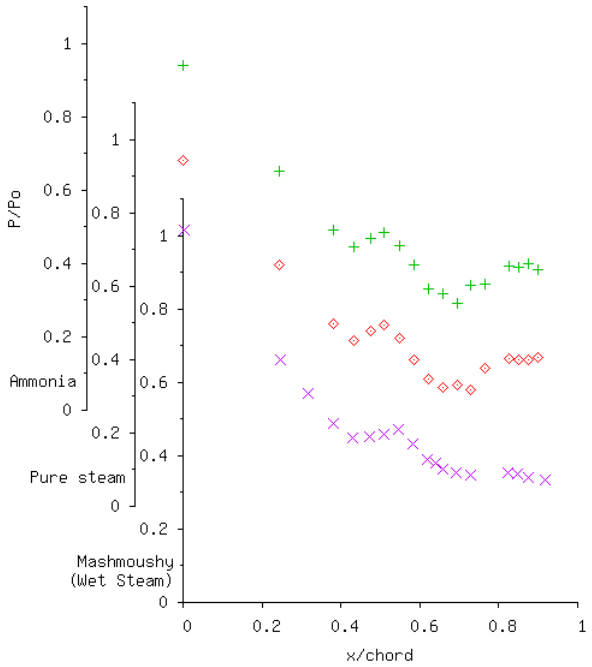

a) P_{ratio} ≈ 2.33, wetness = 2.17%, radius = 0.123µm

Figure 5.17a: Comparison of Mashmoushy's results using wet steam at inlet with ultra-pure steam and steam dosed with 4 ppm ammonia

Key: × indicate results using steam wet at inlet with conventional water treatment

◊ indicate pure steam, + indicate steam dosed with 4 ppm ammonia

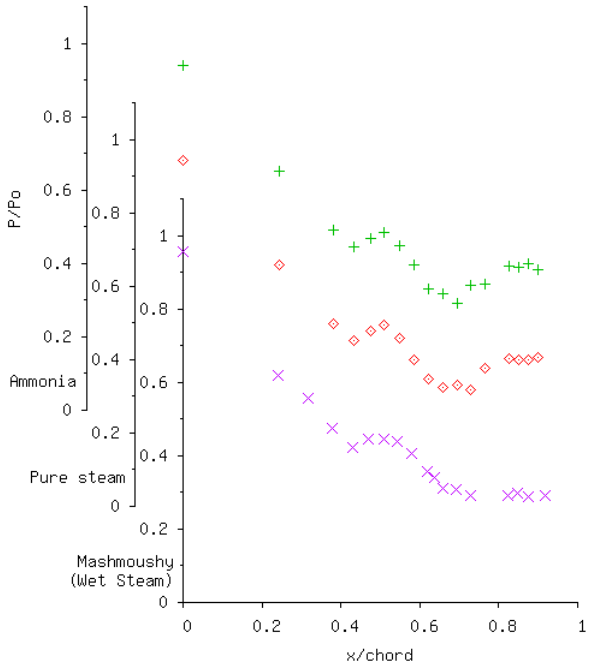

b) $P_{ratio} \approx 2.33$, wetness = 2.09, radius = 0.046μm

Figure 5.17b: Comparison of Mashmoushy's results using wet steam at inlet with ultra-pure steam and steam dosed with 4 ppm ammonia
Key: × indicate results using steam wet at inlet with conventional water treatment
◊ indicate pure steam
+ indicate steam dosed with 4 ppm ammonia

5.5.3 Comparisons of Results at a Pressure Ratio of 3.53

Comparisons of suction surface pressure distributions for steam dry at inlet, at a pressure ratio of 3.53, are shown in Figures 5.18a-c.

In the superheated tests (Figure 5.18a) *Ebrahimi's* expansion ratio is slightly higher compared to the one used in the current work (3.52 compared to 3.05). Consequently the suction surface pressure distributions for ultra-pure steam and for steam dosed with 4 ppm ammonia differ near the trailing edge compared to *Ebrahimi's* distribution. But in the zone of rapid condensation they are identical. All three show the same flat 'knee' in this region.

The suction surface pressure distributions for steam saturated and supercooled at inlet (Figure 5.18b and c) were all run at approximately the same overall pressure ratio and are almost indistinguishable, apart from small differences near the blade outlet. In the zone of rapid condensation the pressure rise in all the tests is very similar. Thus it can be concluded that there is no difference in the nucleation process between the three tests; the flow remains dominated by homogeneous nucleation even when impurities are present.

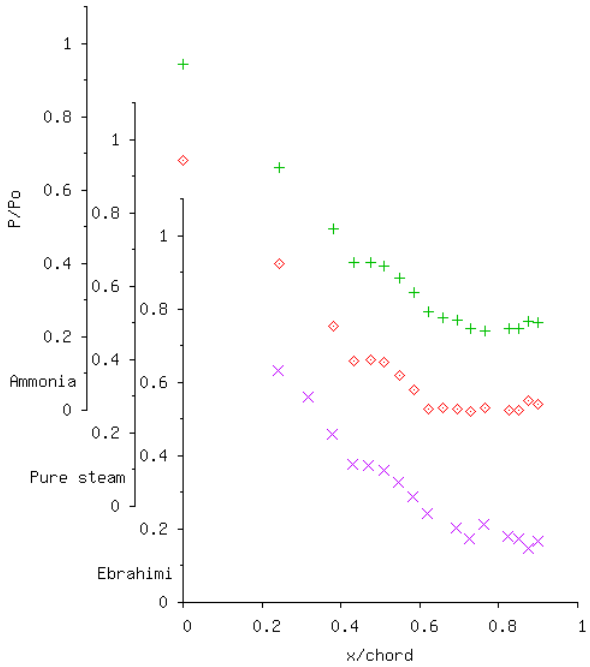

a) $P_{ratio} \approx 3.53$, Superheated

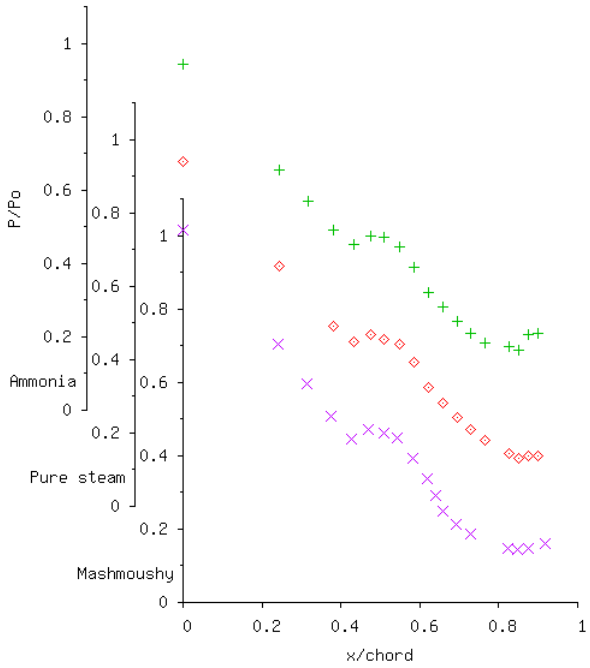

b) $P_{ratio} \approx 3.53$, Saturated

Figure 5.18a-b: Comparison of Ebrahimi/Mashmoushy pressure distributions with ultra-pure steam and steam dosed with 4 ppm ammonia

Key: × indicate results using steam with conventional water treatment

◊ indicate pure steam

+ indicate steam dosed with 4 ppm ammonia

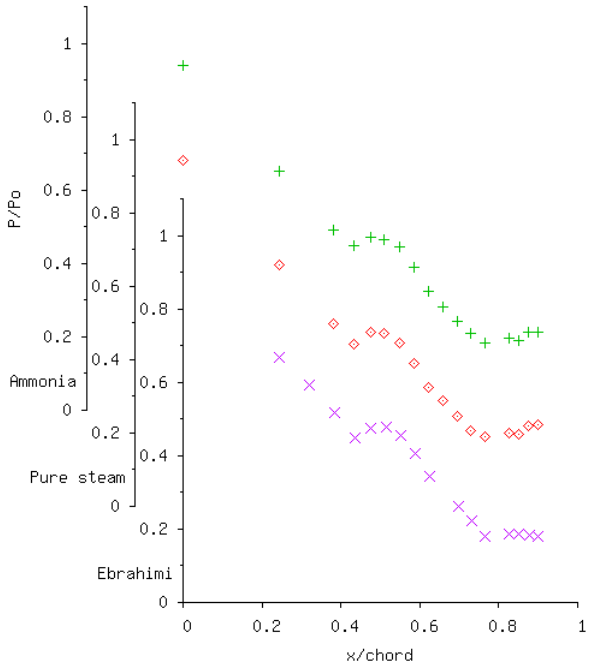

c) $P_{ratio} \approx 3.53$, -10 K Supercool

Figure 5.18c: Comparison of Ebrahimi/Mashmoushy pressure distributions with ultra-pure steam and steam dosed with 4 ppm ammonia
Key: × indicate results using steam with conventional water treatment
◊ indicate pure steam
+ indicate steam dosed with 4 ppm ammonia

5.5.3.1 Comparisons with Steam Wet at Inlet, $P_{ratio} = 3.53$

Figures 5.19a-b show the comparisons with *Mashmoushy's* tests using steam wet at inlet.

In Figure 5.19a the wet steam had a wetness fraction of 1.88% with droplets of 0.189 μm radius. In the zone of rapid condensation there is clearly a difference between the pressure distributions on the suction surface. *Mashmoushy's* pressure distribution looks much more like the superheated distribution in this region (c.f. Figure 5.18a), with a smooth 'knee' in the throat region. In comparison the pressure rise due to the release of latent heat is visible for the two pressure distributions from the current work.

In Figure 5.19b the wet steam had a wetness fraction of 1.82% with smaller droplets of 0.063 μm radius. The pressure distributions in this case are more similar. However the 'knee' in *Mashmoushy's* pressure distribution is flat, corresponding to a pressure rise of 0.017 bar compared to a rise of 0.032 bar for the ultra-pure steam. Downstream the expansions on the suction surface for Figures 5.19a and b are very similar.

The smaller pressure rise in *Mashmoushy's* results is attributed to the presence of small water droplets at inlet to the cascade suppressing homogeneous nucleation in the throat region.

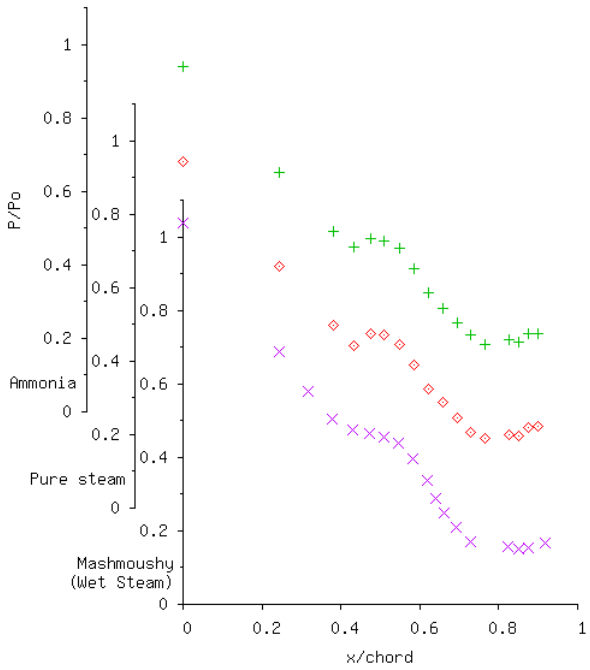

a) $P_{ratio} \approx 3.53$, wetness = 1.88%, radius = 0.189μm

Figure 5.19a: Comparison of Mashmoushy's pressure distributions using wet steam at inlet with ultra-pure steam and steam dosed with 4 ppm ammonia

Key: × indicate results using steam wet at inlet with conventional water treatment

◊ indicate pure steam

+ indicate steam dosed with 4 ppm ammonia

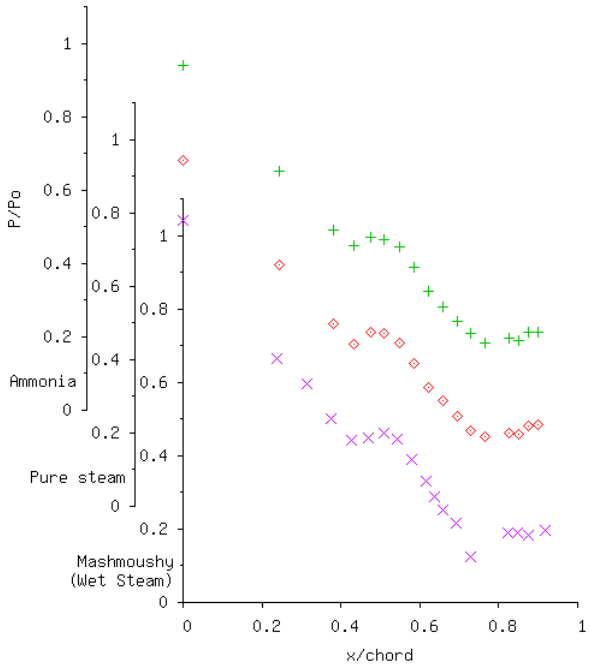

b) $P_{ratio} \approx 3.53$, wetness = 1.82%, radius = 0.063μm

Figure 5.19b: Comparison of Mashmoushy's pressure distributions using wet steam at inlet with ultra-pure steam and steam dosed with 4 ppm ammonia
Key: × indicate results using steam wet at inlet with conventional water treatment
◊ indicate pure steam
+ indicate steam dosed with 4 ppm ammonia

5.6 Discussion

It has been shown by the above comparisons that the similarities between the pressure distributions for ultra-pure steam, for steam dosed with ammonia and for steam containing unknown impurities and dry at inlet, are striking over all the pressure ratios studied. There are some small differences between the pressure distributions, but in the region of interest, the zone of rapid condensation downstream of the blade throat, the distributions are almost identical.

The only major discrepancy between the current pressure distributions and those recorded by previous investigators is the appearance of a pressure rise due to condensation at 60% chord in the superheated tests at a pressure ratio of 2.33. This has been explained by the lower inlet superheat used in the current work, which was not sufficiently high to prevent the flow from supercooling and nucleating during the later part of the expansion through the cascade. There is also evidence of nucleation near the cascade exit in the superheated tests at a pressure ratio of 3.53. Even so, in both these cases the majority of the expansion, including the region around the blade throat, is identical to previous results.

The tests using ultra-pure steam have provided a baseline set of measurements unaffected by the presence of impurities in the steam. It has been shown that for the tests with supersonic outlets, with steam saturated and supercooled at inlet, there is a pressure rise on the suction surface at 40% chord length, just downstream of the blade throat. This pressure rise has been attributed to the release of latent heat occurring when the steam attains a large degree of supercooling upstream of the throat and then nucleates, forming droplets which then grow in the zone of rapid condensation. This process quickly returns the steam to thermodynamic equilibrium and the steam continues to expand or diffuse to match the outlet pressure.

As discussed in chapter 3 the presence of impurities in the steam means that droplets may potentially form at lower degrees of supercooling or even while the steam is saturated. The formation and growth of these droplets would deplete the supercooling. If the number of droplets formed in this way is large and the supercooling is depleted sufficiently so that the flow remains close to thermodynamic equilibrium then homogeneous nucleation will be suppressed and the associated pressure rise in the region of the blade throat would be absent. However if only a small number of droplets are

formed and the expansion is fast then departure of the flow from thermodynamic equilibrium will not be prevented and the steam will nucleate homogeneously when the limiting supersaturation is reached.

In the case of the pressure distributions for steam dosed with ammonia they are almost identical to the baseline set of pressure distributions recorded using ultra-pure steam. Thus it can be concluded that despite very large numbers of ammonia molecules present in the steam, up to 1.3×10^{20} per kg of steam, the ammonia failed to encourage binary nucleation. The flow departed from thermodynamic equilibrium, as it would in the absence of impurities, and the reversion process remained dominated by homogeneous nucleation in the zone of rapid condensation. Increasing the ammonia concentration to 12 ppm, or up to 4.0×10^{20} molecules per kg of steam, did not change matters and the flow was once again dominated by homogeneous nucleation.

Bakhtar and Henson [1999] suggest that to suppress homogeneous nucleation in the expansion through an LP turbine would require of the order of 2×10^{17} impurity particles per kg of steam with a radius of approximately 0.002 μm. It is therefore surprising that the large number of ammonia molecules present in the steam in the current work had no measurable influence on homogeneous nucleation.

As discussed in chapter 3, *Petr and Kolovratnik [1995]* measured the effect of various chemical species on the droplet sizes formed by steam nucleating in a convergent divergent nozzle. An example of their results can be seen in Figure 5.20. The mean droplet size was inferred from light extinction measurements and was normalised by the mean radius for droplets nucleated in pure steam. The normalised radius is plotted against estimated chemical concentration in the figure. Given that the droplet sizes were inferred from light extinction measurements there is some uncertainty in the measurements, this was estimated as ±0.05 and is shown in the figure by the dashed lines. Given this uncertainty the results suggest that ammonia appears to have little or no influence on nucleated droplet size, even for concentrations as large as 100 ppm. In comparison sodium chloride appears to lead to an increase in mean droplet size. These findings concur with the results of this thesis, suggesting that ammonia has very little influence on the nucleation process in condensing flows of steam.

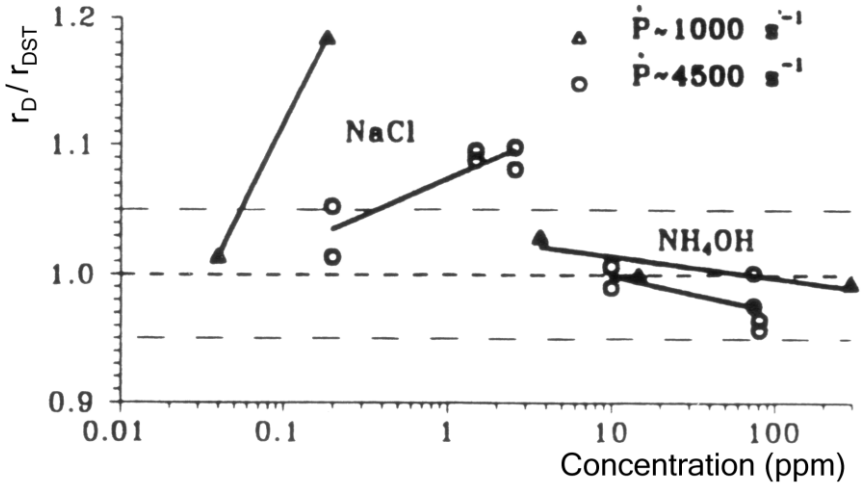

Figure 5.20: Influence of chemical impurities on nucleated droplet radius in a convergent-divergent nozzle. Normalised mean *Sauter* radius is plotted against estimated chemical concentration (from *Petr and Kolovratnik [1995]*)

Comparisons with the results of *Ebrahimi* and *Mashmoushy* for steam dry at inlet, but containing an unknown level of impurities estimated above to be equivalent to 225ppb of ammonia, have shown that these pressure distributions are also very similar to the ultra-pure steam pressure distributions. Thus it can be concluded that the impurities had no influence on the nucleating steam in these studies. As in the case for steam dosed with ammonia, the impurities did not encourage heterogeneous nucleation, or at least not sufficiently to reduce the limiting supersaturation, and the flow remained dominated by homogeneous nucleation. This is not surprising given the relatively low numbers of impurities present in the steam compared to the much higher levels of ammonia used in the current work. This is an important result and means that the baseline of measurements using ultra-pure steam confirms the assumption, made by previous investigators, that their results were uninfluenced by the impurities present in the feed water and steam.

The above conclusions are supported by the observations and theoretical calculations relating to the venturi used by *Mashmoushy* as a wet steam generator (see *Bakhtar, Mashmoushy and Buckley [1997a]*). As already discussed in chapter 3, although droplets did form on the impurities causing problems in the light extinction measurements, the theoretical solutions suggest that the flow was dominated by homogeneous nucleation in the venturi. The effect of the droplets forming on impurities was only to very slightly reduce the limiting supersaturation, but they did not delay the onset of homogeneous nucleation nor change the size of the droplets formed by

homogeneous nucleation. In this case the only significant result of heterogeneous nucleation was the production of a small number of larger droplets with 0.47 μm radius, compared to 0.15 μm radius for the droplets formed by homogeneous nucleation. Rather than influence the thermodynamics of the steam flow through the venturi in *Mashmoushy's* tests, the presence of the impurities was simply a complicating factor. In the case of an operating turbine the presence of larger droplets, containing high concentrations of impurities, probably lead to erosion and corrosion of blades and other surfaces as discussed in chapter 3.

Bakhtar and Henson's [1999] theoretical simulation of nucleating flow through a turbine cascade also supports the above conclusions. Their results were discussed in chapter 3. Despite introducing impurities equivalent to water droplets of 0.15 μm radius and a 0.01% wetness fraction (equivalent to 2.4×10^{12} nucleation sites per kg of steam) they concluded that the impurities had a negligible effect on the reversion process when compared to the same flow containing no impurities. Thus in this case too the reversion process was dominated by homogeneous nucleation, despite the presence of impurities.

In their paper discussing diagnostics of wet steam in LP turbines *Petr and Kolovratnik [2003]* also attempted to model the flow of steam containing impurities. They used three theoretical simulations to produce data for comparison with experimental results from the LP turbines of a 210 MW fossil fuel plant and a 1000 MW PWR nuclear plant. The level of contaminants in the steam was typical of an operating turbine, e.g. downstream of the nuclear LP turbine's L-0 stage the cation conductivity was 0.087 μScm^{-1}. The first theoretical simulation modelled homogeneous nucleation, the second modelled coupled hetero-homogeneous nucleation and the third modelled binary-homogeneous nucleation. Their comparisons with experimental data showed that the homogeneous nucleation model gave the best agreement, supporting the findings of *Bakhtar and Henson [1999]* and of the current work.

Comparisons have also been presented of the current results with *Mashnmoushy's* pressure distributions for steam wet at inlet. These comparisons illustrate the change in suction surface pressure distribution observed when large numbers of small droplets are present upstream of the zone of rapid condensation and inhibit homogeneous nucleation. As reported by *Mashmoushy [1994]* and *Bakhtar, Mashmoushy and Jadayel [1997b]*, in the wet steam tests the population of small droplets, of between 0.2 μm and 0.05 μm radius, at inlet to the blade cascade did inhibit homogeneous nucleation, resulting in a

reduction of the pressure rise on the suction surface, in the zone of rapid condensation. According to *Mashmoushy* in the case of the smallest droplets homogeneous nucleation was suppressed entirely. *Mashmoushy* generated the droplets in a venturi by homogeneous nucleation, but had droplets of the same size and number formed by heterogeneous nucleation on impurities they would have had the same, or similar, effect on the flow. In comparison with the large number of ammonia molecules used in the current work the number of droplets entering the cascade in *Mashmoushy's* tests was only for the order of 10^{15} per kg. Further research is required to ascertain whether a suitable chemical can be found with properties that would inhibit homogeneous nucleation in this way and which would also have properties suitable for use in an operating steam turbine.

In summary the results presented in this chapter have shown that neither the impurities present in earlier tests nor the high concentrations of ammonia added to the steam in the current work have had any effect on the nucleation of the supercooled steam flowing through the blade cascade – the steam condensation process has been dominated by homogeneous nucleation in all cases.

Chapter 6:
Experimental Results – Electrostatics

6.1 Introduction

The second stage of the current investigation has focused on the measurement of electrostatic charge generated in nucleating steam flows. As discussed in chapter 3 electrostatic charges have been measured in LP steam turbine flows by other investigators, e.g. *Hesler and Maurer [1998]*. However, the unique nature of the experimental facility at Birmingham University permits the study of charge in a controlled environment. It has been possible to measure the magnitude and distribution of the charge generated as a result of the first nucleation of droplets during the steam expansion. Also the modifications made to the facility for the current project have made it possible to investigate the effect of pH on the charge.

This chapter summarises electrostatic charge measurements and observations recorded over a range of pressure ratios for ultra-pure steam and for steam dosed with ammonia.

6.2 Range of Measurements

Charge measurements have been recorded using a Langmuir probe mounted upstream and downstream of the cascade of GEC rotor tip blade sections. The position of the upstream probe was fixed. Downstream of the cascade the probe could be traversed across the passage but its position was also fixed for each individual test. To take measurements at a different point it was possible to move the probe across the cascade outlet plane as shown in Figure 6.1. Thus the charge distribution downstream of the two central blade passages has been measured for each set of conditions studied.

The observations were recorded over two pressure ratios, 2.33 and 1.49, using ultra-pure steam, superheated and supercooled at inlet to the cascade. These measurements were repeated for steam dosed with ammonia at 4 ppm and over a limited range at 0.5 ppm at the pressure ratio of 1.49.

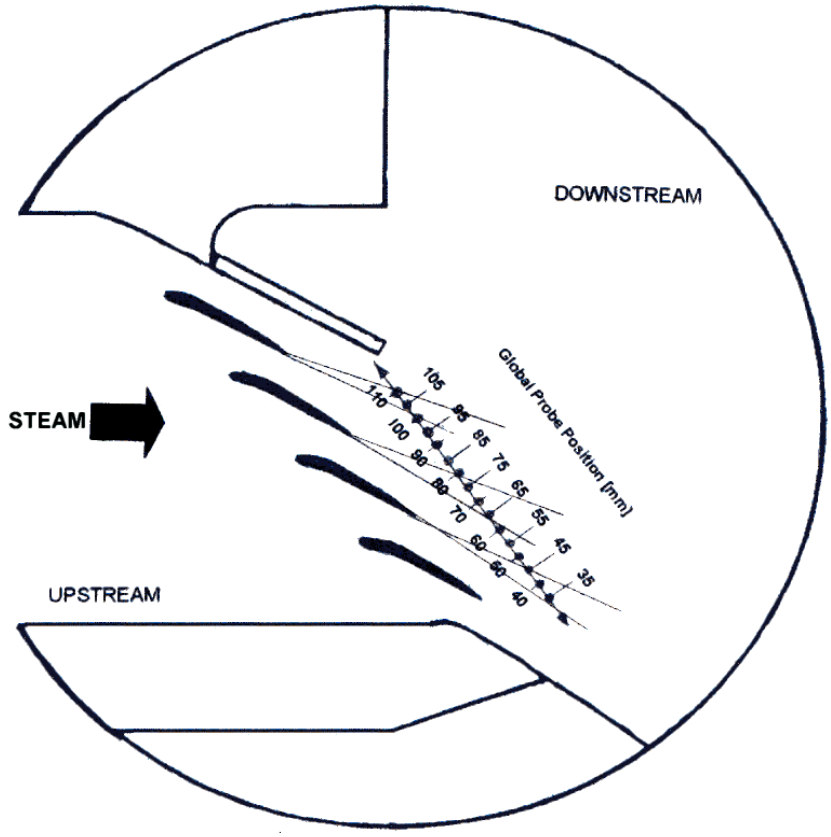

Figure 6.1: Probe positions downstream of the blade cascade.

6.3 Measurements with Ultra-Pure Steam

6.3.1 Probe Leakage Current

Before using the probe to record electrostatic charge in the steam flow it was necessary to gauge the magnitude of any leakage currents. It will be recalled that the operation of the Langmuir probe involves imposing a ramp voltage between the two probe electrodes. This voltage ranged from –10 V to +10 V over one ramp cycle. The ramp cycle period could be adjusted but typically a cycle period of 650 ms was used. The leakage current was measured with the probe mounted in the test section, with a low heater current and no steam flow.

A typical trace of the leakage current flowing between the probe electrodes versus the sampling sequence of the data logger is shown in Figure 6.2. To ensure that the characteristics of the probe were accurately recorded four cycles of the voltage ramp were usually captured. In Figure 6.2 the measured current shown is the sum of leakage through the probe and leads, some noise and a parasitic signal resulting from cross coupling in the

amplifier circuit. In this case the magnitude of the leakage current is of the order of ±50 nA. This was typical of the leakage currents measured throughout the project. It should also be noted that the zero offset for the circuit has not been corrected. It will be seen from the results to be presented that the currents measured in flowing steam were approximately three orders of magnitude larger than the leakage current through the probe. In light of this it was decided to allow a small zero offset in the readings taken in flowing steam and to later correct the measurements using the zero offset measured with low heating and no steam flow. When running blow-down tests using steam, measurements of the leakage current with no steam flow were repeated several times interspersed with the measurements with steam, to ensure that the characteristics of the probe remained unchanged.

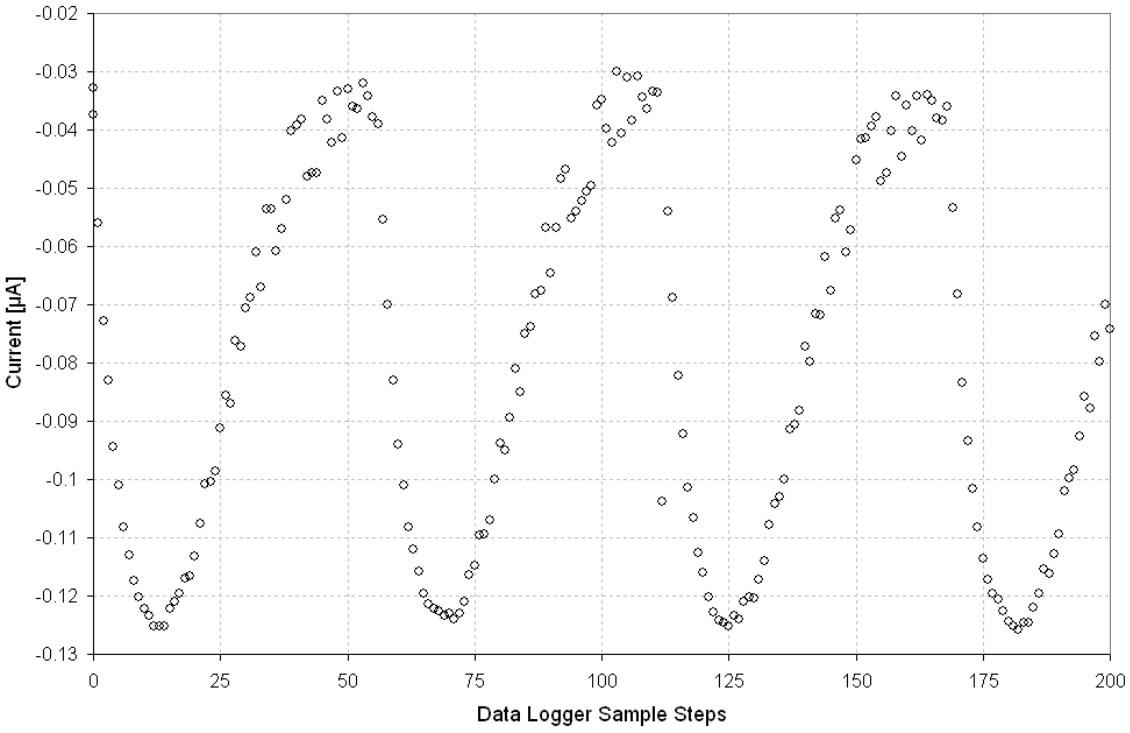

Figure 6.2: Typical trace of probe leakage current versus voltage ramp step number

6.3.2 Measurements at a Pressure Ratio of 2.33

Typical sets of probe current readings for three different traverse locations downstream of the blade cascade and for an overall pressure ratio of 2.33, with steam supercooled at inlet, are shown in Figure 6.3. The probe current was recorded over at least four voltage ramp cycles in order to capture any relation between the current and ramp

voltage. In the figure the probe current in micro-amps is plotted against the data logger sample number. It can be seen from the figure that the probe offset current at all three locations is extremely high in comparison with the currents due to the imposed Langmuir probe voltage ramp, which were expected to be of the order of 10^{-9} A. Indeed to record these readings the amplifier circuit had to be modified. The measurements show fluctuations as a result of turbulence in the steam flow and some general drift with time. These local variations are also larger than the probe currents expected due to the imposed ramp voltage.

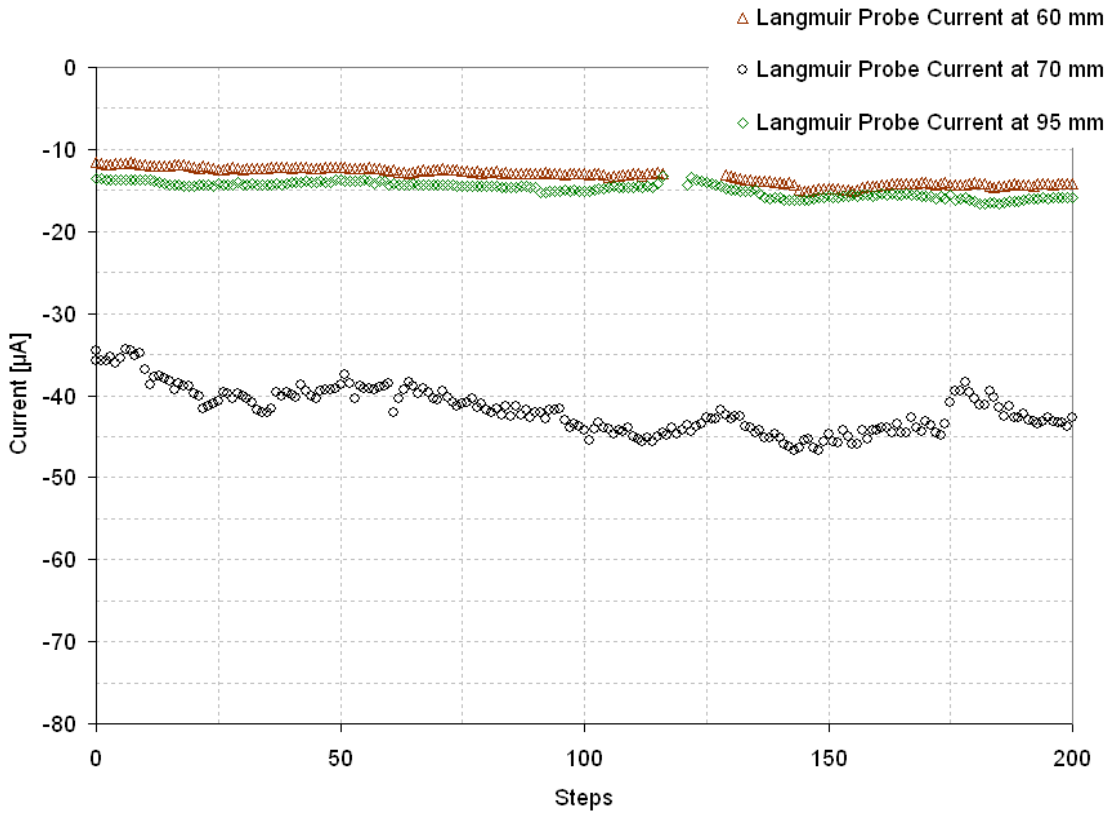

Figure 6.3: Typical Langmuir probe traces obtained at three different traverse positions downstream of the cascade in pure steam, supercooled at inlet. P_{ratio} = 2.33

The variations of mean probe offset current with distance in the pitch direction, downstream of the cascade, have been plotted in Figure 6.4 for steam superheated and supercooled at inlet. Shaded squares represent the offset currents measured in the flow for steam superheated at inlet, and shaded circles represent the offset currents measured in the flow for steam supercooled at inlet. The upstream mean offset currents are shown by single shaded symbols to the top right of the figure. The downstream mean offset currents

are plotted versus the probe's traverse position across the two central blade passages and are shown with the symbols connected by lines.

In addition to the measurements of offset current it was also possible to connect either the probe tip electrode or reference surface electrode directly to ground via a large value resistor and measure the potential difference across the resistor. The measured potential was a result of charge collecting on the probe electrode and then flowing from there to ground. These 'direct' measurements of current are also plotted in Figure 6.4. For the downstream measurements unfilled squares and circles are used for steam superheated and supercooled at inlet respectively. For the upstream measurements unfilled squares and circles with crosses are used.

It can be seen from the figure that upstream of the cascade, for both steam inlet conditions, the probe offset current is very small. This indicates that the overall level of space charge in this region is very small. This is consistent with the results of all other investigators, who have observed that dry steam contains negligible charge. Downstream of the cascade, in the case of the steam superheated at inlet, the offset currents are also very small. This is expected since the superheated steam will remain dry throughout the expansion. In the case of steam supercooled at inlet, which will nucleate just downstream of the blade throat, much larger negative currents can be observed. This is also consistent with the results of other investigators who have found negative charge to be present along most of the blade axis in the wet stages of LP turbines. Returning to Figure 6.4 the largest negative currents occur at positions corresponding to the core of the blade wakes. The regions of smaller negative current correspond to positions in the main part of the blade passage.

The same trends seen in the offset current measurements are apparent in the 'direct' current measurements. Upstream of the cascade the current is very small, as is the current downstream of the cascade for the test using steam superheated at inlet. In the case of nucleating steam downstream of the cascade the 'direct' currents are negative and are larger in the wake region than in the main passage.

The reasonable agreement between the 'direct' current measurements and the offset current measurements is taken as an indication that the probe receives a net charge from the flow. When the instrument is used as a Langmuir probe it still receives charge

from the flow. This charge then finds a way to ground through the insulation of the amplifier circuit and is sensed by the amplifier and shown as an offset current.

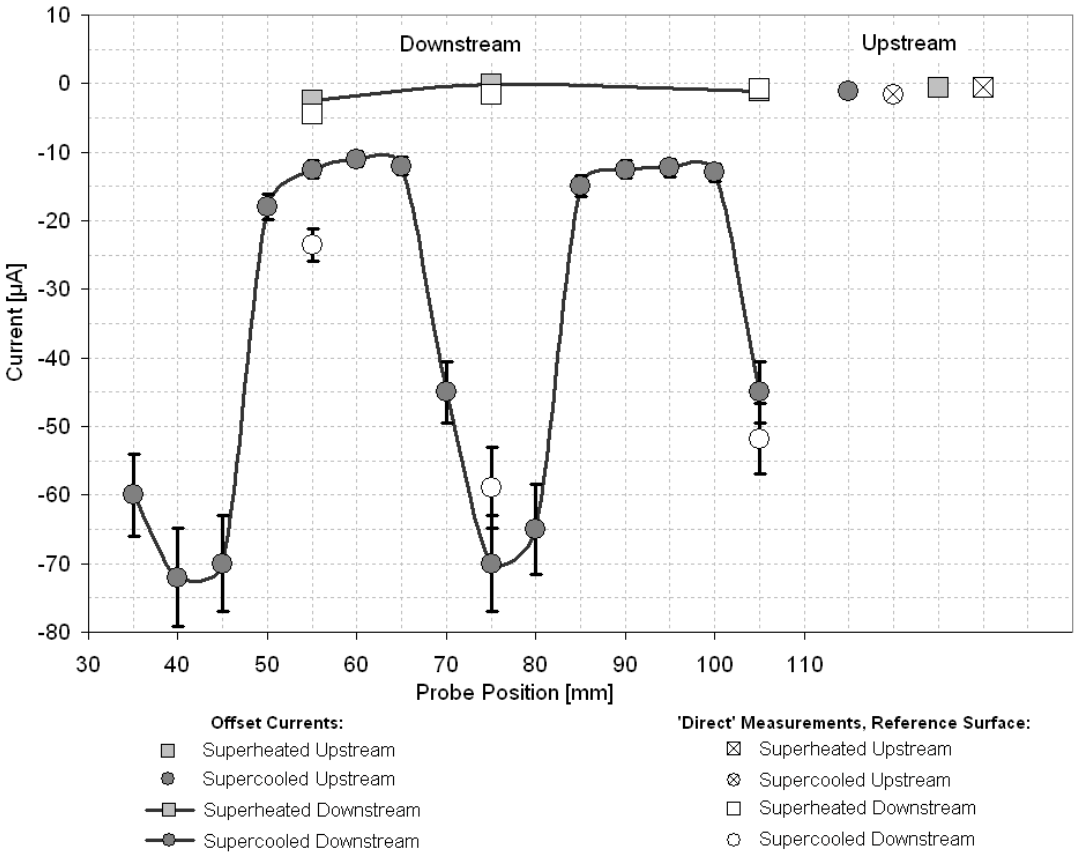

Figure 6.4: Variations in the mean values of probe offset and direct currents for pure steam. P_{ratio} = 2.33

6.3.3 Measurements at a Pressure Ratio of 1.49

Since the flow at outlet from the cascade at an overall pressure ratio of 2.33 was supersonic and contained shock waves it was thought that the level of turbulence would be lower with a subsonic outlet. For this reason the above measurements were repeated at an overall pressure ratio of 1.49. At this pressure ratio the outlet isentropic Mach number is approximately 0.8.

Typical Langmuir probe traces, obtained at three different traverse positions downstream of the cascade are shown in Figure 6.5. Comparing with the traces at a pressure ratio of 2.33 (Figure 6.3) there is very little difference in the fluctuations between the two pressure ratios, if anything they are slightly worse at 1.49.

The mean offset currents and 'direct' currents for steam superheated and supercooled at inlet for a pressure ratio of 1.49 are plotted in Figure 6.6. The same symbols are used as in Figure 6.4. The offset currents follow the same trends as those measured at the higher pressure ratio. The only major difference between the two pressure ratios is that in the case of flow supercooled at inlet the currents downstream of the cascade are smaller in the main blade passage at the lower pressure ratio. In the wake region the magnitude of the offset currents are very similar in both cases. The 'direct' currents are in reasonable agreement with the offset currents.

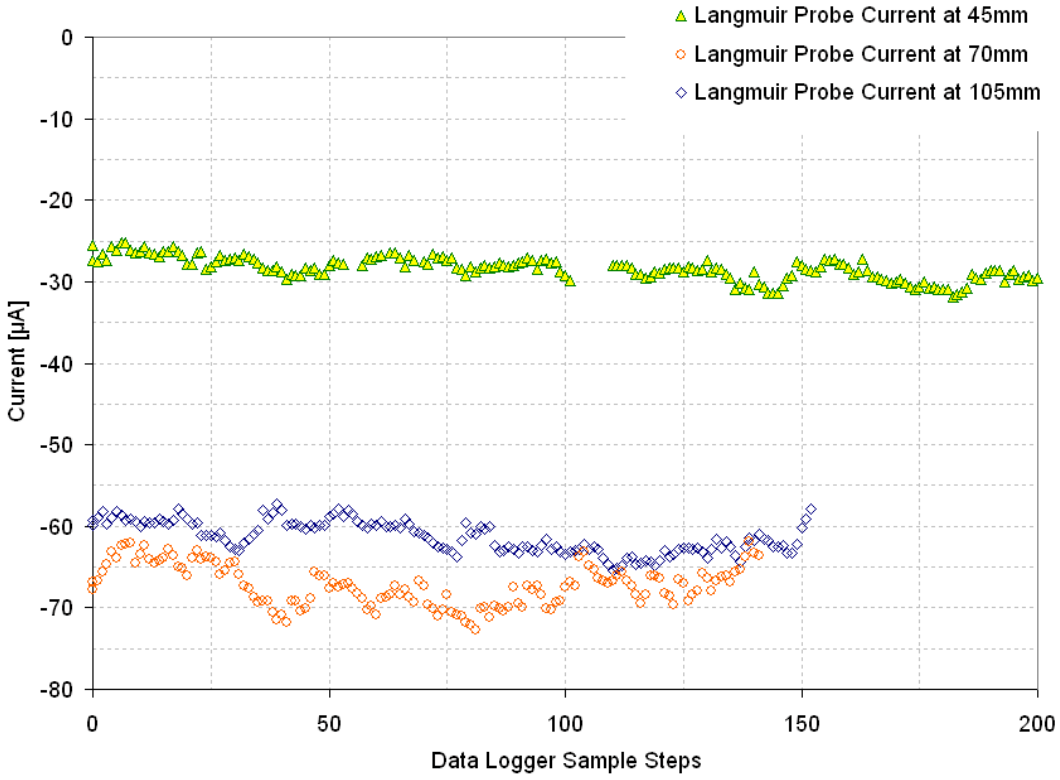

Figure 6.5: Typical Langmuir probe traces obtained at three different traverse positions downstream of the cascade in pure steam, supercooled at inlet. P_{ratio} = 1.49

The relatively large negative currents measured in the wakes at both pressure ratios are taken as an indication that for steam supercooled or wet the main charge generation mechanism is a result of the flow interacting with water films which form on the blade surfaces. The presence of these water films appears to result in charge on the droplets downstream of the wakes.

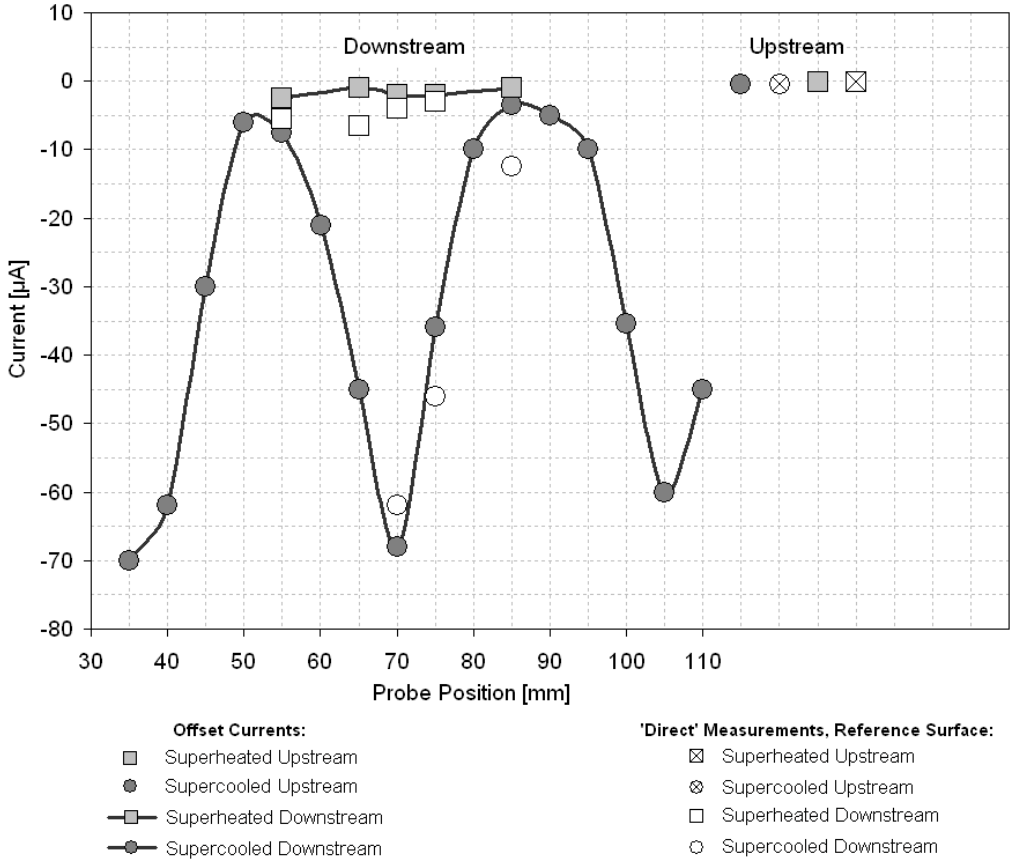

Figure 6.6: Variations in the mean values of probe offset and direct currents for pure steam. P_{ratio} = 1.49

To investigate this possibility further, a set of measurements were carried out downstream of the blades at a pressure ratio of 1.49 with steam *slightly* superheated at inlet (by approximately 10 K). Given this small superheat the flow will supercool as it expands, but not sufficiently to nucleate. However steam will condense on the surface of the blades forming thin water films, which should then result in the generation of charge in the blade wakes.

The measurements of offset and 'direct' currents for steam with a small inlet superheat are shown in Figure 6.7. The measurements for steam supercooled at inlet are also shown for comparison. The same symbols are used as above. It can be seen that although the currents in the main flow region are very small, as expected for the superheated case, the currents in the wake region are larger and negative. This result supports the hypothesis that water films on the blade surfaces are contributing to the space charge in the wake regions.

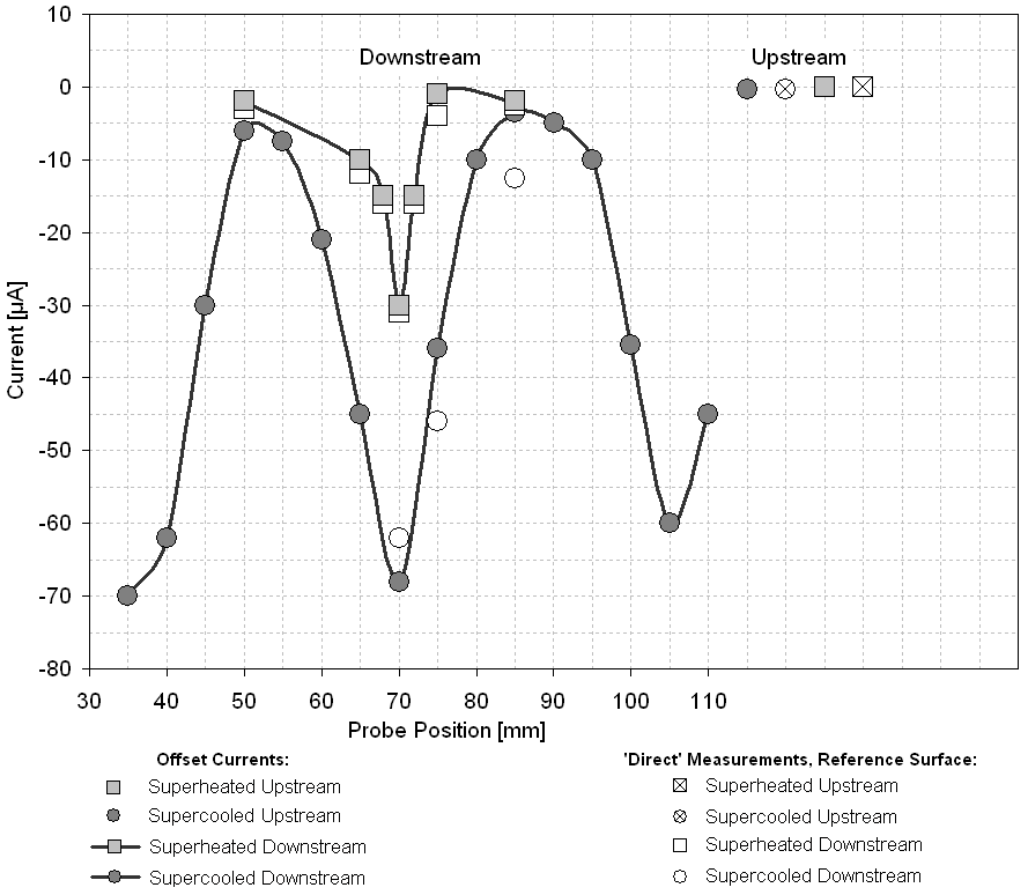

Figure 6.7: Variations in the mean values of probe offset and direct currents for pure steam with a small superheat. P_{ratio} = 1.49

6.3.4 Tabulated Data

The extracted data from the above measurements for ultra-pure steam are summarised in Tables 6.1, 6.2 and 6.3. In these tables the data labelled 'Offset' are the offset currents recorded from the Langmuir probe signal. The data labelled 'Direct' are the direct currents and voltages measured when one of the probe electrodes was connected to ground. For these measurements subscript 'tip' refers to currents and voltages from the probe tip electrode and subscript 'ref' refers to currents and voltages from the probe reference surface.

Table 6.1: Measured currents and voltages for pure steam, P_{ratio} = 2.33

	P_{ratio} = 2.33, Pure Steam DOWNSTREAM									
	Supercooled					**Superheated**				
Probe Position [mm]	**Offset [μA]**	**Direct V_{ref} [Volt]**	**Direct I_{ref} [μA]**	**Direct V_{tip} [Volt]**	**Direct I_{tip} [μA]**	**Offset [μA]**	**Direct V_{ref} [Volt]**	**Direct I_{ref} [μA]**	**Direct V_{tip} [Volt]**	**Direct I_{tip} [μA]**
35	-60.00									
40	-72.00									
45	-70.00									
50	-18.00									
55	-12.50	-236	-32.60	-3.00	-0.30	-2.50	-45	-4.50	-3.0	-0.30
60	-11.00									
65	-12.00									
70	-45.00									
75	-70.00	-590	-59.00	-210	-21.00	-0.10	-16.6	-1.66	-2.3	-0.23
80	-65.00									
85	-15.00									
90	-12.50									
95	-12.30									
100	-13.00									
105	-45.00	-518	-51.8	-150	-15.00	-1.10	-7.8	-0.78	-2.9	-0.29
110										
	UPSTREAM									
	Supercooled					**Superheated**				
Fixed Position	**Offset [μA]**	**Direct V_{ref} [Volt]**	**Direct I_{ref} [μA]**	**Direct V_{tip} [Volt]**	**Direct I_{tip} [μA]**	**Offset [μA]**	**Direct V_{ref} [Volt]**	**Direct I_{ref} [μA]**	**Direct V_{tip} [Volt]**	**Direct I_{tip} [μA]**
	-1.10	-16	-1.60	-0.5	-0.05	-0.60	-6.0	-0.60	-2.0	-0.20

Table 6.2: Measured currents and voltages for pure steam, P_{ratio} = 1.49

	P_{ratio} = 1.49, Pure Steam DOWNSTREAM									
	Supercooled					**Superheated**				
Probe Position [mm]	**Offset [μA]**	**Direct V_{ref} [Volt]**	**Direct I_{ref} [μA]**	**Direct V_{tip} [Volt]**	**Direct I_{tip} [μA]**	**Offset [μA]**	**Direct V_{ref} [Volt]**	**Direct I_{ref} [μA]**	**Direct V_{tip} [Volt]**	**Direct I_{tip} [μA]**
35	-70.00									
40	-62.00									
45	-30.00									
50	-6.00									
55	-7.50					-2.50	-55	-5.50	-3	-0.30
60	-21.00									
65	-45.00					-1.00	-65	-6.50	-4	-0.40
70	-68.00	-620	-62.00	-180	-18.00	-2.05	-40	-4.00	-3	-0.30
75	-36.00	-460	-46.00	-132	-13.20	-2.03	-30	-3.00	-10	-1.00
80	-10.00									
85	-3.50	-135	-13.50	-30	-3.00	-1.0				
90	-5.00									
95	-10.00									
100	-35.50									
105	-60.00									
110	-45.00									
	UPSTREAM									
	Supercooled					**Superheated**				
Fixed Position	**Offset [μA]**	**Direct V_{ref} [Volt]**	**Direct I_{ref} [μA]**	**Direct V_{tip} [Volt]**	**Direct I_{tip} [μA]**	**Offset [μA]**	**Direct V_{ref} [Volt]**	**Direct I_{ref} [μA]**	**Direct V_{tip} [Volt]**	**Direct I_{tip} [μA]**
	-0.40	-4.0	-0.40	-1.0	-0.1	-0.05	-0.5	-0.05	-0.1	-0.01

Table 6.3: Measured currents and voltages for pure steam with a small superheat, P_{ratio} = 1.49

	P_{ratio} = 1.49, Pure Steam DOWNSTREAM									
	Supercooled					**Slightly Superheated**				
Probe Position [mm]	**Offset [µA]**	**Direct V_{ref} [Volt]**	**Direct I_{ref} [µA]**	**Direct V_{tip} [Volt]**	**Direct I_{tip} [µA]**	**Offset [µA]**	**Direct V_{ref} [Volt]**	**Direct I_{ref} [µA]**	**Direct V_{tip} [Volt]**	**Direct I_{tip} [µA]**
35	-70.00									
40	-62.00									
45	-30.00									
50	-6.00					-2	-30	-3.0	-10	-1.0
55	-7.50									
60	-21.00									
65	-45.00					-10	-120	-12.0	-10	-1.0
68						-15	-160	-16.0	-15	-1.5
70	-68.00	-620	-62.0	-180	-18.0	-30	-310	-31.0	-11	-1.1
72						-15	-160	-16.0	-4	-0.4
75	-36.00	-460	-46.0	-132	-13.2	-1	-40	-4.0	-10	-1.0
80	-10.00									
85	-3.50	-125	-12.5	-30	-3.0	-2	-25	-2.5	-12	-1.2
90	-5.00									
95	-10.00									
100	-35.50									
105	-60.00									
110	-45.00									
	UPSTREAM									
	Supercooled					**Slightly Superheated**				
Fixed Position	**Offset [µA]**	**Direct V_{ref} [Volt]**	**Direct I_{ref} [µA]**	**Direct V_{tip} [Volt]**	**Direct I_{tip} [µA]**	**Offset [µA]**	**Direct V_{ref} [Volt]**	**Direct I_{ref} [µA]**	**Direct V_{tip} [Volt]**	**Direct I_{tip} [µA]**
	-0.5	-4	-0.4	-1	-0.1	-0.05	-0.5	-0.05	-0.1	-0.01

6.4 Measurements with Steam Dosed with Ammonia

To investigate the influence of pH on charge present in nucleating steam the measurements with ultra-pure steam were repeated for steam dosed with ammonia. At pressure ratios of 2.33 and 1.49 the steam was dosed with approximately 4 ppm of ammonia, which produces a pH of 9.7. A more limited number of measurements were also taken at a pressure ratio of 1.49 for steam dosed with 0.5 ppm of ammonia, which produces a pH of 9.2. These measurements are described in the following sections.

6.4.1 Measurements at a Pressure Ratio of 2.33

The measured offset currents and directly measured probe to ground currents at a pressure ratio of 2.33 are shown in Figure 6.8 for steam dosed with 4 ppm of ammonia. The symbols in the figure have the same meaning as those used previously.

It can be seen that the currents upstream of the cascade, are small and very similar to those measured in pure steam. The same is true for the currents measured downstream of the cascade for steam superheated at inlet. In the case of steam supercooled at inlet, downstream of the cascade the form of the current distribution is the same as for pure steam. Although the offset currents are still negative and show a large increase in the wake regions, the current peaks are smaller by around 10 μA in the wake regions and by around 5 μA in the main flow regions compared to the same peaks for ultra-pure steam. In the case of the directly measured currents, although they are generally in good agreement with the offset currents, the peak in the wake, measured at a probe position of 75 mm, is smaller than the corresponding offset current by around 20 μA. This is a somewhat anomalous result given that in all the other tests there is much better agreement between the probe offset currents and ‘direct’ currents.

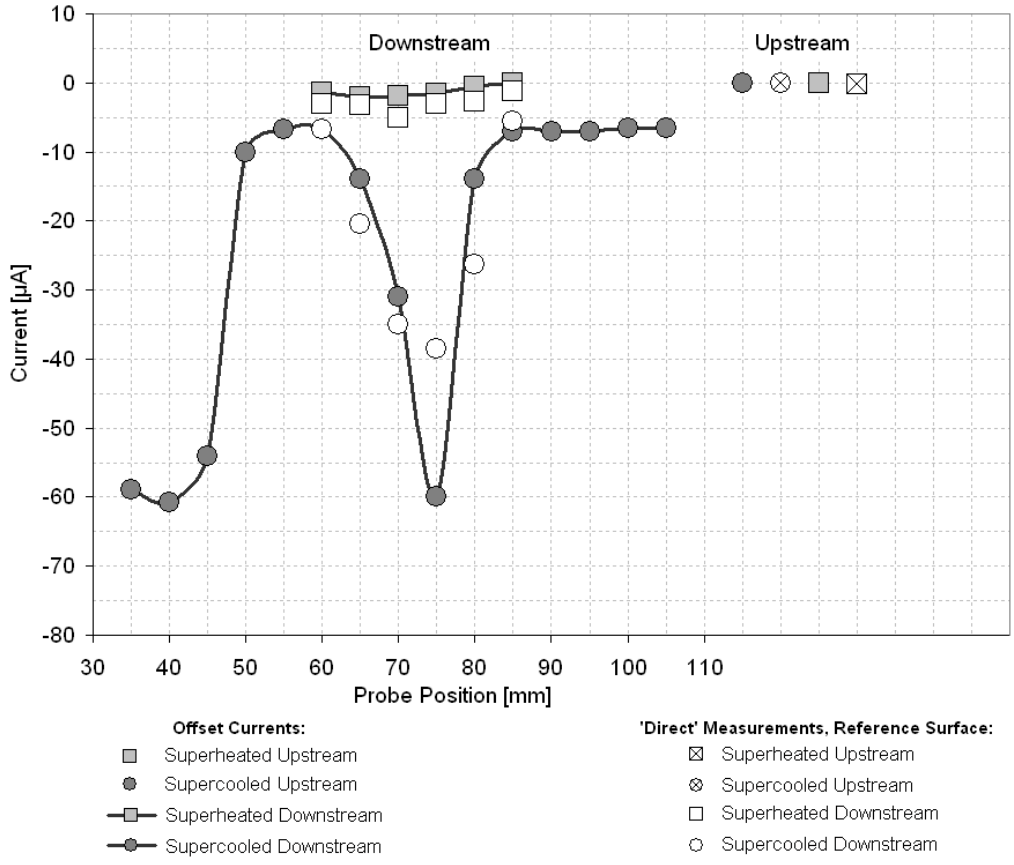

Figure 6.8: Variations of mean values of offset and direct currents for steam dosed with 4 ppm ammonia, P_{ratio} = 2.33

6.4.2 Measurements at a Pressure Ratio of 1.49

The measured offset currents and directly measured probe to ground currents for a pressure ratio of 1.49 are shown in Figure 6.9 for steam dosed with 4 ppm of ammonia. As usual the symbols have the same meaning as those used previously.

The trends in measured currents are again very similar to those for ultra-pure steam. In the case of the downstream currents for steam supercooled at inlet the peaks in the wake regions are slightly smaller than the corresponding peaks for ultra-pure steam, by around 5 µA.

The directly measured currents are in better agreement with the offset currents than at the pressure ratio of 2.33 for steam dosed with ammonia.

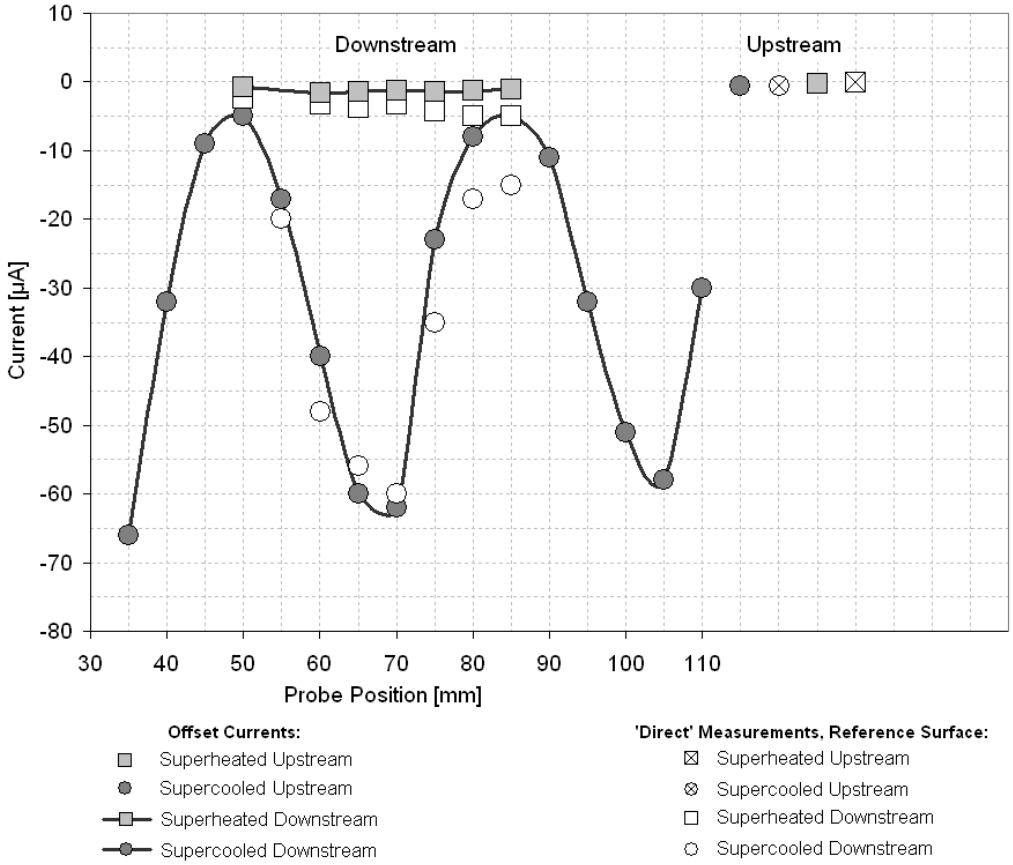

Figure 6.9: Variations of mean values of offset and direct currents for steam dosed with 4 ppm ammonia, P_{ratio} = 1.49

Measurements of offset and direct currents for steam dosed with 0.5 ppm of ammonia at a pressure ratio of 1.49 are shown in Figure 6.10. In this case no measurements were made downstream of the cascade for steam superheated at inlet. Otherwise the symbols have the same meaning as usual.

For steam supercooled at inlet the measured offset currents again show the same trends as in all the previous results. However in this case the negative current peak in the wake regions is lower than at the same pressure ratio with ultra-pure steam and with steam dosed with 4 ppm of ammonia. Compared to the peaks for ultra-pure steam the peaks in this case are around 15 μA smaller. They are around 10 μA smaller than the same peaks for steam dosed with 4 ppm of ammonia.

The agreement between the offset and direct current measurements is reasonable.

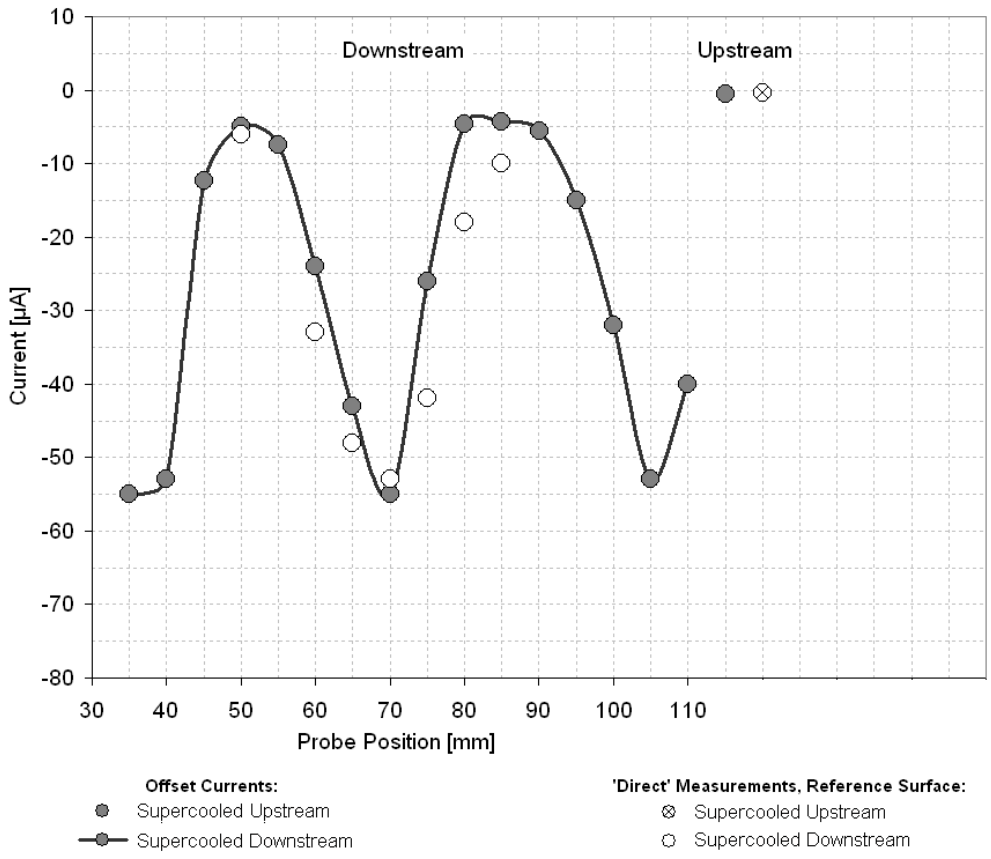

Figure 6.10: Variations of mean values of offset and direct currents for steam dosed with 0.5 ppm ammonia, P_{ratio} = 1.49

6.4.3 Tabulated Data

The extracted data from the above measurements for steam dosed with ammonia are summarised in the following three tables.

Table 6.4: Measured currents and voltages for steam dosed with 4 ppm ammonia, P_{ratio} = 2.33

	R = 2.33, 4ppm Ammonia - Dosed Steam DOWNSTREAM									
	Supercooled					**Superheated**				
Probe Position [mm]	**Offset [µA]**	**Direct V_{ref} [Volt]**	**Direct I_{ref} [µA]**	**Direct V_{tip} [Volt]**	**Direct I_{tip} [µA]**	**Offset [µA]**	**Direct V_{ref} [Volt]**	**Direct I_{ref} [µA]**	**Direct V_{tip} [Volt]**	**Direct I_{tip} [µA]**
35	-59.00									
40	-60.70									
45	-54.00									
50	-10.00									
55	-6.80									
60	-6.80	-67	-6.70	-1.00	-0.10	-1.30	-30	-3.00	-8	-0.80
65	-14.00	-205	-20.50	-1.00	-0.10	-2.00	-32	-3.20	-10	-1.00
70	-31.00	-350	-35.00	-12.75	-1.27	-1.80	-50	-5.00	-16	-1.60
75	-60.00	-385	-38.50	-1.00	-0.10	-1.50	-30	-3.00	-10	-1.00
80	-14.00	-263	-26.30	-10.10	-1.01	-0.50	-27	-2.70	-10	-1.00
85	-7.00	-56	-5.60	-0.52	-0.05	-0.10	-12.6	-1.26	-1.5	-0.15
90	-7.00									
95	-7.00									
100	-6.50									
105	-6.50									
110										
	UPSTREAM									
	Supercooled					**Superheated**				
Fixed Position	**Offset [µA]**	**Direct V_{ref} [Volt]**	**Direct I_{ref} [µA]**	**Direct V_{tip} [Volt]**	**Direct I_{tip} [µA]**	**Offset [µA]**	**Direct V_{ref} [Volt]**	**Direct I_{ref} [µA]**	**Direct V_{tip} [Volt]**	**Direct I_{tip} [µA]**
	0.00	-1	-0.10	-0.10	0.00	-0.10	-2	-0.20	-1.5	-0.15

Table 6.5: Measured currents and voltages for steam dosed with 4 ppm ammonia, P_{ratio} = 1.49

	R = 1.49, 4ppm Ammonia - Dosed Steam DOWNSTREAM									
	Supercooled					Superheated				
Probe Position [mm]	**Offset [µA]**	**Direct V_{ref} [Volt]**	**Direct I_{ref} [µA]**	**Direct V_{tip} [Volt]**	**Direct I_{tip} [µA]**	**Offset [µA]**	**Direct V_{ref} [Volt]**	**Direct I_{ref} [µA]**	**Direct V_{tip} [Volt]**	**Direct I_{tip} [µA]**
35	-66.00									
40	-32.00									
45	-9.00									
50	-5.00	-15.0	-1.50	-15	-1.50	-0.75	-25.2	-2.52	-6.7	-0.67
55	-17.00									
60	-40.00	-480	-48.00	-120	-12.00	-1.60	-33.1	-3.31	-8.8	-0.88
65	-60.00	-560	-56.00	-204	-20.40	-1.40	-37.3	-3.73	-13.6	-1.36
70	-62.00	-600	-60.00	-155	-15.50	-1.20	-32.2	-3.22	-8.0	-0.80
75	-23.00	-350	-35.00	-50	-5.00	-1.50	-43.0	-4.30	-10.0	-1.00
80	-8.00	-170	-17.00	-15	-1.50	-0.30	-49.0	-5.00	-14.0	-1.40
85	-5.00	-150	-15.00	-20	-2.00	0.10	-49.0	-6.00	-28.0	-2.80
90	-11.00									
95	-32.00									
100	-51.00									
105	-58.00									
110	-30.00									
	UPSTREAM									
	Supercooled					Superheated				
Fixed Position	**Offset [µA]**	**Direct V_{ref} [Volt]**	**Direct I_{ref} [µA]**	**Direct V_{tip} [Volt]**	**Direct I_{tip} [µA]**	**Offset [µA]**	**Direct V_{ref} [Volt]**	**Direct I_{ref} [µA]**	**Direct V_{tip} [Volt]**	**Direct I_{tip} [µA]**
	-0.62	-6.7	-0.67	-0.9	-0.09	-0.20	-0.5	-0.05	-0.5	-1.05

Table 6.6: Measured currents and voltages for steam dosed with 0.5 ppm ammonia, P_{ratio} = 1.49

	R = 1.49, 0.5ppm Ammonia - Dosed Steam DOWNSTREAM									
	Supercooled					Superheated				
Probe Position [mm]	Offset [µA]	Direct V_{ref} [Volt]	Direct I_{ref} [µA]	Direct V_{tip} [Volt]	Direct I_{tip} [µA]	Offset [µA]	Direct V_{ref} [Volt]	Direct I_{ref} [µA]	Direct V_{tip} [Volt]	Direct I_{tip} [µA]
35	-55.00									
40	-53.00									
45	-12.30									
50	-5.00	-60	-6.00	-10	-1.00					
55	-7.50					-2.50	-55	-5.50	-3	-0.30
60	-24.00	-330	-33.00	-100	-10.00					
65	-43.00	-480	-48.00	-200	-20.00	-1.00	-65	-6.50	-4	-0.40
70	-55.00	-530	-53.00	-170	-17.00	-2.05	-40	-4.00	-3	-0.30
75	-26.00	-420	-42.00	-80	-8.00	-2.03	-30	-3.00	-10	-1.00
80	-4.60	-180	-18.00	-20	-2.00					
85	-4.30	-100	-10.00	-20	-2.00	-1.00				
90	-5.50									
95	-15.00									
100	-32.00									
105	-53.00									
110	-40.00									
	UPSTREAM									
	Supercooled					Superheated				
Fixed Position	Offset [µA]	Direct V_{ref} [Volt]	Direct I_{ref} [µA]	Direct V_{tip} [Volt]	Direct I_{tip} [µA]	Offset [µA]	Direct V_{ref} [Volt]	Direct I_{ref} [µA]	Direct V_{tip} [Volt]	Direct I_{tip} [µA]
	-0.40	-4	-0.40	-1	-0.09	-0.05	-0.5	-0.05	-0.5	-0.05

6.5 Experimental Uncertainty

With reference to Figure 6.3, showing the Langmuir probe current traces at a pressure ratio of 2.33, it can be seen that there are some fluctuations in the measured currents especially at a probe traverse position of 70 mm. There are also some fluctuations in the traces at a pressure ratio of 1.49. In general the measurements from the first and last voltage ramp cycles were disregarded and only the data from the middle two cycles have been used in further analysis.

In the case of the trace at a probe position of 70 mm in Figure 6.3 all the measurements fall within ±10% of the mean value. The variation of the individual points from the mean value are at their highest for this pressure ratio and probe position. Typical variations from the mean value are considerably lower for the majority of the data. It can

therefore be concluded that the experimental uncertainty can be regarded as better than ±10%. The error bars in Figure 6.4 show this uncertainty, which should be similar for the rest of the results.

6.6 Analysis and Discussion of Results

6.6.1 Overall Characteristics

In order to estimate the space charge present in the steam, the currents measured by the probe can to be related to the space charge via an estimation of the collection efficiencies of the probe electrodes. This requires detailed information about the steam flow to be known. Fortunately, as mentioned elsewhere, the GEC rotor tip section under investigation has been studied extensively, both experimentally and theoretically and a great deal of information about its characteristics is available. Relevant flow properties are summarised in Table 6.7. The flow velocities are measured values while the droplet sizes and numbers are from theoretical solutions and are for droplets formed by homogenous nucleation, rather than for any droplets produced from re-entrainment of water films downstream of the blade wakes.

Table 6.7: Summary of flow properties

	P_{ratio} = 2.33		P_{ratio} = 1.49	
	Mid-passage	**Wake**	**Mid-passage**	**Wake**
Flow velocity (ms^{-1})	560	520	320	260
Droplet radius (μm)	0.035	0.035	0.032	0.043
Number of droplets (m^{-3})	62.2×10^{15}	62.2×10^{15}	107×10^{15}	41.3×10^{15}
K.E. of one droplet (J)	28.2×10^{-15}	24.3×10^{-15}	7.0×10^{-15}	11.3×10^{-15}

Since large currents have only been measured in areas of the flow where water droplets are present it seems likely that it is water droplets that are the carriers of charge. Therefore to estimate the level of charge in the flow the deposition rate of droplets on the probe electrodes must be estimated. Values of Stokes number[1] and Reynolds number for these surfaces, calculated using the data in Table 6.7, are given in Table 6.8. The Stokes numbers on the probe reference surface are extremely low and therefore the deposition

[1] Corrected for non-continuum effects.

rates on this surface must be very small. The Stokes numbers on the probe tip are slightly higher, but are still small. In an investigation by *Crane et. al. [1973]* it was shown that in cases of boundary layer bubble separation the re-attaching stream provides a mechanism for depositing small droplets on a surface. The calculated Reynolds numbers for the probe reference surface and tip indicate that they would be subject to bubble separation (e.g. see *Houghton and Carpenter [1993]*). However there appear to be no investigations that provide estimates of the actual deposition rates due to this mechanism.

Considering other studies of deposition rates on turbine blading for similar sized droplets it would be expected that the deposition rate on the front of the reference surface would be very small. Assuming that there is some deposition on the remainder of the reference surface, particularly due to boundary layer re-attachment, it is estimated that the collection efficiency would be of the order of a few percent. Since the probe tip has a larger Stokes number it will have a slightly higher collection efficiency. In the following calculations a collection efficiency of 5% has been assumed for both probe electrodes.

Table 6.8: Summary of Stokes and Reynolds numbers for the probe electrodes

	P_{ratio} = 2.33		P_{ratio} = 1.49	
	Mid-passage	**Wake**	**Mid-passage**	**Wake**
Stokes no. reference surface	0.05	0.047	0.018	0.02
Stokes no. probe tip	0.55	0.51	0.19	0.22
Re no. reference surface	74.8×10^3	69.5×10^3	62.9×10^3	51.0×10^3
Re no. probe tip	6.9×10^3	6.4×10^3	5.8×10^3	4.7×10^3

It is assumed that the droplets are the carriers of charge in the flow and that their impingement on the probe surface transfers this charge to the probe. Thus the probe surface will be at a higher potential than ground and a current will flow from the probe to ground. Given this assumption and the estimation of probe collection efficiency, the average number of single electron charges per droplet can be estimated. Table 6.9 shows the calculated rates of droplet flow onto the projected areas of probe tip and reference surface and also the number of single electron charges collected for different flow conditions. In the water droplets the charge will be the result of a net negative or positive ion concentration, e.g. hydroxyl (OH^-), hydronium (H_3O^+) ions etc.

In the case of the mid-passage flow at a pressure ratio of 2.33 there are 4089×10^{12} droplets crossing the projected area of the reference surface per second. Assuming a nominal collector efficiency of 5% for the reference surface the number of droplets depositing on the surface is around 200×10^{12} s^{-1}. This is still more than the number of single electron charges captured, which is 75×10^{12} s^{-1} for pure steam. Thus the amount of charge present is less than one electron charge per water droplet for these flow conditions. The situation is generally similar in the mid-passage for the other flow conditions.

Table 6.9: Summary of droplet impingement rates and charge characteristics

		P_{ratio} = 2.33		P_{ratio} = 1.49	
		Mid-passage	**Wake**	**Mid-passage**	**Wake**
No. droplets traversing projected area of reference surface (s^{-1})		4089×10^{12}	3087×10^{12}	4030×10^{12}	1257×10^{12}
No. single electron charges collected by reference surface (s^{-1})	**Pure steam**	75×10^{12}	450×10^{12}	21.9×10^{12}	425×10^{12}
	Dosed steam	42.5×10^{12}	375×10^{12}	31×10^{12}	375×10^{12}
No. droplets traversing projected area of probe tip (s^{-1})		160×10^{12}	149×10^{12}	156×10^{12}	49.2×10^{12}
No. single electron charges collected by probe tip (s^{-1})	**Pure steam**	1.8×10^{12}	131×10^{12}	18×10^{12}	112.5×10^{12}
	Dosed steam	0.5×10^{12}	7.9×10^{12}	9.4×10^{12}	125×10^{12}

The current measured in the wake regions was substantially higher than in the mid-passage. Using the same reasoning as above the number of single electron charges per droplet in the wakes, estimated for the reference surface, is larger than 1 at a pressure ratio of 2.33 and slightly higher at the lower pressure ratio. The *estimated* number of electron charges per droplet, calculated using the reference surface measurements for both the mid-passage and wake regions, are summarised in Figures 6.11a and b for the pressure ratios 2.33 and 1.49 respectively. The estimates for each pressure ratio are plotted in separate figures to deter quantitative comparisons between them since the estimate for collection efficiency means that such comparisons would not make sense. The general trends described above can be seen in these figures, notably larger negative charge in the wake regions and slightly lower negative charge for steam dosed with ammonia.

The same calculations for the probe tip, also using a collection efficiency of 5%, reveal a similar number of electron charges per drop in the mid-passage. However in the wakes, the calculations indicate a higher number of electron charges per droplet when compared to the same numbers calculated for the reference surface. One explanation for this may be that because the probe tip was not heated directly water droplets depositing on the tip surface may have stripped off generating charge, which would have influenced the measurements. Despite this the probe tip measurements do indicate the same overall trends as the reference surface and since the collection efficiency of both the probe tip and reference surface have been estimated and taken to the be same, quantitative comparisons between the two electrodes have little meaning.

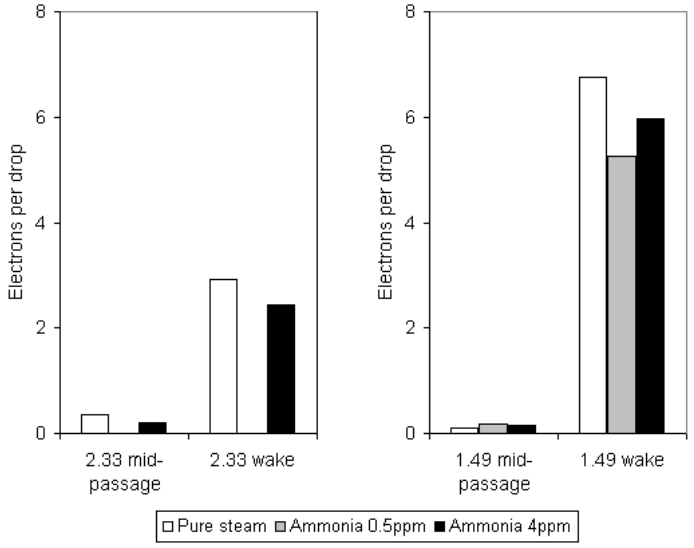

Figure 6.11: *Estimated* number of single electron charges captured by probe reference surface (assuming 5% collection efficiency)
Note1: This figure indicates trends only.
Note2: No measurements at 2.33 with steam dosed with 0.5 ppm ammonia.

The space charge in the steam has also been estimated, again by making assumptions about the collection efficiency of the probe electrodes. Space charge, estimated from the probe reference surface measurements, is shown in Figure 6.12 for all flow conditions. It can be seen from the figure that the overall space charge in the steam is extremely low. However, following the general trends discussed above, the space charge in the wake regions is larger than the charge in the mid-passage regions.

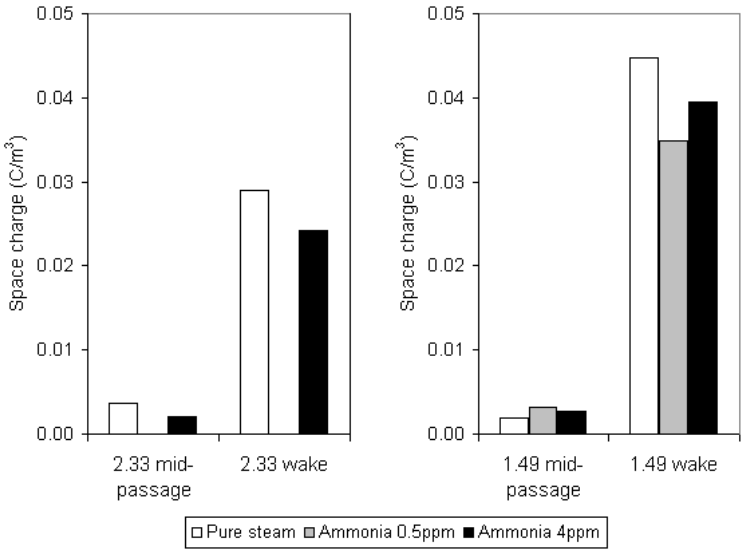

Figure 6.12: *Estimated* Space Charge measured by probe reference surface (assuming 5% efficiency)
Note1: This figure indicates trends only.
Note2: No measurements at 2.33 with steam dosed with 0.5 ppm ammonia.

6.6.2 Langmuir Probe Performance

It has been mentioned that the Langmuir probe did not perform as expected. Particularly there was no evidence that the charge carriers in the flow were influenced by the electric field generated by the ramp voltage. It will be recalled that the probe ramp voltage ranged from –10 V to +10 V. Therefore the maximum electric potential energy exerted by the ramp electric field on a single electron would be 1.6×10^{-18} J. Since the likely number of electron charges on a single droplet appears to be of the order of 1 then the electric potential energy exerted by the ramp electric field would be approximately three orders of magnitude less than the kinetic energy of the droplet (see Table 6.7). It is therefore not surprising that the effect of the voltage imposed by the ramp is not easily evident from the measured currents.

During the experimental work it was not possible to raise the Langmuir probe voltage significantly, partly because the ramp and amplification circuits could not support higher voltages without major modifications, which were not practical at the time. In addition to this a large ramp voltage such as 1000 V may introduce other problems, such as generation of ions around the probe, potentially influencing the measurements.

6.6.3 The Influence of pH

It can be seen from the data, especially Figures 6.11 and 6.12, that adding ammonia to the steam appears to have some influence on the measurements. In order to examine this influence further, the number of single electron charges captured by the probe electrodes in steam dosed with 4 ppm of ammonia, have been plotted in Figure 6.13 against the number of electron charges captured by the same electrodes in ultra-pure steam. It has already been shown, in chapter 5, that the presence of small quantities of ammonia in steam does not affect the nucleation characteristics of the steam. Therefore it can be assumed that the population of droplets in each case is the same and any change in charge is due to the presence of ammonia only. Despite the scatter in the results and the experimental uncertainty, the relation between the measured currents is linear. In the case of steam dosed with 4 ppm of ammonia this relationship indicates that the amount of electrical charge generated is around 15 – 20% less than the charge in ultra-pure steam.

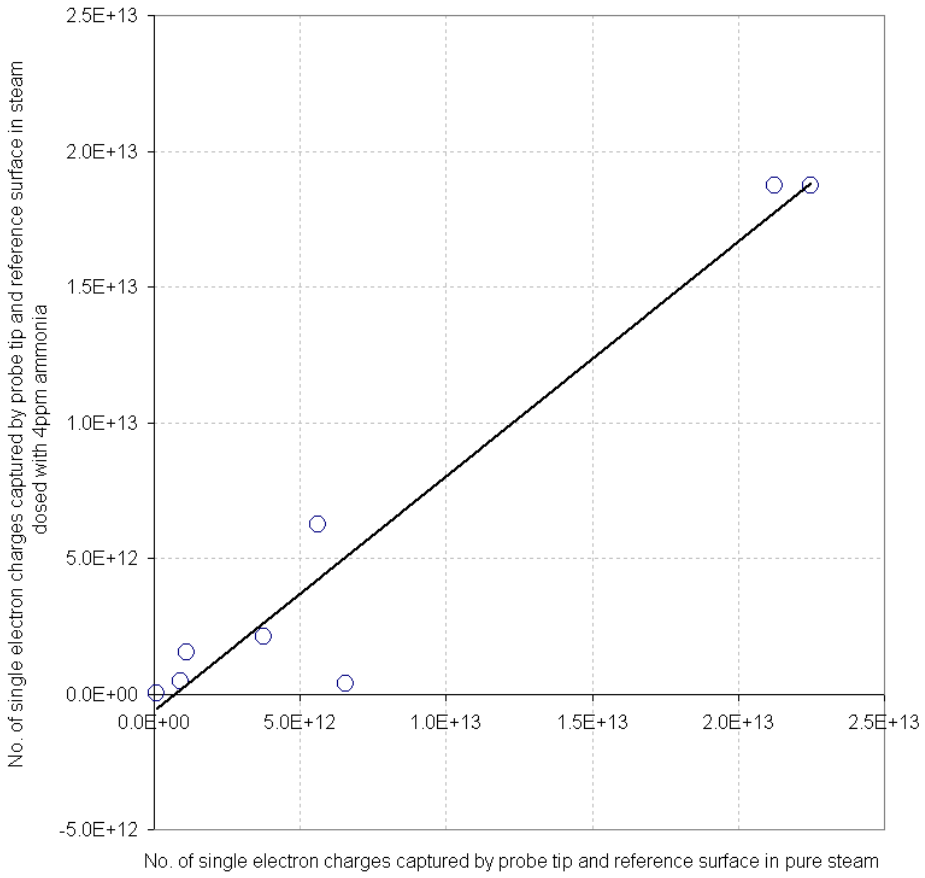

Figure 6.13: Variation of number of single electron charges captured by reference surface and probe tip in pure steam and steam dosed with 4ppm ammonia

The relationship between pure steam and steam dosed with 0.5 ppm of ammonia is also linear. In this case the drop in charge, in the presence of the smaller concentration of ammonia, is larger (20 – 25%).

Other investigators who have studied the effect of pH on electrostatic charge in wet and nucleating steam have noticed a positive correlation; increasing pH seems to increase the level of positive charge in the steam (e.g. *Hesler [1998]*). This is somewhat supported by the results described above. Increasing the pH does indeed lower the amount of negative charge in the steam. However the fact that the magnitude of negative charge was actually less at a pH of 9.2 than a pH of 9.7 is anomalous. It is quite possible that the influence of pH is not quite so straight forward as is suggested by the results of previous investigations. The chemistry of the water droplets, rather than simply the pH, may influence the charge present in the steam. In the case of the current project it has been suggested by *Mr. M. Ball*[2] that the charges measured were affected by the presence of carbon dioxide in the steam. During the electrostatic charge measurements no precautions were taken to prevent atmospheric air coming into contact with water in the hotwell. It is therefore likely that the boiler feed water contained some carbon dioxide in solution. This would have made the resulting steam slightly acidic, due to the presence of carbonic acid and could have contributed to the electrical charges measured. The addition of 0.5 ppm of ammonia neutralised the effect of the carbonic acid and reduced the electrostatic charges generated. Further addition of ammonia then increased the alkalinity, which led to an increase in the negative charges generated.

There is certainly no evidence of a clear relationship between pH and charge in this case.

6.6.4 Charge Generation in the Wakes

It appears from the trends highlighted in the above results that the majority of space charge present in wet and nucleating steam is found downstream of the blade surfaces in the blade wakes. Downstream of the zone of rapid condensation in the centre of the blade passage only a very small amount charge has been detected. However in the wake regions downstream of the blades much larger negative charges have been measured. Thus it appears that interaction of water droplets and water films with the blade surfaces is the primary mechanism of charge generation, rather than the

[2] Private communication

condensation process itself. This conclusion is further supported by the measurements with steam slightly superheated at inlet. In this case despite the absence of nucleation in the main flow, charge was measured in the wake regions, as a result of steam condensing on the blade surfaces, forming water films and subsequently generating charge.

The charging mechanisms at work are open to speculation. It is possible that the water films on the blade surfaces form an electric-double layer, as described in chapter 3, and as the flow passes, charge is stripped off. Alternatively, re-entrainment of the water film at the blade trailing edge and subsequent shattering of larger water droplets downstream of the blade may generate charged droplets in the flow. However, the exact nature of the charge generation mechanism is unfortunately beyond the scope of the current work. Since the charge measured by the probe electrodes has been negative it may be that positive charge remains on the blades and then flows to ground; it would be possible to measure this current. Positive charge may also be present on larger droplets in the flow, as observed by other investigators (e.g. *Petr and Kolovratnik [2003]*). In the current work only the net charge has been measured, no attempt has been made to measure the charge associated with different droplet size populations. However, it would be insightful to do so in future.

6.6.5 Nucleation in the Wakes

There are some reports in the literature of nucleation in the blade wakes, in addition to nucleation in the blade mid-passage in the zone of rapid condensation. For example see *Filippov et. al. [1970]* and *Stastny et. al. [1997]*. As discussed in chapter 3, the presence of electric charge significantly reduces the supersaturation necessary for droplets to nucleate and grow and it is possible that nucleation of the steam downstream of the wakes is a consequence of the electrostatic charge measured in the flow in this region. However it should be noted that such nucleation has not been observed in the blade cascade used in the current work and further research would be necessary to investigate the effect of electrostatic charge on nucleation in the blade wakes.

6.7 Conclusions

The results presented here are consistent with the findings of previous investigators working in LP turbines, e.g. *Hesler and Maurer [1998]* and *Petr and Kolovratnik [2003]*. In the current work and in all previous investigations no charge has been measured in dry steam, however once the steam has nucleated a net negative charge has been measured. Downstream of the wet turbine stages previous investigators have measured a net negative charge along most of the blade axis from the root. Only in the blade tip region, where larger droplets are found as a result of centrifugal forces, have net positive charges been measured. *Petr and Kolovratnik [2003]* went further and were able to distinguish between the charge present on fine and coarse droplets at the same radial position. They found that the smaller droplets carried a negative charge and the larger droplets a positive charge. However in this case also, the overall net charge was negative.

In the current work significantly larger negative charge has been measured in the blade wakes, in comparison with the very low charge measured in the mid-passage. In previous investigations the local variation of charge between the blade wakes and mid-passage region has not been measured and therefore this correlation between charge and the blade wake regions has not previously been observed.

In summary:

1. It has been possible to construct a Langmuir probe for use in wet and nucleating steam. But when using such a probe in flowing steam the measurements were dominated by the charge collected by the probe from the flow.
2. When steam is superheated or supercooled but dry, the charge is extremely small.
3. The charge is appreciable when the steam has nucleated and is wet.
4. The polarity of the current collected by the probe is negative, indicating that the particles collected by the probe are negatively charged.
5. In the body of the flow, some distance from the influence of solid boundaries the measured charge is very low. The charge is considerably higher in the wake region downstream of a solid surface such as a blade. The charge is

many electron charges per droplet in the blade wakes. This suggests that interaction of the flow with water films formed on the blade surfaces in nucleating and wet steam is the source of the charge.

6. When the steam has a relatively low superheat at inlet to the cascade, the fluid becomes supercooled on expansion through the passage but not sufficiently to nucleate. Under these conditions it is possible for water films to form on the surface of the blades leading to charge appearing in the blade wakes. This also indicates that the charge is not generated as a result of the nucleation process, but as a result of liquid interacting with the blade surfaces.

7. In steam containing ammonia at a concentration of 4 ppm the measured charges are around 15-20% lower than in ultra-pure steam. The drop in generated charges was higher with an ammonia concentration of 0.5 ppm. However the influence of pH has been complicated because no precautions were taken to prevent contamination of the feed water with carbon dioxide from atmospheric air and no clear trend has emerged.

Chapter 7:
Conclusions and Further Work

7.1 Conclusions

7.1.1 Effect of Impurities

Significant modifications to the steam blow down experimental facility have been completed in order to provide a supply of ultra-pure steam to the test section and blade cascade. Conductivity measurements and water/steam analysis have shown that very high water/steam purity has been achieved throughout the system. In addition to this equipment has been installed to dose the boiler feed water with a controlled concentration of aqueous ammonia.

It has been shown that a satisfactory set of baseline measurements using ultra-pure steam have been completed over a number of different inlet conditions and pressure ratios, representative of steam turbine conditions.

Comparison of the baseline pressure distributions with those from previous studies, which used steam containing an unknown number of impurities, has demonstrated that the prior assumption that these impurities did not influence the nucleation process was correct. It can be concluded that in these studies the steam reversion process was dominated by homogeneous nucleation, despite the presence of impurities.

Comparison of the baseline pressure distributions with the pressure distributions for steam dosed with 4 ppm and 12 ppm of ammonia has shown that in neither case did the ammonia have any significant effect on the nucleation process. In both cases the pressure distributions were identical with and without ammonia. Thus, despite the high concentrations of the ammonia in the steam, the reversion process was dominated by homogeneous nucleation.

7.1.2 Electrostatic Charge

A Langmuir probe has been designed and constructed that is able to successfully operate in dry, nucleating and wet steam conditions in the short duration test section. The precautions to avoid water films forming on the probe surfaces have proved to be successful. When using the probe in flowing steam the readings were dominated by charge collected by the probe from the flow.

Negligible charge has been measured in dry steam both upstream and downstream of the blade cascade, indicating that dry steam carries no appreciable charge. However, when the steam nucleates and becomes wet, significant negative charges have been measured. Under these conditions the charge is relatively low in the mid-passage, far from the blade surfaces, but is noticeably larger in the blade wakes downstream of the blade trailing edge.

These results suggest that the condensation process itself does not generate charge. Interaction of water droplets and films with the blade surfaces appears to be the source of the charge. However, the charge mechanism(s) responsible are at present unknown and are open to speculation.

Increasing the alkalinity of the steam has reduced the magnitude of negative charge measured in the steam. However, the relationship between pH and charge is not clear and the results have been complicated by the lack of precautions taken to avoid contamination of the feed water with carbon dioxide.

7.2 Suggestions for Further Work

7.2.1 Effect of Impurities

1. Investigate the influence of other volatile chemicals on the nucleation process.
2. Investigate the influence of non-volatile chemicals on the nucleation process. It would be particularly interesting to investigate the effect of salts, such as sodium chloride, which have been known to lead to nucleation around the saturation line in the ‘salt zone’.

3. Study the effect of chemicals, such as some organic compounds, which reduce the surface tension of water. Any chemical that reduced the surface tension would tend to encourage nucleation at a lower supersaturation ratio.
4. Measure droplet size distributions upstream of the zone of rapid condensation in order to determine the size of droplets generated by heterogeneous nucleation.
5. Study heterogeneous nucleation on impurities for other blade geometries and expansion rates.

7.2.2 Electrostatic Charge

1. Investigate the mechanisms causing droplets to acquire charge downstream of the blade surfaces.
2. Investigate more thoroughly the exact nature of the correlation between steam/water chemistry, pH and charge polarity and magnitude.
3. Investigate the size distribution of droplets in the wakes and main flow – and correlate with the measured charge distributions.
4. Do charged particles introduced into the flow upstream of the zone of rapid condensation encourage heterogeneous nucleation and would they reduce the limiting supersaturation?

Appendix A:

GEC Rotor Blade Tip Profile and Tapping Point Locations

A.1 GEC Rotor Blade Tip Profile

Table A.1: Blade Profile Equations (all dimensions are in mm)

Suction Surface	Pressure Surface
Points LE (0.0, 0.0) and BS1 (1.2756, 0.6998) Joined by circle of radius 0.8361 and centre (0.8301, 0.0)	Points LE (0.0, 0.0) and BP1 (0.1716, -0.5052) Joined by circle of radius 0.8361 and centre (0.8301, 0.0)
Points BS1 (1.2756, 0.6998) and BS2 (8.245, -7.4941) Joined by circle of radius 18.2753 and centre (-8.5298, 14.7008)	Points BP1 (0.1716, -0.5052) and BP2 (2.8372, -4.4122) Joined by circle of radius 42.8803 and centre (-33.8587, -26.59)
Points BS2 (8.245, -7.4941) and BS3 (9.2577, -9.9576) Joined by circle of radius 85.2009 and centre (-70.0375, -41.1241)	Points BP2 (2.8372, -4.4122) and BP3 (9.702, -17.7608) Joined by circle of radius 109.544 and centre (-90.9191, -61.0672)
Points BS3 (9.2577, -9.9576) and BS4 (19.1532, -37.9631) Joined by circle of radius 426.004 and centre (-387.237, -165.798)	Points BP3 (9.702, -17.7608) and BP4 (18.5008, -38.2053) Joined by a straight line
Points BS4 (19.1532,-37.9631) and TE (19.169, -38.0678) Joined by circle of radius 0.3481 and centre (18.8209, -38.0678)	Points BP4 (18.5008, -38.2053) and TE (19.169, -38.0678) Joined by circle of radius 0.3481 and centre (18.8209, -38.0678)

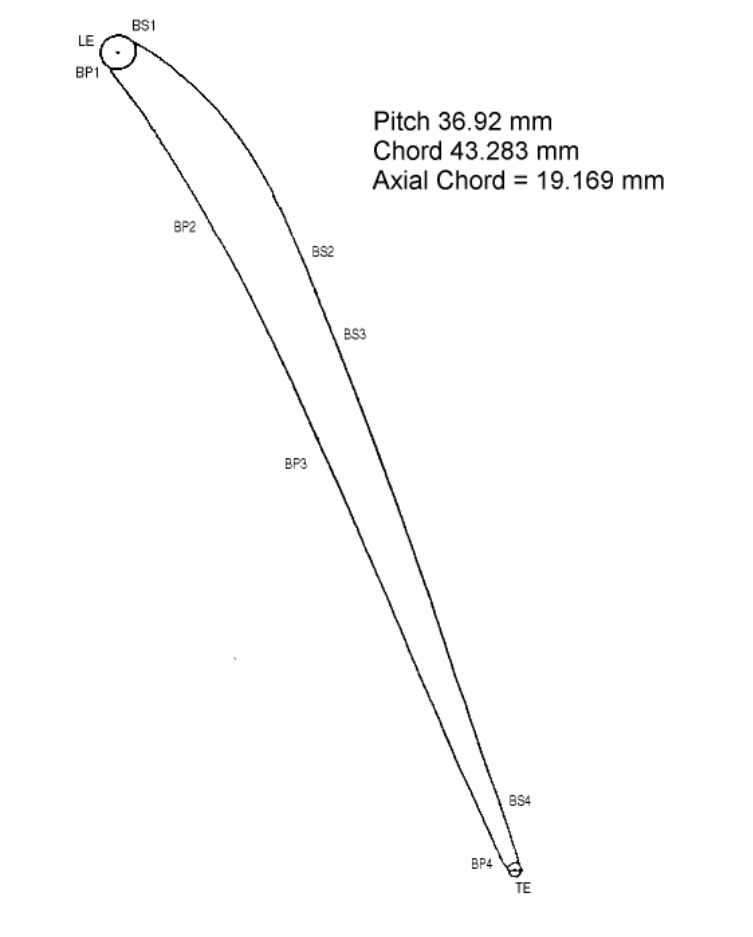

Figure A.1: GEC Blade Tip Profile

A.2 Blade Pressure Tapping Point Locations

The following two tables provide the locations, in non-dimensional distance, of the blade surface pressure tapping points and wall pressure tapping points relative to the blade leading edge.

Table A.2: Blade Surface Pressure Tapping Point Locations
Key: PS – Pressure surface, SS – Suction surface
Axial chord = 19.169 mm

Tapping Point	x/chord
PS10	0.128
PS1	0.180
PS11	0.233
PS2	0.283
PS12	0.333
PS3	0.378
PS13	0.421
PS4	0.465
PS5	0.550
PS15	0.590
PS6	0.633
PS16	0.673
PS7	0.715
PS17	0.745
PS8	0.778
PS18	0.808
PS9	0.838

Tapping Point	x/chord
SSLE	0.000
SS10	0.245
SS1	0.318
SS11	0.381
SS2	0.433
SS12	0.475
SS3	0.510
SS13	0.548
SS4	0.585
SS14	0.622
SS5	0.660
SS15	0.695
SS6	0.730
SS16	0.765
SS17	0.825
SS8	0.850
SS18	0.876
SS9	0.900

Table A.3: Wall Pressure Tapping Point Coordinates
Key: MP – Blade mid-passage (normalised by axial chord)
US – Traverse tapping points upstream of the blade cascade
DS – Traverse tapping points downstream of the blade cascade

Tapping Point	x/chord
MP2	-0.350
MP3	-0.137
MP7	0.300
MP11	0.446
MP14	0.570
MP16	0.648
MP17	0.761
MP19	0.834
MP21	0.908
MP23	0.949
MP25	0.990
MP27	1.058

Tapping Point	x (mm)	y (mm)
US1	-51.412	40.65
US2	-51.412	22.15
US3	-51.412	3.70
US4	-51.412	-14.70
US5	-51.412	-33.20

Tapping Point	x (mm)	y (mm)
DS1	26.935	3.842
DS2	26.935	-0.319
DS4	26.887	-8.466
DS5	26.935	-12.635
DS6	26.887	-16.804
DS7	26.791	-20.781
DS8	26.935	-24.854
DS9	26.935	-28.975
DS10	26.887	-33.096
DS11	26.791	-37.313
DS12	26.839	-41.290
DS13	26.887	-45.507
DS14	26.887	-49.533
DS15	26.886	-53.606

Appendix B:

Chemical Analysis and Conductivity Measurements

B.1 Estimation of Ammonia Concentration

The concentration of ammonia in the steam was estimated using the graph in Figure B-0 provided by M. Ball, consultant to EPRI. The estimated values were corrected using the results of the chemical analysis of the steam and pure water by ELGA's laboratory. The correction factor was defined as the ratio of the ammonia concentration measured by the laboratory divided by the ammonia concentration estimated using the conductivity measurements. In the receiver the correction factor was 1.36.

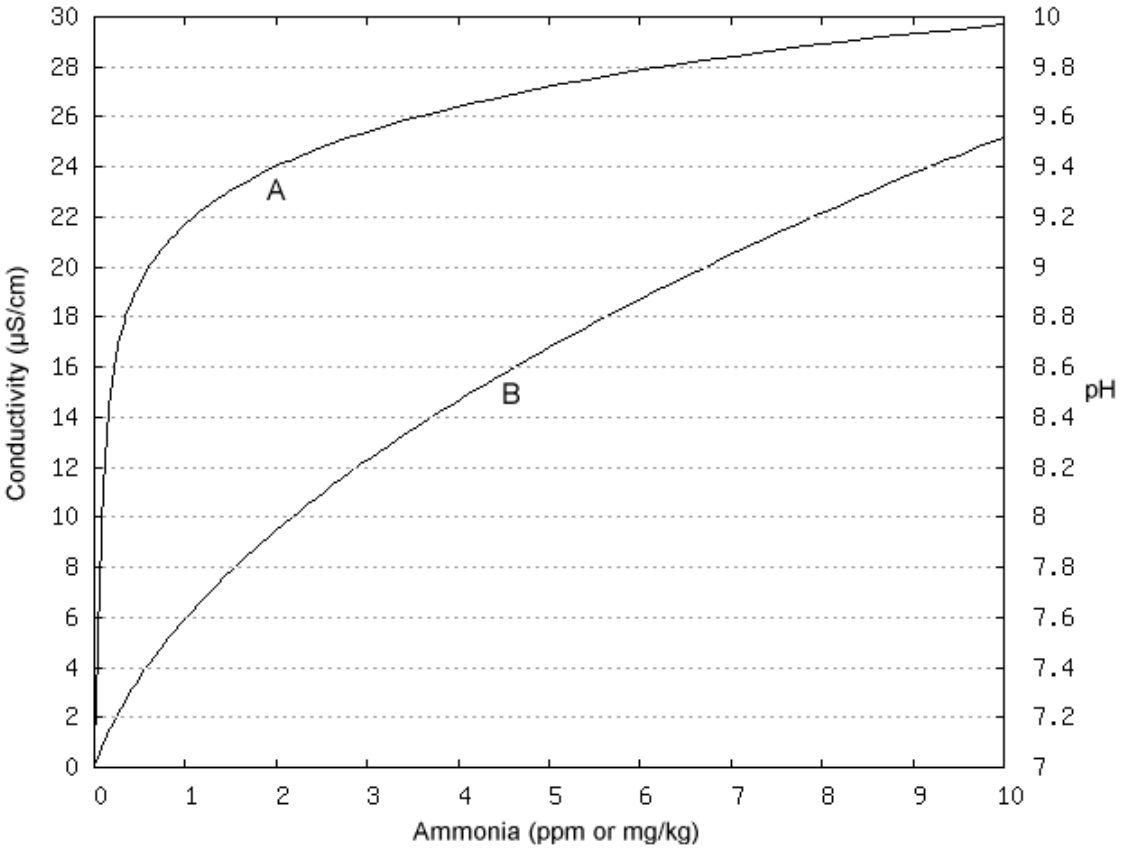

Figure B.1: Relationship between conductivity, pH and ammonia at 25 °C
Curve A shows the relationship between ammonia concentration and pH – the right hand scale
Curve B shows the relationship between ammonia concentration and conductivity – the left hand scale

B.2 Chemical Analysis

Tables B-1 to B-2 present the results of a detailed chemical analysis of water and steam samples taken from the steam rig on three separate dates. All values are in ppb unless otherwise stated. Many values are maximum concentrations because the levels are at the limit of detection.

Table B.1: Ion concentrations sampled on 31.07.98

a) cations

Sample Point	Fluoride (F-)	Chloride (Cl-)	Nitrite (NO2-)	Bromide (Br-)	Nitrate (NO3-)	Phosphate (PO4 3-)	Sulphate (SO4 2-)
S0		< 20	< 0.5	< 0.5	< 0.5	< 0.5	< 0.5
S8	0.07	0.04	< 0.02	< 0.02	< 0.02	0.09	1.2
S6		< 20	< 0.5	< 0.5	< 0.5	< 0.5	7.9
S3		< 20	< 0.5	< 0.5	< 0.5	0.9	7.8
S2		< 20	< 0.5	< 0.5	< 0.5	1.5	9.7

b) anions

Sample Point	Sodium (Na+)	Ammonium (NH4+)	Potassium (K+)	Magnesium (Mg 2+)	Calcium (Ca 2+)
S0	0.4	< 1.0	0.4	< 0.4	< 1.0
S8	0.7	< 0.02	0.05	0.05	2.5
S6	3.3	2.0	1.1	< 0.4	6.0
S3	5.4	< 1.0	3.5	3.0	150.0
S2	5.0	< 1.0	5.7	1.4	41.0

Table B.2: Ion concentrations sampled on 12.03.99

a) cations

Sample Point	Chloride (Cl-)	Nitrite (NO2-)	Bromide (Br-)	Nitrate (NO3-)	Phosphate (PO4 3-)	Sulphate (SO4 2-)
S0	< 0.5	< 0.5	< 0.5	< 0.5	< 0.5	< 0.5
S8	< 0.5	< 0.5	< 0.5	< 0.5	1.0	< 0.5
S6	< 0.5	< 0.5	< 0.5	< 0.5	< 0.5	< 0.5
S3	< 0.5	< 0.5	< 0.5	< 0.5	< 0.5	< 0.5
S2	< 0.5	< 0.5	< 0.5	< 0.5	< 0.5	< 0.5

b) anions

Sample Point	Sodium (Na+)	Ammonium (NH4+)	Potassium (K+)	Magnesium (Mg 2+)	Calcium (Ca 2+)
S0	< 2.0	< 1.0	< 0.5	< 0.5	< 3.0
S8	< 2.0	< 1.0	< 0.5	< 0.5	< 3.0
S6	< 2.0	< 1.0	< 0.5	< 0.5	< 3.0
S3	< 2.0	9.0	< 0.5	< 0.5	< 3.0
S2	< 2.0	10.0	< 0.5	< 0.5	< 3.0

Table B.3: Ion concentrations sampled on 14.04.99

a) cations

Sample Point	Chloride (Cl-)	Nitrite (NO2-)	Bromide (Br-)	Nitrate (NO3-)	Phosphate (PO4 3-)	Sulphate (SO4 2-)
S0	1.0	<0.5	<0.5	<0.5	8.0	<0.5
S8	<0.2	<0.5	<0.5	<0.5	32.0	0.9
S6	<0.2	<0.5	<0.5	<0.5	<0.5	<0.5
S3	<0.2	<0.5	<0.5	<0.5	<0.5	<0.6
S2	0.7	<0.5	<0.5	1.0	0.6	3.5

b) anions

Sample Point	Sodium (Na+)	Ammonium (NH4+)	Potassium (K+)	Magnesium (Mg 2+)	Calcium (Ca 2+)
S0	< 20	< 20	< 20	< 20	80
S8	< 20	3.2 ppm	< 20	50	410
S6	< 20	4.7 ppm	< 20	< 20	30
S3	< 20	4.8 ppm	< 20	20	30
S2	< 20	4.7 ppm	< 20	120	310

B.3 Conductivity Measurements

Table B.4: Direct and cation conductivity measurements for the pressure measurements.
Values are in µSiemens/cm

Date	ELGA System (S0)		Boiler Feed water (S8)		Steam supply (S6)		Rear Receiver (S3)		Front Receiver (S2)	
	Direct	Cation	Direct	Cation	Direct	Cation	Direct	Cation	Direct	Cation
31.07.98*	0.054	-	25.000	-	0.854	-	1.795	-		
03.08.98			25.000	-	0.854	-	1.666	-		
11.09.98			0.500	-	0.833	-				
15.08.98			0.500	-	0.800	-				
22.09.98			0.455	-	0.694	-				
23.09.98			0.444	-	0.769	-				
28.09.98			0.476	-	0.819	-	1.515	-	1.923	-
02.10.98			0.400	-	0.819	-	1.818	-	1.851	-
09.10.98			0.400	-	0.816	-	1.142	-	1.025	-
12.10.98			0.417	-						
30.10.98			0.385	-	0.833	-	0.976	-		
04.11.98							1.176	-		
11.11.98			0.385	-			1.099			
13.11.98			0.385	-	0.755	-	0.976	-		
17.11.98							1.111			
03.02.99	0.056	-	0.119	0.333	0.286	0.909	0.833	1.111		
10.02.99			0.098	0.364	0.222	0.667	0.571	0.870		
18.02.99			0.100	0.286	0.244	0.556	0.597	0.784		
24.02.99							0.581	-		
02.03.99			0.344	0.549	0.444	0.694	0.884	1.111		
05.03.99			0.385	0.613	0.658	0.727	0.909	1.111	1.429	2.105
09.03.99			0.204	0.500			0.976	1.429	0.806	1.163
12.03.99*	0.054	-	0.089	0.250	0.167	0.364	0.333	0.575	0.869	1.064
16.03.99^			2.941	0.588	4.167	0.621	4.348	0.787		
19.03.99^			6.211	0.541	7.752	0.602	7.937	0.667		
23.03.99^			13.514	0.714	17.241	0.800	17.544	0.676		
26.03.99^			7.407	0.500	9.434	0.526	9.170	0.714		
29.03.99^			10.638	0.641	13.333	0.658	13.514	0.800		
01.04.99^			13.158	0.357	15.385	0.500	16.949	0.641		
12.04.99^			11.628	0.455	18.519	0.476	22.222	0.769		
14.04.99^*	0.055	-	11.111	1.111	13.333	0.806	13.333	0.806	13.514	1.176
16.04.99^			12.048	0.719	15.625	0.699	15.625	0.855		

Date	ELGA System (S0)		Boiler Feed water (S8)		Steam supply (S6)		Rear Receiver (S3)		Front Receiver (S2)	
	Direct	Cation	Direct	Cation	Direct	Cation	Direct	Cation	Direct	Cation
19.04.99^			16.129	1.000	18.519	0.990	17.860	1.081		
21.04.99^			22.727	0.763	28.571	0.781	28.571	0.961		
23.04.99			6.098	0.568	5.747	1.064				
27.04.99			0.303	0.500	0.400	0.588	0.741	0.826		
29.04.99			0.323	0.526	0.392	0.562	0.4	0.645		

Notes: * Indicates water samples were taken on this date
^ Indicates dosing with Ammonia solution into the hotwell on this date

Table B.5: Direct and cation conductivity measurements for the electrostatic measurements. Values are in µSiemens/cm

Test Type	Boiler Feed water (S8)		Steam supply (S6)	
	Direct	Cation	Direct	Cation
Pure steam	1.000	1.000	1.750	1.500
Dosed steam	6.550	0.750	4.000	1.500
Dosed steam	6.550	0.500	12.500	0.800
Dosed steam	8.550	0.700	12.500	0.900
Dosed steam	11.200	0.750	15.500	0.900
Dosed steam	13.500	0.700	18.400	1.100
Dosed steam			14.250	1.500
Dosed steam	16.700	2.000	16.700	1.800
Dosed steam			20.000	1.800
Dosed steam			20.000	1.900

Appendix C:

Preparation of Ammonia Solution

The concentration of ammonia in the reservoir feeding the dosing pump was determined using the following calculations.

The ELGA pure water pump, feeding the hotwell from the pure water storage tank, could deliver a flow rate of 21 l/min. The peristaltic dosing pump was set-up to operate at a flow rate of 0.034 l/min and pumped ammonia solution from a reservoir into the hotwell. The dosing pump was set-up to switch on and off in sync with the pure water pump.

For a target concentration of C_{feed} ppm of ammonia in the hotwell, the ammonia reservoir concentration C_{res} is given by:

$$C_{feed} \times 21.034 = C_{res} \times 0.034 \tag{C.1}$$

$$C_{res} \approx \left(C_{feed} \times 21\right) / 0.034 \,\text{ppm} \tag{C.2}$$

To calculate the percentage weight/volume (g/ml) required for these flow rates it is assumed that 1 ppm is almost exactly equivalent to 1 mg/l

$$\therefore \text{ w/v} = C_{res} \times 10^{-3}/1000 \times 100\ \% \tag{C.3}$$

For a target of 4 ppm NH_3 (i.e. 4mg/l solution) in the feed-water based on the pure water pump flow rate and the ammonia dosing pump flow rate:

$$4 \text{ ppm} \times 21 \text{ l/min} = C_{res} \text{ ppm} \times 0.034 \text{ l/min} \tag{C.4}$$

$$C_{res} = \left(4 \times 21\right) / 0.034 \tag{C.5}$$

$$C_{res} = 2400 \text{ ppm} \tag{C.6}$$

To calculate percentage weight/volume required for these flow rates:

$$\text{w/v} = 2400 \times 10^{-3}/1000 \times 100 \tag{C.7}$$

$$\text{w/v} = 0.24\ \% \tag{C.8}$$

Stock ammonia solution, with a concentration of 35 % w/v was used to make up the reservoir solution. The stock solution was diluted by the appropriate amount with pure, distilled water to reach the target reservoir concentration.

Appendix D:

Experimental Results – Pressure Measurements

D.1 Tables of Experimental Conditions

Table D.1: Pure Steam - Overall conditions for surface pressure measurements

Test ref.	P01 (bar)	ΔT (K)	P2S (bar)	P01/P2S	Steam Cond. (μS/cm)
2704e	1.114	33.04	0.587	1.846	0.74
1802e	1.100	-0.69	0.587	1.876	0.597
1802m	1.108	-0.59	0.587	1.889	0.597
1802p	1.106	-0.69	0.603	1.834	0.597
1802q	1.104	-0.69	0.619	1.783	0.597
0203e	1.052	-2.18	0.594	1.771	0.884
0203g	1.064	-1.98	0.591	1.800	0.884
0203h	1.058	-1.98	0.599	1.816	0.884
0203l	1.043	-11.69	0.571	1.879	0.884
0203m	1.063	-11.40	0.581	1.886	0.884
0203n	1.051	-11.40	0.593	1.772	0.884
0203o	1.068	-10.83	0.603	1.771	0.884
0203p	1.073	-10.83	0.590	1.868	0.884
0203q	1.064	-10.83	0.608	1.796	0.884
0203s	1.082	-11.12	0.620	1.791	0.884
0503p	1.089	-11.50	0.592	1.897	1.169
0203t	1.066	-12.76	0.593	1.846	0.884
0203u	1.060	-13.51	0.600	1.810	0.884
0203v	1.071	-12.47	0.598	1.844	0.884
0203w	1.066	-12.47	0.597	1.848	0.884
0203x	1.051	-12.85	0.583	1.802	0.884
0503v	1.088	-14.16	0.603	1.856	1.169
2904ab	1.111	-16.99	0.594	1.870	0.400
2904ac	1.105	-16.90	0.608	1.818	0.400
2904ad	1.109	-21.19	0.607	1.827	0.400
1203b	1.065	27.98	0.430	2.474	0.601
2704a	1.142	27.15	0.497	2.297	0.740
2704b	1.125	31.06	0.415	2.713	0.740
2704i	1.112	26.50	0.470	2.367	0.740
1002e	1.099	-0.89	0.492	2.235	0.571
1002j	1.106	-0.99	0.470	2.354	0.571
1002k	1.112	-1.18	0.455	2.446	0.571
0503a	1.095	-1.58	0.417	2.630	1.169
0503b	1.097	-1.48	0.443	2.477	1.169
0503c	1.087	-1.58	0.460	2.361	1.169
2904d	1.117	-0.49	0.490	2.279	0.400
2904e	1.109	-0.59	0.487	2.277	0.400
1002n	1.082	-10.45	0.504	2.148	0.571
2904f	1.156	-10.45	0.506	2.282	0.400
2904g	1.133	-10.55	0.488	2.323	0.400
2904h	1.133	-10.07	0.491	2.308	0.400
2904i	1.137	-10.07	0.501	2.270	0.400
2904v	1.113	-17.18	0.504	2.210	0.400
2904x	1.108	-16.90	0.494	2.241	0.400
2904af	1.113	-21.19	0.483	2.305	0.400

Test ref.	P01 (bar)	ΔT (K)	P2S (bar)	P01/P2S	Steam Cond. (μS/cm)
2704g	1.117	32.35	0.366	3.054	0.740
0903c	1.094	-1.78	0.314	3.488	0.891
0903d	1.085	-1.88	0.301	3.610	0.891
0903e	1.086	-1.78	0.313	3.469	0.891
0903t	1.075	-10.17	0.341	3.152	0.891
2904j	1.135	-10.17	0.350	3.245	0.400
2904k	1.127	-10.07	0.348	3.235	0.400
2904p	1.114	-10.45	0.305	3.651	0.400
2904r	1.098	-16.99	0.342	3.213	0.400
2904s	1.115	-16.99	0.344	3.241	0.400

Table D.2: Steam Dosed with nominal 4ppm Ammonia - Overall conditions for surface pressure measurements

Test ref.	P01 (bar)	ΔT (K)	P2S (bar)	P01/P2S	Steam Cond. (μS/cm)	NH_3 conc. (ppm)
1904c	1.102	34.04	0.619	1.780	17.857	6.809
1603a	1.093	-0.39	0.614	1.821	4.348	0.943
1603c	1.117	-0.79	0.613	1.871	4.348	0.943
1603d	1.100	-0.29	0.610	1.852	4.348	0.943
2603b	1.091	-0.49	0.602	1.864	9.170	2.898
2603c	1.072	-0.19	0.608	1.810	9.170	2.898
2603d	1.081	-0.19	0.616	1.800	9.170	2.898
2903a	1.077	-1.98	0.584	1.843	13.510	4.784
2903b	1.083	-1.78	0.593	1.825	13.510	4.784
0104a	1.098	-11.02	0.591	1.858	16.950	6.373
0104c	1.098	-10.83	0.603	1.820	16.950	6.373
0104d	1.088	-10.93	0.593	1.836	16.950	6.373
0104e	1.093	-10.74	0.593	1.843	16.950	6.373
0104i	1.093	-13.32	0.613	1.784	16.950	6.373
0104j	1.096	-13.32	0.614	1.784	16.950	6.373
2303v	1.088	-17.23	0.593	1.883	17.540	6.670
0104k	1.090	-17.36	0.586	1.859	16.950	6.373
0104l	1.100	-17.18	0.607	1.813	16.950	6.373
0104m	1.091	-17.36	0.593	1.841	16.950	6.373
0104n	1.093	-17.36	0.595	1.839	16.950	6.373
1904a	1.113	27.64	0.473	2.355	17.857	6.809
1904b	1.114	32.57	0.486	2.293	17.857	6.809
1603h	1.103	-0.49	0.501	2.201	4.348	0.943
1603i	1.102	-0.39	0.496	2.200	4.348	0.943
1603m	1.094	-0.79	0.501	2.186	4.348	0.943
1603v	1.093	-1.18	0.466	2.343	4.348	0.943
1903d	1.099	-1.48	0.467	2.354	7.937	2.392
2603e	1.088	-0.69	0.446	2.438	9.170	2.898
2603f	1.086	-0.19	0.497	2.188	9.170	2.898
2603g	1.083	-0.40	0.451	2.400	9.170	2.898
2603h	1.083	-1.10	0.485	2.235	9.170	2.898
2903f	1.085	-1.18	0.466	2.328	13.510	4.784
2903g	1.085	-1.48	0.488	2.223	13.510	4.784
2903h	1.090	-1.58	0.465	2.343	13.510	4.784
1903i	1.094	-11.02	0.442	2.472	7.937	2.392
1903j	1.099	-10.93	0.459	2.392	7.937	2.392
1903l	1.098	-10.93	0.473	2.322	7.937	2.392

Test ref.	P01 (bar)	ΔT (K)	P2S (bar)	P01/P2S	Steam Cond. (μS/cm)	NH_3 conc. (ppm)
2303b	1.072	-8.45	0.455	2.355	17.540	6.670
2303c	1.077	-7.60	0.466	2.312	17.540	6.670
2603s	1.070	-11.71	0.475	2.252	9.170	2.898
2303m	1.068	-13.31	0.422	2.531	17.540	6.670
2303n	1.083	-12.94	0.454	2.386	17.540	6.670
2303q	1.076	-12.76	0.468	2.298	17.540	6.670
2303t	1.080	-17.95	0.488	2.212	17.540	6.670
2903n	1.092	-17.36	0.501	2.181	13.510	4.784
2903o	1.085	-17.45	0.463	2.343	13.510	4.784
2903p	1.080	-17.54	0.451	2.395	13.510	4.784
2903r	1.081	-17.54	0.462	2.340	13.510	4.784
1404f	1.068	-17.73	0.434	2.463	13.420	4.749
1404j	1.072	-17.18	0.430	2.496	13.420	4.749
1604c	1.083	-21.19	0.450	2.405	15.630	5.762
1604d	1.077	-21.10	0.459	2.348	15.630	5.762
1604f	1.076	-21.01	0.475	2.265	15.630	5.762
1904e	1.111	31.88	0.369	3.015	17.857	6.809
1904f	1.098	33.85	0.359	3.060	17.857	6.809
1603y	1.092	-1.08	0.333	3.274	4.348	0.943
1603z	1.097	-0.99	0.337	3.254	4.348	0.943
1903e	1.098	-1.48	0.295	3.722	7.937	2.392
2603k	1.078	-1.30	0.306	3.522	9.170	2.898
2603n	1.087	-0.19	0.318	3.417	9.170	2.898
2603o	1.079	-0.30	0.312	3.453	9.170	2.898
2903i	1.090	-1.68	0.332	3.283	13.510	4.784
2903j	1.084	-1.68	0.280	3.870	13.510	4.784
2303f	1.084	-8.64	0.306	3.542	17.540	6.670
2303g	1.090	-8.83	0.303	3.594	17.540	6.670
2303l	1.085	-13.96	0.300	3.623	17.540	6.670
2303o	1.344	-12.57	0.403	3.338	17.540	6.670
2603p	1.088	-17.45	0.322	3.378	9.170	2.898
2603q	1.086	-17.45	0.304	3.577	9.170	2.898
1404c	1.064	-17.91	0.341	3.117	13.420	4.749
1404d	1.066	-17.91	0.289	3.691	13.420	4.749
1404g	1.084	-17.54	0.354	3.060	13.420	4.749
1404h	1.066	-17.36	0.288	3.696	13.420	4.749
1604a	1.071	-21.46	0.304	3.525	15.630	5.762
1604b	1.088	-21.64	0.360	3.025	15.630	5.762

Table D.3: Steam Dosed with nominal 12ppm Ammonia - Overall conditions for surface pressure measurements

Test ref.	P01 (bar)	ΔT (K)	P2S (bar)	P01/P2S	Steam Cond. (μS/cm)	NH_3 conc. (ppm)
2104c	1.085	-3.39	0.455	2.383	28.571	12.362
2104d	1.087	-3.20	0.460	2.361	28.571	12.362
2104e	1.094	-3.10	0.474	2.309	28.571	12.362
2104s	1.084	-11.50	0.461	2.349	28.571	12.362
2104t	1.093	-10.64	0.463	2.362	28.571	12.362
2104u	1.084	-10.74	0.477	2.271	28.571	12.362
2104w	1.093	-17.91	0.456	2.396	28.571	12.362
2104x	1.090	-17.18	0.462	2.360	28.571	12.362
2104y	1.089	-17.45	0.455	2.393	28.571	12.362

Test ref.	P01 (bar)	ΔT (K)	P2S (bar)	P01/P2S	Steam Cond. (μS/cm)	NH_3 conc. (ppm)
2104f	1.089	-2.90	0.337	3.229	28.571	12.362
2104h	1.089	-2.90	0.339	3.214	28.571	12.362
2104j	1.097	-3.69	0.299	3.673	28.571	12.362
2104l	1.088	-3.30	0.323	3.369	28.571	12.362
2104o	1.078	-10.74	0.321	3.360	28.571	12.362
2104q	1.079	-10.74	0.310	3.481	28.571	12.362
2104r	1.079	-10.74	0.318	3.390	28.571	12.362
2104ac	1.094	-16.99	0.376	2.908	28.571	12.362
2104af	1.094	-16.99	0.368	2.968	28.571	12.362

D.2 Surface Pressure Distributions

The surface pressure distributions for each test listed in Tables D.1 to D3 are plotted below in the following sections.

D.2.1 Pure Steam

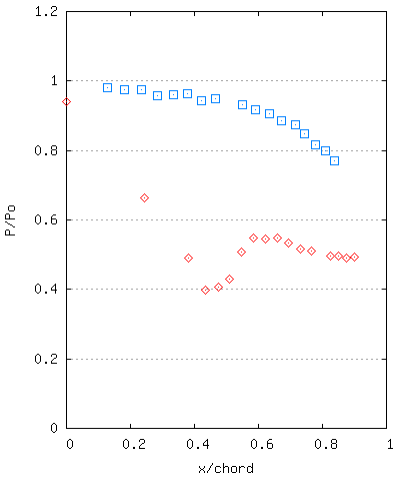

Test: 2704e
P_{ratio} = 1.85, ΔT = +33.04 K, P_0 = 1.11

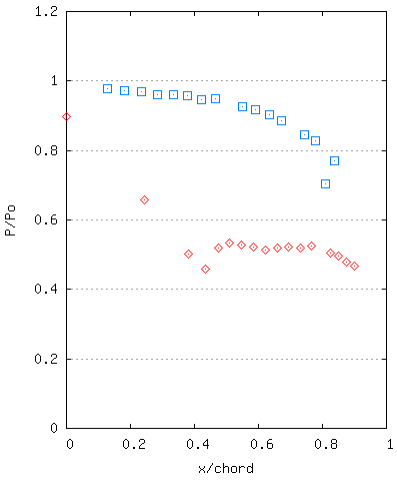

Test: 1802e
P_{ratio} = 1.88, ΔT = -0.69 K, P_0 = 1.10

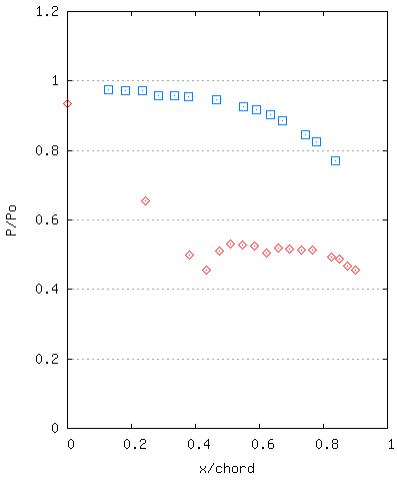

Test: 1802e
P_{ratio} = 1.88, ΔT = -0.69 K, P_0 = 1.10

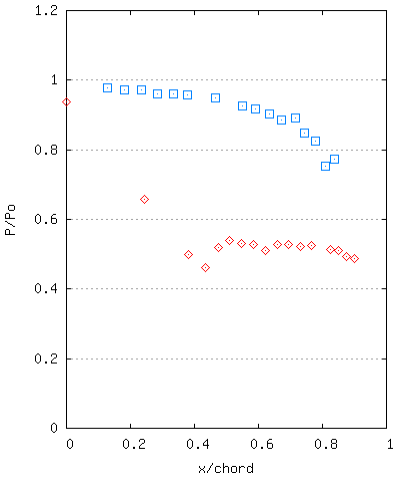

Test: 1802p
P_{ratio} = 1.83, ΔT = -0.69 K, P_0 = 1.11

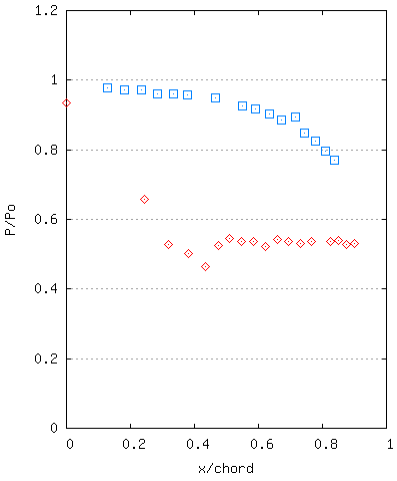

Test: 1802q
P_{ratio} = 1.78, ΔT = -0.69 K, P_0 = 1.10

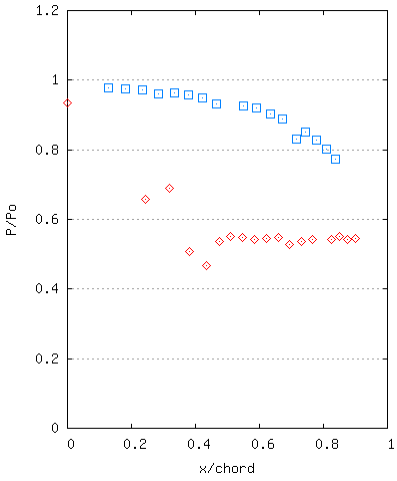

Test: 0203e
P_{ratio} = 1.77, ΔT = -2.18 K, P_0 = 1.05

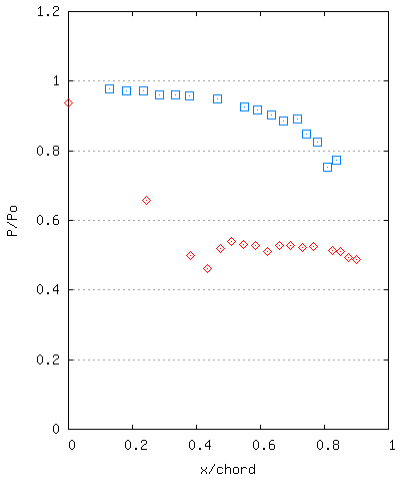

Test: 1802p
P_{ratio} = 1.83, ΔT = -0.69 K, P_0 = 1.11

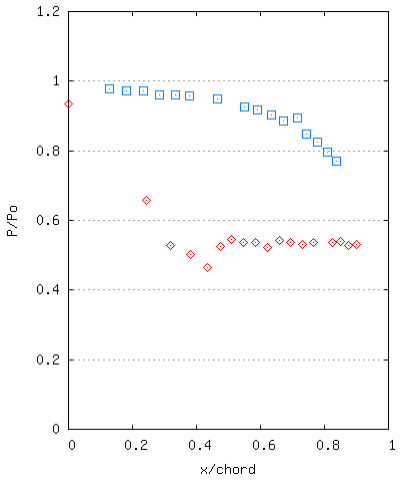

Test: 1802q
P_{ratio} = 1.78, ΔT = -0.69 K, P_0 = 1.10

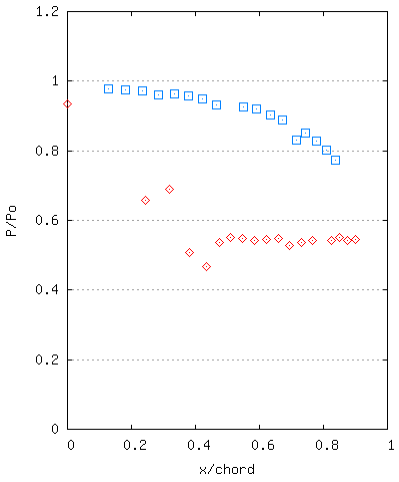

Test: 0203e
P_{ratio} = 1.77, ΔT = -2.18 K, P_0 = 1.05

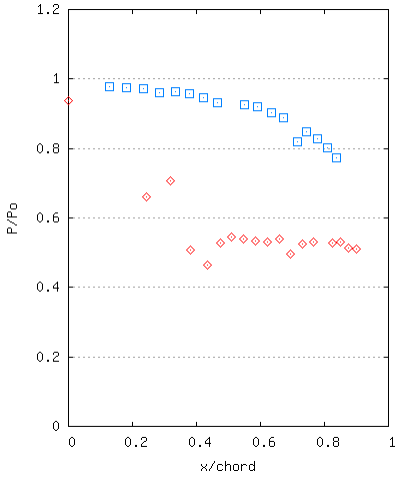

Test: 0203g
P_{ratio} = 1.80, ΔT = -1.98 K, P_0 = 1.06

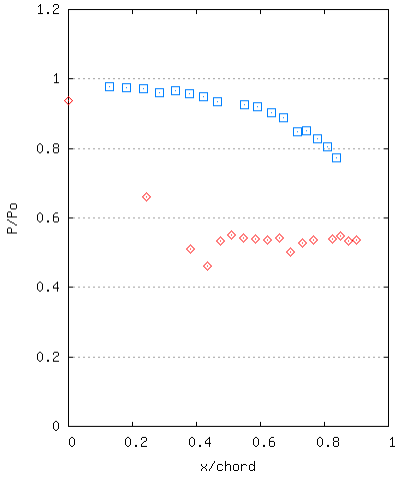

Test: 0203h
P_{ratio} = 1.82, ΔT = -1.98 K, P_0 = 1.06

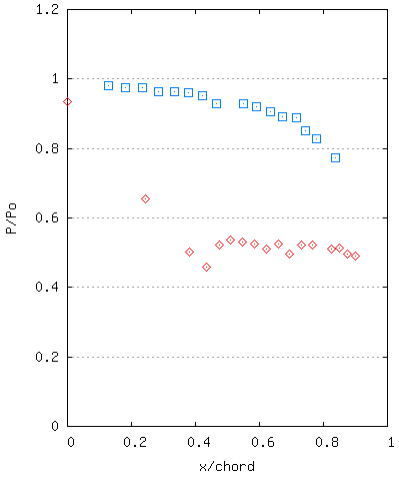

Test: 0203l
P_{ratio} = 1.88, ΔT = -11.69 K, P_0 = 1.04

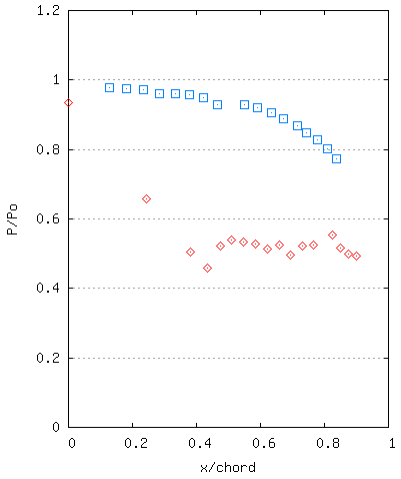

Test: 0203m
P_{ratio} = 1.89, ΔT = -11.40 K, P_0 = 1.06

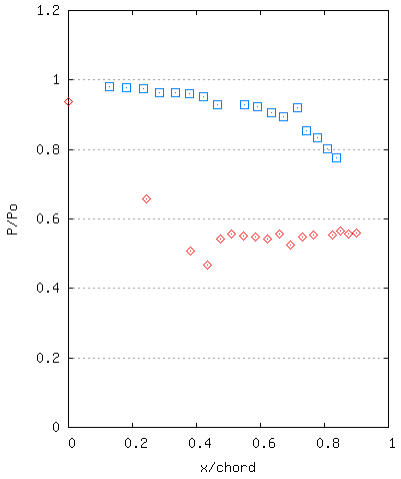

Test: 0203n
P_{ratio} = 1.77, ΔT = -11.40 K, P_0 = 1.05

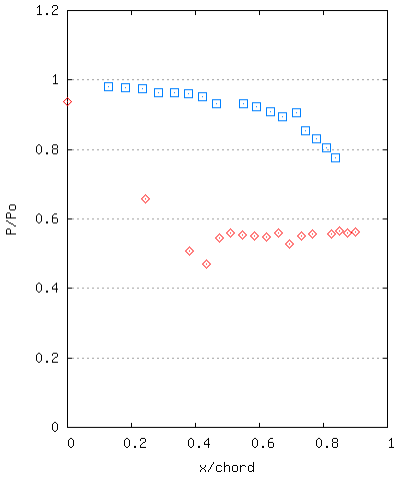

Test: 0203o
P_{ratio} = 1.77, ΔT = -10.83 K, P_0 = 1.07

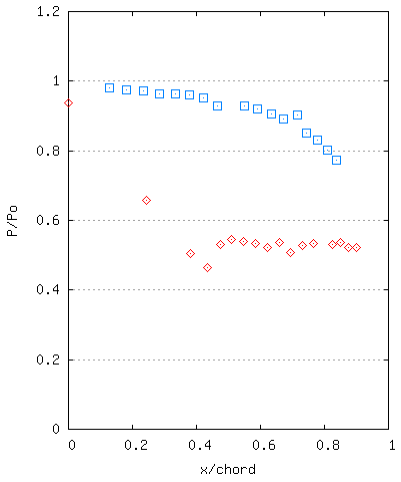

Test: 0203p
P_{ratio} = 1.87, ΔT = -10.83 K, P_0 = 1.07

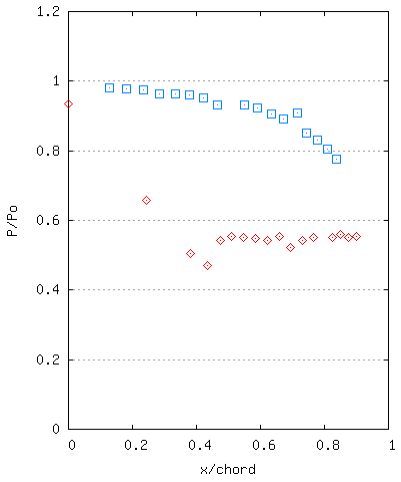

Test: 0203q
P_{ratio} = 1.80, ΔT = -10.83 K, P_0 = 1.06

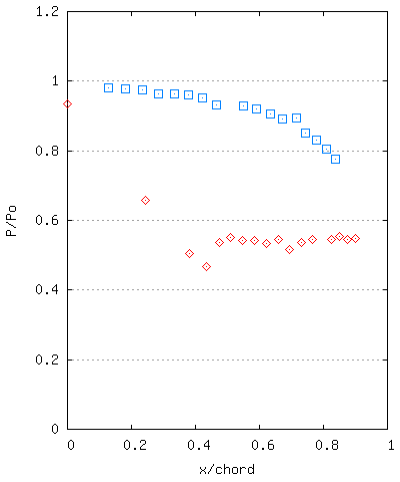

Test: 0203s
P_{ratio} = 1.79, ΔT = -11.12 K, P_0 = 1.08

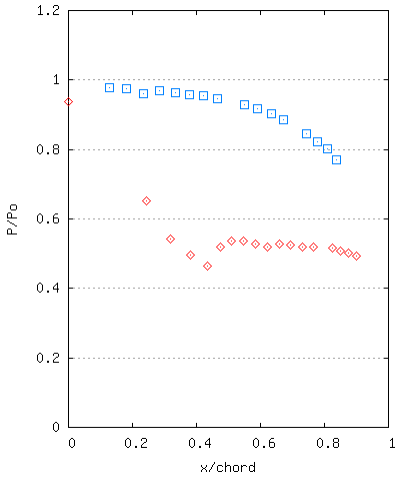

Test: 0503p
P_{ratio} = 1.90, ΔT = -11.50 K, P_0 = 1.09

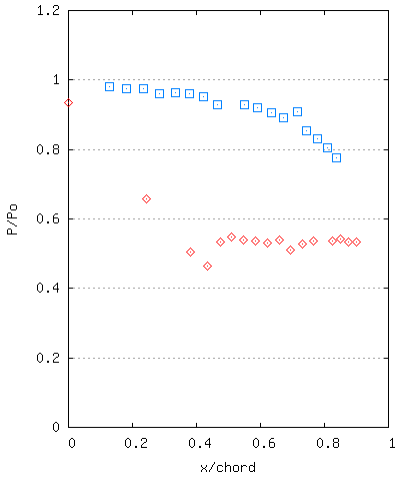

Test: 0203t
P_{ratio} = 1.85, ΔT = -12.76 K, P_0 = 1.07

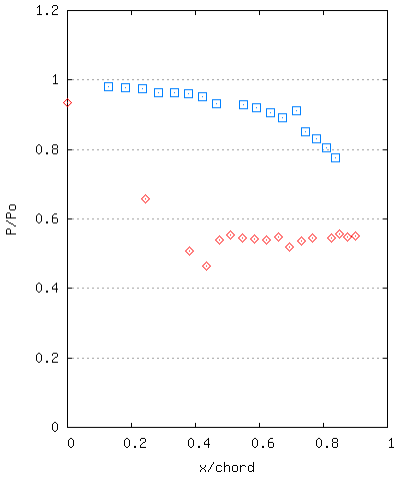

Test: 0203u
P_{ratio} = 1.81, ΔT = -13.51 K, P_0 = 1.06

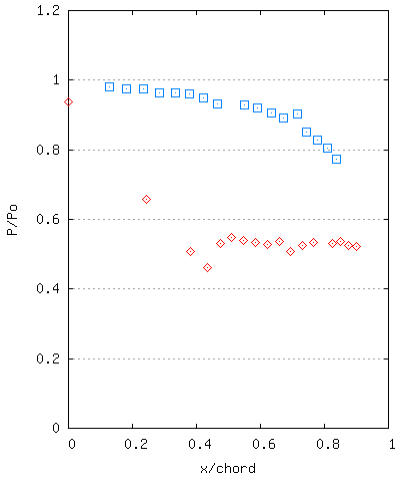

Test: 0203v
P_{ratio} = 1.84, ΔT = -12.47 K, P_0 = 1.07

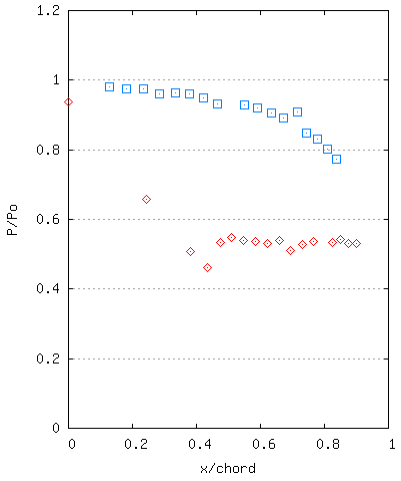

Test: 0203w
P_{ratio} = 1.85, ΔT = -12.47 K, P_0 = 1.07

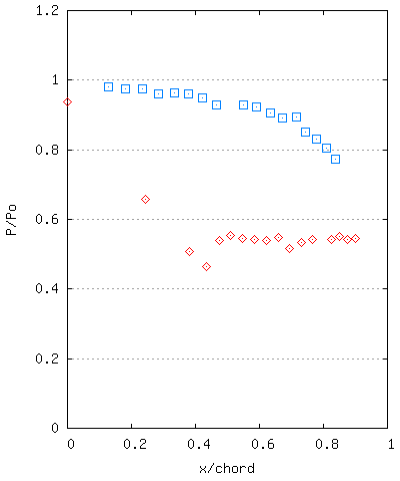

Test: 0203x
P_{ratio} = 1.80, ΔT = -12.85 K, P_0 = 1.05

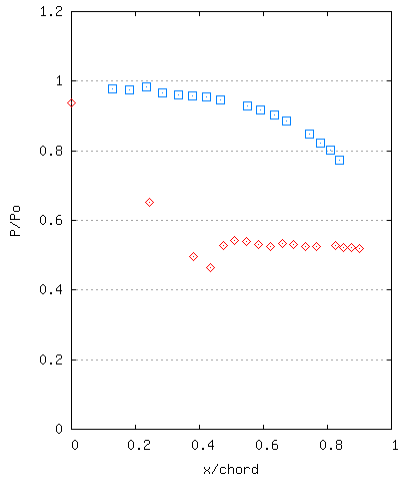

Test: 0503v
P_{ratio} = 1.86, ΔT = -14.16 K, P_0 = 1.09

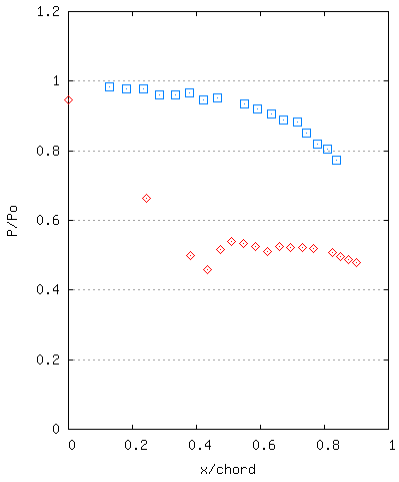

Test: 2904ab
P_{ratio} = 1.87, ΔT = -16.99 K, P_0 = 1.11

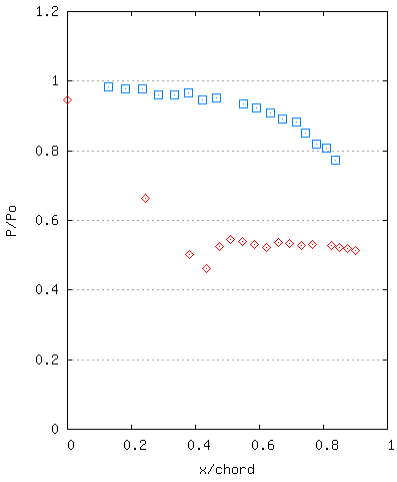

Test: 2904ac
P_{ratio} = 1.87, ΔT = -16.90 K, P_0 = 1.10

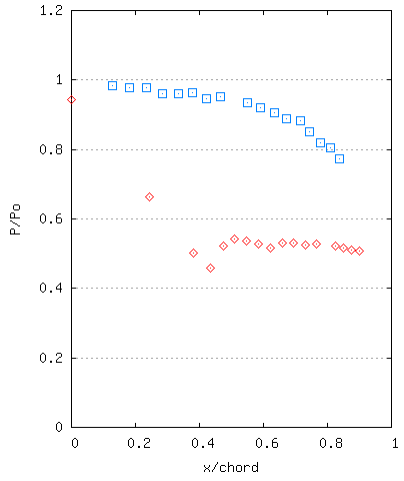

Test: 2904ad
P_{ratio} = 1.83, ΔT = -21.19 K, P_0 = 1.11

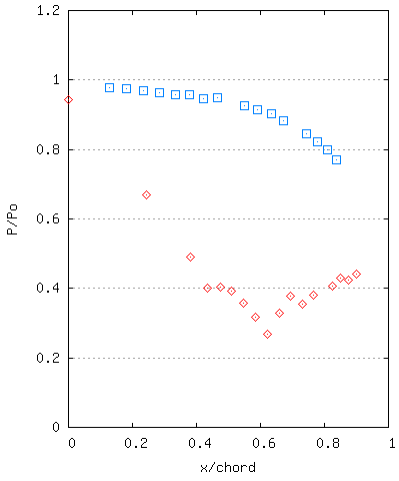

Test: 1203b
P_{ratio} = 2.47, ΔT = 27.98 K, P_0 = 1.07

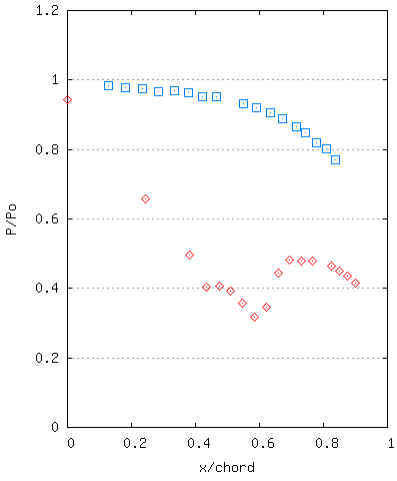

Test: 2704a
P_{ratio} = 2.30, ΔT = 27.15 K, P_0 = 1.14

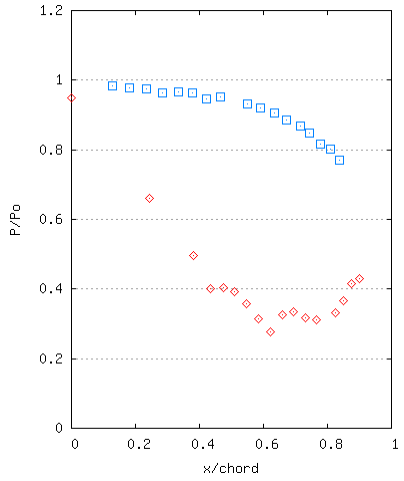

Test: 2704b
P_{ratio} = 2.71, ΔT = 31.06 K, P_0 = 1.13

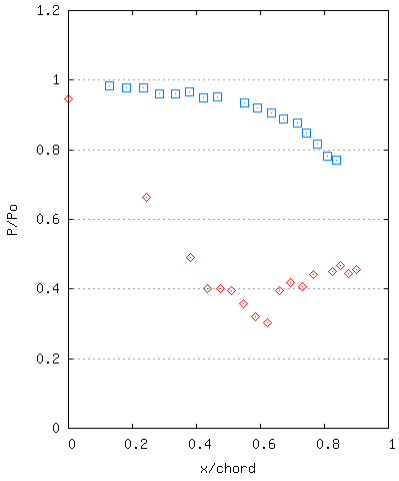

Test: 2704i
P_{ratio} = 2.37, ΔT = 26.50 K, P_0 = 1.11

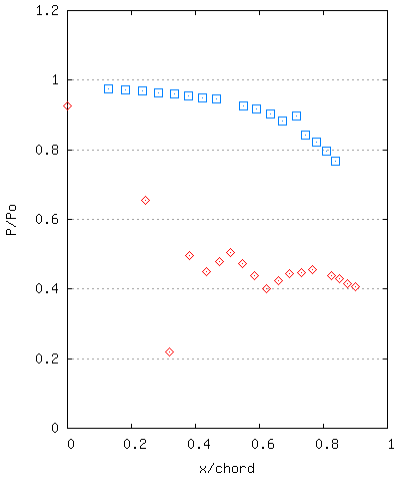

Test: 1002e
P_{ratio} = 2.24, ΔT = -0.89 K, P_0 = 1.10

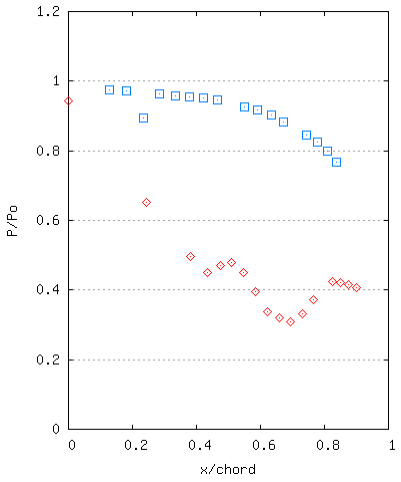

Test: 1002j
P_{ratio} = 2.35, ΔT = -0.99 K, P_0 = 1.11

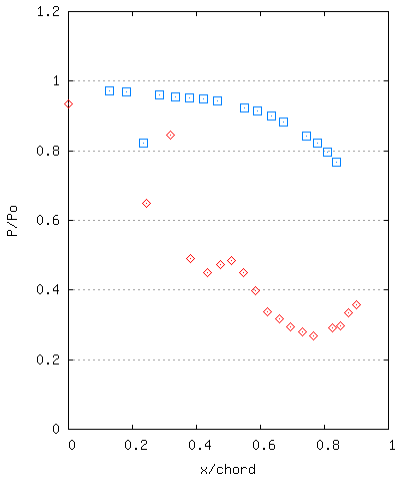

Test: 1002k
P_{ratio} = 2.45, ΔT = -1.18 K, P_0 = 1.11

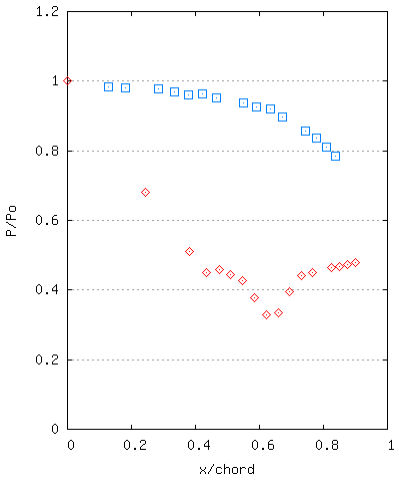

Test: 0503a
P_{ratio} = 2.63, ΔT = -1.58 K, P_0 = 1.10

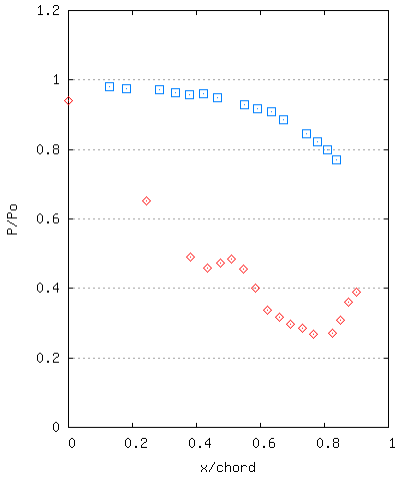

Test: 0503b
P_{ratio} = 2.48, ΔT = -1.48 K, P_0 = 1.10

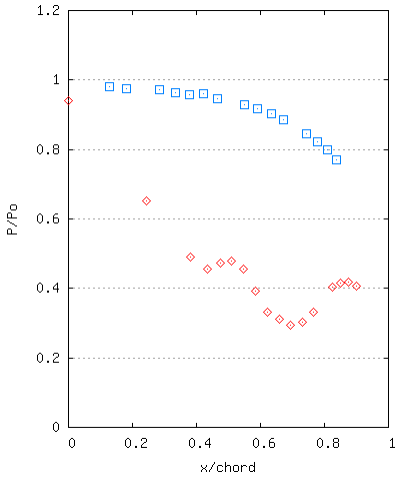

Test: 0503c
P_{ratio} = 2.36, ΔT = -1.58 K, P_0 = 1.09

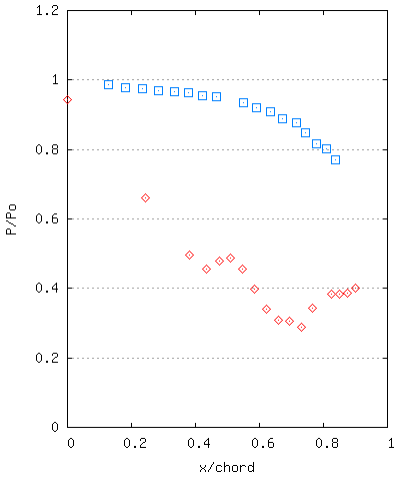

Test: 2904d
P_{ratio} = 2.28, ΔT = -0.49 K, P_0 = 1.12

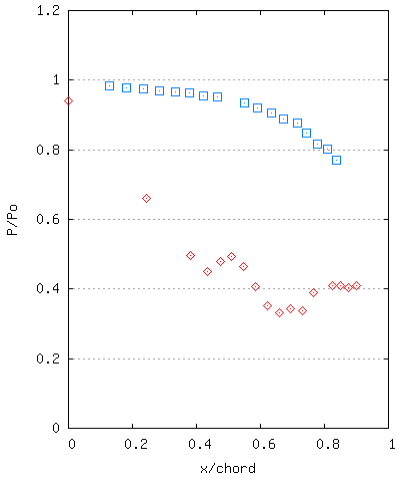

Test: 2904e
P_{ratio} = 2.28, ΔT = -0.59 K, P_0 = 1.11

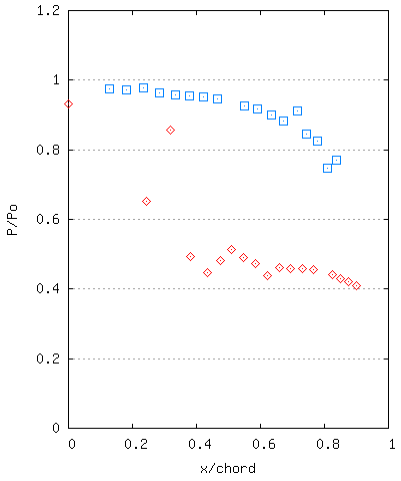

Test: 1002n
P_{ratio} = 2.15, ΔT = -10.45 K, P_0 = 1.08

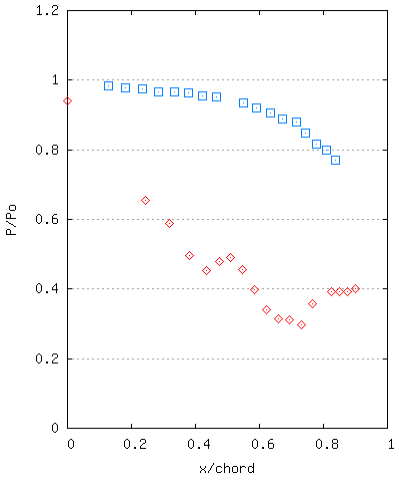

Test: 2904f
P_{ratio} = 2.28, ΔT = -10.45 K, P_0 = 1.16

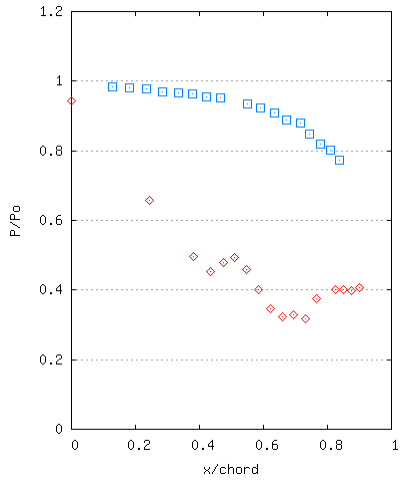

Test: 2904g
P_{ratio} = 2.32, ΔT = -10.55 K, P_0 = 1.13

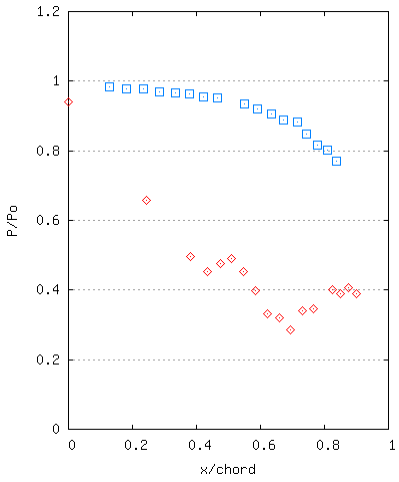

Test: 2904h
P_{ratio} = 2.31, ΔT = -10.07 K, P_0 = 1.13

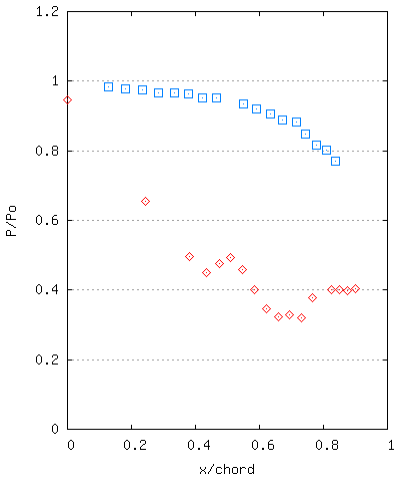

Test: 2904i
P_{ratio} = 2.27, ΔT = -10.07 K, P_0 = 1.14

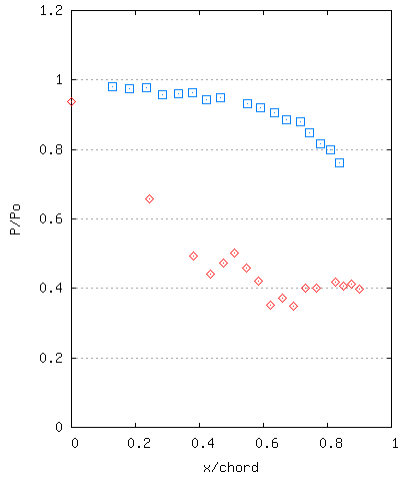

Test: 2904v
P_{ratio} = 2.21, ΔT = -17.18 K, P_0 = 1.11

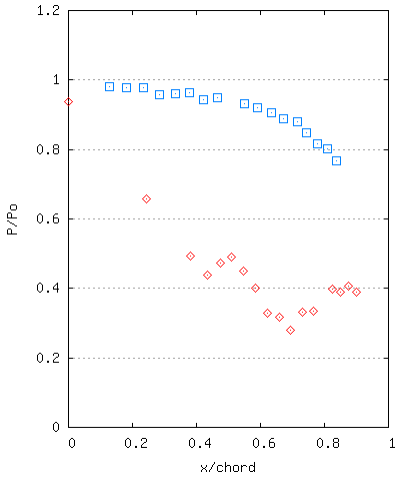

Test: 2904x
P_{ratio} = 2.24, ΔT = -16.90 K, P_0 = 1.11

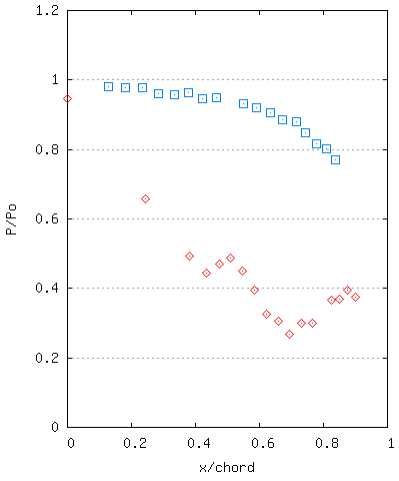

Test: 2904af
P_{ratio} = 2.31, ΔT = -21.19 K, P_0 = 1.11

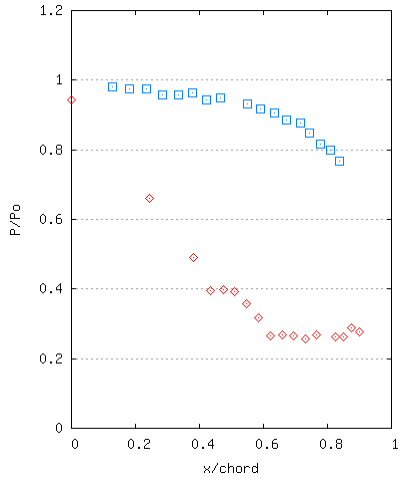

Test: 2704g
P_{ratio} = 3.05, ΔT = 32.35 K, P_0 = 1.12

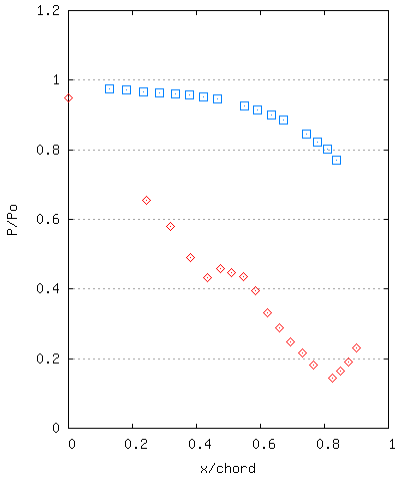

Test: 0903c
P_{ratio} = 3.49, ΔT = -1.78 K, P_0 = 1.09

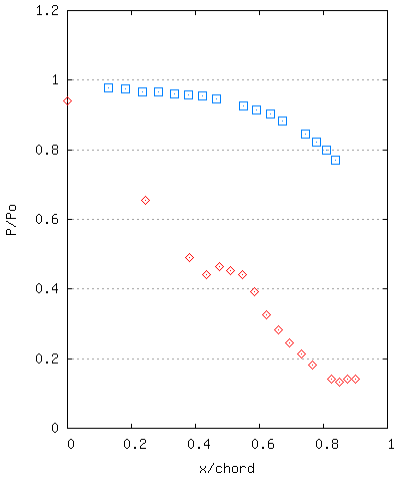

Test: 0903d
P_{ratio} = 3.61, ΔT = -1.88 K, P_0 = 1.09

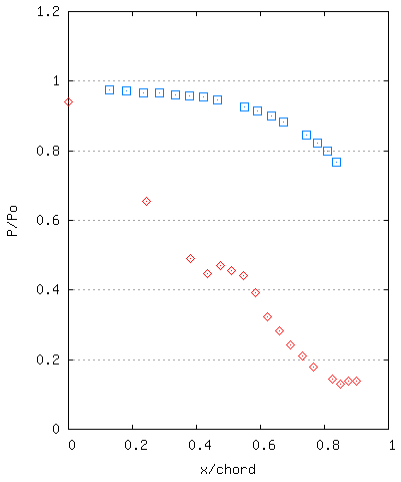

Test: 0903e
P_{ratio} = 3.47, ΔT = -1.78 K, P_0 = 1.09

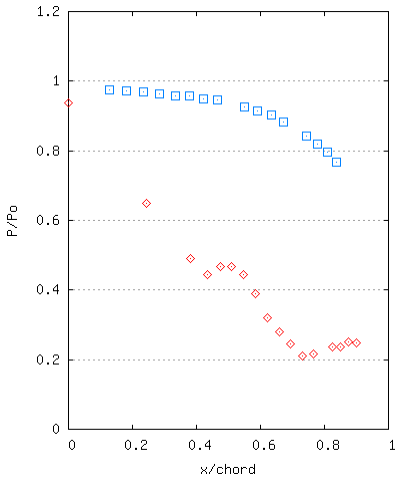

Test: 0903t
P_{ratio} = 3.15, ΔT = -10.17 K, P_0 = 1.08

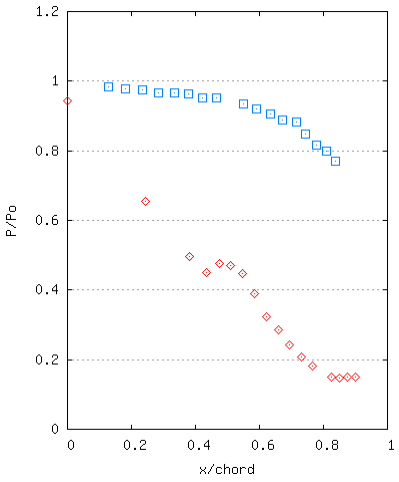

Test: 2904j
P_{ratio} = 3.25, ΔT = -10.17 K, P_0 = 1.14

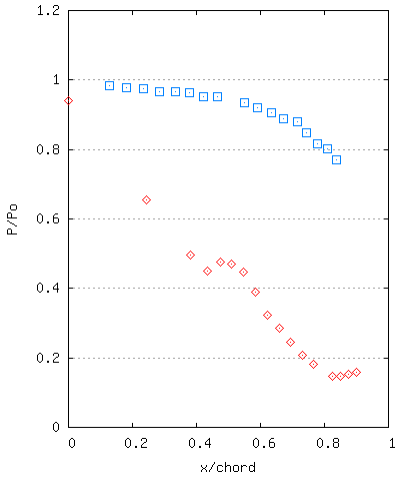

Test: 2904k
P_{ratio} = 3.24, ΔT = -10.07 K, P_0 = 1.13

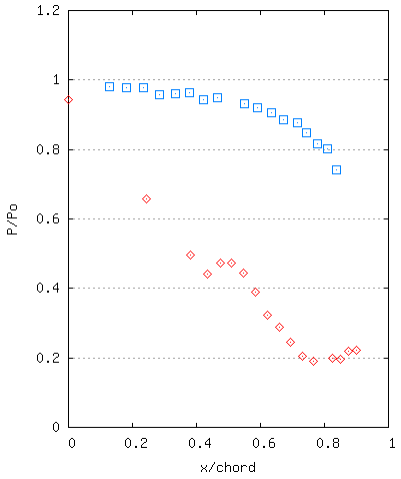

Test: 2904p
P_{ratio} = 3.65, ΔT = -10.45 K, P_0 = 1.11

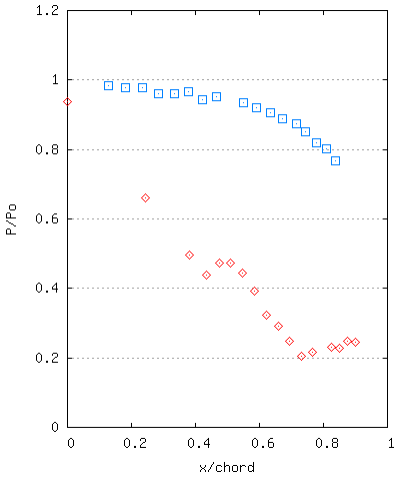

Test: 2904r
P_{ratio} = 3.21, ΔT = -16.99 K, P_0 = 1.10

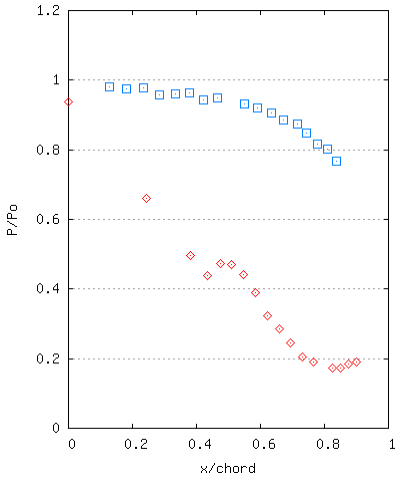

Test: 2904s
P_{ratio} = 3.24, ΔT = -16.99 K, P_0 = 1.12

D.2.2 Steam Dosed with 4ppm of Ammonia

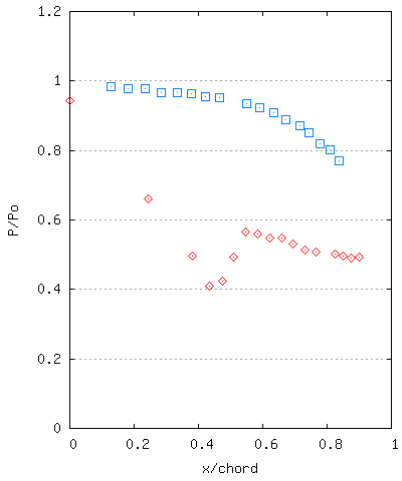

Test: 1904c
P_{ratio} = 1.78, ΔT = +34.04 K, P_0 = 1.10

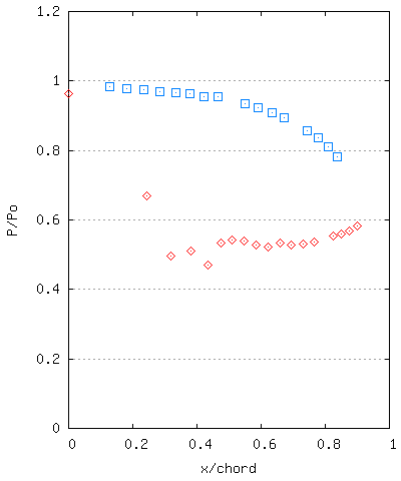

Test: 1603a
P_{ratio} = 1.82, ΔT = -0.39 K, P_0 = 1.09

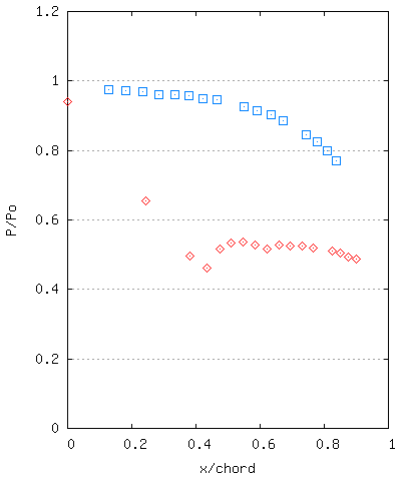

Test: 1603c
P_{ratio} = 1.82, ΔT = -0.79 K, P_0 = 1.12

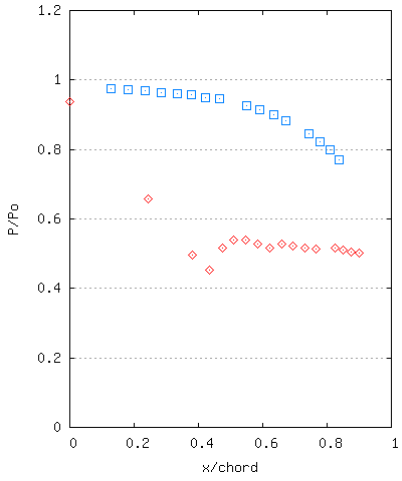

Test: 1603d
P_{ratio} = 1.85, ΔT = -0.29 K, P_0 = 1.10

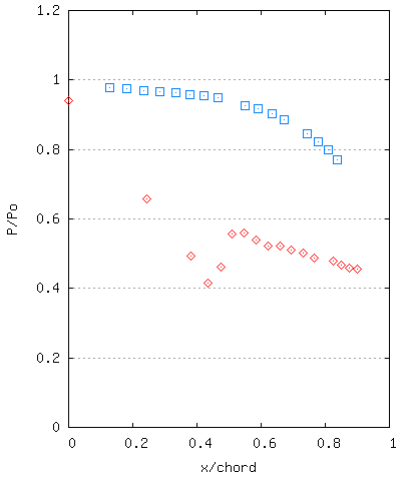

Test: 2603b
P_{ratio} = 1.86, ΔT = -0.49 K, P_0 = 1.09

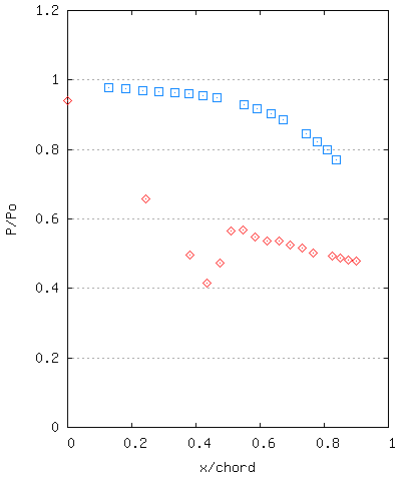

Test: 2603c
P_{ratio} = 1.81, ΔT = -0.19 K, P_0 = 1.07

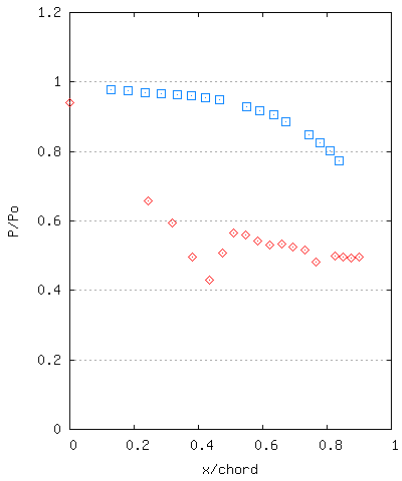

Test: 2603d
P_{ratio} = 1.80, ΔT = -0.19, P_0 = 1.08

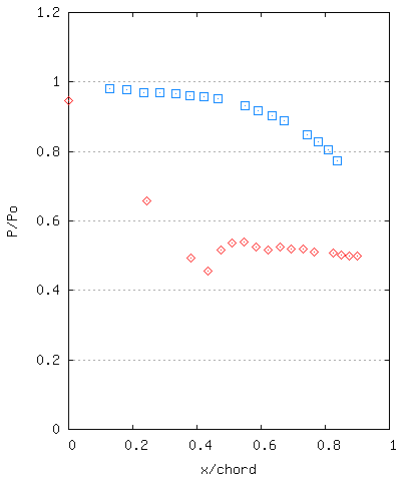

Test: 2903a
P_{ratio} = 1.84, ΔT = -1.98 K, P_0 = 1.08

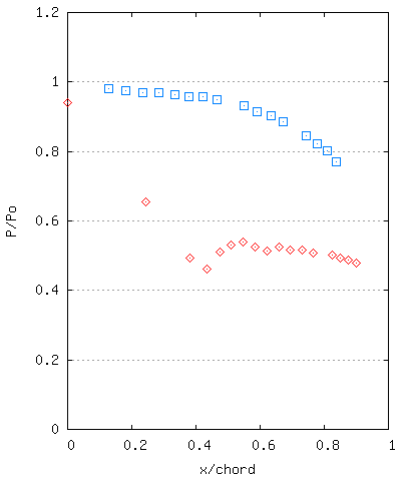

Test: 2903b
P_{ratio} = 1.83, ΔT = -1.78 K, P_0 = 1.08

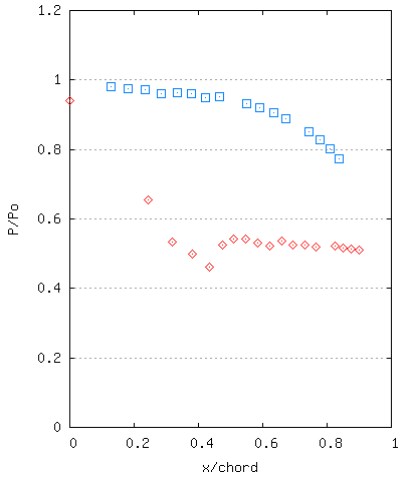

Test: 0104a
P_{ratio} = 1.86, ΔT = -11.02 K, P_0 = 1.10

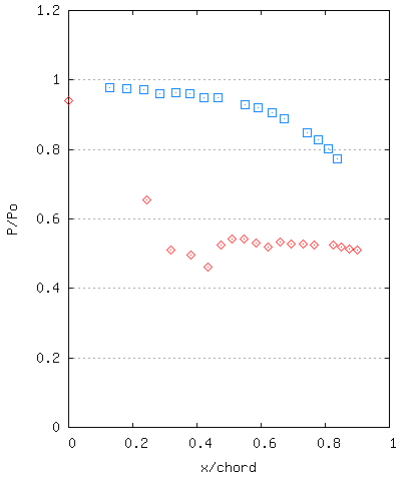

Test: 0104c
P_{ratio} = 1.82, ΔT = -10.83 K, P_0 = 1.10

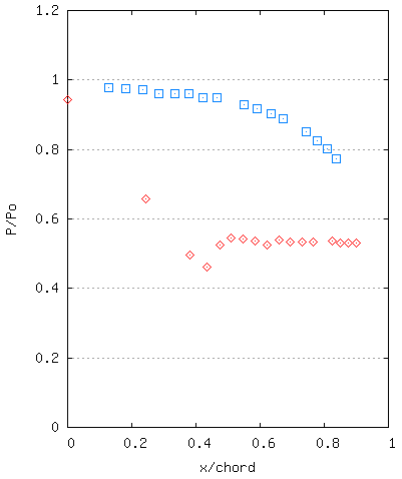

Test: 0104d
P_{ratio} = 1.84, ΔT = -10.93 K, P_0 = 1.09

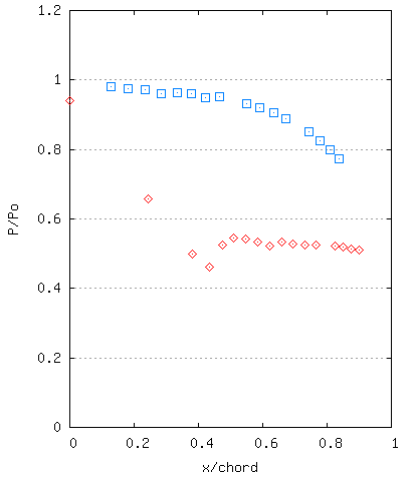

Test: 0104e
P_{ratio} = 1.84, ΔT = -10.74 K, P_0 = 1.09

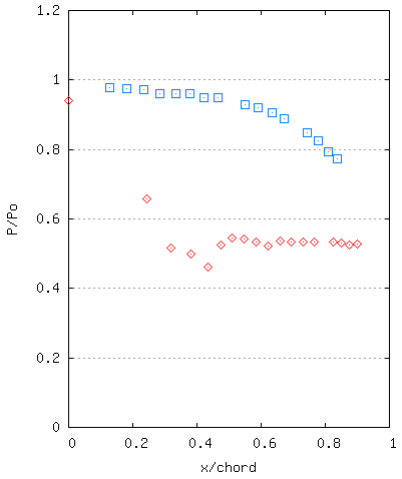

Test: 0104i
P_{ratio} = 1.78, ΔT = -13.32 K, P_0 = 1.09

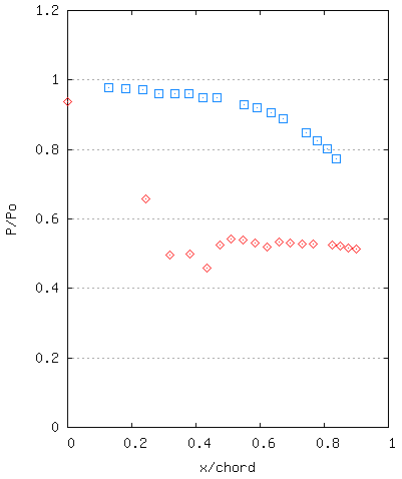

Test: 0104j
P_{ratio} = 1.78, ΔT = -13.32 K, P_0 = 1.10

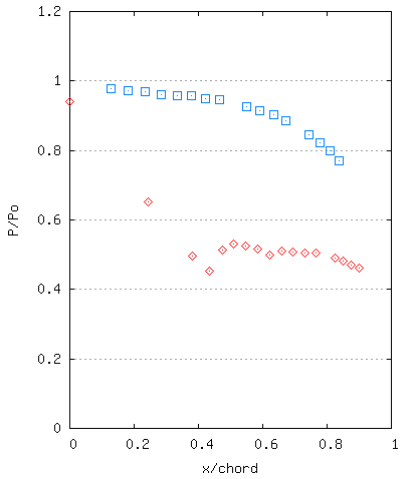

Test: 2303v
P_{ratio} = 1.88, ΔT = -17.23 K, P_0 = 1.09

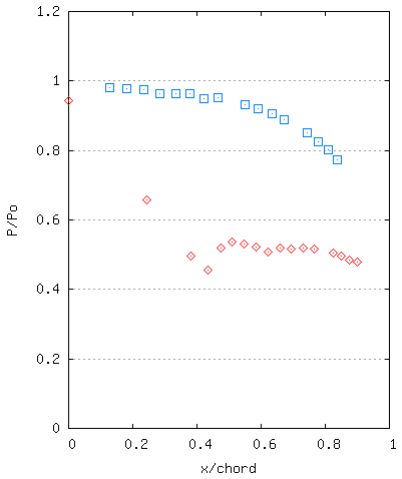

Test: 0104k
P_{ratio} = 1.86, ΔT = -17.36 K, P_0 = 1.09

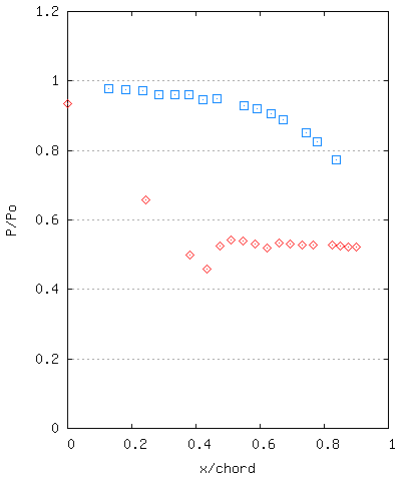

Test: 0104l
P_{ratio} = 1.81, ΔT = -17.18 K, P_0 = 1.10

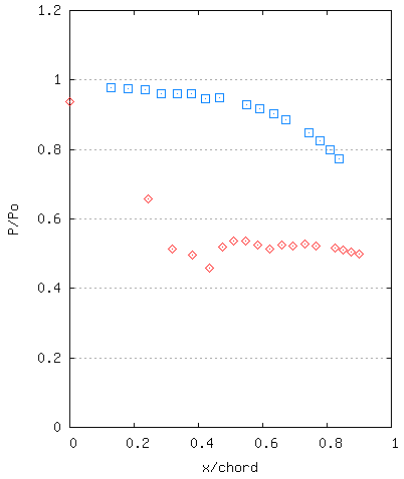

Test: 0104m
P_{ratio} = 1.84, ΔT = -17.36 K, P_0 = 1.09

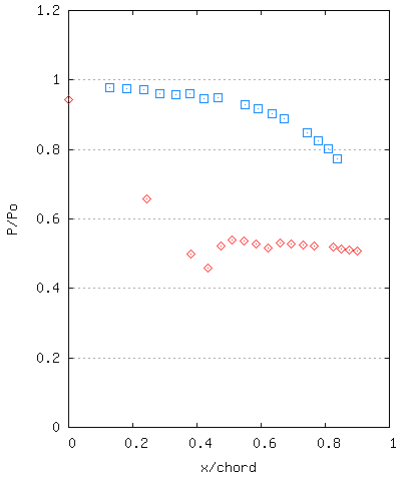

Test: 0104n
P_{ratio} = 1.84, ΔT = -17.36 K, P_0 = 1.09

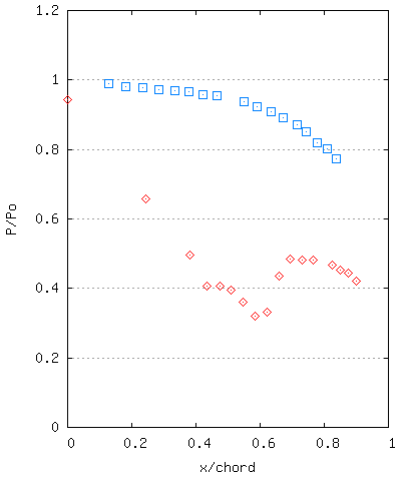

Test: 1904a
P_{ratio} = 2.36, ΔT = +27.64 K, P_0 = 1.11

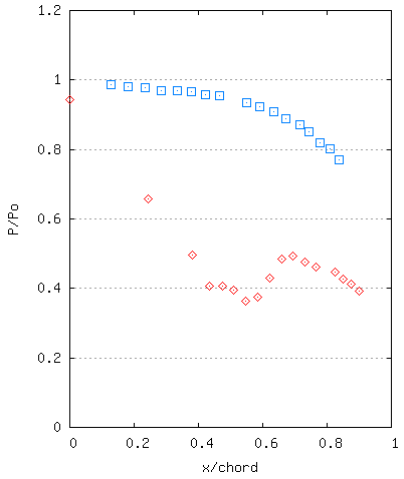

Test: 1904b
P_{ratio} = 2.29, ΔT = +32.57 K, P_0 = 1.11

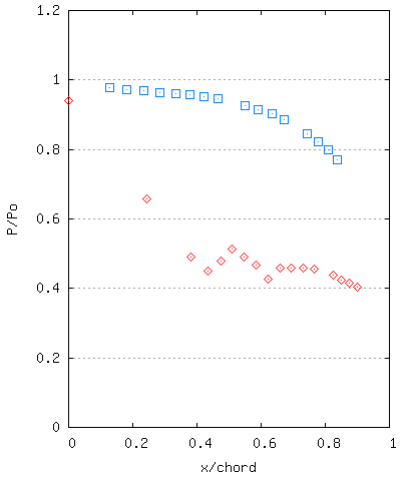

Test: 1603h
P_{ratio} = 2.20, ΔT = -0.49 K, P_0 = 1.10

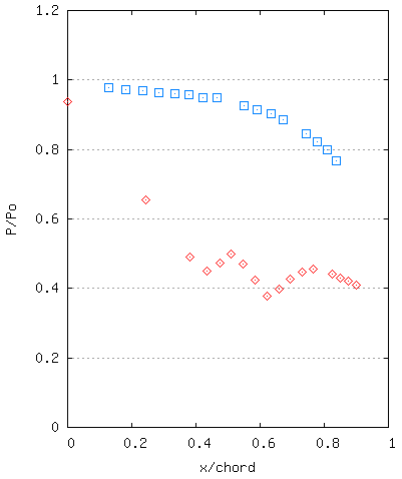

Test: 1603i
P_{ratio} = 2.20, ΔT = -0.39 K, P_0 = 1.10

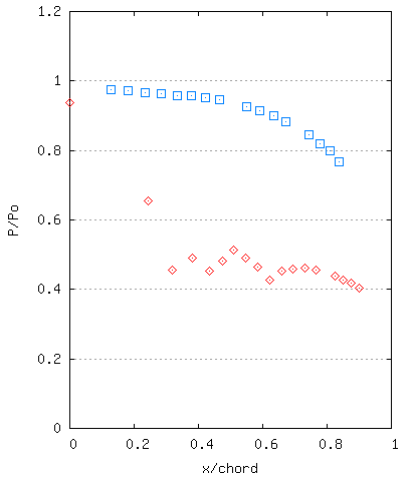

Test: 1603m
P_{ratio} = 2.19, ΔT = -0.79 K, P_0 = 1.09

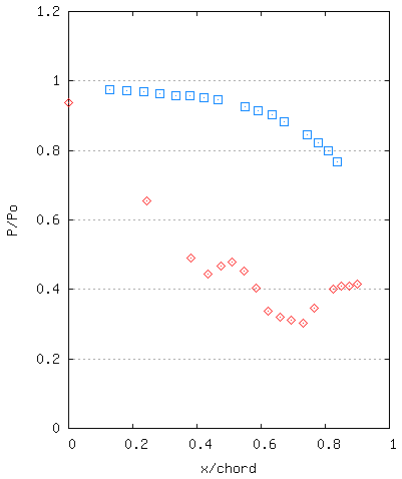

Test: 1603v
P_{ratio} = 2.34, ΔT = -1.18 K, P_0 = 1.09

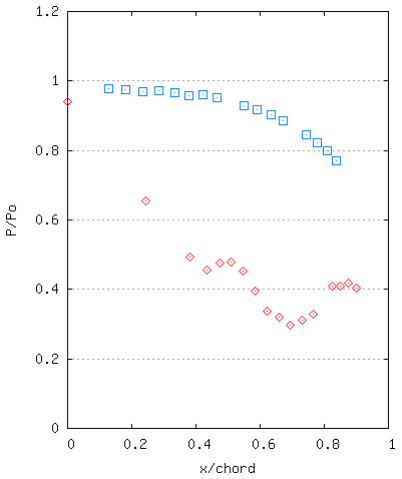

Test: 1903d
P_{ratio} = 2.35, ΔT = -1.48 K, P_0 = 1.10

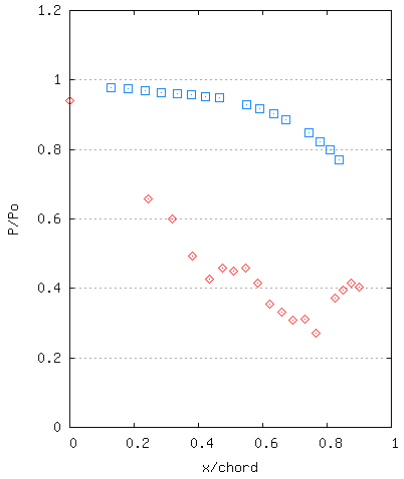

Test: 2603e
P_{ratio} = 2.44, ΔT = -0.69 K, P_0 = 1.09

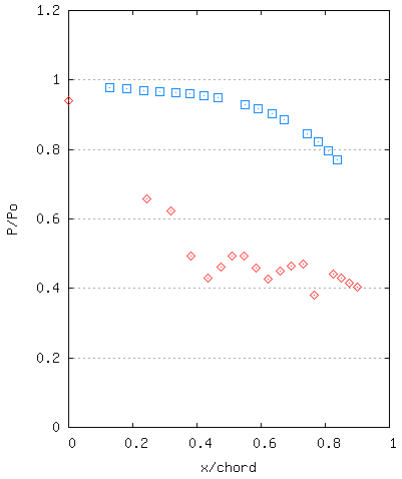

Test: 2603f
P_{ratio} = 2.19, ΔT = -0.19 K, P_0 = 1.09

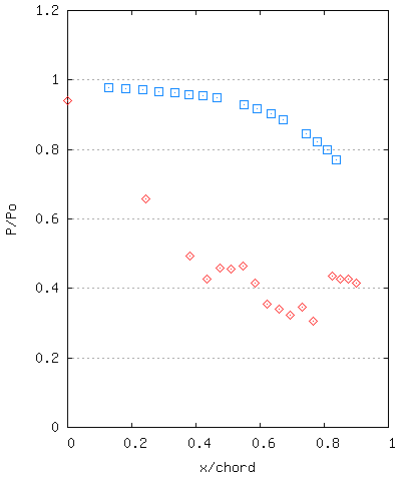

Test: 2603g
P_{ratio} = 2.40, ΔT = -0.40 K, P_0 = 1.08

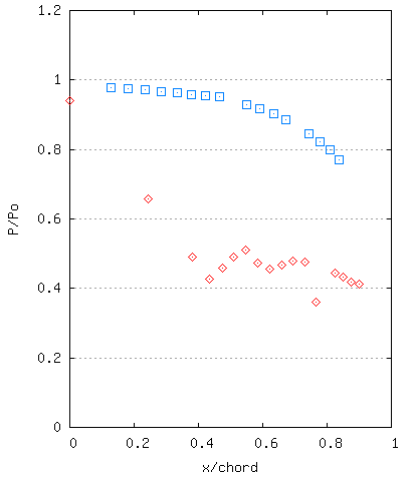

Test: 2603h
P_{ratio} = 2.24, ΔT = -1.10 K, P_0 = 1.08

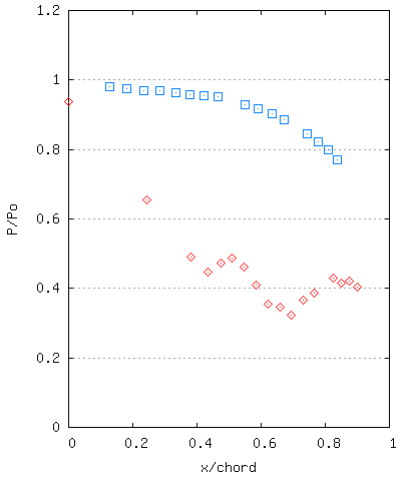

Test: 2903f
P_{ratio} = 2.33, ΔT = -1.18 K, P_0 = 1.09

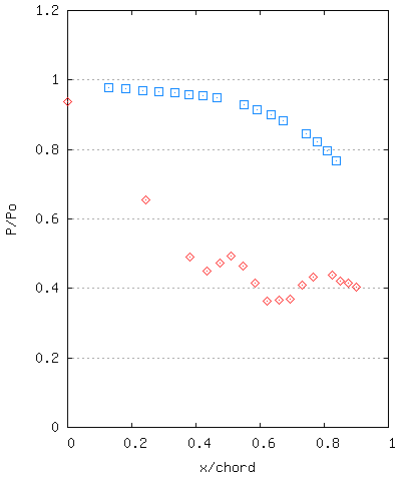

Test: 2903g
P_{ratio} = 2.22, ΔT = -1.48 K, P_0 = 1.09

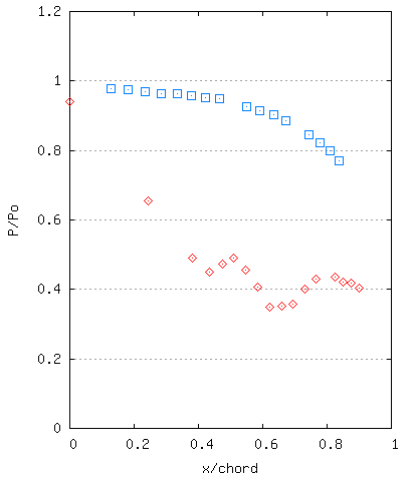

Test: 2903h
P_{ratio} = 2.34, ΔT = -1.58 K, P_0 = 1.09

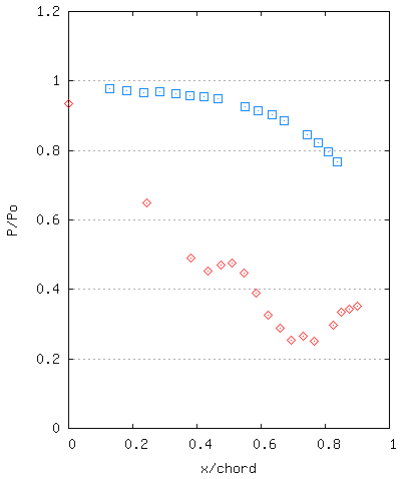

Test: 1903i
P_{ratio} = 2.47, ΔT = -11.02 K, P_0 = 1.09

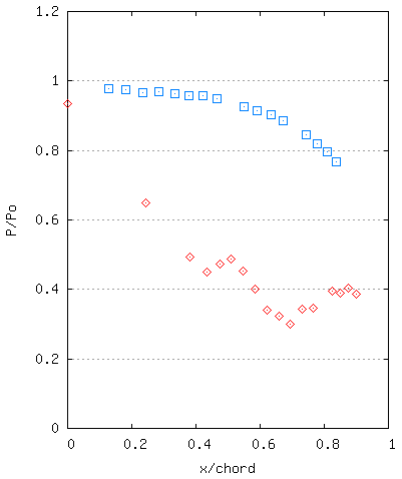

Test: 1903j
P_{ratio} = 2.39, ΔT = -10.93 K, P_0 = 1.10

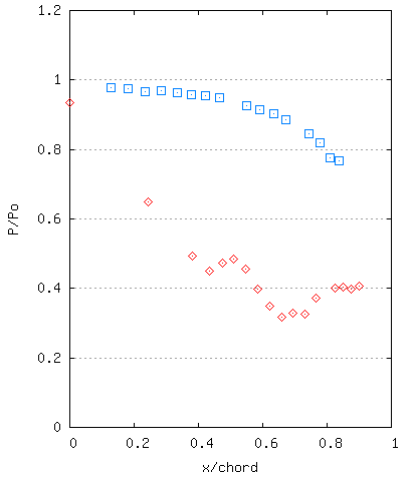

Test: 1903l
P_{ratio} = 2.32, ΔT = -10.93 K, P_0 = 1.10

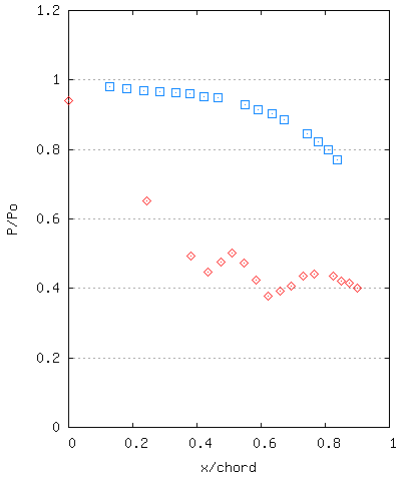

Test: 2303b
P_{ratio} = 2.36, ΔT = -8.45 K, P_0 = 1.07

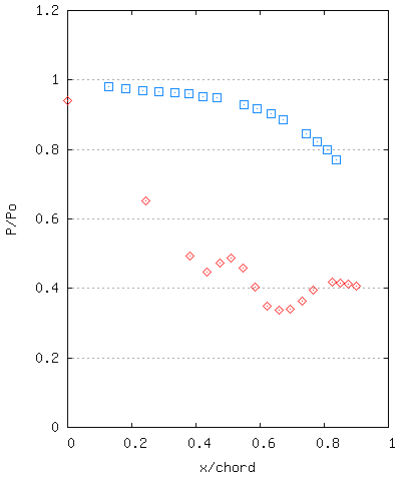

Test: 2303c
P_{ratio} = 2.31, ΔT = -7.60 K, P_0 = 1.08

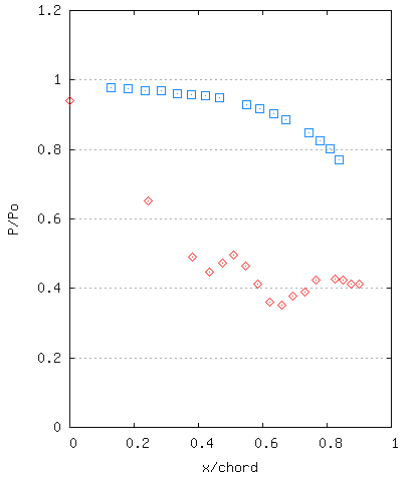

Test: 2603s
P_{ratio} = 2.25, ΔT = -11.71 K, P_0 = 1.07

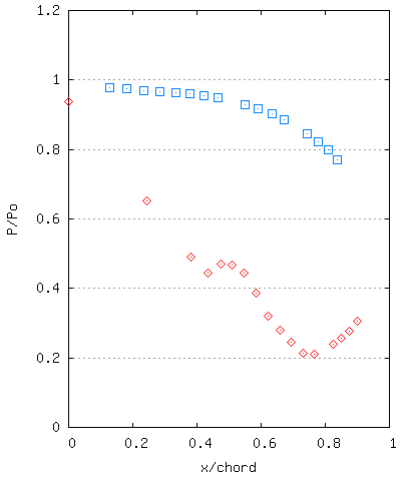

Test: 2303m
P_{ratio} = 2.53, ΔT = -13.31 K, P_0 = 1.07

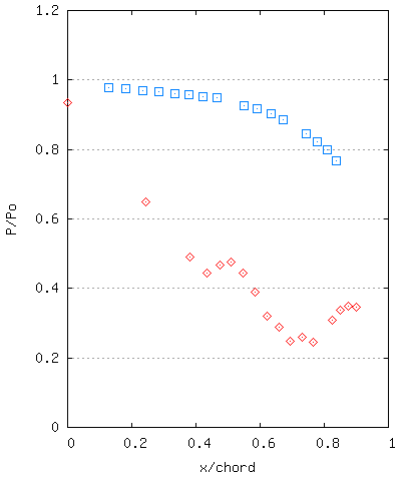

Test: 2303n
P_{ratio} = 2.39, ΔT = -12.94 K, P_0 = 1.08

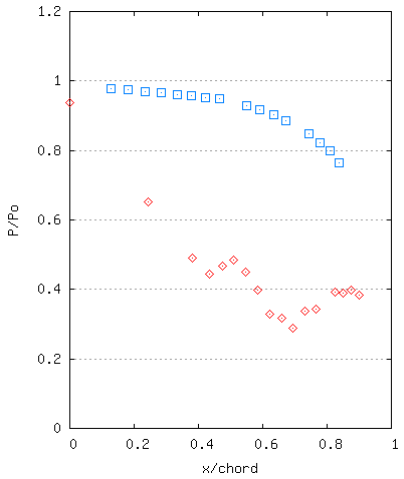

Test: 2303q
P_{ratio} = 2.30, ΔT = -12.76 K, P_0 = 1.08

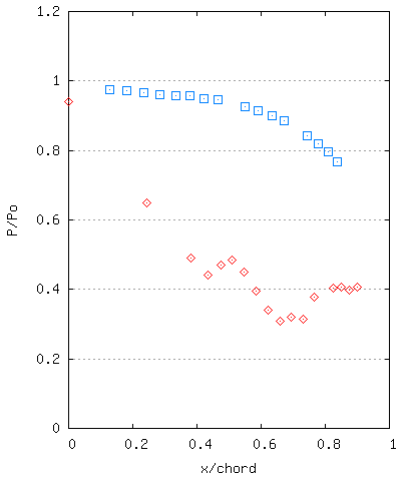

Test: 2303t
P_{ratio} = 2.21, ΔT = -17.95 K, P_0 = 1.08

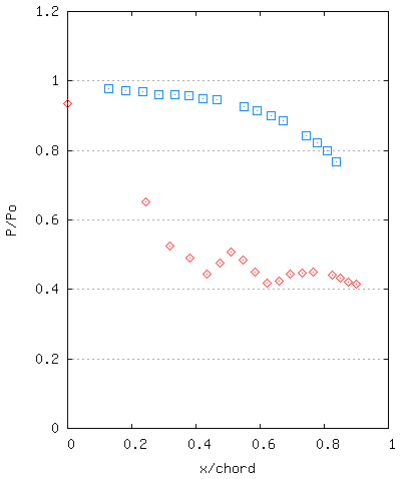

Test: 2903n
P_{ratio} = 2.18, ΔT = -17.36 K, P_0 = 1.09

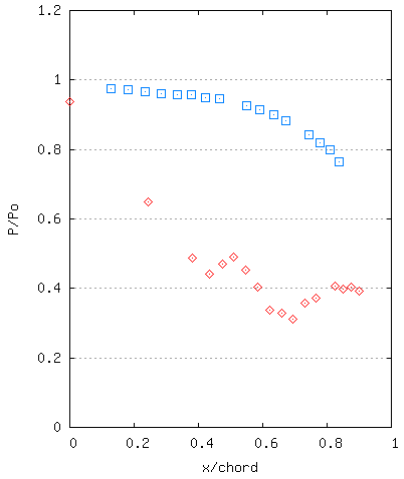

Test: 2903o
P_{ratio} = 2.34, ΔT = -17.45 K, P_0 = 1.09

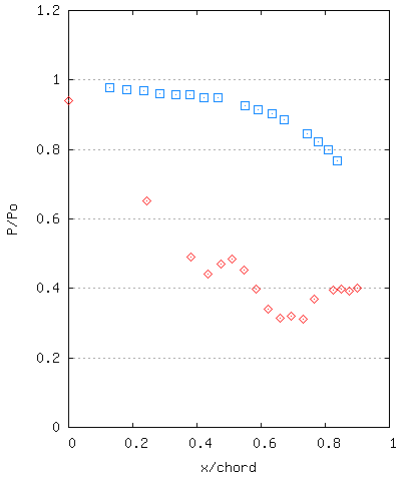

Test: 2903p
P_{ratio} = 2.40, ΔT = -17.54 K, P_0 = 1.08

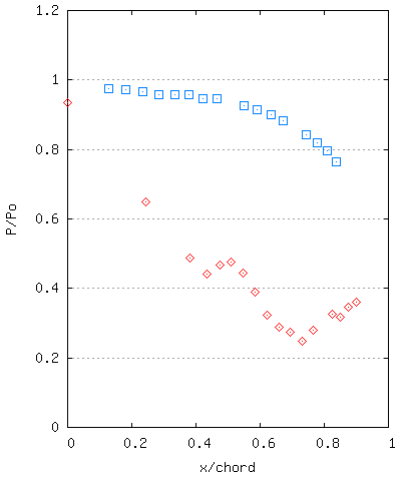

Test: 2903r
P_{ratio} = 2.34, ΔT = -17.54 K, P_0 = 1.08

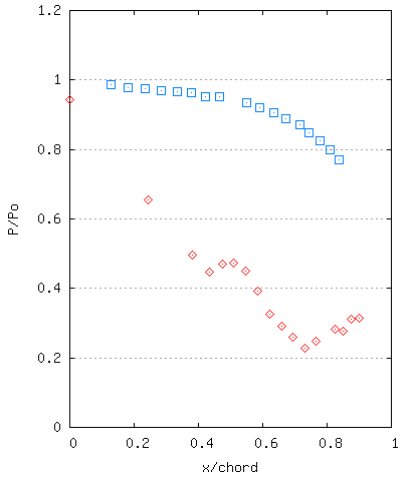

Test: 1404f
P_{ratio} = 2.46, ΔT = -17.73 K, P_0 = 1.07

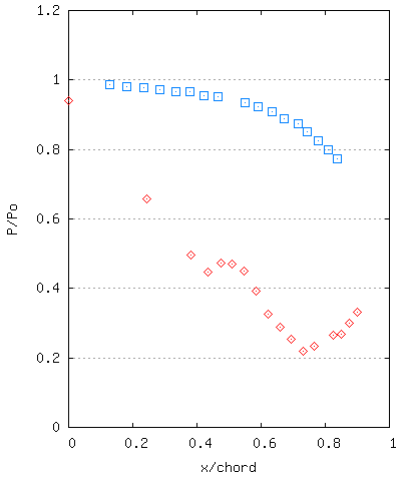

Test: 1404j
P_{ratio} = 2.50, ΔT = -17.18 K, P_0 = 1.07

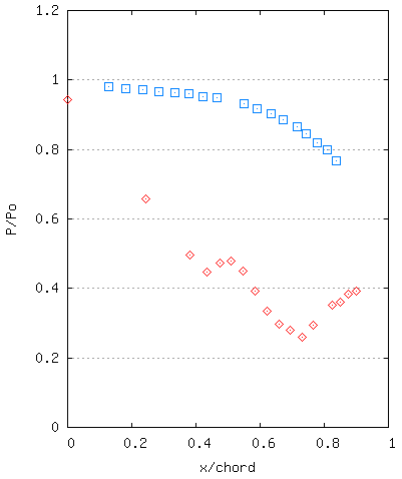

Test: 1604c
P_{ratio} = 2.41, ΔT = -21.19 K, P_0 = 1.08

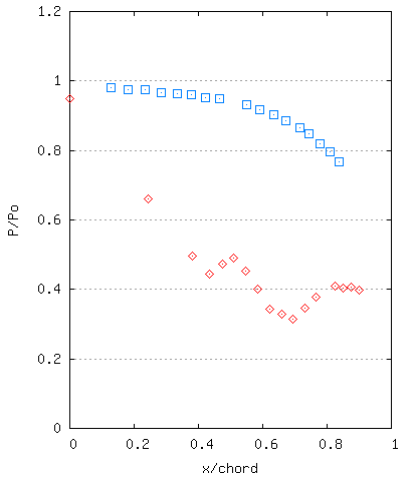

Test: 1604d
P_{ratio} = 2.35, ΔT = -21.10 K, P_0 = 1.08

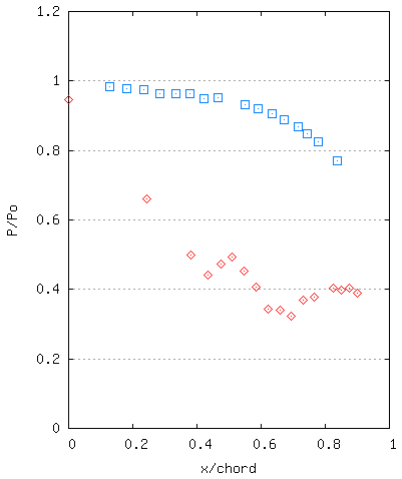

Test: 1604f
P_{ratio} = 2.27, ΔT = -21.01 K, P_0 = 1.08

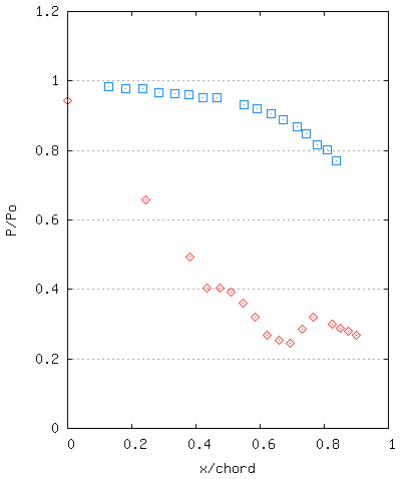

Test: 1904e
P_{ratio} = 3.02, ΔT = +31.88 K, P_0 = 1.11

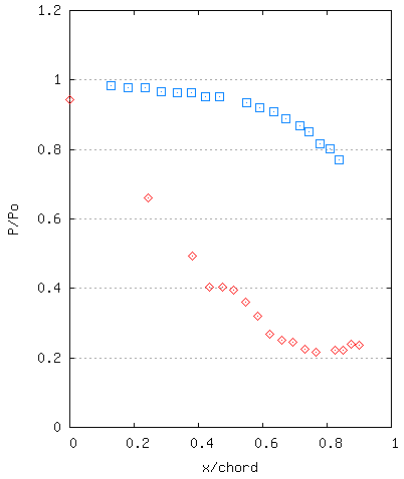

Test: 1904f
P_{ratio} = 3.06, ΔT = +33.85 K, P_0 = 1.10

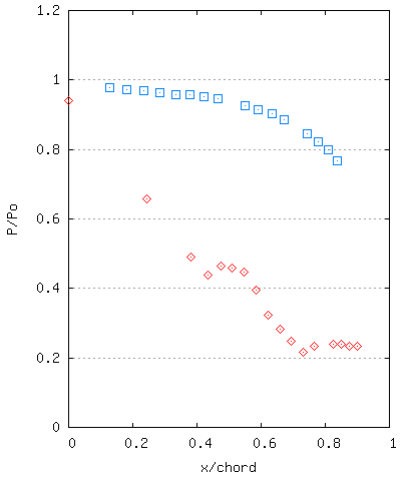

Test: 1603y
P_{ratio} = 3.27, ΔT = -1.08 K, P_0 = 1.09

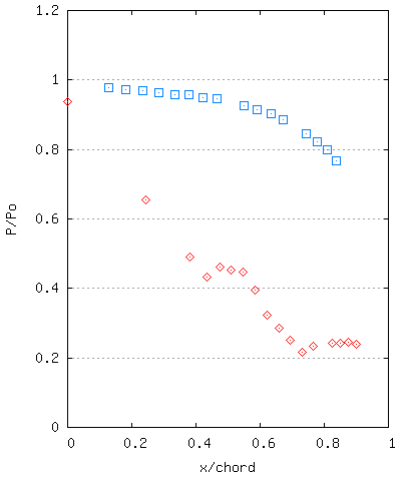

Test: 1603z
P_{ratio} = 3.25, ΔT = -0.99 K, P_0 = 1.10

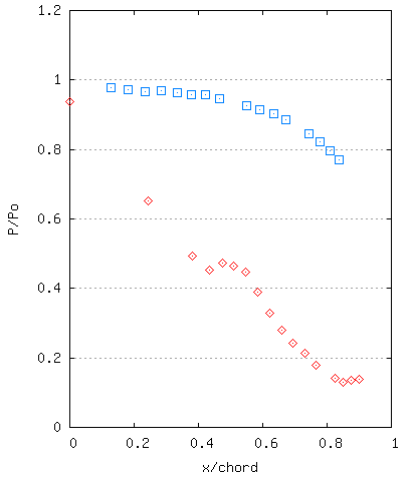

Test: 1903e
P_{ratio} = 3.72, ΔT = -1.48 K, P_0 = 1.10

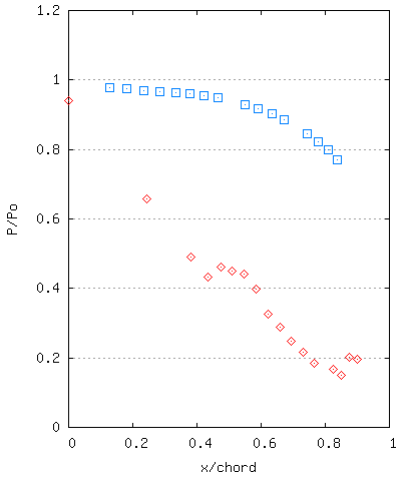

Test: 2603k
P_{ratio} = 3.52, ΔT = -1.30 K, P_0 = 1.08

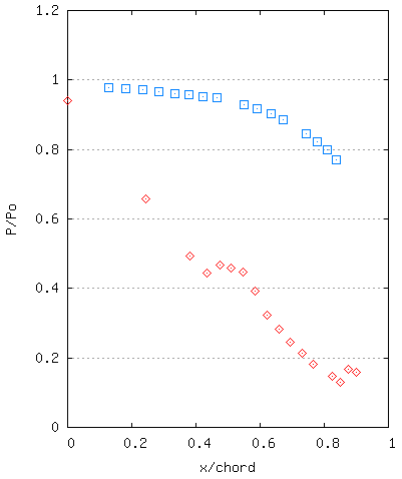

Test: 2603n
P_{ratio} = 3.42, ΔT = -0.19 K, P_0 = 1.09

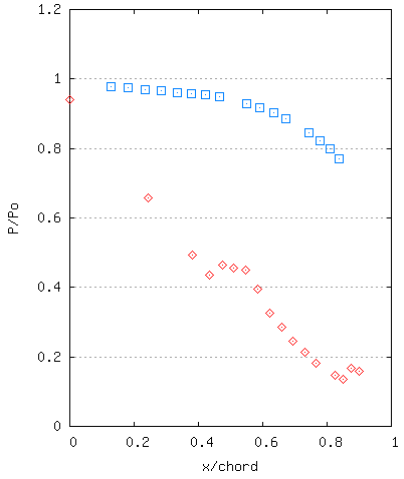

Test: 2603o
P_{ratio} = 3.45, ΔT = -0.30 K, P_0 = 1.08

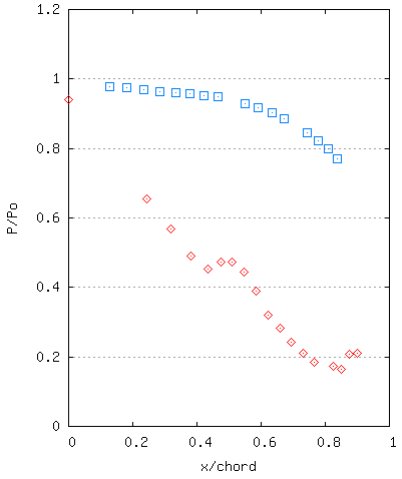

Test: 2903i
P_{ratio} = 3.28, ΔT = -1.68 K, P_0 = 1.09

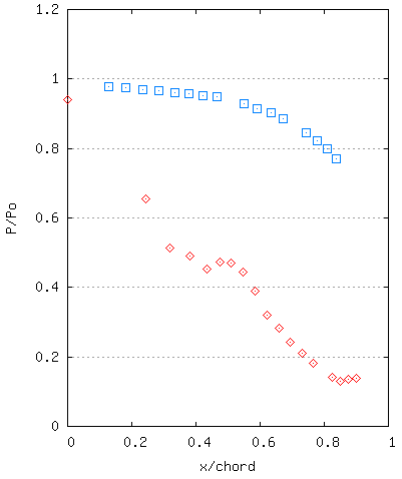

Test: 2903j
P_{ratio} = 3.87, ΔT = -1.68 K, P_0 = 1.08

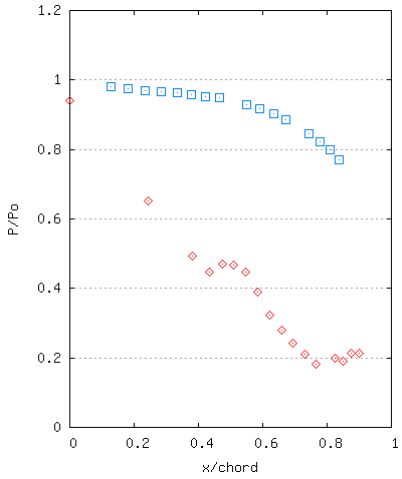

Test: 2303f
P_{ratio} = 3.54, ΔT = -8.64 K, P_0 = 1.08

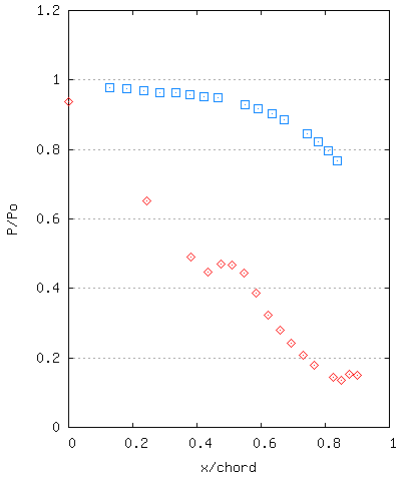

Test: 2303g
P_{ratio} = 3.59, ΔT = -8.83 K, P_0 = 1.09

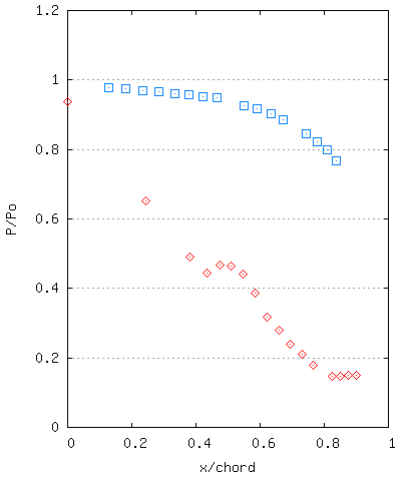

Test: 2303l
P_{ratio} = 3.62, ΔT = -13.96 K, P_0 = 1.09

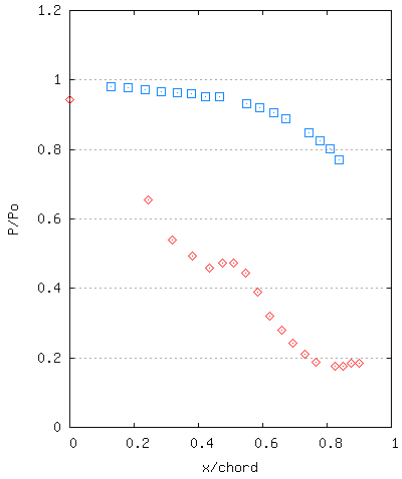

Test: 2303o
P_{ratio} = 3.34, ΔT = -12.57 K, P_0 = 1.34

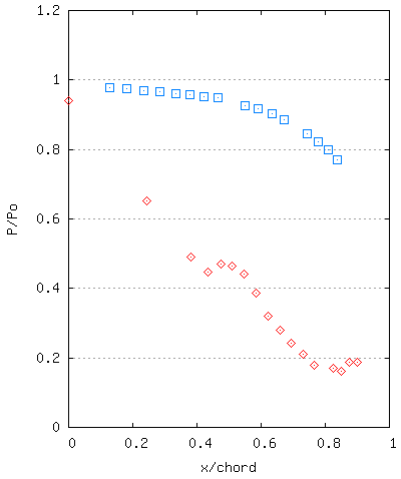

Test: 2603p
P_{ratio} = 3.38, ΔT = -17.45 K, P_0 = 1.09

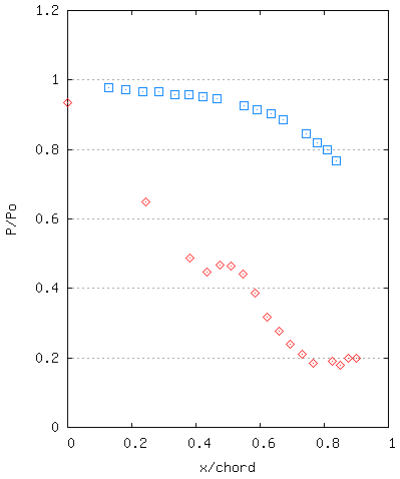

Test: 2603q
P_{ratio} = 3.58, ΔT = -17.45 K, P_0 = 1.09

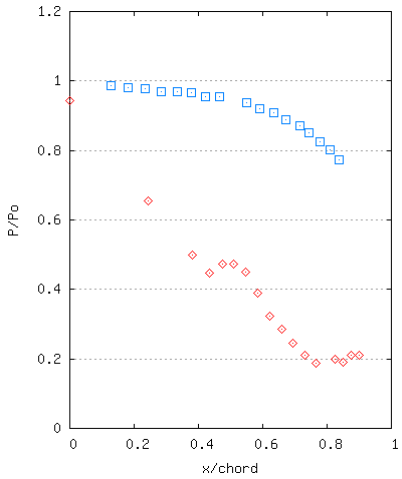

Test: 1404c
P_{ratio} = 3.12, ΔT = -17.91 K, P_0 = 1.06

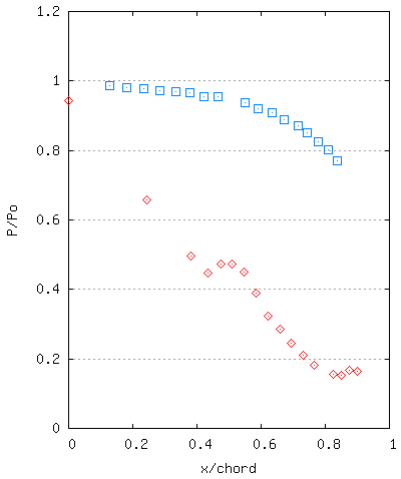

Test: 1404d
P_{ratio} = 3.69, ΔT = -17.91 K, P_0 = 1.07

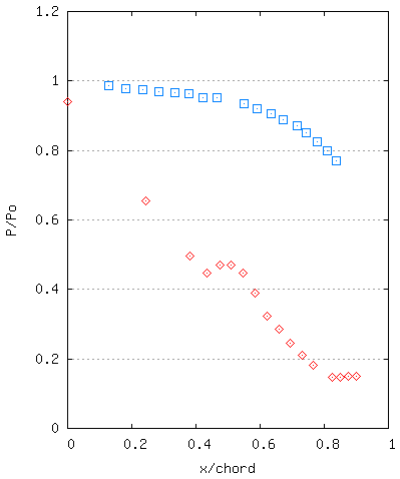

Test: 1404g
P_{ratio} = 3.06, ΔT = -17.54 K, P_0 = 1.08

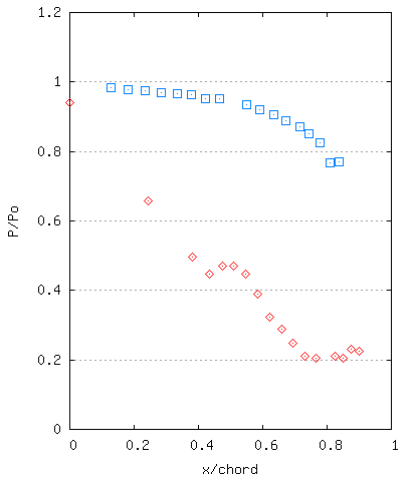

Test: 1404h
P_{ratio} = 3.70, ΔT = -17.36 K, P_0 = 1.07

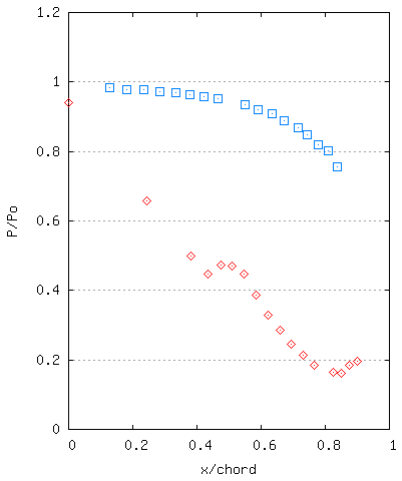

Test: 1604a
P_{ratio} = 3.53, ΔT = -21.46 K, P_0 = 1.07

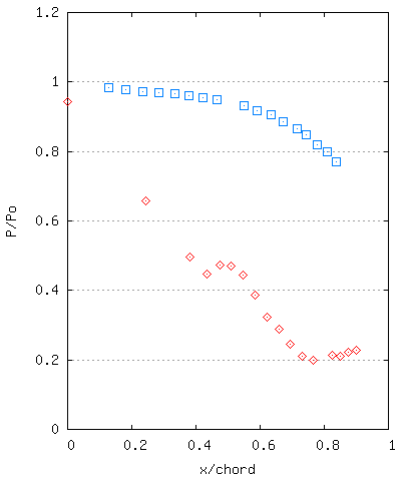

Test: 1604b
P_{ratio} = 3.03, ΔT = -21.64 K, P_0 = 1.09

D.2.3 Steam Dosed with 12ppm of Ammonia

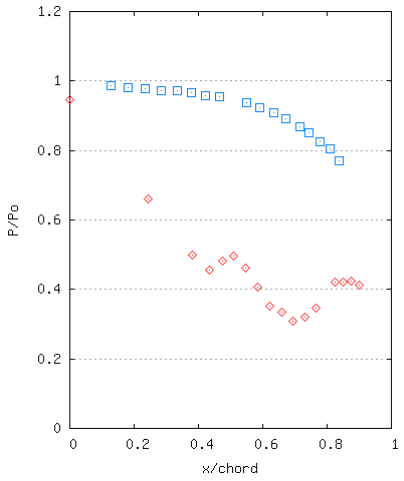

Test: 2104c
P_{ratio} = 2.38, ΔT = -3.39 K, P_0 = 1.09

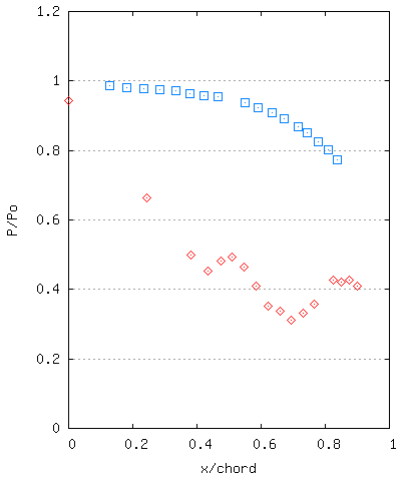

Test: 2104d
P_{ratio} = 2.36, ΔT = -3.20 K, P_0 = 1.09

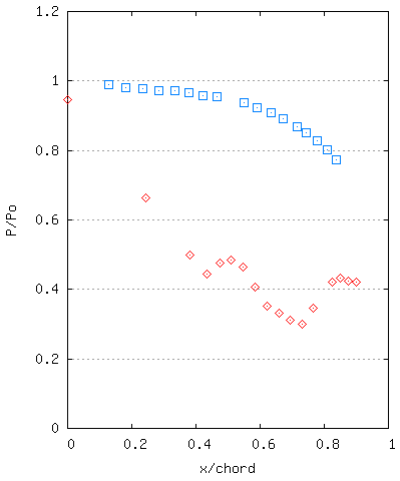

Test: 2104e
P_{ratio} = 2.31, ΔT = -3.10 K, P_0 = 1.09

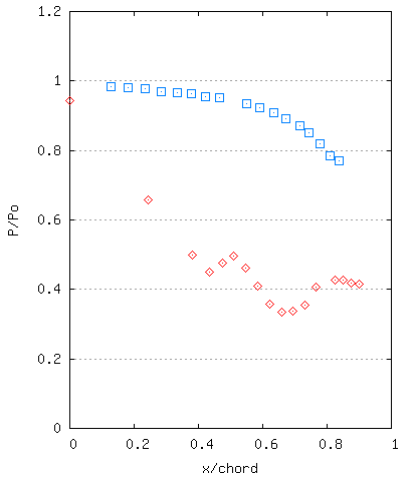

Test: 2104s
P_{ratio} = 2.35, ΔT = -11.50 K, P_0 = 1.08

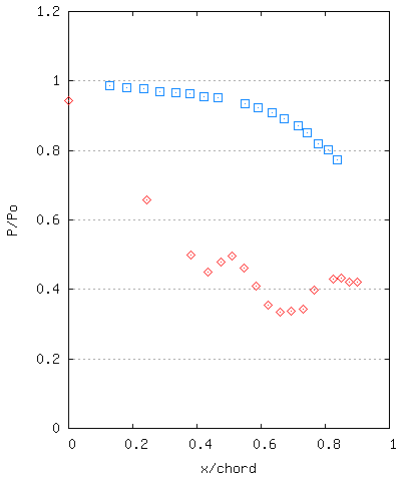

Test: 2104t
P_{ratio} = 2.36, ΔT = -10.64 K, P_0 = 1.09

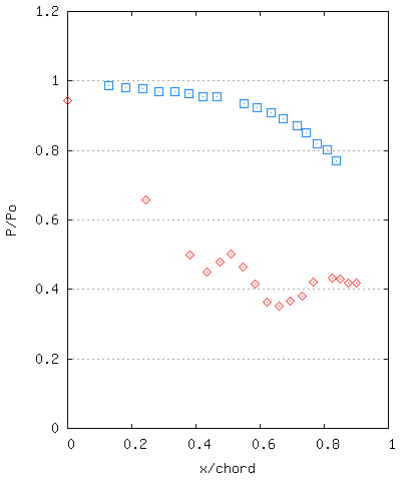

Test: 2104u
P_{ratio} = 2.27, ΔT = -10.74 K, P_0 = 1.08

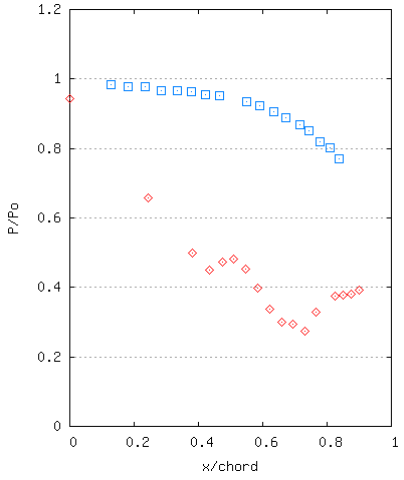

Test: 2104w
P_{ratio} = 2.40, ΔT = -17.91 K, P_0 = 1.09

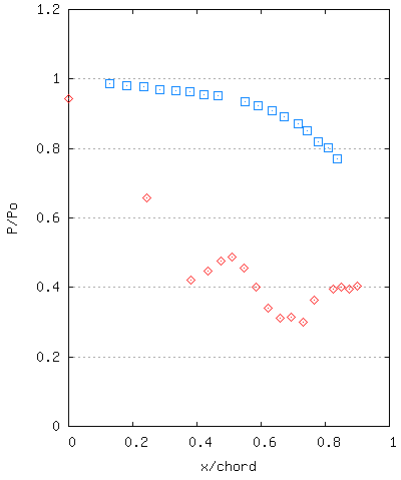

Test: 2104x
P_{ratio} = 2.36, ΔT = -17.18 K, P_0 = 1.09

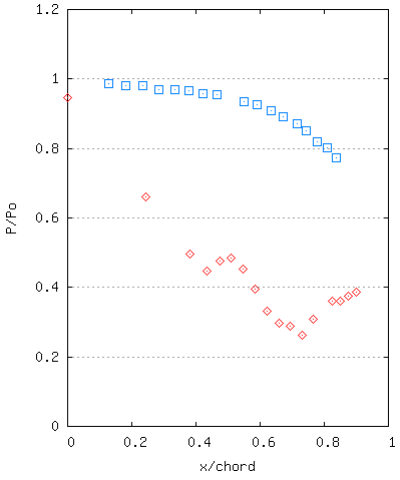

Test: 2104y
P_{ratio} = 2.39, ΔT = -17.45 K, P_0 = 1.09

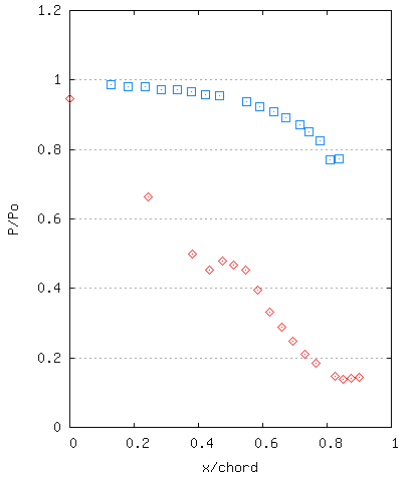

Test: 2104f
P_{ratio} = 3.23, ΔT = -2.90 K, P_0 = 1.09

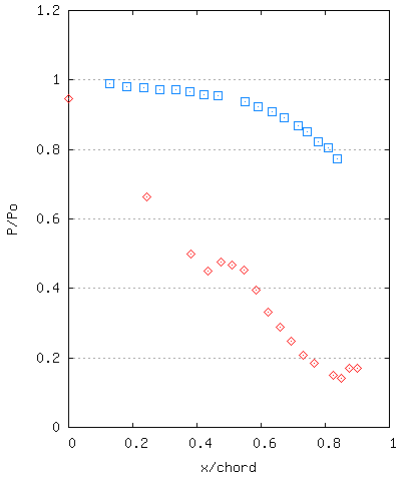

Test: 2104h
P_{ratio} = 3.21, ΔT = -2.90 K, P_0 = 1.09

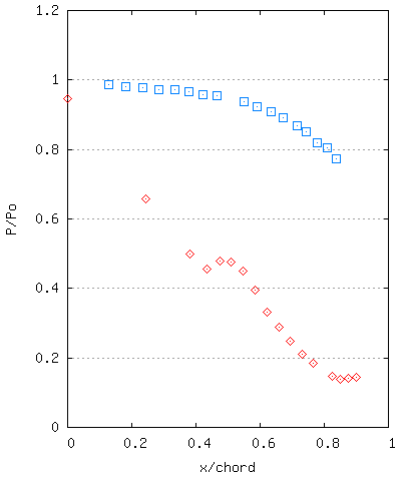

Test: 2104j
P_{ratio} = 3.67, ΔT = -3.69 K, P_0 = 1.10

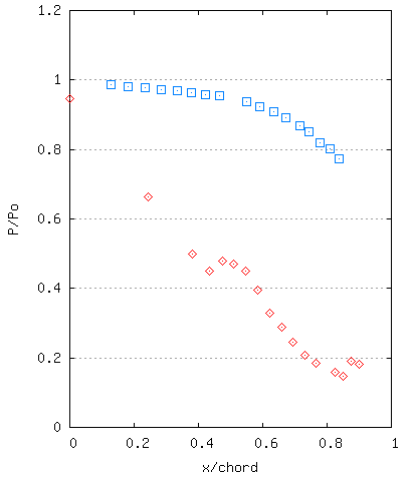

Test: 2104l
P_{ratio} = 3.37, ΔT = -3.30 K, P_0 = 1.09

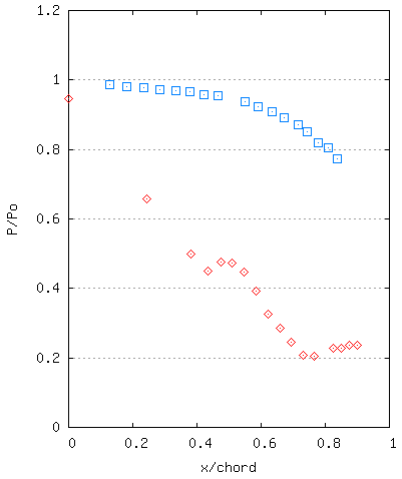

Test: 2104o
P_{ratio} = 3.36, ΔT = -10.74 K, P_0 = 1.08

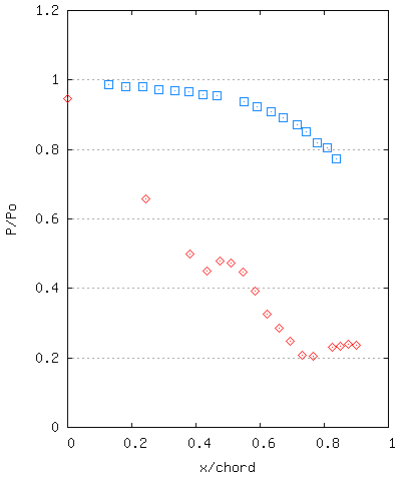

Test: 2104q
P_{ratio} = 3.48, ΔT = -10.74 K, P_0 = 1.08

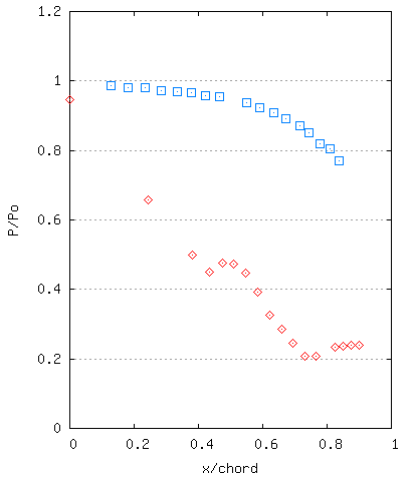

Test: 2104r
P_{ratio} = 3.39, ΔT = -10.74 K, P_0 = 1.08

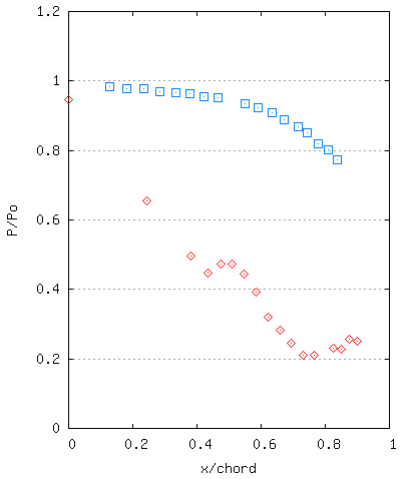

Test: 2104ac
P_{ratio} = 2.91, ΔT = -16.99 K, P_0 = 1.09

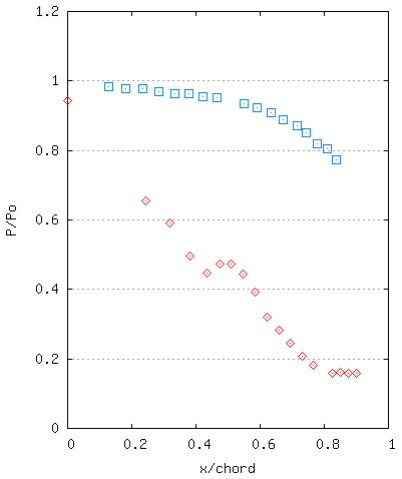

Test: 2104af
P_{ratio} = 2.97, ΔT = -16.99 K, P_0 = 1.09

D.3 Tables of Pressure Readings

D.3.1 Pure Steam

Table D.4a: Pressure readings (bar) at individual tapping points for pure steam results

Tapping Point	X/chord	Test 270499e	Test 180299e	Test 180299m	Test 180299p	Test 180299q	Test 020399e	Test 020399g	Test 020399h
WMP2	-0.350	1.0239	1.0179	1.0300	1.0297	1.0283	0.9748	0.9857	0.9800
WMP3	-0.137	1.0258	1.0199	1.0304	1.0296	1.0295	0.9769	0.9874	0.9838
WMP7	0.300	0.9874	0.9843	0.9955	0.9945	0.9922	0.9431	0.9527	0.9487
WMP11	0.446	0.7599	0.9135	0.9254	0.9255	0.9244	0.8784	0.8880	0.8849
WMP14	0.570	0.7984	0.7948	0.8063	0.8051	0.8051	0.7657	0.7742	0.7708
WMP16	0.648	0.7042	0.3873	0.6265	0.3842	0.4002	0.2581	0.2759	0.2882
WMP17	0.761	0.6092	0.6162	0.6228	0.6264	0.6294	0.6112	0.3764	0.3830
WMP19	0.834	0.5547	0.5936	0.5966	0.6017	0.6090	0.5969	0.6000	0.5926
WMP21	0.908	0.5553	0.5428	0.5439	0.5550	0.5688	0.5499	0.5287	0.5265
WMP23	0.949	0.5620	0.5466	0.5470	0.5548	0.5684	0.5664	0.5636	0.5526
WMP25	0.990	0.5289	0.5111	0.4914	0.4988	0.5146	0.5606	0.5430	0.5326
WMP27	1.058	0.5608	0.5488	0.5490	0.5601	0.5770	0.5597	0.5501	0.5518
WDS1	3.842	0.5708	0.5451	0.5365	0.5600	0.5804	0.5754	0.5672	0.5621
WDS2	-0.319	0.5977	0.5961	0.5922	0.6043	0.6199	0.6140	0.6072	0.6054
WDS4	-8.466	0.5993	0.5971	0.5999	0.6093	0.6202	0.6123	0.6114	0.6025
WDS5	-12.635	0.5963	0.5906	0.5899	0.5987	0.6116	0.6074	0.6068	0.5960
WDS6	-16.804	0.5834	0.5785	0.5777	0.5890	0.6038	0.6004	0.5991	0.5879
WDS7	-20.781	0.5889	0.5748	0.5782	0.5910	0.6067	0.5946	0.5922	0.5828
WDS8	-24.854	0.3890	0.3730	0.3637	0.3875	0.4135	0.4184	0.4100	0.4010
WDS9	-28.975	0.5909	0.5553	0.5437	0.5781	0.6089	0.6025	0.5992	0.5889
WDS10	-33.096	0.6094	0.2689	-0.9799	0.6113	0.6011	0.4851	0.4515	0.4702
WDS11	-37.313	0.6256	0.5976	0.5967	0.6200	0.6416	0.6253	0.6235	0.6149
WDS12	-41.290	0.6332	0.6119	0.6184	0.6322	0.6507	0.6309	0.6307	0.6234
WDS13	-45.507	0.6321	0.6091	0.6178	0.6295	0.6495	0.6284	0.6271	0.6193
WDS14	-49.533	0.6169	0.5964	0.6017	0.6149	0.6365	0.6193	0.6154	0.6077
PS10	0.128	1.0920	1.0747	1.0813	1.0811	1.0791	1.0296	1.0404	1.0356
PS1	0.180	1.0861	1.0695	1.0765	1.0764	1.0743	1.0244	1.0355	1.0310
PS11	0.233	1.0876	1.0670	1.0761	1.0747	1.0740	1.0222	1.0327	1.0285
PS2	0.283	1.0655	1.0563	1.0611	1.0623	1.0600	1.0099	1.0202	1.0160
PS12	0.333	1.0695	1.0577	1.0615	1.0613	1.0595	1.0143	1.0250	1.0209
PS3	0.378	1.0729	1.0536	1.0594	1.0585	1.0571	1.0078	1.0187	1.0142
PS13	0.421	1.0501	1.0426	-1.1350	-1.4201	-1.3544	0.9978	1.0078	1.0036
PS4	0.465	1.0574	1.0439	1.0500	1.0497	1.0482	0.9811	0.9914	0.9873
PS5	0.550	1.0376	1.0189	1.0255	1.0256	1.0236	0.9751	0.9853	0.9808
PS15	0.590	1.0235	1.0095	1.0163	1.0159	1.0140	0.9671	0.9772	0.9733
PS6	0.633	1.0082	0.9926	0.9995	0.9998	0.9980	0.9504	0.9605	0.9562
PS16	0.673	0.9867	0.9736	0.9805	0.9806	0.9788	0.9347	0.9444	0.9399
PS7	0.715	0.9741	0.7795	-0.4388	0.9877	0.9877	0.8751	0.8724	0.8966
PS17	0.745	0.9443	0.9309	0.9367	0.9382	0.9354	0.8939	0.9022	0.8992
PS8	0.778	0.9111	0.9105	0.9140	0.9142	0.9123	0.8719	0.8809	0.8766
PS18	0.808	0.8916	0.7742	0.7773	0.8329	0.8807	0.8440	0.8518	0.8501
PS9	0.838	0.8571	0.8476	0.8535	0.8549	0.8519	0.8128	0.8215	0.8174
SSLE	0.000	1.0477	0.9871	1.0358	1.0364	1.0330	0.9848	0.9968	0.9923
SS10	0.245	0.7402	0.7225	0.7265	0.7268	0.7263	0.6927	0.7023	0.6998
SS1	0.318	0.3754	-0.0191	0.7725	0.4475	0.5833	0.7247	0.7515	0.7468
SS11	0.381	0.5477	0.5538	0.5528	0.5529	0.5529	0.5348	0.5405	0.5387
SS2	0.433	0.4429	0.5039	0.5054	0.5100	0.5139	0.4917	0.4936	0.4890
SS12	0.475	0.4519	0.5706	0.5673	0.5737	0.5788	0.5639	0.5611	0.5648
SS3	0.510	0.4791	0.5871	0.5885	0.5956	0.6020	0.5799	0.5788	0.5823

Tapping Point	X/chord	Test 270499e	Test 180299e	Test 180299m	Test 180299p	Test 180299q	Test 020399e	Test 020399g	Test 020399h
SS13	0.548	0.5642	0.5812	0.5837	0.5876	0.5931	0.5754	0.5729	0.5739
SS4	0.585	0.6121	0.5753	0.5813	0.5850	0.5922	0.5711	0.5686	0.5705
SS14	0.622	0.6071	0.5662	0.5607	0.5654	0.5773	0.5738	0.5646	0.5677
SS5	0.660	0.6113	0.5725	0.5751	0.5834	0.5977	0.5781	0.5726	0.5752
SS15	0.695	0.5936	0.5745	0.5725	0.5831	0.5935	0.5556	0.5272	0.5302
SS6	0.730	0.5767	0.5702	0.5684	0.5779	0.5865	0.5631	0.5598	0.5592
SS16	0.765	0.5687	0.5770	0.5686	0.5819	0.5936	0.5700	0.5656	0.5669
SS17	0.825	0.5519	0.5541	0.5464	0.5667	0.5911	0.5704	0.5611	0.5699
SS8	0.850	0.5533	0.5465	0.5412	0.5659	0.5963	0.5794	0.5644	0.5784
SS18	0.876	0.5455	0.5257	0.5172	0.5456	0.5828	0.5702	0.5473	0.5650
SS9	0.900	0.5499	0.5128	0.5063	0.5400	0.5860	0.5742	0.5425	0.5678

Table D.4b: Pressure readings (bar) at individual tapping points for pure steam contd.

Tapping Point	X/chord	Test 020399l	Test 020399m	Test 020399n	Test 020399o	Test 020399p	Test 020399q	Test 020399s	Test 050399p
WMP2	-0.350	0.9700	0.9921	0.9798	0.9966	0.9996	0.9912	1.0090	1.0158
WMP3	-0.137	0.9757	0.9938	0.9812	0.9973	1.0021	0.9932	1.0093	1.0183
WMP7	0.300	0.9417	0.9596	0.9483	0.9640	0.9672	0.9594	0.9756	0.9836
WMP11	0.446	0.8843	0.8954	0.8864	0.9004	0.9030	0.8970	0.9119	0.9146
WMP14	0.570	0.7705	0.7800	0.7723	0.7856	0.7859	0.7809	0.7955	0.7969
WMP16	0.648	0.2353	0.2154	0.2428	0.2563	0.2434	0.2766	0.2487	0.6561
WMP17	0.761	0.3861	0.4045	0.4140	0.4269	0.4362	0.4305	0.4450	0.6508
WMP19	0.834	0.5721	0.5818	0.5947	0.6049	0.5878	0.5963	0.6054	0.5968
WMP21	0.908	0.5211	0.5334	0.5544	0.5637	0.5424	0.5539	0.5628	0.5600
WMP23	0.949	0.5256	0.5337	0.5605	0.5704	0.5400	0.5557	0.5659	0.5522
WMP25	0.990	0.4765	0.4864	0.5174	0.5268	0.4980	0.5122	0.5241	0.5231
WMP27	1.058	0.5262	0.5407	0.5666	0.5756	0.5503	0.5624	0.5724	0.5553
WDS1	3.842	0.5332	0.5421	0.5769	0.5831	0.5556	0.5752	0.5839	0.5481
WDS2	-0.319	0.5690	0.5827	0.6028	0.6115	0.5913	0.6054	0.6124	0.5822
WDS4	-8.466	0.5747	0.5842	0.6061	0.6152	0.5894	0.6043	0.6149	0.6009
WDS5	-12.635	0.5606	0.5719	0.5964	0.6056	0.5783	0.5923	0.6038	0.5846
WDS6	-16.804	0.5601	0.5661	0.5930	0.6035	0.5748	0.5894	0.6012	0.5808
WDS7	-20.781	0.5603	0.5693	0.5941	0.6051	0.5783	0.5912	0.6031	0.5812
WDS8	-24.854	0.3736	0.3778	0.4215	0.4285	0.3898	0.4108	0.4225	0.3796
WDS9	-28.975	0.5491	0.5610	0.6027	0.6133	0.5734	0.5985	0.6118	0.5692
WDS10	-33.096	0.4614	0.4544	0.5593	0.5848	0.5758	0.6201	0.6323	-0.5644
WDS11	-37.313	0.5893	0.5993	0.6286	0.6405	0.6114	0.6271	0.6405	0.6108
WDS12	-41.290	0.6026	0.6114	0.6364	0.6485	0.6220	0.6359	0.6489	0.6241
WDS13	-45.507	0.5997	0.6082	0.6343	0.6452	0.6194	0.6333	0.6472	0.6202
WDS14	-49.533	0.5856	0.5943	0.6244	0.6360	0.6074	0.6228	0.6361	0.6074
PS10	0.128	1.0221	1.0405	1.0301	1.0475	1.0509	1.0443	1.0613	1.0653
PS1	0.180	1.0178	1.0368	1.0265	1.0436	1.0470	1.0400	1.0569	1.0615
PS11	0.233	1.0152	1.0337	1.0235	1.0405	1.0440	1.0370	1.0545	1.0470
PS2	0.283	1.0036	1.0224	1.0120	1.0292	1.0325	1.0252	1.0414	1.0547
PS12	0.333	1.0045	1.0227	1.0130	1.0293	1.0328	1.0259	1.0426	1.0479
PS3	0.378	1.0004	1.0193	1.0086	1.0258	1.0293	1.0223	1.0391	1.0432
PS13	0.421	0.9927	1.0106	1.0005	1.0172	1.0207	1.0137	1.0295	1.0401
PS4	0.465	0.9699	0.9887	0.9775	0.9950	0.9978	0.9916	1.0079	1.0308
PS5	0.550	0.9685	0.9864	0.9769	0.9938	0.9966	0.9905	1.0059	1.0108
PS15	0.590	0.9602	0.9781	0.9688	0.9847	0.9878	0.9812	0.9975	0.9996
PS6	0.633	0.9444	0.9621	0.9528	0.9690	0.9718	0.9654	0.9812	0.9841

Tapping Point	X/chord	Test 020399l	Test 020399m	Test 020399n	Test 020399o	Test 020399p	Test 020399q	Test 020399s	Test 050399p
PS16	0.673	0.9289	0.9461	0.9382	0.9539	0.9563	0.9497	0.9648	0.9644
PS7	0.715	0.9270	0.9224	0.9660	0.9675	0.9675	0.9675	0.9675	-0.1397
PS17	0.745	0.8868	0.9030	0.8959	0.9105	0.9134	0.9061	0.9215	0.9208
PS8	0.778	0.8647	0.8815	0.8756	0.8883	0.8914	0.8850	0.8998	0.8952
PS18	0.808	0.6778	0.8543	0.8416	0.8591	0.8610	0.8575	0.8705	0.8723
PS9	0.838	0.8075	0.8216	0.8141	0.8298	0.8302	0.8257	0.8393	0.8402
SSLE	0.000	0.9753	0.9944	0.9840	1.0004	1.0055	0.9962	1.0131	1.0225
SS10	0.245	0.6838	0.6987	0.6909	0.7034	0.7055	0.7007	0.7113	0.7112
SS1	0.318	0.8421	0.7951	0.8609	0.7499	0.7573	0.8900	0.8157	0.5911
SS11	0.381	0.5244	0.5357	0.5322	0.5410	0.5416	0.5385	0.5472	0.5408
SS2	0.433	0.4770	0.4881	0.4925	0.5028	0.4972	0.4994	0.5045	0.5061
SS12	0.475	0.5433	0.5542	0.5688	0.5821	0.5688	0.5759	0.5793	0.5663
SS3	0.510	0.5606	0.5727	0.5850	0.5971	0.5858	0.5910	0.5963	0.5842
SS13	0.548	0.5528	0.5663	0.5786	0.5916	0.5781	0.5850	0.5879	0.5853
SS4	0.585	0.5487	0.5608	0.5773	0.5897	0.5736	0.5821	0.5861	0.5739
SS14	0.622	0.5331	0.5460	0.5710	0.5847	0.5611	0.5768	0.5772	0.5641
SS5	0.660	0.5462	0.5583	0.5849	0.5965	0.5765	0.5885	0.5911	0.5737
SS15	0.695	0.5162	0.5281	0.5516	0.5644	0.5441	0.5566	0.5578	0.5716
SS6	0.730	0.5434	0.5550	0.5754	0.5873	0.5668	0.5771	0.5797	0.5668
SS16	0.765	0.5442	0.5574	0.5819	0.5944	0.5729	0.5858	0.5886	0.5647
SS17	0.825	0.5332	0.5887	0.5824	0.5938	0.5684	0.5853	0.5886	0.5633
SS8	0.850	0.5366	0.5490	0.5930	0.6041	0.5749	0.5946	0.5989	0.5522
SS18	0.876	0.5181	0.5300	0.5839	0.5964	0.5611	0.5872	0.5887	0.5469
SS9	0.900	0.5109	0.5232	0.5883	0.6003	0.5603	0.5903	0.5925	0.5387

Table D.4c: Pressure readings (bar) at individual tapping points for pure steam contd.

Tapping Point	X/chord	Test 020399t	Test 020399u	Test 020399v	Test 020399w	Test 020399x	Test 050399v	Test 290499ab	Test 290499ac
WMP2	-0.350	0.9924	0.9873	0.9952	0.9916	0.9771	1.0118	1.0349	1.0302
WMP3	-0.137	0.9940	0.9893	0.9981	0.9921	0.9794	1.0126	1.0379	1.0308
WMP7	0.300	0.9590	0.9539	0.9620	0.9581	0.9437	0.9793	0.9983	0.9937
WMP11	0.446	0.8951	0.8911	0.8980	0.8953	0.8828	0.9090	0.9283	0.9246
WMP14	0.570	0.7797	0.7765	0.7822	0.7794	0.7680	0.7945	0.8147	0.8116
WMP16	0.648	0.3802	0.3748	0.3791	0.3455	0.2283	0.6530	0.5551	0.5267
WMP17	0.761	0.4425	0.4171	0.4075	0.4376	0.4025	0.6699	0.6290	0.6293
WMP19	0.834	0.5882	0.5904	0.5920	0.5896	0.5875	0.5996	0.5979	0.6021
WMP21	0.908	0.5453	0.5485	0.5451	0.5455	0.5431	0.5655	0.5590	0.5640
WMP23	0.949	0.5429	0.5486	0.5456	0.5426	0.5478	0.5604	0.5448	0.5544
WMP25	0.990	0.5059	0.5129	0.5086	0.5086	0.5124	0.5290	0.5004	0.5073
WMP27	1.058	0.5503	0.5572	0.5543	0.5542	0.5567	0.5715	0.5550	0.5645
WDS1	3.842	0.5646	0.5706	0.5683	0.5697	0.5696	0.5627	0.5571	0.5701
WDS2	-0.319	0.5924	0.5932	0.5908	0.5906	0.5893	0.5899	0.5916	0.5998
WDS4	-8.466	0.5934	0.5973	0.5968	0.5945	0.5947	0.6083	0.5977	0.6066
WDS5	-12.635	0.5801	0.5863	0.5849	0.5819	0.5848	0.5942	0.5841	0.5945
WDS6	-16.804	0.5767	0.5840	0.5814	0.5788	0.5820	0.5900	0.5761	0.5863
WDS7	-20.781	0.5792	0.5861	0.5841	0.5819	0.5850	0.5917	0.5856	0.5971
WDS8	-24.854	0.3949	0.4091	0.4015	0.4002	0.4108	0.4003	0.3809	0.4023
WDS9	-28.975	0.5815	0.5953	0.5902	0.5883	0.5929	0.5916	0.5640	0.5923
WDS10	-33.096	0.5714	0.5869	0.5640	0.5367	0.5223	-0.5398	0.5853	0.6114
WDS11	-37.313	0.6154	0.6233	0.6195	0.6178	0.6205	0.6250	0.6164	0.6317
WDS12	-41.290	0.6250	0.6323	0.6280	0.6265	0.6271	0.6339	0.6288	0.6396

Tapping Point	X/chord	Test 020399t	Test 020399u	Test 020399v	Test 020399w	Test 020399x	Test 050399v	Test 290499ab	Test 290499ac
WDS13	-45.507	0.6216	0.6300	0.6255	0.6244	0.6256	0.6295	0.6288	0.6393
WDS14	-49.533	0.6097	0.6188	0.6128	0.6119	0.6150	0.6177	0.6109	0.6236
PS10	0.128	1.0447	1.0392	1.0490	1.0456	1.0301	1.0638	1.0910	1.0870
PS1	0.180	1.0401	1.0352	1.0449	1.0410	1.0255	1.0600	1.0858	1.0808
PS11	0.233	1.0376	1.0327	1.0425	1.0391	1.0238	1.0702	1.0858	1.0808
PS2	0.283	1.0248	1.0199	1.0302	1.0250	1.0098	1.0526	1.0668	1.0621
PS12	0.333	1.0258	1.0209	1.0303	1.0263	1.0117	1.0459	1.0671	1.0606
PS3	0.378	1.0227	1.0184	1.0281	1.0240	1.0085	1.0423	1.0716	1.0665
PS13	0.421	1.0132	1.0079	1.0169	1.0129	0.9979	1.0378	1.0514	1.0468
PS4	0.465	0.9908	0.9891	0.9966	0.9926	0.9763	1.0294	1.0556	1.0508
PS5	0.550	0.9896	0.9857	0.9949	0.9905	0.9758	1.0094	1.0374	1.0326
PS15	0.590	0.9812	0.9768	0.9860	0.9822	0.9690	0.9983	1.0226	1.0183
PS6	0.633	0.9655	0.9613	0.9701	0.9668	0.9519	0.9831	1.0072	1.0029
PS16	0.673	0.9497	0.9461	0.9551	0.9510	0.9368	0.9631	0.9870	0.9836
PS7	0.715	0.9675	0.9675	0.9675	0.9675	0.9398	-0.1409	0.9799	0.9760
PS17	0.745	0.9083	0.9029	0.9100	0.9059	0.8938	0.9214	0.9451	0.9417
PS8	0.778	0.8851	0.8816	0.8877	0.8857	0.8718	0.8937	0.9086	0.9048
PS18	0.808	0.8564	0.8530	0.8614	0.8548	0.8454	0.8713	0.8926	0.8915
PS9	0.838	0.8255	0.8219	0.8287	0.8253	0.8136	0.8402	0.8581	0.8549
SSLE	0.000	0.9974	0.9902	1.0025	0.9996	0.9854	1.0189	1.0504	1.0447
SS10	0.245	0.7004	0.6980	0.7041	0.7012	0.6916	0.7097	0.7353	0.7323
SS1	0.318	0.7808	0.8676	0.7833	0.8577	0.8242	0.5298	0.3729	0.3938
SS11	0.381	0.5393	0.5383	0.5423	0.5404	0.5340	0.5407	0.5543	0.5535
SS2	0.433	0.4934	0.4934	0.4945	0.4926	0.4866	0.5044	0.5084	0.5098
SS12	0.475	0.5688	0.5732	0.5688	0.5696	0.5670	0.5735	0.5727	0.5809
SS3	0.510	0.5845	0.5869	0.5854	0.5858	0.5819	0.5897	0.5975	0.6040
SS13	0.548	0.5761	0.5781	0.5764	0.5766	0.5730	0.5886	0.5925	0.5975
SS4	0.585	0.5719	0.5759	0.5726	0.5727	0.5696	0.5771	0.5832	0.5879
SS14	0.622	0.5642	0.5715	0.5642	0.5663	0.5665	0.5701	0.5674	0.5758
SS5	0.660	0.5759	0.5817	0.5750	0.5760	0.5745	0.5797	0.5836	0.5934
SS15	0.695	0.5442	0.5499	0.5448	0.5449	0.5440	0.5763	0.5811	0.5900
SS6	0.730	0.5640	0.5690	0.5635	0.5630	0.5598	0.5716	0.5787	0.5843
SS16	0.765	0.5722	0.5792	0.5717	0.5718	0.5701	0.5706	0.5758	0.5855
SS17	0.825	0.5702	0.5791	0.5671	0.5691	0.5698	0.5747	0.5630	0.5822
SS8	0.850	0.5775	0.5889	0.5733	0.5769	0.5778	0.5672	0.5521	0.5760
SS18	0.876	0.5673	0.5810	0.5610	0.5670	0.5700	0.5672	0.5421	0.5723
SS9	0.900	0.5676	0.5847	0.5595	0.5673	0.5730	0.5652	0.5320	0.5682

Table D.4d: Pressure readings (bar) at individual tapping points for pure steam contd.

Tapping Point	X/chord	Test 290499ad	Test 120399b	Test 270499a	Test 270499b	Test 270499i	Test 100299e	Test 100299j	Test 100299k
WMP2	-0.350	1.0342	0.9767	1.0533	1.0368	1.0249	0.9900	1.0300	1.0319
WMP3	-0.137	1.0359	0.9807	1.0525	1.0374	1.0255	0.9867	1.0306	1.0326
WMP7	0.300	0.9975	0.9448	1.0185	1.0014	0.9903	0.9534	0.9974	0.9989
WMP11	0.446	0.9275	0.8774	0.7446	0.7600	0.9196	0.8859	0.9276	0.9282
WMP14	0.570	0.8129	0.7591	0.8188	0.8058	0.7979	0.7672	0.8055	0.8065
WMP16	0.648	0.6186	0.6337	0.7084	0.6968	0.7100	0.6456	0.6764	0.6776
WMP17	0.761	0.6291	0.6365	0.6121	0.5999	0.5961	0.5838	0.6040	0.6055
WMP19	0.834	0.6005	0.4035	0.4781	0.4214	0.4186	0.5553	0.5599	0.5626
WMP21	0.908	0.5640	0.3541	0.4325	0.3433	0.3768	0.5127	0.4569	0.4256
WMP23	0.949	0.5515	0.3931	0.4641	0.3822	0.4583	0.5046	0.4424	0.4238

Tapping Point	X/chord	Test 290499ad	Test 120399b	Test 270499a	Test 270499b	Test 270499i	Test 100299e	Test 100299j	Test 100299k
WMP25	0.990	0.5053	0.3940	0.4536	0.3732	0.4165	0.4485	0.4060	0.3779
WMP27	1.058	0.5635	0.4297	0.4783	0.3780	0.5068	0.4731	0.4123	0.3838
WDS1	3.842	0.5701	0.3542	0.4715	0.3306	0.3683	0.4545	0.3850	0.3408
WDS2	-0.319	0.5985	0.3917	0.5150	0.3357	0.4308	0.5368	0.4894	0.4403
WDS4	-8.466	0.6057	0.4711	0.5289	0.4703	0.5040	0.5544	0.5329	0.5236
WDS5	-12.635	0.5926	0.4717	0.5032	0.4773	0.5180	0.5365	0.5243	0.5203
WDS6	-16.804	0.5856	0.4569	0.4933	0.4533	0.5137	0.5171	0.4859	0.4803
WDS7	-20.781	0.5960	0.4391	0.5104	0.4102	0.5127	0.4984	0.4368	0.4259
WDS8	-24.854	0.4008	0.3040	0.3330	0.2993	0.3315	0.3128	0.2993	0.2871
WDS9	-28.975	0.5916	0.4076	0.4863	0.3735	0.4694	0.4400	0.3936	0.3841
WDS10	-33.096	0.6125	0.4442	0.4998	0.3899	0.4787	0.3940	-1.1553	-1.1992
WDS11	-37.313	0.6331	0.4378	0.5125	0.4042	0.4633	0.5099	0.4832	0.4500
WDS12	-41.290	0.6395	0.4771	0.5536	0.4753	0.5151	0.5494	0.5368	0.5298
WDS13	-45.507	0.6377	0.4807	0.5412	0.4934	0.5126	0.5560	0.5413	0.5443
WDS14	-49.533	0.6220	0.4586	0.5155	0.4758	0.4908	0.5326	0.5290	0.5286
PS10	0.128	1.0894	1.0399	1.1247	1.1047	1.0934	1.0724	1.0783	1.0814
PS1	0.180	1.0839	1.0374	1.1180	1.0984	1.0877	1.0676	1.0738	1.0773
PS11	0.233	1.0847	1.0312	1.1148	1.0966	1.0877	1.0652	0.9891	0.9124
PS2	0.283	1.0654	1.0248	1.1048	1.0832	1.0697	1.0575	1.0654	1.0687
PS12	0.333	1.0646	1.0211	1.1058	1.0855	1.0675	1.0546	1.0594	1.0627
PS3	0.378	1.0696	1.0211	1.0994	1.0824	1.0743	1.0500	1.0564	1.0594
PS13	0.421	1.0502	1.0089	1.0879	1.0656	1.0553	1.0436	1.0519	1.0552
PS4	0.465	1.0540	1.0099	1.0865	1.0694	1.0573	1.0394	1.0467	1.0497
PS5	0.550	1.0357	0.9865	1.0657	1.0475	1.0383	1.0180	1.0234	1.0275
PS15	0.590	1.0217	0.9742	1.0508	1.0337	1.0236	1.0066	1.0132	1.0163
PS6	0.633	1.0059	0.9617	1.0348	1.0189	1.0085	0.9906	0.9971	0.9994
PS16	0.673	0.9861	0.9414	1.0138	0.9974	0.9879	0.9709	0.9768	0.9798
PS7	0.715	0.9793	-0.1685	0.9899	0.9762	0.9746	0.9844	-0.3637	-0.4090
PS17	0.745	0.9442	0.8995	0.9682	0.9536	0.9444	0.9264	0.9341	0.9365
PS8	0.778	0.9083	0.8753	0.9343	0.9184	0.9092	0.9045	0.9130	0.9135
PS18	0.808	0.8938	0.8523	0.9150	0.9007	0.8711	0.8758	0.8829	0.8852
PS9	0.838	0.8573	0.8191	0.8784	0.8650	0.8555	0.8441	0.8499	0.8521
SSLE	0.000	1.0460	1.0058	1.0759	1.0681	1.0519	1.0175	1.0427	1.0401
SS10	0.245	0.7349	0.7130	0.7499	0.7424	0.7373	0.7184	0.7224	0.7222
SS1	0.318	0.3841	0.3361	0.8002	0.5932	0.4119	0.2396	0.9395	0.9383
SS11	0.381	0.5554	0.5214	0.5650	0.5576	0.5456	0.5437	0.5495	0.5465
SS2	0.433	0.5090	0.4264	0.4597	0.4521	0.4470	0.4932	0.4977	0.4998
SS12	0.475	0.5801	0.4290	0.4632	0.4544	0.4454	0.5263	0.5213	0.5248
SS3	0.510	0.6023	0.4169	0.4484	0.4412	0.4394	0.5560	0.5310	0.5388
SS13	0.548	0.5958	0.3821	0.4098	0.4008	0.3988	0.5210	0.4973	0.5000
SS4	0.585	0.5849	0.3377	0.3633	0.3551	0.3571	0.4824	0.4360	0.4419
SS14	0.622	0.5718	0.2868	0.3950	0.3110	0.3375	0.4406	0.3716	0.3768
SS5	0.660	0.5898	0.3497	0.5065	0.3660	0.4404	0.4653	0.3537	0.3517
SS15	0.695	0.5876	0.4015	0.5489	0.3753	0.4667	0.4872	0.3405	0.3275
SS6	0.730	0.5832	0.3767	0.5467	0.3580	0.4530	0.4924	0.3654	0.3120
SS16	0.765	0.5840	0.4052	0.5468	0.3517	0.4896	0.5004	0.4121	0.2972
SS17	0.825	0.5782	0.4329	0.5292	0.3745	0.4992	0.4833	0.4680	0.3235
SS8	0.850	0.5714	0.4562	0.5153	0.4116	0.5198	0.4710	0.4650	0.3318
SS18	0.876	0.5658	0.4522	0.4968	0.4671	0.4943	0.4574	0.4601	0.3734
SS9	0.900	0.5623	0.4699	0.4745	0.4843	0.5059	0.4468	0.4506	0.3985

Table D.4e: Pressure readings (bar) at individual tapping points for pure steam contd.

Tapping Point	X/chord	Test 050399a	Test 050399b	Test 050399c	Test 290499d	Test 290499e	Test 100299n	Test 290499f	Test 290499g
WMP2	-0.350	1.0313	1.0206	1.0114	1.0400	1.0338	1.0048	1.0823	1.0616
WMP3	-0.137	1.0312	1.0221	1.0106	1.0427	1.0344	1.0062	1.0836	1.0634
WMP7	0.300	1.0020	0.9904	0.9809	1.0068	0.9986	0.9738	1.0446	1.0242
WMP11	0.446	0.9330	0.9174	0.9078	0.9299	0.9219	0.9075	0.9679	0.9475
WMP14	0.570	0.8154	0.7962	0.7894	0.8113	0.8033	0.7888	0.8493	0.8261
WMP16	0.648	0.6730	0.6579	0.6516	0.7178	0.7078	0.6674	0.7327	0.7201
WMP17	0.761	0.6465	0.6250	0.6514	0.6083	0.6037	0.5934	0.6355	0.6199
WMP19	0.834	0.4958	0.5510	0.5613	0.5519	0.5565	0.5608	0.6036	0.5669
WMP21	0.908	0.4148	0.4189	0.4545	0.3973	0.3987	0.5140	0.4704	0.4150
WMP23	0.949	0.3455	0.4200	0.4390	0.3557	0.3931	0.4651	0.4756	0.4008
WMP25	0.990	0.3043	0.3703	0.4172	0.3167	0.3448	0.4224	0.4032	0.3454
WMP27	1.058	0.3530	0.3801	0.4092	0.3731	0.3964	0.4553	0.4316	0.3817
WDS1	3.842	0.2891	0.3265	0.3769	0.3525	0.3653	0.4370	0.4046	0.3067
WDS2	-0.319	0.3571	0.4248	0.4766	0.4139	0.4303	0.5351	0.5274	0.4284
WDS4	-8.466	0.4093	0.5174	0.5274	0.4844	0.5080	0.5444	0.5765	0.5156
WDS5	-12.635	0.4203	0.5156	0.5215	0.5177	0.5251	0.5349	0.5519	0.5316
WDS6	-16.804	0.3962	0.4773	0.4865	0.4977	0.4978	0.5126	0.5124	0.5029
WDS7	-20.781	0.3703	0.4219	0.4339	0.4496	0.4483	0.4797	0.4631	0.4546
WDS8	-24.854	0.3217	0.2807	0.2916	0.3102	0.3071	0.3157	0.3141	0.3128
WDS9	-28.975	0.4351	0.3777	0.3935	0.4705	0.4489	0.4417	0.4289	0.4343
WDS10	-33.096	0.8277	0.7394	-0.7826	0.5427	0.5059	0.4921	0.4586	0.5030
WDS11	-37.313	0.4843	0.4403	0.4486	0.5692	0.5535	0.5322	0.5511	0.5626
WDS12	-41.290	0.4966	0.5067	0.5222	0.5877	0.5828	0.5821	0.6018	0.5982
WDS13	-45.507	0.5090	0.5175	0.5310	0.5943	0.5881	0.5832	0.6090	0.6043
WDS14	-49.533	0.5091	0.5075	0.5140	0.5824	0.5704	0.5607	0.5840	0.5853
PS10	0.128	1.0764	1.0753	1.0645	1.1012	1.0925	1.0558	1.1378	1.1156
PS1	0.180	1.0731	1.0706	1.0602	1.0935	1.0856	1.0514	1.1316	1.1096
PS11	0.233	0.5230	0.4740	0.6417	1.0908	1.0829	1.0584	1.1281	1.1064
PS2	0.283	1.0700	1.0668	1.0558	1.0829	1.0745	1.0430	1.1183	1.0971
PS12	0.333	1.0614	1.0582	1.0479	1.0812	1.0730	1.0372	1.1175	1.0959
PS3	0.378	1.0536	1.0508	1.0413	1.0762	1.0682	1.0344	1.1132	1.0915
PS13	0.421	1.0567	1.0524	1.0426	1.0667	1.0587	1.0307	1.1023	1.0811
PS4	0.465	1.0433	1.0396	1.0287	1.0640	1.0565	1.0246	1.1004	1.0787
PS5	0.550	1.0255	1.0194	1.0092	1.0437	1.0358	1.0024	1.0794	1.0585
PS15	0.590	1.0143	1.0076	0.9976	1.0293	1.0214	0.9920	1.0641	1.0443
PS6	0.633	1.0071	0.9954	0.9820	1.0137	1.0062	0.9752	1.0477	1.0277
PS16	0.673	0.9814	0.9718	0.9624	0.9928	0.9852	0.9563	1.0263	1.0066
PS7	0.715	1.1145	1.1145	-0.1234	0.9791	0.9715	0.9858	1.0159	0.9971
PS17	0.745	0.9396	0.9285	0.9186	0.9484	0.9413	0.9141	0.9808	0.9620
PS8	0.778	0.9161	0.9022	0.8923	0.9128	0.9067	0.8919	0.9439	0.9273
PS18	0.808	0.8886	0.8761	0.8691	0.8955	0.8888	0.8085	0.9220	0.9083
PS9	0.838	0.8596	0.8460	0.8368	0.8615	0.8547	0.8324	0.8897	0.8746
SSLE	0.000	1.0970	1.0306	1.0210	1.0536	1.0442	1.0069	1.0859	1.0686
SS10	0.245	0.7469	0.7138	0.7080	0.7367	0.7336	0.7045	0.7568	0.7445
SS1	0.318	-0.4318	0.0145	0.2655	0.2860	0.4528	0.9280	0.6808	0.5163
SS11	0.381	0.5603	0.5364	0.5322	0.5558	0.5506	0.5341	0.5726	0.5621
SS2	0.433	0.4945	0.5018	0.4940	0.5101	0.4986	0.4852	0.5218	0.5128
SS12	0.475	0.5009	0.5203	0.5141	0.5362	0.5299	0.5208	0.5521	0.5416
SS3	0.510	0.4864	0.5319	0.5213	0.5461	0.5464	0.5551	0.5671	0.5579
SS13	0.548	0.4689	0.5010	0.4944	0.5093	0.5141	0.5321	0.5275	0.5196
SS4	0.585	0.4153	0.4389	0.4274	0.4445	0.4499	0.5133	0.4601	0.4543
SS14	0.622	0.3600	0.3714	0.3604	0.3806	0.3913	0.4753	0.3939	0.3925
SS5	0.660	0.3659	0.3481	0.3385	0.3454	0.3667	0.5010	0.3626	0.3657
SS15	0.695	0.4327	0.3246	0.3205	0.3431	0.3820	0.4968	0.3609	0.3736

Tapping Point	X/chord	Test 050399a	Test 050399b	Test 050399c	Test 290499d	Test 290499e	Test 100299n	Test 290499f	Test 290499g
SS6	0.730	0.4848	0.3137	0.3293	0.3237	0.3734	0.4960	0.3441	0.3602
SS16	0.765	0.4917	0.2932	0.3591	0.3846	0.4333	0.4936	0.4125	0.4257
SS17	0.825	0.5078	0.2983	0.4394	0.4279	0.4541	0.4779	0.4525	0.4556
SS8	0.850	0.5127	0.3374	0.4503	0.4286	0.4532	0.4646	0.4530	0.4547
SS18	0.876	0.5186	0.3962	0.4541	0.4319	0.4468	0.4548	0.4547	0.4516
SS9	0.900	0.5255	0.4277	0.4434	0.4478	0.4551	0.4434	0.4646	0.4612

Table D.4f: Pressure readings (bar) at individual tapping points for pure steam contd.

Tapping Point	X/chord	Test 290499h	Test 290499i	Test 290499v	Test 290499x	Test 290499af	Test 270499g	Test 090399c	Test 090399d
WMP2	-0.350	1.0613	1.0653	1.0347	1.0300	1.0351	1.0261	1.0132	1.0040
WMP3	-0.137	1.0598	1.0632	1.0355	1.0317	1.0370	1.0279	1.0130	1.0062
WMP7	0.300	1.0242	1.0279	0.9973	0.9931	0.9981	0.9901	0.9807	0.9733
WMP11	0.446	0.9478	0.9525	0.9262	0.9207	0.9286	0.9190	0.9102	0.9047
WMP14	0.570	0.8262	0.8325	0.8104	0.8031	0.8112	0.7972	0.7902	0.7844
WMP16	0.648	0.7221	0.7260	0.6596	0.6224	0.6655	0.7120	0.5869	0.5741
WMP17	0.761	0.6202	0.6252	0.6116	0.6054	0.6105	0.5989	0.6379	0.6327
WMP19	0.834	0.5731	0.5936	0.5763	0.5669	0.5526	0.4111	0.5088	0.5087
WMP21	0.908	0.4347	0.4578	0.5212	0.5041	0.4655	0.3091	0.3600	0.3570
WMP23	0.949	0.4200	0.4733	0.4905	0.4720	0.4398	0.2872	0.2810	0.2725
WMP25	0.990	0.3601	0.3968	0.4183	0.3888	0.3658	0.2260	0.2559	0.2284
WMP27	1.058	0.4099	0.4285	0.4456	0.4275	0.4038	0.2702	0.2358	0.2229
WDS1	3.842	0.3646	0.3984	0.4443	0.4187	0.3803	0.2271	0.2201	0.2069
WDS2	-0.319	0.4624	0.5200	0.5479	0.5279	0.5042	0.2354	0.2669	0.2504
WDS4	-8.466	0.5355	0.5674	0.5652	0.5576	0.5453	0.3611	0.3678	0.3618
WDS5	-12.635	0.5362	0.5442	0.5395	0.5323	0.5234	0.3799	0.3735	0.3619
WDS6	-16.804	0.5012	0.5061	0.5058	0.4947	0.4859	0.3674	0.3517	0.3396
WDS7	-20.781	0.4500	0.4607	0.4799	0.4627	0.4448	0.3551	0.3071	0.3023
WDS8	-24.854	0.3095	0.3117	0.3072	0.3034	0.2984	0.2573	0.2076	0.2063
WDS9	-28.975	0.4260	0.4265	0.4260	0.4223	0.4100	0.3461	0.2350	0.2244
WDS10	-33.096	0.4779	0.4574	0.4561	0.4526	0.4388	0.3800	0.2345	0.2339
WDS11	-37.313	0.5525	0.5460	0.5333	0.5327	0.5290	0.4230	0.3140	0.2815
WDS12	-41.290	0.5923	0.5961	0.5847	0.5789	0.5750	0.4603	0.3740	0.3517
WDS13	-45.507	0.5972	0.6012	0.5911	0.5847	0.5820	0.4825	0.4070	0.3909
WDS14	-49.533	0.5754	0.5769	0.5657	0.5587	0.5582	0.4799	0.4183	0.3968
PS10	0.128	1.1150	1.1193	1.0919	1.0879	1.0917	1.0949	1.0681	1.0604
PS1	0.180	1.1087	1.1131	1.0864	1.0823	1.0869	1.0890	1.0641	1.0568
PS11	0.233	1.1060	1.1101	1.0871	1.0835	1.0870	1.0894	1.0573	1.0501
PS2	0.283	1.0962	1.1000	1.0655	1.0621	1.0681	1.0691	1.0555	1.0478
PS12	0.333	1.0956	1.0994	1.0680	1.0641	1.0659	1.0711	1.0504	1.0424
PS3	0.378	1.0910	1.0952	1.0724	1.0686	1.0723	1.0775	1.0476	1.0381
PS13	0.421	1.0804	1.0841	1.0491	1.0458	1.0519	1.0544	1.0426	1.0362
PS4	0.465	1.0783	1.0826	1.0562	1.0520	1.0559	1.0599	1.0347	1.0282
PS5	0.550	1.0581	1.0621	1.0371	1.0333	1.0381	1.0407	1.0125	1.0049
PS15	0.590	1.0435	1.0473	1.0233	1.0195	1.0241	1.0259	1.0008	0.9928
PS6	0.633	1.0267	1.0316	1.0071	1.0034	1.0073	1.0112	0.9860	0.9789
PS16	0.673	1.0060	1.0096	0.9864	0.9833	0.9870	0.9890	0.9678	0.9586
PS7	0.715	0.9987	1.0028	0.9786	0.9758	0.9796	0.9784	-0.1392	-0.1493
PS17	0.745	0.9617	0.9653	0.9441	0.9405	0.9442	0.9465	0.9246	0.9175
PS8	0.778	0.9255	0.9290	0.9072	0.9054	0.9082	0.9118	0.8982	0.8921
PS18	0.808	0.9078	0.9113	0.8900	0.8878	0.8940	0.8936	0.8759	0.8684

Tapping Point	X/chord	Test 290499h	Test 290499i	Test 290499v	Test 290499x	Test 290499af	Test 270499g	Test 090399c	Test 090399d
PS9	0.838	0.8731	0.8755	0.8481	0.8489	0.8557	0.8580	0.8423	0.8354
SSLE	0.000	1.0660	1.0746	1.0444	1.0392	1.0536	1.0522	1.0391	1.0212
SS10	0.245	0.7449	0.7462	0.7317	0.7300	0.7332	0.7380	0.7150	0.7102
SS1	0.318	0.5335	0.3234	0.3500	0.3504	0.3491	0.3213	0.6356	0.4616
SS11	0.381	0.5625	0.5636	0.5502	0.5468	0.5501	0.5475	0.5374	0.5319
SS2	0.433	0.5114	0.5115	0.4898	0.4866	0.4928	0.4421	0.4733	0.4795
SS12	0.475	0.5403	0.5430	0.5266	0.5226	0.5231	0.4459	0.5027	0.5042
SS3	0.510	0.5553	0.5598	0.5591	0.5445	0.5422	0.4398	0.4888	0.4911
SS13	0.548	0.5137	0.5222	0.5119	0.4985	0.5008	0.4001	0.4765	0.4781
SS4	0.585	0.4512	0.4567	0.4695	0.4429	0.4414	0.3552	0.4331	0.4257
SS14	0.622	0.3766	0.3950	0.3931	0.3642	0.3640	0.2965	0.3635	0.3548
SS5	0.660	0.3616	0.3665	0.4155	0.3503	0.3395	0.3012	0.3143	0.3077
SS15	0.695	0.3226	0.3733	0.3901	0.3085	0.2990	0.2953	0.2709	0.2663
SS6	0.730	0.3851	0.3648	0.4460	0.3678	0.3345	0.2881	0.2365	0.2311
SS16	0.765	0.3917	0.4302	0.4466	0.3716	0.3340	0.3003	0.1999	0.1966
SS17	0.825	0.4525	0.4570	0.4641	0.4399	0.4090	0.2942	0.1583	0.1537
SS8	0.850	0.4418	0.4545	0.4518	0.4314	0.4108	0.2931	0.1806	0.1432
SS18	0.876	0.4615	0.4528	0.4602	0.4516	0.4382	0.3210	0.2083	0.1537
SS9	0.900	0.4421	0.4604	0.4440	0.4327	0.4182	0.3094	0.2527	0.1523

Table D.4g: Pressure readings (bar) at individual tapping points for pure steam contd.

Tapping Point	X/chord	Test 090399e	Test 090399t	Test 290499j	Test 290499k	Test 290499p	Test 290499r	Test 290499s
WMP2	-0.350	1.0056	0.9991	1.0620	1.0548	1.0408	1.0233	1.0367
WMP3	-0.137	1.0074	0.9989	1.0614	1.0536	1.0420	1.0246	1.0375
WMP7	0.300	0.9739	0.9664	1.0253	1.0182	1.0027	0.9861	0.9989
WMP11	0.446	0.9045	0.8977	0.9505	0.9439	0.9315	0.9144	0.9265
WMP14	0.570	0.7861	0.7791	0.8302	0.8240	0.8131	0.7983	0.8093
WMP16	0.648	0.5775	0.6363	0.7229	0.7074	0.6209	0.6330	0.6579
WMP17	0.761	0.6154	0.6543	0.6223	0.6170	0.6112	0.5992	0.6067
WMP19	0.834	0.5153	0.5047	0.5461	0.5397	0.5298	0.5091	0.5205
WMP21	0.908	0.3562	0.3545	0.3763	0.3718	0.3646	0.3576	0.3658
WMP23	0.949	0.2854	0.2703	0.2898	0.2875	0.2725	0.2677	0.3088
WMP25	0.990	0.2366	0.2014	0.2168	0.2119	0.1909	0.1839	0.2210
WMP27	1.058	0.2379	0.2231	0.2316	0.2308	0.2181	0.2168	0.2593
WDS1	3.842	0.2148	0.1996	0.2144	0.2082	0.1983	0.1951	0.2201
WDS2	-0.319	0.2380	0.1927	0.2094	0.2018	0.1986	0.1936	0.2446
WDS4	-8.466	0.3729	0.3797	0.3868	0.3955	0.3637	0.3651	0.4132
WDS5	-12.635	0.3712	0.3670	0.3666	0.3835	0.3380	0.3496	0.4123
WDS6	-16.804	0.3501	0.3464	0.3467	0.3615	0.3111	0.3297	0.3762
WDS7	-20.781	0.3159	0.3124	0.3169	0.3263	0.2868	0.3095	0.3426
WDS8	-24.854	0.2169	0.2133	0.2263	0.2261	0.2067	0.2261	0.2326
WDS9	-28.975	0.2529	0.2750	0.2728	0.2593	0.2263	0.2994	0.2774
WDS10	-33.096	0.2340	0.3541	0.3528	0.3263	0.2515	0.3734	0.2719
WDS11	-37.313	0.3072	0.4088	0.4123	0.4002	0.3214	0.4107	0.3286
WDS12	-41.290	0.3774	0.4434	0.4460	0.4380	0.3766	0.4402	0.4228
WDS13	-45.507	0.4074	0.4703	0.4892	0.4902	0.4384	0.4759	0.4689
WDS14	-49.533	0.4123	0.4715	0.5060	0.5109	0.4480	0.4752	0.4601
PS10	0.128	1.0603	1.0489	1.1161	1.1083	1.0932	1.0796	1.0935
PS1	0.180	1.0564	1.0457	1.1099	1.1022	1.0880	1.0741	1.0884
PS11	0.233	1.0510	1.0410	1.1070	1.0996	1.0878	1.0744	1.0887

Tapping Point	X/chord	Test 090399e	Test 090399t	Test 290499j	Test 290499k	Test 290499p	Test 290499r	Test 290499s
PS2	0.283	1.0487	1.0355	1.0969	1.0891	1.0679	1.0535	1.0679
PS12	0.333	1.0427	1.0293	1.0965	1.0881	1.0708	1.0566	1.0707
PS3	0.378	1.0395	1.0284	1.0922	1.0847	1.0734	1.0604	1.0741
PS13	0.421	1.0361	1.0220	1.0812	1.0732	1.0511	1.0373	1.0514
PS4	0.465	1.0277	1.0177	1.0797	1.0724	1.0583	1.0450	1.0586
PS5	0.550	1.0064	0.9957	1.0591	1.0521	1.0385	1.0252	1.0390
PS15	0.590	0.9932	0.9830	1.0445	1.0371	1.0246	1.0115	1.0252
PS6	0.633	0.9793	0.9698	1.0283	1.0211	1.0084	0.9958	1.0092
PS16	0.673	0.9600	0.9494	1.0077	1.0000	0.9878	0.9772	0.9883
PS7	0.715	-0.1459	-0.1589	1.0011	0.9924	0.9778	0.9592	0.9739
PS17	0.745	0.9186	0.9068	0.9624	0.9569	0.9453	0.9333	0.9456
PS8	0.778	0.8922	0.8808	0.9264	0.9207	0.9089	0.8984	0.9095
PS18	0.808	0.8689	0.8563	0.9076	0.9025	0.8921	0.8815	0.8950
PS9	0.838	0.8347	0.8258	0.8741	0.8670	0.8271	0.8436	0.8550
SSLE	0.000	1.0208	1.0096	1.0693	1.0611	1.0517	1.0308	1.0461
SS10	0.245	0.7114	0.6989	0.7442	0.7388	0.7325	0.7241	0.7348
SS1	0.318	0.1112	0.2611	0.2377	0.4056	0.3972	0.3659	0.3645
SS11	0.381	0.5322	0.5265	0.5620	0.5586	0.5522	0.5447	0.5526
SS2	0.433	0.4854	0.4791	0.5106	0.5070	0.4921	0.4818	0.4901
SS12	0.475	0.5094	0.5031	0.5385	0.5358	0.5277	0.5202	0.5260
SS3	0.510	0.4954	0.5027	0.5341	0.5304	0.5259	0.5208	0.5246
SS13	0.548	0.4804	0.4767	0.5062	0.5022	0.4948	0.4887	0.4935
SS4	0.585	0.4259	0.4174	0.4422	0.4391	0.4352	0.4294	0.4344
SS14	0.622	0.3516	0.3429	0.3674	0.3637	0.3605	0.3556	0.3591
SS5	0.660	0.3065	0.3000	0.3231	0.3209	0.3198	0.3203	0.3184
SS15	0.695	0.2644	0.2633	0.2765	0.2749	0.2731	0.2725	0.2729
SS6	0.730	0.2290	0.2272	0.2357	0.2344	0.2280	0.2258	0.2285
SS16	0.765	0.1948	0.2334	0.2073	0.2059	0.2125	0.2376	0.2118
SS17	0.825	0.1561	0.2549	0.1686	0.1645	0.2220	0.2527	0.1930
SS8	0.850	0.1422	0.2540	0.1676	0.1654	0.2189	0.2515	0.1919
SS18	0.876	0.1515	0.2703	0.1712	0.1737	0.2428	0.2716	0.2074
SS9	0.900	0.1513	0.2663	0.1713	0.1783	0.2466	0.2680	0.2114

D.3.2 Steam Dosed with 4 ppm Ammonia

Table D.5a: Pressure readings (bar) at individual tapping points for steam dosed with 4 ppm ammonia

Tapping Point	X/chord	Test 190499c	Test 160399a	Test 160399c	Test 160399d	Test 260399b	Test 260399c	Test 260399d	Test 290399a
WMP2	-0.350	1.0181	1.0198	1.0319	1.0170	1.0049	0.9871	0.9972	1.0017
WMP3	-0.137	1.0183	1.0234	1.0337	1.0210	1.0077	0.9897	1.0000	1.0039
WMP7	0.300	0.9841	0.9905	1.0012	0.9855	0.9743	0.9563	0.9659	0.9719
WMP11	0.446	0.8203	0.9182	0.9270	0.9125	0.8998	0.8840	0.8943	0.8975
WMP14	0.570	0.7944	0.8020	0.8062	0.7957	0.7876	0.7758	0.7834	0.7835
WMP16	0.648	0.5670	0.6176	0.6841	0.6786	0.6698	0.6599	0.6749	0.6733
WMP17	0.761	0.6130	0.6985	0.7031	0.7007	0.6745	0.6661	0.6817	0.6463
WMP19	0.834	0.5959	0.5882	0.6056	0.6007	0.5987	0.5980	0.6092	0.5796
WMP21	0.908	0.5735	0.5570	0.5587	0.5579	0.5519	0.5585	0.5620	0.5411
WMP23	0.949	0.5855	0.5631	0.5743	0.5691	0.5668	0.5748	0.5811	0.5482
WMP25	0.990	0.5518	0.5475	0.5375	0.5339	0.5377	0.5667	0.5626	0.5247
WMP27	1.058	0.5776	0.5765	0.5740	0.5704	0.5520	0.5641	0.5696	0.5476

Tapping Point	X/chord	Test 190499c	Test 160399a	Test 160399c	Test 160399d	Test 260399b	Test 260399c	Test 260399d	Test 290399a
WDS1	3.842	0.5824	0.5458	0.5620	0.5592	0.5591	0.5795	0.5757	0.5374
WDS2	-0.319	0.6191	0.5945	0.6124	0.6074	0.6023	0.6073	0.6123	0.5857
WDS4	-8.466	0.6274	0.6071	0.6215	0.6177	0.6116	0.6181	0.6243	0.5942
WDS5	-12.635	0.6208	0.6001	0.6144	0.6111	0.6035	0.6109	0.6160	0.5856
WDS6	-16.804	0.6091	0.5892	0.6020	0.5990	0.5915	0.6005	0.6069	0.5781
WDS7	-20.781	0.6086	0.5931	0.5994	0.5964	0.5851	0.5931	0.6025	0.5748
WDS8	-24.854	0.4135	0.4420	0.4027	0.4039	0.3904	0.4045	0.4152	0.3863
WDS9	-28.975	0.6084	0.6021	0.5985	0.5970	0.5856	0.5937	0.6062	0.5618
WDS10	-33.096	0.6191	0.6353	0.6154	0.6124	0.6004	0.6043	0.6171	0.5834
WDS11	-37.313	0.6343	0.6490	0.6316	0.6292	0.6184	0.6193	0.6314	0.6016
WDS12	-41.290	0.6395	0.6535	0.6407	0.6378	0.6283	0.6284	0.6390	0.6087
WDS13	-45.507	0.6361	0.6506	0.6366	0.6326	0.6237	0.6241	0.6359	0.6051
WDS14	-49.533	0.6252	0.6431	0.6236	0.6202	0.6116	0.6142	0.6249	0.5956
PS10	0.128	1.0840	1.0740	1.0902	1.0742	1.0675	1.0492	1.0577	1.0571
PS1	0.180	1.0786	1.0704	1.0847	1.0702	1.0634	1.0456	1.0545	1.0518
PS11	0.233	1.0764	1.0644	1.0813	1.0652	1.0573	1.0395	1.0490	1.0441
PS2	0.283	1.0664	1.0583	1.0740	1.0594	1.0546	1.0363	1.0439	1.0454
PS12	0.333	1.0649	1.0572	1.0729	1.0563	1.0513	1.0331	1.0410	1.0412
PS3	0.378	1.0619	1.0535	1.0679	1.0532	1.0456	1.0280	1.0368	1.0341
PS13	0.421	1.0507	1.0447	1.0602	1.0446	1.0407	1.0220	1.0309	1.0324
PS4	0.465	1.0506	1.0429	1.0562	1.0416	1.0359	1.0184	1.0272	1.0245
PS5	0.550	1.0294	1.0215	1.0340	1.0189	1.0119	0.9951	1.0037	1.0036
PS15	0.590	1.0159	1.0089	1.0214	1.0064	0.9995	0.9831	0.9927	0.9893
PS6	0.633	1.0007	0.9948	1.0076	0.9919	0.9850	0.9683	0.9781	0.9737
PS16	0.673	0.9784	0.9765	0.9883	0.9724	0.9648	0.9492	0.9577	0.9562
PS7	0.715	0.9601	-0.1306	-0.1180	-0.1365	-0.1196	-0.1579	-0.1272	-0.1545
PS17	0.745	0.9373	0.9354	0.9437	0.9302	0.9233	0.9070	0.9157	0.9145
PS8	0.778	0.9021	0.9139	0.9207	0.9053	0.8970	0.8813	0.8910	0.8901
PS18	0.808	0.8843	0.8873	0.8922	0.8787	0.8720	0.8572	0.8663	0.8654
PS9	0.838	0.8503	0.8552	0.8603	0.8471	0.8402	0.8255	0.8342	0.8329
SSLE	0.000	1.0391	1.0525	1.0505	1.0326	1.0261	1.0080	1.0148	1.0193
SS10	0.245	0.7277	0.7331	0.7317	0.7231	0.7168	0.7061	0.7114	0.7097
SS1	0.318	0.5641	0.5434	0.3680	0.3841	0.2997	0.4136	0.6415	-0.6406
SS11	0.381	0.5467	0.5583	0.5532	0.5445	0.5369	0.5307	0.5359	0.5324
SS2	0.433	0.4499	0.5136	0.5152	0.4982	0.4534	0.4463	0.4631	0.4920
SS12	0.475	0.4658	0.5819	0.5770	0.5697	0.5047	0.5058	0.5476	0.5576
SS3	0.510	0.5443	0.5920	0.5969	0.5923	0.6090	0.6075	0.6102	0.5770
SS13	0.548	0.6228	0.5894	0.6001	0.5922	0.6117	0.6093	0.6047	0.5824
SS4	0.585	0.6183	0.5763	0.5887	0.5801	0.5881	0.5868	0.5850	0.5654
SS14	0.622	0.6040	0.5706	0.5752	0.5669	0.5690	0.5744	0.5721	0.5547
SS5	0.660	0.6047	0.5845	0.5898	0.5805	0.5706	0.5758	0.5770	0.5653
SS15	0.695	0.5849	0.5786	0.5863	0.5747	0.5583	0.5623	0.5681	0.5599
SS6	0.730	0.5673	0.5799	0.5847	0.5697	0.5475	0.5543	0.5586	0.5577
SS16	0.765	0.5600	0.5856	0.5805	0.5654	0.5335	0.5394	0.5220	0.5507
SS17	0.825	0.5522	0.6054	0.5710	0.5679	0.5218	0.5286	0.5382	0.5474
SS8	0.850	0.5475	0.6106	0.5630	0.5618	0.5102	0.5236	0.5352	0.5410
SS18	0.876	0.5418	0.6223	0.5525	0.5558	0.5013	0.5161	0.5316	0.5370
SS9	0.900	0.5446	0.6370	0.5452	0.5514	0.4967	0.5147	0.5376	0.5385

Table D.5b: Pressure readings (bar) at individual tapping points for steam dosed with 4 ppm ammonia contd.

Tapping Point	X/chord	Test 290399b	Test 010499a	Test 010499c	Test 010499d	Test 010499e	Test 010499i	Test 010499j	Test 230399v
WMP2	-0.350	1.0030	1.0213	1.0213	1.0126	1.0178	1.0160	1.0197	1.0076
WMP3	-0.137	1.0063	1.0241	1.0256	1.0165	1.0212	1.0199	1.0232	1.0098
WMP7	0.300	0.9736	0.9886	0.9882	0.9798	0.9849	0.9824	0.9860	0.9738
WMP11	0.446	0.8995	0.9162	0.9175	0.9097	0.9149	0.9101	0.9127	0.9057
WMP14	0.570	0.7877	0.8018	0.8039	0.7957	0.8017	0.7959	0.8014	0.7939
WMP16	0.648	0.6689	0.6685	0.6644	0.6620	0.6392	0.6689	0.6658	0.6531
WMP17	0.761	0.6695	0.7289	0.7285	0.7380	0.7370	0.7304	0.7314	0.6853
WMP19	0.834	0.5886	0.5954	0.6029	0.5921	0.5969	0.6052	0.6045	0.5901
WMP21	0.908	0.5446	0.5640	0.5674	0.5604	0.5590	0.5697	0.5652	0.5440
WMP23	0.949	0.5583	0.5532	0.5603	0.5497	0.5527	0.5661	0.5639	0.5373
WMP25	0.990	0.5307	0.5372	0.5300	0.5159	0.5161	0.5382	0.5353	0.4953
WMP27	1.058	0.5537	0.5521	0.5632	0.5526	0.5524	0.5697	0.5720	0.5579
WDS1	3.842	0.5398	0.5448	0.5741	0.5593	0.5655	0.5819	0.5853	0.5430
WDS2	-0.319	0.5917	0.5944	0.6054	0.5945	0.5946	0.6029	0.6041	0.5844
WDS4	-8.466	0.6039	0.6017	0.6112	0.5975	0.6039	0.6133	0.6154	0.5943
WDS5	-12.635	0.5949	0.5902	0.5974	0.5857	0.5881	0.6002	0.6013	0.5808
WDS6	-16.804	0.5874	0.5807	0.5879	0.5772	0.5790	0.5938	0.5955	0.5767
WDS7	-20.781	0.5826	0.5789	0.5900	0.5786	0.5808	0.5981	0.5998	0.5823
WDS8	-24.854	0.3924	0.3785	0.3945	0.3859	0.3837	0.4130	0.4123	0.3926
WDS9	-28.975	0.5765	0.5621	0.5833	0.5707	0.5688	0.6020	0.6039	0.5815
WDS10	-33.096	0.5929	0.5852	0.6010	0.5876	0.5872	0.6193	0.6205	0.5985
WDS11	-37.313	0.6105	0.6094	0.6196	0.6091	0.6080	0.6335	0.6349	0.6173
WDS12	-41.290	0.6198	0.6213	0.6312	0.6234	0.6218	0.6415	0.6439	0.6264
WDS13	-45.507	0.6149	0.6177	0.6265	0.6204	0.6178	0.6396	0.6409	0.6235
WDS14	-49.533	0.6034	0.6041	0.6135	0.6071	0.6026	0.6261	0.6277	0.6097
PS10	0.128	1.0603	1.0765	1.0752	1.0651	1.0710	1.0698	1.0734	1.0624
PS1	0.180	1.0549	1.0714	1.0715	1.0614	1.0674	1.0661	1.0698	1.0575
PS11	0.233	1.0481	1.0662	1.0664	1.0568	1.0627	1.0621	1.0657	1.0529
PS2	0.283	1.0487	1.0553	1.0554	1.0455	1.0513	1.0502	1.0537	1.0450
PS12	0.333	1.0434	1.0577	1.0566	1.0464	1.0519	1.0502	1.0536	1.0415
PS3	0.378	1.0373	1.0560	1.0560	1.0460	1.0515	1.0509	1.0543	1.0406
PS13	0.421	1.0356	1.0415	1.0416	1.0314	1.0370	1.0356	1.0389	1.0317
PS4	0.465	1.0287	1.0447	1.0433	1.0335	1.0394	1.0382	1.0416	1.0302
PS5	0.550	1.0073	1.0221	1.0214	1.0115	1.0173	1.0161	1.0195	1.0074
PS15	0.590	0.9910	1.0088	1.0089	0.9997	1.0052	1.0040	1.0073	0.9954
PS6	0.633	0.9781	0.9934	0.9940	0.9839	0.9899	0.9892	0.9919	0.9806
PS16	0.673	0.9580	0.9747	0.9740	0.9654	0.9704	0.9696	0.9731	0.9629
PS7	0.715	-0.1509	-0.1260	-0.1249	-0.1406	-0.1342	-0.1323	-0.1307	-0.1226
PS17	0.745	0.9163	0.9331	0.9328	0.9244	0.9300	0.9282	0.9313	0.9198
PS8	0.778	0.8913	0.9101	0.9091	0.8968	0.9029	0.9004	0.9035	0.8940
PS18	0.808	0.8671	0.8819	0.8814	0.8725	0.8738	0.8673	0.8800	0.8683
PS9	0.838	0.8341	0.8480	0.8486	0.8415	0.8451	0.8449	0.8470	0.8368
SSLE	0.000	1.0176	1.0321	1.0327	1.0252	1.0296	1.0270	1.0265	1.0241
SS10	0.245	0.7092	0.7202	0.7197	0.7144	0.7185	0.7189	0.7204	0.7103
SS1	0.318	0.0485	0.5856	0.5619	0.5229	0.5408	0.5628	0.5430	0.2009
SS11	0.381	0.5326	0.5474	0.5445	0.5414	0.5448	0.5438	0.5455	0.5382
SS2	0.433	0.4990	0.5060	0.5068	0.5025	0.5035	0.5039	0.5034	0.4940
SS12	0.475	0.5524	0.5769	0.5761	0.5727	0.5743	0.5749	0.5757	0.5590
SS3	0.510	0.5756	0.5958	0.5954	0.5939	0.5950	0.5957	0.5950	0.5768
SS13	0.548	0.5833	0.5946	0.5942	0.5914	0.5918	0.5924	0.5921	0.5701
SS4	0.585	0.5673	0.5818	0.5830	0.5826	0.5821	0.5826	0.5820	0.5611
SS14	0.622	0.5553	0.5717	0.5707	0.5710	0.5697	0.5720	0.5701	0.5433
SS5	0.660	0.5675	0.5876	0.5860	0.5872	0.5848	0.5871	0.5853	0.5558
SS15	0.695	0.5605	0.5779	0.5807	0.5816	0.5785	0.5829	0.5805	0.5528

Tapping Point	X/chord	Test 290399b	Test 010499a	Test 010499c	Test 010499d	Test 010499e	Test 010499i	Test 010499j	Test 230399v
SS6	0.730	0.5579	0.5761	0.5789	0.5794	0.5745	0.5819	0.5787	0.5500
SS16	0.765	0.5510	0.5714	0.5777	0.5794	0.5731	0.5828	0.5790	0.5483
SS17	0.825	0.5430	0.5719	0.5770	0.5830	0.5722	0.5833	0.5771	0.5346
SS8	0.850	0.5340	0.5681	0.5700	0.5783	0.5668	0.5798	0.5715	0.5245
SS18	0.876	0.5262	0.5629	0.5636	0.5764	0.5616	0.5752	0.5651	0.5120
SS9	0.900	0.5188	0.5607	0.5599	0.5770	0.5588	0.5768	0.5643	0.5031

Table D.5c: Pressure readings (bar) at individual tapping points for steam dosed with 4 ppm ammonia contd.

Tapping Point	X/chord	Test 010499k	Test 010499l	Test 010499m	Test 010499n	Test 190499a	Test 190499b	Test 160399h	Test 160399i
WMP2	-0.350	1.0134	1.0205	1.0116	1.0100	1.0298	1.0299	1.0209	1.0195
WMP3	-0.137	1.0173	1.0252	1.0155	1.0155	1.0291	1.0288	1.0250	1.0211
WMP7	0.300	0.9800	0.9868	0.9781	0.9781	0.9966	0.9962	0.9889	0.9869
WMP11	0.446	0.9091	0.9155	0.9076	0.9076	0.8870	0.8686	0.9156	0.9148
WMP14	0.570	0.7961	0.8029	0.7957	0.7957	0.8020	0.8035	0.7968	0.7941
WMP16	0.648	0.6388	0.6392	0.6393	0.6393	0.6060	0.6809	0.6025	0.5838
WMP17	0.761	0.7184	0.7272	0.7427	0.7427	0.5979	0.5984	0.6772	0.6846
WMP19	0.834	0.5896	0.6001	0.5912	0.5912	0.4580	0.4715	0.5739	0.5734
WMP21	0.908	0.5523	0.5639	0.5531	0.5531	0.4170	0.4338	0.5019	0.4806
WMP23	0.949	0.5379	0.5560	0.5426	0.5426	0.4441	0.4580	0.4999	0.5055
WMP25	0.990	0.5085	0.5263	0.5425	0.5425	0.4173	0.4386	0.4301	0.4269
WMP27	1.058	0.5456	0.5632	0.5514	0.5514	0.4553	0.4529	0.4664	0.4570
WDS1	3.842	0.5624	0.5816	0.5677	0.5677	0.4468	0.4821	0.4486	0.4410
WDS2	-0.319	0.5833	0.5991	0.5864	0.5864	0.4912	0.5038	0.5392	0.5341
WDS4	-8.466	0.5908	0.6085	0.5950	0.5950	0.5118	0.5137	0.5609	0.5621
WDS5	-12.635	0.5752	0.5951	0.5807	0.5807	0.4843	0.4886	0.5466	0.5422
WDS6	-16.804	0.5685	0.5875	0.5743	0.5743	0.4655	0.4773	0.5169	0.5148
WDS7	-20.781	0.5730	0.5928	0.5800	0.5800	0.4770	0.4884	0.4868	0.4843
WDS8	-24.854	0.3759	0.4013	0.3865	0.3865	0.3191	0.3266	0.3124	0.3086
WDS9	-28.975	0.5597	0.5933	0.5724	0.5724	0.4473	0.4588	0.4316	0.4225
WDS10	-33.096	0.5813	0.6104	0.5934	0.5934	0.4760	0.4860	0.4525	0.4431
WDS11	-37.313	0.6056	0.6265	0.6128	0.6128	0.4823	0.5091	0.5171	0.5093
WDS12	-41.290	0.6188	0.6351	0.6236	0.6236	0.5264	0.5455	0.5755	0.5695
WDS13	-45.507	0.6153	0.6318	0.6202	0.6202	0.5242	0.5323	0.5790	0.5733
WDS14	-49.533	0.6001	0.6172	0.6053	0.6053	0.4954	0.5052	0.5512	0.5459
PS10	0.128	1.0684	1.0762	1.0666	1.0666	1.1002	1.0980	1.0780	1.0756
PS1	0.180	1.0654	1.0725	1.0630	1.0630	1.0929	1.0936	1.0739	1.0715
PS11	0.233	1.0613	1.0687	1.0591	1.0591	1.0895	1.0892	1.0683	1.0662
PS2	0.283	1.0485	1.0558	1.0475	1.0475	1.0828	1.0813	1.0636	1.0610
PS12	0.333	1.0501	1.0559	1.0465	1.0465	1.0800	1.0789	1.0592	1.0571
PS3	0.378	1.0501	1.0571	1.0473	1.0473	1.0759	1.0756	1.0564	1.0547
PS13	0.421	1.0344	1.0416	1.0332	1.0332	1.0665	1.0658	1.0495	1.0466
PS4	0.465	1.0370	1.0442	1.0348	1.0348	1.0625	1.0628	1.0453	1.0438
PS5	0.550	1.0153	1.0225	1.0134	1.0134	1.0428	1.0419	1.0220	1.0199
PS15	0.590	1.0029	1.0115	1.0009	1.0009	1.0271	1.0286	1.0100	1.0087
PS6	0.633	0.9876	0.9949	0.9854	0.9854	1.0121	1.0113	0.9949	0.9931
PS16	0.673	0.9692	0.9768	0.9667	0.9667	0.9917	0.9897	0.9765	0.9741
PS7	0.715	-0.1259	-0.1239	-0.1336	-0.1336	0.9686	0.9701	-0.1335	-0.1357
PS17	0.745	0.9271	0.9356	0.9255	0.9255	0.9472	0.9482	0.9322	0.9299
PS8	0.778	0.8997	0.9066	0.8988	0.8988	0.9107	0.9126	0.9075	0.9047
PS18	0.808	0.8740	0.6466	0.8725	0.8725	0.8936	0.8949	0.8827	0.8803

Tapping Point	X/chord	Test 010499k	Test 010499l	Test 010499m	Test 010499n	Test 190499a	Test 190499b	Test 160399h	Test 160399i
PS9	0.838	0.8436	0.8488	0.8429	0.8429	0.8597	0.8591	0.8487	0.8457
SSLE	0.000	1.0293	1.0285	1.0219	1.0219	1.0509	1.0516	1.0377	1.0337
SS10	0.245	0.7173	0.7226	0.7163	0.7163	0.7332	0.7333	0.7242	0.7225
SS1	0.318	0.5379	0.5542	0.5586	0.5586	-0.2071	0.0511	0.1807	0.1943
SS11	0.381	0.5417	0.5476	0.5424	0.5424	0.5519	0.5518	0.5420	0.5408
SS2	0.433	0.4958	0.5057	0.4991	0.4991	0.4526	0.4546	0.4963	0.4945
SS12	0.475	0.5653	0.5786	0.5676	0.5676	0.4528	0.4522	0.5289	0.5222
SS3	0.510	0.5849	0.5965	0.5868	0.5868	0.4399	0.4393	0.5679	0.5493
SS13	0.548	0.5792	0.5928	0.5855	0.5855	0.4029	0.4059	0.5410	0.5167
SS4	0.585	0.5684	0.5826	0.5723	0.5723	0.3552	0.4192	0.5170	0.4672
SS14	0.622	0.5518	0.5724	0.5612	0.5612	0.3685	0.4796	0.4718	0.4175
SS5	0.660	0.5649	0.5869	0.5720	0.5720	0.4834	0.5400	0.5053	0.4387
SS15	0.695	0.5617	0.5832	0.5704	0.5704	0.5384	0.5487	0.5061	0.4690
SS6	0.730	0.5662	0.5808	0.5753	0.5753	0.5373	0.5297	0.5065	0.4927
SS16	0.765	0.5628	0.5811	0.5696	0.5696	0.5362	0.5132	0.5024	0.5018
SS17	0.825	0.5509	0.5812	0.5644	0.5644	0.5195	0.4983	0.4833	0.4859
SS8	0.850	0.5421	0.5760	0.5564	0.5564	0.5039	0.4762	0.4685	0.4739
SS18	0.876	0.5285	0.5742	0.5509	0.5509	0.4948	0.4590	0.4586	0.4642
SS9	0.900	0.5222	0.5736	0.5458	0.5458	0.4688	0.4362	0.4455	0.4524

Table D.5d: Pressure readings (bar) at individual tapping points for steam dosed with 4 ppm ammonia contd.

Tapping Point	X/chord	Test 160399m	Test 160399v	Test 190399d	Test 260399e	Test 260399f	Test 260399g	Test 260399h	Test 290399f
WMP2	-0.350	1.0168	1.0129	1.0200	1.0043	1.0024	0.9997	0.9999	1.0055
WMP3	-0.137	1.0192	1.0169	1.0216	1.0059	1.0047	1.0010	1.0028	1.0082
WMP7	0.300	0.9836	0.9824	0.9899	0.9737	0.9713	0.9671	0.9679	0.9752
WMP11	0.446	0.9107	0.9080	0.9140	0.8992	0.8985	0.8952	0.8954	0.9004
WMP14	0.570	0.7911	0.7894	0.7951	0.7846	0.7846	0.7808	0.7824	0.7868
WMP16	0.648	0.6716	0.6662	0.4383	0.6738	0.6733	0.6655	0.6641	0.6630
WMP17	0.761	0.6603	0.6612	0.6667	0.6570	0.6591	0.6559	0.6622	0.6427
WMP19	0.834	0.5689	0.5387	0.5719	0.5347	0.5613	0.5443	0.5545	0.5601
WMP21	0.908	0.4970	0.4085	0.4474	0.4305	0.4987	0.4348	0.4741	0.4501
WMP23	0.949	0.4935	0.3742	0.4625	0.4191	0.5063	0.4279	0.4837	0.4548
WMP25	0.990	0.4260	0.3258	0.4162	0.3841	0.4536	0.3799	0.4246	0.4056
WMP27	1.058	0.4669	0.3806	0.4199	0.3987	0.4692	0.4043	0.4473	0.4073
WDS1	3.842	0.4554	0.3177	0.4057	0.3682	0.4489	0.3587	0.4263	0.3660
WDS2	-0.319	0.5391	0.4211	0.4861	0.4664	0.5290	0.4643	0.5156	0.4790
WDS4	-8.466	0.5557	0.4819	0.5359	0.5079	0.5587	0.5134	0.5436	0.5360
WDS5	-12.635	0.5428	0.5194	0.5253	0.5104	0.5398	0.5109	0.5276	0.5227
WDS6	-16.804	0.5164	0.4927	0.4904	0.4766	0.5189	0.4758	0.5030	0.4900
WDS7	-20.781	0.4856	0.4399	0.4444	0.4242	0.4962	0.4288	0.4726	0.4434
WDS8	-24.854	0.3115	0.2955	0.2954	0.2862	0.3126	0.2888	0.3050	0.2957
WDS9	-28.975	0.4314	0.4118	0.3990	0.3863	0.4371	0.3898	0.4171	0.3987
WDS10	-33.096	0.4514	0.4533	0.4117	0.3953	0.4553	0.4006	0.4366	0.4147
WDS11	-37.313	0.5178	0.5293	0.4675	0.4431	0.5036	0.4557	0.4960	0.4790
WDS12	-41.290	0.5734	0.5702	0.5390	0.5087	0.5577	0.5246	0.5580	0.5471
WDS13	-45.507	0.5770	0.5752	0.5452	0.5216	0.5627	0.5373	0.5616	0.5544
WDS14	-49.533	0.5501	0.5541	0.5242	0.5068	0.5354	0.5169	0.5369	0.5316
PS10	0.128	1.0682	1.0669	1.0762	1.0655	1.0636	1.0594	1.0602	1.0634
PS1	0.180	1.0642	1.0631	1.0718	1.0603	1.0599	1.0558	1.0565	1.0587
PS11	0.233	1.0586	1.0577	1.0637	1.0558	1.0538	1.0515	1.0516	1.0506

Tapping Point	X/chord	Test 160399m	Test 160399v	Test 190399d	Test 260399e	Test 260399f	Test 260399g	Test 260399h	Test 290399f
PS2	0.283	1.0551	1.0532	1.0697	1.0495	1.0495	1.0460	1.0478	1.0512
PS12	0.333	1.0496	1.0471	1.0615	1.0460	1.0453	1.0420	1.0424	1.0466
PS3	0.378	1.0495	1.0479	1.0528	1.0434	1.0421	1.0386	1.0387	1.0405
PS13	0.421	1.0413	1.0397	1.0554	1.0363	1.0365	1.0332	1.0330	1.0372
PS4	0.465	1.0354	1.0338	1.0451	1.0336	1.0319	1.0271	1.0299	1.0315
PS5	0.550	1.0135	1.0122	1.0211	1.0093	1.0088	1.0044	1.0054	1.0079
PS15	0.590	1.0011	1.0005	1.0074	0.9975	0.9966	0.9926	0.9936	0.9952
PS6	0.633	0.9861	0.9852	0.9938	0.9833	0.9823	0.9781	0.9790	0.9796
PS16	0.673	0.9674	0.9661	0.9723	0.9622	0.9623	0.9588	0.9593	0.9606
PS7	0.715	-0.1433	-0.1421	-0.1299	-0.1170	-0.1146	-0.1181	-0.1142	-0.1475
PS17	0.745	0.9239	0.9226	0.9301	0.9216	0.9193	0.9161	0.9162	0.9168
PS8	0.778	0.8981	0.8978	0.9045	0.8947	0.8941	0.8901	0.8916	0.8925
PS18	0.808	0.8742	0.8727	0.8777	0.8697	0.8638	0.8661	0.8660	0.8674
PS9	0.838	0.8401	0.8394	0.8471	0.8378	0.8377	0.8340	0.8334	0.8356
SSLE	0.000	1.0270	1.0248	1.0332	1.0234	1.0220	1.0180	1.0190	1.0184
SS10	0.245	0.7174	0.7169	0.7197	0.7145	0.7150	0.7115	0.7119	0.7118
SS1	0.318	0.4978	0.3152	-0.1228	0.6531	0.6773	0.4897	0.2823	0.3459
SS11	0.381	0.5369	0.5356	0.5406	0.5354	0.5354	0.5327	0.5327	0.5333
SS2	0.433	0.4951	0.4849	0.4996	0.4655	0.4673	0.4631	0.4612	0.4843
SS12	0.475	0.5261	0.5110	0.5227	0.4987	0.5019	0.4975	0.4973	0.5117
SS3	0.510	0.5609	0.5219	0.5264	0.4911	0.5369	0.4951	0.5302	0.5287
SS13	0.548	0.5366	0.4957	0.4976	0.5006	0.5371	0.5037	0.5522	0.5019
SS4	0.585	0.5096	0.4398	0.4344	0.4510	0.4989	0.4508	0.5133	0.4444
SS14	0.622	0.4669	0.3686	0.3708	0.3869	0.4640	0.3847	0.4924	0.3841
SS5	0.660	0.4947	0.3512	0.3509	0.3600	0.4880	0.3675	0.5074	0.3745
SS15	0.695	0.5012	0.3405	0.3266	0.3357	0.5060	0.3510	0.5176	0.3512
SS6	0.730	0.5037	0.3310	0.3411	0.3381	0.5101	0.3744	0.5154	0.3970
SS16	0.765	0.4994	0.3797	0.3627	0.2942	0.4123	0.3304	0.3896	0.4186
SS17	0.825	0.4803	0.4381	0.4511	0.4060	0.4799	0.4724	0.4821	0.4665
SS8	0.850	0.4661	0.4488	0.4503	0.4299	0.4658	0.4632	0.4689	0.4492
SS18	0.876	0.4565	0.4472	0.4608	0.4525	0.4519	0.4630	0.4543	0.4565
SS9	0.900	0.4435	0.4535	0.4445	0.4407	0.4402	0.4503	0.4458	0.4375

Table D.5e: Pressure readings (bar) at individual tapping points for steam dosed with 4 ppm ammonia contd.

Tapping Point	X/chord	Test 290399g	Test 290399h	Test 190399i	Test 190399j	Test 190399l	Test 230399b	Test 230399c	Test 260399s
WMP2	-0.350	1.0050	1.0103	1.0170	1.0222	1.0216	0.9971	1.0027	0.9951
WMP3	-0.137	1.0070	1.0148	1.0194	1.0251	1.0227	0.9987	1.0013	0.9978
WMP7	0.300	0.9746	0.9783	0.9867	0.9909	0.9897	0.9651	0.9698	0.9626
WMP11	0.446	0.8993	0.9061	0.9140	0.9181	0.9173	0.8925	0.8927	0.8902
WMP14	0.570	0.7853	0.7915	0.7942	0.7978	0.7967	0.7771	0.7795	0.7793
WMP16	0.648	0.6597	0.6602	0.6498	0.6547	0.6526	0.6462	0.6496	0.6492
WMP17	0.761	0.6350	0.6484	0.6456	0.6544	0.6633	0.6538	0.6628	0.6524
WMP19	0.834	0.5660	0.5487	0.5498	0.5627	0.5431	0.5457	0.5548	0.5322
WMP21	0.908	0.4812	0.4481	0.4362	0.4633	0.4033	0.4748	0.4879	0.4251
WMP23	0.949	0.4931	0.4180	0.4093	0.4306	0.3705	0.4176	0.4607	0.4025
WMP25	0.990	0.4615	0.3621	0.3729	0.4048	0.3593	0.4055	0.4298	0.3513
WMP27	1.058	0.4428	0.4094	0.3702	0.3926	0.3705	0.4031	0.4255	0.4085
WDS1	3.842	0.4439	0.3445	0.3363	0.3639	0.3214	0.3490	0.3967	0.3497
WDS2	-0.319	0.5244	0.4711	0.4434	0.4708	0.4188	0.4733	0.5095	0.4357
WDS4	-8.466	0.5520	0.5199	0.5081	0.5268	0.4930	0.5172	0.5346	0.5068

Tapping Point	X/chord	Test 290399g	Test 290399h	Test 190399i	Test 190399j	Test 190399l	Test 230399b	Test 230399c	Test 260399s
WDS5	-12.635	0.5331	0.5247	0.5045	0.5154	0.5144	0.5161	0.5200	0.5207
WDS6	-16.804	0.5082	0.4951	0.4669	0.4763	0.4892	0.4775	0.4855	0.4927
WDS7	-20.781	0.4729	0.4436	0.4080	0.4248	0.4395	0.4299	0.4443	0.4454
WDS8	-24.854	0.3041	0.3021	0.2698	0.2818	0.2961	0.2912	0.2945	0.3070
WDS9	-28.975	0.4136	0.4082	0.3666	0.3882	0.4160	0.3968	0.3975	0.4338
WDS10	-33.096	0.4346	0.4240	0.3822	0.4035	0.4918	0.4103	0.4137	0.4677
WDS11	-37.313	0.4982	0.4755	0.4606	0.4801	0.5463	0.4570	0.4690	0.5342
WDS12	-41.290	0.5588	0.5460	0.5367	0.5514	0.5777	0.5351	0.5336	0.5697
WDS13	-45.507	0.5625	0.5566	0.5447	0.5567	0.5795	0.5433	0.5408	0.5681
WDS14	-49.533	0.5364	0.5348	0.5240	0.5328	0.5633	0.5212	0.5185	0.5485
PS10	0.128	1.0611	1.0657	1.0688	1.0744	1.0733	1.0505	1.0554	1.0482
PS1	0.180	1.0564	1.0613	1.0646	1.0700	1.0692	1.0453	1.0510	1.0445
PS11	0.233	1.0504	1.0552	1.0577	1.0636	1.0624	1.0388	1.0440	1.0388
PS2	0.283	1.0475	1.0504	1.0604	1.0657	1.0644	1.0361	1.0413	1.0370
PS12	0.333	1.0440	1.0485	1.0529	1.0579	1.0566	1.0339	1.0382	1.0290
PS3	0.378	1.0383	1.0435	1.0461	1.0513	1.0506	1.0288	1.0336	1.0267
PS13	0.421	1.0342	1.0379	1.0457	1.0512	1.0495	1.0218	1.0266	1.0236
PS4	0.465	1.0291	1.0331	1.0362	1.0415	1.0407	1.0180	1.0233	1.0167
PS5	0.550	1.0060	1.0101	1.0129	1.0183	1.0174	0.9955	1.0007	0.9944
PS15	0.590	0.9924	0.9976	1.0007	1.0059	1.0051	0.9819	0.9871	0.9829
PS6	0.633	0.9776	0.9831	0.9864	0.9909	0.9901	0.9678	0.9726	0.9680
PS16	0.673	0.9583	0.9640	0.9671	0.9730	0.9715	0.9493	0.9543	0.9494
PS7	0.715	-0.1496	-0.1432	-0.1392	-0.1336	-0.1331	-0.1487	-0.1045	-0.1384
PS17	0.745	0.9155	0.9209	0.9244	0.9286	0.9279	0.9059	0.9102	0.9088
PS8	0.778	0.8915	0.8966	0.8977	0.9019	0.9009	0.8812	0.8854	0.8838
PS18	0.808	0.8645	0.8710	0.8702	0.8748	0.8518	0.8559	0.8599	0.8571
PS9	0.838	0.8332	0.8382	0.8396	0.8433	0.8431	0.8246	0.8290	0.8235
SSLE	0.000	1.0177	1.0242	1.0224	1.0278	1.0275	1.0074	1.0121	1.0073
SS10	0.245	0.7093	0.7135	0.7106	0.7140	0.7138	0.7000	0.7032	0.6981
SS1	0.318	0.2457	0.3485	-0.1392	-0.1447	-0.2849	-0.1428	0.0038	0.3027
SS11	0.381	0.5329	0.5335	0.5356	0.5405	0.5406	0.5279	0.5299	0.5249
SS2	0.433	0.4888	0.4920	0.4937	0.4951	0.4939	0.4796	0.4825	0.4783
SS12	0.475	0.5141	0.5162	0.5157	0.5190	0.5197	0.5104	0.5088	0.5062
SS3	0.510	0.5363	0.5346	0.5192	0.5354	0.5332	0.5386	0.5251	0.5310
SS13	0.548	0.5041	0.4973	0.4899	0.4987	0.5011	0.5061	0.4949	0.4960
SS4	0.585	0.4493	0.4417	0.4271	0.4394	0.4385	0.4560	0.4345	0.4431
SS14	0.622	0.3932	0.3806	0.3570	0.3726	0.3826	0.4050	0.3771	0.3870
SS5	0.660	0.3974	0.3835	0.3154	0.3539	0.3497	0.4196	0.3647	0.3780
SS15	0.695	0.3997	0.3907	0.2775	0.3293	0.3599	0.4357	0.3672	0.4053
SS6	0.730	0.4436	0.4381	0.2887	0.3787	0.3573	0.4666	0.3927	0.4181
SS16	0.765	0.4681	0.4670	0.2747	0.3809	0.4088	0.4737	0.4253	0.4548
SS17	0.825	0.4741	0.4760	0.3256	0.4357	0.4404	0.4671	0.4510	0.4583
SS8	0.850	0.4574	0.4590	0.3654	0.4286	0.4425	0.4516	0.4487	0.4538
SS18	0.876	0.4515	0.4551	0.3747	0.4427	0.4384	0.4445	0.4434	0.4410
SS9	0.900	0.4369	0.4394	0.3843	0.4260	0.4452	0.4309	0.4372	0.4401

Table D.5f: Pressure readings (bar) at individual tapping points for steam dosed with 4 ppm ammonia contd.

Tapping Point	X/chord	Test 230399m	Test 230399n	Test 230399q	Test 230399t	Test 290399n	Test 290399o	Test 290399p	Test 290399r
WMP2	-0.350	0.9914	1.0049	0.9985	0.9991	1.0107	1.0044	1.0003	0.9990
WMP3	-0.137	0.9936	1.0074	1.0014	1.0031	1.0160	1.0087	1.0047	1.0037
WMP7	0.300	0.9591	0.9718	0.9652	0.9654	0.9786	0.9718	0.9677	0.9660
WMP11	0.446	0.8877	0.8991	0.8946	0.8981	0.9038	0.8966	0.8944	0.8932
WMP14	0.570	0.7738	0.7865	0.7815	0.7853	0.7928	0.7878	0.7832	0.7828
WMP16	0.648	0.6431	0.6542	0.6465	0.6479	0.6600	0.6497	0.6483	0.6427
WMP17	0.761	0.6607	0.6642	0.6664	0.6675	0.6175	0.6357	0.6008	0.6346
WMP19	0.834	0.5160	0.5503	0.5534	0.5575	0.5578	0.5536	0.5234	0.5358
WMP21	0.908	0.3830	0.4371	0.4765	0.4426	0.4948	0.4696	0.3982	0.4510
WMP23	0.949	0.3802	0.4154	0.4406	0.4785	0.4649	0.4409	0.3611	0.4116
WMP25	0.990	0.3240	0.3586	0.3911	0.4162	0.4109	0.3729	0.3087	0.3371
WMP27	1.058	0.3448	0.3827	0.4036	0.4433	0.4459	0.4025	0.3513	0.3992
WDS1	3.842	0.2949	0.3545	0.3844	0.4099	0.3971	0.3797	0.2717	0.3466
WDS2	-0.319	0.3986	0.4675	0.4899	0.5115	0.5131	0.4890	0.3974	0.4896
WDS4	-8.466	0.4859	0.5160	0.5317	0.5463	0.5561	0.5264	0.4775	0.5090
WDS5	-12.635	0.4851	0.5000	0.5070	0.5228	0.5436	0.5107	0.4944	0.5073
WDS6	-16.804	0.4454	0.4630	0.4742	0.5009	0.5104	0.4742	0.4696	0.4725
WDS7	-20.781	0.3940	0.4158	0.4347	0.4774	0.4812	0.4311	0.4220	0.4303
WDS8	-24.854	0.2607	0.2779	0.2895	0.3040	0.3158	0.2894	0.2947	0.2922
WDS9	-28.975	0.3513	0.3804	0.3991	0.4225	0.4505	0.3920	0.3891	0.3892
WDS10	-33.096	0.3664	0.4047	0.4239	0.4456	0.4721	0.4105	0.4549	0.4179
WDS11	-37.313	0.4508	0.4920	0.5031	0.5138	0.5391	0.4826	0.5255	0.4977
WDS12	-41.290	0.5169	0.5471	0.5555	0.5688	0.5834	0.5503	0.5581	0.5546
WDS13	-45.507	0.5253	0.5522	0.5593	0.5720	0.5843	0.5549	0.5620	0.5609
WDS14	-49.533	0.5073	0.5304	0.5374	0.5500	0.5635	0.5281	0.5457	0.5383
PS10	0.128	1.0452	1.0589	1.0527	1.0541	1.0670	1.0591	1.0553	1.0542
PS1	0.180	1.0414	1.0546	1.0488	1.0494	1.0621	1.0549	1.0511	1.0504
PS11	0.233	1.0358	1.0493	1.0435	1.0444	1.0577	1.0495	1.0460	1.0458
PS2	0.283	1.0322	1.0453	1.0387	1.0381	1.0502	1.0426	1.0384	1.0359
PS12	0.333	1.0274	1.0406	1.0339	1.0337	1.0477	1.0395	1.0353	1.0340
PS3	0.378	1.0243	1.0371	1.0318	1.0328	1.0453	1.0381	1.0346	1.0340
PS13	0.421	1.0181	1.0312	1.0248	1.0239	1.0370	1.0292	1.0247	1.0226
PS4	0.465	1.0143	1.0268	1.0210	1.0219	1.0346	1.0272	1.0238	1.0229
PS5	0.550	0.9916	1.0037	0.9983	0.9995	1.0121	1.0048	1.0010	1.0000
PS15	0.590	0.9794	0.9921	0.9864	0.9873	0.9989	0.9918	0.9884	0.9879
PS6	0.633	0.9643	0.9765	0.9715	0.9720	0.9838	0.9769	0.9736	0.9728
PS16	0.673	0.9465	0.9587	0.9531	0.9548	0.9660	0.9592	0.9558	0.9542
PS7	0.715	-0.1299	-0.1155	-0.1166	-0.1314	-0.1410	-0.1493	-0.1535	-0.1538
PS17	0.745	0.9037	0.9151	0.9123	0.9110	0.9212	0.9152	0.9139	0.9113
PS8	0.778	0.8780	0.8889	0.8844	0.8856	0.8967	0.8903	0.8881	0.8865
PS18	0.808	0.8534	0.8653	0.8594	0.8597	0.8727	0.8656	0.8627	0.8620
PS9	0.838	0.8221	0.8307	0.8238	0.8270	0.8377	0.8307	0.8281	0.8276
SSLE	0.000	1.0003	1.0124	1.0097	1.0158	1.0213	1.0158	1.0145	1.0094
SS10	0.245	0.6965	0.7040	0.7010	0.7022	0.7109	0.7047	0.7037	0.7024
SS1	0.318	0.7120	0.7053	0.3191	-0.1703	0.5743	0.5379	0.5488	0.4971
SS11	0.381	0.5248	0.5310	0.5283	0.5300	0.5350	0.5303	0.5295	0.5282
SS2	0.433	0.4747	0.4815	0.4775	0.4768	0.4854	0.4796	0.4773	0.4757
SS12	0.475	0.5009	0.5072	0.5043	0.5067	0.5207	0.5086	0.5072	0.5042
SS3	0.510	0.4980	0.5144	0.5223	0.5229	0.5529	0.5322	0.5247	0.5131
SS13	0.548	0.4736	0.4808	0.4841	0.4872	0.5290	0.4905	0.4885	0.4806
SS4	0.585	0.4142	0.4222	0.4275	0.4282	0.4902	0.4371	0.4293	0.4218
SS14	0.622	0.3418	0.3470	0.3547	0.3663	0.4557	0.3659	0.3672	0.3508
SS5	0.660	0.3001	0.3120	0.3400	0.3343	0.4643	0.3571	0.3392	0.3128
SS15	0.695	0.2614	0.2701	0.3119	0.3442	0.4849	0.3391	0.3459	0.2970

Tapping Point	X/chord	Test 230399m	Test 230399n	Test 230399q	Test 230399t	Test 290399n	Test 290399o	Test 290399p	Test 290399r
SS6	0.730	0.2267	0.2809	0.3644	0.3386	0.4882	0.3883	0.3369	0.2679
SS16	0.765	0.2247	0.2661	0.3704	0.4077	0.4928	0.4025	0.3999	0.3029
SS17	0.825	0.2569	0.3334	0.4226	0.4369	0.4806	0.4403	0.4275	0.3526
SS8	0.850	0.2738	0.3647	0.4196	0.4404	0.4720	0.4313	0.4307	0.3439
SS18	0.876	0.2942	0.3775	0.4282	0.4313	0.4599	0.4393	0.4229	0.3750
SS9	0.900	0.3280	0.3763	0.4132	0.4376	0.4539	0.4244	0.4322	0.3909

Table D.5g: Pressure readings (bar) at individual tapping points for steam dosed with 4 ppm ammonia contd.

Tapping Point	X/chord	Test 140499f	Test 140499j	Test 160499c	Test 160499d	Test 160499f	Test 190499e	Test 190499f	Test 160399y
WMP2	-0.350	0.9983	1.0032	1.0319	1.0170	1.0211	1.0238	1.0124	1.0125
WMP3	-0.137	0.9978	1.0016	1.0337	1.0210	1.0246	1.0244	1.0139	1.0158
WMP7	0.300	0.9628	0.9674	1.0012	0.9855	0.9885	0.9916	0.9793	0.9807
WMP11	0.446	0.8996	0.9033	0.9270	0.9125	0.9156	0.8349	0.8324	0.9080
WMP14	0.570	0.7789	0.7806	0.8062	0.7957	0.7956	0.7960	0.7900	0.7890
WMP16	0.648	0.6658	0.6537	0.6841	0.6786	0.5933	0.6748	0.6715	0.6542
WMP17	0.761	0.5829	0.5849	0.7031	0.7007	0.6829	0.5957	0.5906	0.6658
WMP19	0.834	0.5369	0.5223	0.6056	0.6007	0.5742	0.4168	0.4112	0.5170
WMP21	0.908	0.4113	0.3853	0.5587	0.5579	0.5035	0.3148	0.3029	0.3552
WMP23	0.949	0.3958	0.3857	0.5743	0.5691	0.5137	0.3143	0.3083	0.2717
WMP25	0.990	0.3302	0.3178	0.5375	0.5339	0.4477	0.2708	0.2639	0.2041
WMP27	1.058	0.3566	0.3556	0.5740	0.5704	0.4760	0.2988	0.2944	0.2228
WDS1	3.842	0.3111	0.3004	0.5620	0.5592	0.4502	0.2553	0.2600	0.2027
WDS2	-0.319	0.4322	0.4087	0.6124	0.6074	0.5409	0.2866	0.2597	0.2041
WDS4	-8.466	0.4975	0.4883	0.6215	0.6177	0.5675	0.3897	0.3880	0.3731
WDS5	-12.635	0.4907	0.4908	0.6144	0.6111	0.5524	0.4100	0.4071	0.3645
WDS6	-16.804	0.4511	0.4523	0.6020	0.5990	0.5272	0.3971	0.3894	0.3458
WDS7	-20.781	0.3995	0.4006	0.5994	0.5964	0.4997	0.3706	0.3623	0.3119
WDS8	-24.854	0.2711	0.2707	0.4027	0.4039	0.3134	0.2657	0.2594	0.2203
WDS9	-28.975	0.3591	0.3560	0.5985	0.5970	0.4385	0.3356	0.3237	0.2571
WDS10	-33.096	0.3775	0.3755	0.6154	0.6124	0.4594	0.3416	0.3335	0.3298
WDS11	-37.313	0.4612	0.4655	0.6316	0.6292	0.5158	0.3859	0.3700	0.3785
WDS12	-41.290	0.5276	0.5266	0.6407	0.6378	0.5731	0.4366	0.4253	0.4099
WDS13	-45.507	0.5390	0.5350	0.6366	0.6326	0.5763	0.4579	0.4455	0.4553
WDS14	-49.533	0.5185	0.5141	0.6236	0.6202	0.5479	0.4601	0.4415	0.4805
PS10	0.128	1.0521	1.0570	1.0902	1.0742	1.0777	1.0921	1.0802	1.0665
PS1	0.180	1.0454	1.0512	1.0847	1.0702	1.0747	1.0869	1.0747	1.0623
PS11	0.233	1.0424	1.0484	1.0813	1.0652	1.0679	1.0864	1.0730	1.0572
PS2	0.283	1.0347	1.0416	1.0740	1.0594	1.0623	1.0742	1.0616	1.0522
PS12	0.333	1.0317	1.0372	1.0729	1.0563	1.0599	1.0713	1.0588	1.0462
PS3	0.378	1.0294	1.0352	1.0679	1.0532	1.0566	1.0691	1.0577	1.0461
PS13	0.421	1.0180	1.0238	1.0602	1.0446	1.0483	1.0577	1.0456	1.0377
PS4	0.465	1.0166	1.0221	1.0562	1.0416	1.0451	1.0577	1.0447	1.0333
PS5	0.550	0.9985	1.0035	1.0340	1.0189	1.0230	1.0368	1.0261	1.0109
PS15	0.590	0.9824	0.9887	1.0214	1.0064	1.0099	1.0235	1.0117	0.9996
PS6	0.633	0.9681	0.9734	1.0076	0.9919	0.9956	1.0080	0.9964	0.9843
PS16	0.673	0.9480	0.9538	0.9883	0.9724	0.9748	0.9865	0.9757	0.9655
PS7	0.715	0.9302	0.9364	-0.1180	-0.1365	-0.1323	0.9662	0.9552	-0.1456
PS17	0.745	0.9069	0.9121	0.9437	0.9302	0.9331	0.9438	0.9335	0.9219
PS8	0.778	0.8795	0.8853	0.9207	0.9053	0.9088	0.9077	0.8971	0.8975
PS18	0.808	0.8535	0.8584	0.8922	0.8787	0.8827	0.8900	0.8797	0.8722

Tapping Point	X/chord	Test 140499f	Test 140499j	Test 160499c	Test 160499d	Test 160499f	Test 190499e	Test 190499f	Test 160399y
PS9	0.838	0.8232	0.8280	0.8603	0.8471	0.8484	0.8555	0.8468	0.8382
SSLE	0.000	1.0072	1.0096	1.0505	1.0326	1.0381	1.0482	1.0361	1.0265
SS10	0.245	0.7006	0.7057	0.7317	0.7231	0.7200	0.7314	0.7248	0.7164
SS1	0.318	0.0529	0.1621	0.3680	0.3841	0.2616	-0.3238	0.4554	0.3575
SS11	0.381	0.5283	0.5324	0.5532	0.5445	0.5427	0.5469	0.5426	0.5359
SS2	0.433	0.4781	0.4788	0.5152	0.4982	0.4988	0.4486	0.4438	0.4799
SS12	0.475	0.5034	0.5059	0.5770	0.5697	0.5248	0.4483	0.4436	0.5078
SS3	0.510	0.5062	0.5057	0.5969	0.5923	0.5457	0.4374	0.4325	0.5008
SS13	0.548	0.4807	0.4823	0.6001	0.5922	0.5105	0.4001	0.3952	0.4886
SS4	0.585	0.4196	0.4202	0.5887	0.5801	0.4564	0.3553	0.3511	0.4301
SS14	0.622	0.3483	0.3490	0.5752	0.5669	0.4060	0.2990	0.2940	0.3516
SS5	0.660	0.3099	0.3097	0.5898	0.5805	0.4181	0.2822	0.2765	0.3098
SS15	0.695	0.2773	0.2726	0.5863	0.5747	0.4537	0.2728	0.2682	0.2717
SS6	0.730	0.2420	0.2357	0.5847	0.5697	0.4836	0.3182	0.2462	0.2348
SS16	0.765	0.2647	0.2506	0.5805	0.5654	0.4982	0.3555	0.2387	0.2538
SS17	0.825	0.3013	0.2853	0.5710	0.5679	0.4872	0.3346	0.2445	0.2598
SS8	0.850	0.2943	0.2867	0.5630	0.5618	0.4768	0.3201	0.2454	0.2623
SS18	0.876	0.3321	0.3205	0.5525	0.5558	0.4602	0.3102	0.2644	0.2565
SS9	0.900	0.3361	0.3566	0.5452	0.5514	0.4514	0.2989	0.2610	0.2559

Table D.5h: Pressure readings (bar) at individual tapping points for steam dosed with 4 ppm ammonia contd.

Tapping Point	X/chord	Test 160399z	Test 190399e	Test 260399k	Test 260399n	Test 260399o	Test 290399i	Test 290399j	Test 230399f
WMP2	-0.350	1.0178	1.0176	0.9985	1.0079	0.9995	1.0123	1.0055	1.0102
WMP3	-0.137	1.0196	1.0212	0.9998	1.0094	1.0015	1.0163	1.0104	1.0117
WMP7	0.300	0.9832	0.9880	0.9649	0.9749	0.9658	0.9803	0.9759	0.9775
WMP11	0.446	0.9120	0.9131	0.8921	0.9012	0.8927	0.9042	0.8977	0.9044
WMP14	0.570	0.7905	0.7953	0.7796	0.7862	0.7795	0.7922	0.7850	0.7880
WMP16	0.648	0.6638	0.4539	0.5644	0.6694	0.6675	0.6645	0.6598	0.4485
WMP17	0.761	0.6685	0.6341	0.6629	0.6570	0.6442	0.6461	0.6472	0.6659
WMP19	0.834	0.5122	0.5268	0.5022	0.5154	0.5121	0.5223	0.5185	0.5137
WMP21	0.908	0.3554	0.3591	0.3496	0.3525	0.3502	0.3549	0.3516	0.3584
WMP23	0.949	0.2744	0.2819	0.2684	0.2748	0.2682	0.2736	0.2669	0.2753
WMP25	0.990	0.2031	0.2895	0.2143	0.2264	0.2168	0.2170	0.2022	0.2421
WMP27	1.058	0.2256	0.2144	0.2116	0.2177	0.2153	0.2341	0.2043	0.2230
WDS1	3.842	0.2038	0.2308	0.1991	0.2048	0.2023	0.2104	0.1964	0.2093
WDS2	-0.319	0.2053	0.2069	0.1914	0.1941	0.1923	0.2293	0.1870	0.1961
WDS4	-8.466	0.3745	0.3721	0.3591	0.3712	0.3640	0.3866	0.3604	0.3699
WDS5	-12.635	0.3697	0.3593	0.3439	0.3642	0.3529	0.3794	0.3369	0.3494
WDS6	-16.804	0.3498	0.3393	0.3316	0.3446	0.3376	0.3569	0.3175	0.3278
WDS7	-20.781	0.3152	0.3020	0.2995	0.3070	0.3028	0.3160	0.2849	0.2972
WDS8	-24.854	0.2248	0.2066	0.2127	0.2167	0.2131	0.2140	0.2038	0.2088
WDS9	-28.975	0.2760	0.2293	0.2298	0.2474	0.2312	0.2409	0.2174	0.2393
WDS10	-33.096	0.3430	0.2131	0.2290	0.2983	0.2494	0.2873	0.2066	0.2261
WDS11	-37.313	0.3774	0.2488	0.3306	0.3314	0.3409	0.3627	0.2359	0.3130
WDS12	-41.290	0.4093	0.3513	0.3781	0.3745	0.3833	0.4053	0.3353	0.3795
WDS13	-45.507	0.4546	0.3908	0.4249	0.4286	0.4332	0.4530	0.3880	0.4288
WDS14	-49.533	0.4790	0.3828	0.4496	0.4532	0.4582	0.4744	0.3724	0.4355
PS10	0.128	1.0714	1.0726	1.0557	1.0629	1.0558	1.0668	1.0601	1.0621
PS1	0.180	1.0678	1.0678	1.0515	1.0593	1.0520	1.0618	1.0562	1.0580
PS11	0.233	1.0621	1.0611	1.0459	1.0558	1.0458	1.0551	1.0511	1.0515

Tapping Point	X/chord	Test 160399z	Test 190399e	Test 260399k	Test 260399n	Test 260399o	Test 290399i	Test 290399j	Test 230399f
PS2	0.283	1.0574	1.0641	1.0430	1.0505	1.0434	1.0517	1.0477	1.0475
PS12	0.333	1.0509	1.0563	1.0380	1.0444	1.0375	1.0483	1.0428	1.0447
PS3	0.378	1.0503	1.0499	1.0357	1.0416	1.0345	1.0454	1.0382	1.0400
PS13	0.421	1.0422	1.0502	1.0300	1.0359	1.0285	1.0382	1.0333	1.0337
PS4	0.465	1.0386	1.0400	1.0238	1.0313	1.0241	1.0343	1.0281	1.0296
PS5	0.550	1.0162	1.0169	1.0019	1.0084	1.0014	1.0125	1.0059	1.0070
PS15	0.590	1.0046	1.0047	0.9890	0.9963	0.9900	0.9984	0.9931	0.9942
PS6	0.633	0.9891	0.9896	0.9749	0.9815	0.9743	0.9846	0.9778	0.9787
PS16	0.673	0.9703	0.9707	0.9549	0.9624	0.9556	0.9655	0.9589	0.9610
PS7	0.715	-0.1404	-0.1343	-0.1421	-0.1311	-0.1413	-0.1436	-0.1498	-0.1132
PS17	0.745	0.9264	0.9275	0.9121	0.9193	0.9122	0.9226	0.9156	0.9176
PS8	0.778	0.9009	0.9024	0.8878	0.8945	0.8879	0.8976	0.8926	0.8911
PS18	0.808	0.8762	0.8753	0.8627	0.8687	0.8621	0.8721	0.8661	0.8673
PS9	0.838	0.8425	0.8442	0.8302	0.8366	0.8294	0.8383	0.8345	0.8341
SSLE	0.000	1.0298	1.0298	1.0134	1.0227	1.0159	1.0266	1.0187	1.0197
SS10	0.245	0.7195	0.7148	0.7091	0.7147	0.7093	0.7124	0.7101	0.7065
SS1	0.318	0.1205	-0.1703	-0.3037	-0.2913	-0.3223	0.6198	0.5565	-0.0645
SS11	0.381	0.5382	0.5404	0.5295	0.5363	0.5310	0.5343	0.5317	0.5339
SS2	0.433	0.4759	0.4980	0.4670	0.4818	0.4713	0.4928	0.4907	0.4854
SS12	0.475	0.5073	0.5199	0.4967	0.5089	0.5022	0.5166	0.5130	0.5098
SS3	0.510	0.4977	0.5108	0.4856	0.4996	0.4914	0.5143	0.5109	0.5052
SS13	0.548	0.4910	0.4913	0.4750	0.4876	0.4842	0.4853	0.4825	0.4834
SS4	0.585	0.4345	0.4269	0.4283	0.4276	0.4260	0.4235	0.4220	0.4212
SS14	0.622	0.3555	0.3610	0.3526	0.3509	0.3504	0.3494	0.3477	0.3501
SS5	0.660	0.3133	0.3081	0.3107	0.3077	0.3070	0.3071	0.3057	0.3042
SS15	0.695	0.2762	0.2657	0.2673	0.2657	0.2650	0.2641	0.2628	0.2623
SS6	0.730	0.2388	0.2347	0.2332	0.2309	0.2295	0.2282	0.2294	0.2288
SS16	0.765	0.2575	0.1974	0.1981	0.1970	0.1969	0.2001	0.1975	0.1978
SS17	0.825	0.2651	0.1540	0.1797	0.1586	0.1590	0.1872	0.1540	0.2144
SS8	0.850	0.2644	0.1410	0.1604	0.1423	0.1448	0.1785	0.1403	0.2052
SS18	0.876	0.2698	0.1495	0.2162	0.1818	0.1814	0.2257	0.1476	0.2301
SS9	0.900	0.2641	0.1509	0.2118	0.1714	0.1717	0.2293	0.1498	0.2317

Table D.5i: Pressure readings (bar) at individual tapping points for steam dosed with 4 ppm ammonia contd.

Tapping Point	X/chord	Test 230399g	Test 230399l	Test 230399o	Test 260399p	Test 260399q	Test 140499c	Test 140499d	Test 140499g
WMP2	-0.350	1.0144	1.0060	1.2549	1.0096	1.0060	0.9956	0.9981	1.0130
WMP3	-0.137	1.0144	1.0090	1.2567	1.0116	1.0078	0.9942	0.9978	1.0117
WMP7	0.300	0.9809	0.9733	1.2114	0.9766	0.9731	0.9618	0.9633	0.9765
WMP11	0.446	0.9087	0.9001	1.1242	0.9042	0.9005	0.8985	0.8998	0.9132
WMP14	0.570	0.7924	0.7869	0.9854	0.7937	0.7908	0.7767	0.7786	0.7905
WMP16	0.648	0.4525	0.6551	0.8274	0.6678	0.6608	0.6773	0.6735	0.6690
WMP17	0.761	0.6695	0.6645	0.8114	0.6590	0.6529	0.5810	0.5824	0.5906
WMP19	0.834	0.5174	0.5018	0.6583	0.5121	0.5127	0.5029	0.5016	0.5117
WMP21	0.908	0.3584	0.3571	0.4497	0.3588	0.3571	0.3583	0.3573	0.3636
WMP23	0.949	0.2850	0.2707	0.3471	0.2780	0.2770	0.3021	0.2711	0.2799
WMP25	0.990	0.2395	0.2250	0.2872	0.2178	0.2089	0.2456	0.2137	0.2174
WMP27	1.058	0.2235	0.2085	0.2825	0.2168	0.2102	0.2386	0.2127	0.2276
WDS1	3.842	0.2078	0.2025	0.2561	0.2048	0.2026	0.2105	0.1948	0.2004
WDS2	-0.319	0.2004	0.1854	0.2433	0.1896	0.1841	0.2127	0.1895	0.1946
WDS4	-8.466	0.3765	0.3479	0.4661	0.3709	0.3602	0.3974	0.3542	0.3927

Tapping Point	X/chord	Test 230399g	Test 230399l	Test 230399o	Test 260399p	Test 260399q	Test 140499c	Test 140499d	Test 140499g
WDS5	-12.635	0.3593	0.3208	0.4490	0.3449	0.3297	0.3943	0.3249	0.3825
WDS6	-16.804	0.3372	0.2957	0.4291	0.3278	0.3106	0.3737	0.3006	0.3647
WDS7	-20.781	0.3045	0.2672	0.3838	0.2999	0.2809	0.3379	0.2721	0.3280
WDS8	-24.854	0.2093	0.1861	0.2591	0.2143	0.1986	0.2354	0.1973	0.2316
WDS9	-28.975	0.2411	0.2150	0.3034	0.2509	0.2254	0.2783	0.2130	0.2786
WDS10	-33.096	0.2271	0.2965	0.3429	0.2858	0.2499	0.2836	0.2148	0.3613
WDS11	-37.313	0.2767	0.3493	0.4539	0.3749	0.3420	0.3568	0.3035	0.4236
WDS12	-41.290	0.3688	0.3835	0.5026	0.4174	0.3873	0.4282	0.3575	0.4565
WDS13	-45.507	0.4196	0.4237	0.5616	0.4532	0.4358	0.4617	0.4166	0.4906
WDS14	-49.533	0.4148	0.4211	0.5841	0.4540	0.4398	0.4668	0.4156	0.5002
PS10	0.128	1.0664	1.0618	1.3180	1.0641	1.0610	1.0495	1.0523	1.0683
PS1	0.180	1.0621	1.0575	1.3138	1.0601	1.0565	1.0428	1.0460	1.0604
PS11	0.233	1.0561	1.0519	1.3067	1.0547	1.0506	1.0399	1.0428	1.0578
PS2	0.283	1.0516	1.0477	1.2977	1.0513	1.0480	1.0317	1.0348	1.0497
PS12	0.333	1.0488	1.0437	1.2958	1.0452	1.0414	1.0298	1.0325	1.0470
PS3	0.378	1.0447	1.0399	1.2922	1.0427	1.0386	1.0279	1.0303	1.0442
PS13	0.421	1.0371	1.0339	1.2794	1.0370	1.0335	1.0160	1.0182	1.0325
PS4	0.465	1.0341	1.0292	1.2788	1.0318	1.0279	1.0144	1.0170	1.0316
PS5	0.550	1.0114	1.0065	1.2516	1.0093	1.0057	0.9964	0.9991	1.0128
PS15	0.590	0.9986	0.9954	1.2360	0.9969	0.9936	0.9795	0.9823	0.9971
PS6	0.633	0.9832	0.9792	1.2175	0.9821	0.9799	0.9655	0.9680	0.9823
PS16	0.673	0.9647	0.9614	1.1937	0.9626	0.9607	0.9459	0.9482	0.9626
PS7	0.715	-0.1098	-0.1129	0.1584	-0.1065	-0.1069	0.9264	0.9297	0.9440
PS17	0.745	0.9223	0.9185	1.1412	0.9202	0.9165	0.9041	0.9066	0.9210
PS8	0.778	0.8956	0.8910	1.1089	0.8949	0.8910	0.8779	0.8804	0.8928
PS18	0.808	0.8670	0.8660	1.0776	0.8699	0.8664	0.8530	0.8551	0.8658
PS9	0.838	0.8379	0.8336	1.0373	0.8373	0.8340	0.8214	0.8218	0.8357
SSLE	0.000	1.0227	1.0180	1.2687	1.0240	1.0163	1.0032	1.0044	1.0184
SS10	0.245	0.7098	0.7066	0.8792	0.7082	0.7043	0.6981	0.7002	0.7106
SS1	0.318	0.0966	-0.0302	0.7255	0.0941	0.1929	-0.1129	0.0086	-0.5431
SS11	0.381	0.5357	0.5314	0.6647	0.5348	0.5307	0.5295	0.5291	0.5369
SS2	0.433	0.4866	0.4832	0.6153	0.4876	0.4844	0.4772	0.4778	0.4845
SS12	0.475	0.5120	0.5081	0.6356	0.5103	0.5076	0.5036	0.5046	0.5113
SS3	0.510	0.5085	0.5054	0.6373	0.5055	0.5056	0.5025	0.5038	0.5104
SS13	0.548	0.4841	0.4791	0.5980	0.4814	0.4799	0.4779	0.4784	0.4838
SS4	0.585	0.4222	0.4197	0.5231	0.4206	0.4194	0.4152	0.4157	0.4228
SS14	0.622	0.3508	0.3458	0.4314	0.3470	0.3442	0.3442	0.3443	0.3493
SS5	0.660	0.3051	0.3032	0.3778	0.3034	0.3020	0.3050	0.3053	0.3098
SS15	0.695	0.2627	0.2604	0.3256	0.2627	0.2616	0.2615	0.2613	0.2652
SS6	0.730	0.2276	0.2270	0.2823	0.2290	0.2275	0.2247	0.2251	0.2278
SS16	0.765	0.1955	0.1944	0.2508	0.1962	0.1992	0.1984	0.1942	0.1964
SS17	0.825	0.1570	0.1592	0.2350	0.1839	0.2069	0.2122	0.1669	0.1602
SS8	0.850	0.1486	0.1584	0.2367	0.1760	0.1952	0.2016	0.1629	0.1603
SS18	0.876	0.1671	0.1639	0.2468	0.2047	0.2170	0.2243	0.1789	0.1620
SS9	0.900	0.1650	0.1631	0.2467	0.2055	0.2157	0.2232	0.1749	0.1614

Table D.5j: Pressure readings (bar) at individual tapping points for steam dosed with 4 ppm ammonia contd.

Tapping Point	X/chord	Test 140499h	Test 160499a	Test 160499b
WMP2	-0.350	0.9972	1.0007	1.0127
WMP3	-0.137	0.9961	1.0005	1.0119
WMP7	0.300	0.9613	0.9670	0.9788
WMP11	0.446	0.8986	0.8991	0.9118
WMP14	0.570	0.7788	0.7801	0.7900
WMP16	0.648	0.6285	0.6551	0.6639
WMP17	0.761	0.5811	0.5823	0.5906
WMP19	0.834	0.5030	0.5010	0.5086
WMP21	0.908	0.3580	0.3606	0.3649
WMP23	0.949	0.2720	0.2745	0.3006
WMP25	0.990	0.2013	0.2568	0.2538
WMP27	1.058	0.2118	0.2122	0.2392
WDS1	3.842	0.1949	0.2165	0.2107
WDS2	-0.319	0.1896	0.1958	0.2079
WDS4	-8.466	0.3537	0.3549	0.4064
WDS5	-12.635	0.3224	0.3303	0.4067
WDS6	-16.804	0.2973	0.3079	0.3894
WDS7	-20.781	0.2701	0.2786	0.3509
WDS8	-24.854	0.1947	0.2030	0.2454
WDS9	-28.975	0.2092	0.2223	0.2928
WDS10	-33.096	0.2378	0.2490	0.3138
WDS11	-37.313	0.2993	0.3426	0.4018
WDS12	-41.290	0.3517	0.3828	0.4611
WDS13	-45.507	0.4107	0.4303	0.4917
WDS14	-49.533	0.4180	0.4362	0.4959
PS10	0.128	1.0496	1.0549	1.0687
PS1	0.180	1.0432	1.0483	1.0622
PS11	0.233	1.0408	1.0459	1.0585
PS2	0.283	1.0331	1.0403	1.0527
PS12	0.333	1.0296	1.0367	1.0495
PS3	0.378	1.0274	1.0312	1.0452
PS13	0.421	1.0159	1.0243	1.0375
PS4	0.465	1.0148	1.0198	1.0331
PS5	0.550	0.9960	1.0004	1.0139
PS15	0.590	0.9809	0.9861	0.9991
PS6	0.633	0.9663	0.9718	0.9845
PS16	0.673	0.9469	0.9517	0.9639
PS7	0.715	0.9291	0.9293	0.9417
PS17	0.745	0.9056	0.9087	0.9216
PS8	0.778	0.8793	0.8787	0.8910
PS18	0.808	0.8173	0.8578	0.8690
PS9	0.838	0.8212	0.8089	0.8366
SSLE	0.000	1.0037	1.0078	1.0253
SS10	0.245	0.7008	0.7043	0.7149
SS1	0.318	0.2963	-0.3930	0.2836
SS11	0.381	0.5290	0.5338	0.5399
SS2	0.433	0.4765	0.4785	0.4862
SS12	0.475	0.5023	0.5077	0.5140
SS3	0.510	0.5020	0.5031	0.5099
SS13	0.548	0.4770	0.4800	0.4845
SS4	0.585	0.4164	0.4144	0.4215
SS14	0.622	0.3452	0.3521	0.3517
SS5	0.660	0.3061	0.3074	0.3123
SS15	0.695	0.2644	0.2634	0.2681

Tapping Point	X/chord	Test 140499h	Test 160499a	Test 160499b
SS6	0.730	0.2260	0.2286	0.2294
SS16	0.765	0.2178	0.1964	0.2152
SS17	0.825	0.2239	0.1758	0.2315
SS8	0.850	0.2198	0.1725	0.2278
SS18	0.876	0.2446	0.1973	0.2421
SS9	0.900	0.2413	0.2105	0.2472

D.3.3 Steam Dosed with 12 ppm Ammonia

Table D.6a: Pressure readings (bar) at individual tapping points for steam dosed with 12 ppm ammonia

Tapping Point	X/chord	Test 210499c	Test 210499d	Test 210499e	Test 210499s	Test 210499t	Test 210499u	Test 210499w	Test 210499x
WMP2	-0.350	1.0136	1.0140	1.0189	1.0160	1.0253	1.0175	1.0214	1.0188
WMP3	-0.137	1.0125	1.0122	1.0177	1.0172	1.0263	1.0159	1.0223	1.0184
WMP7	0.300	0.9816	0.9822	0.9869	0.9821	0.9902	0.9826	0.9868	0.9845
WMP11	0.446	0.8926	0.8942	0.8977	0.8955	0.9026	0.8960	0.8981	0.8950
WMP14	0.570	0.7897	0.7916	0.7932	0.7968	0.8015	0.7958	0.8008	0.7950
WMP16	0.648	0.6910	0.6912	0.6911	0.6840	0.6856	0.6729	0.6787	0.6756
WMP17	0.761	0.5955	0.5956	0.5999	0.5972	0.6014	0.5968	0.5990	0.5969
WMP19	0.834	0.5634	0.5554	0.5726	0.5357	0.5526	0.5415	0.5285	0.5358
WMP21	0.908	0.4585	0.4609	0.4669	0.4094	0.4301	0.4170	0.3882	0.3883
WMP23	0.949	0.4446	0.4247	0.4822	0.3778	0.4172	0.3914	0.3385	0.3820
WMP25	0.990	0.4059	0.3949	0.4304	0.3509	0.3726	0.3481	0.3055	0.3235
WMP27	1.058	0.4088	0.4143	0.4279	0.3686	0.4003	0.4038	0.3256	0.3593
WDS1	3.842	0.3853	0.3503	0.3965	0.2754	0.2979	0.2961	0.2680	0.2824
WDS2	-0.319	0.4871	0.4837	0.4957	0.4084	0.4388	0.4342	0.3826	0.4014
WDS4	-8.466	0.5269	0.5245	0.5494	0.4845	0.5236	0.5027	0.4627	0.4935
WDS5	-12.635	0.5159	0.5273	0.5291	0.5119	0.5274	0.5278	0.4848	0.5063
WDS6	-16.804	0.4813	0.4921	0.4978	0.4872	0.4894	0.4982	0.4686	0.4791
WDS7	-20.781	0.4309	0.4381	0.4558	0.4361	0.4367	0.4449	0.4269	0.4335
WDS8	-24.854	0.2935	0.3015	0.3041	0.3025	0.3004	0.3121	0.2983	0.2980
WDS9	-28.975	0.3925	0.4054	0.4075	0.4038	0.4058	0.4356	0.3965	0.4060
WDS10	-33.096	0.4006	0.4177	0.4245	0.4499	0.4269	0.4800	0.4966	0.4739
WDS11	-37.313	0.4481	0.4578	0.4794	0.5288	0.4924	0.5455	0.5427	0.5326
WDS12	-41.290	0.5176	0.5261	0.5407	0.5723	0.5613	0.5824	0.5651	0.5680
WDS13	-45.507	0.5307	0.5402	0.5519	0.5786	0.5687	0.5847	0.5743	0.5735
WDS14	-49.533	0.5105	0.5197	0.5277	0.5585	0.5452	0.5621	0.5657	0.5560
PS10	0.128	1.0716	1.0733	1.0811	1.0676	1.0766	1.0686	1.0752	1.0741
PS1	0.180	1.0649	1.0673	1.0743	1.0617	1.0707	1.0632	1.0695	1.0684
PS11	0.233	1.0619	1.0638	1.0714	1.0600	1.0689	1.0611	1.0682	1.0669
PS2	0.283	1.0563	1.0588	1.0650	1.0501	1.0588	1.0515	1.0579	1.0567
PS12	0.333	1.0542	1.0568	1.0635	1.0489	1.0576	1.0497	1.0560	1.0547
PS3	0.378	1.0481	1.0483	1.0566	1.0449	1.0533	1.0459	1.0522	1.0510
PS13	0.421	1.0404	1.0421	1.0492	1.0347	1.0434	1.0360	1.0425	1.0415
PS4	0.465	1.0363	1.0371	1.0447	1.0326	1.0415	1.0338	1.0402	1.0390
PS5	0.550	1.0179	1.0189	1.0266	1.0135	1.0218	1.0144	1.0205	1.0193
PS15	0.590	1.0017	1.0024	1.0104	0.9995	1.0084	1.0010	1.0076	1.0063
PS6	0.633	0.9872	0.9879	0.9954	0.9839	0.9923	0.9852	0.9913	0.9905
PS16	0.673	0.9661	0.9679	0.9746	0.9657	0.9738	0.9655	0.9714	0.9714
PS7	0.715	0.9439	0.9445	0.9509	0.9433	0.9508	0.9446	0.9495	0.9490

Tapping Point	X/chord	Test 210499c	Test 210499d	Test 210499e	Test 210499s	Test 210499t	Test 210499u	Test 210499w	Test 210499x
PS17	0.745	0.9243	0.9259	0.9325	0.9230	0.9292	0.9238	0.9288	0.9274
PS8	0.778	0.8962	0.8956	0.9045	0.8872	0.8956	0.8880	0.8942	0.8930
PS18	0.808	0.8720	0.8729	0.8781	0.8515	0.8755	0.8701	0.8761	0.8749
PS9	0.838	0.8372	0.8414	0.8459	0.8356	0.8449	0.8337	0.8425	0.8402
SSLE	0.000	1.0259	1.0266	1.0347	1.0215	1.0324	1.0219	1.0297	1.0283
SS10	0.245	0.7183	0.7200	0.7262	0.7118	0.7192	0.7139	0.7182	0.7180
SS1	0.318	0.2959	0.1527	0.0829	0.2202	0.1832	0.2737	0.3213	-0.3689
SS11	0.381	0.5413	0.5426	0.5466	0.5406	0.5446	0.5396	0.5446	0.4598
SS2	0.433	0.4956	0.4918	0.4874	0.4863	0.4920	0.4877	0.4905	0.4886
SS12	0.475	0.5230	0.5220	0.5212	0.5163	0.5224	0.5206	0.5179	0.5183
SS3	0.510	0.5372	0.5361	0.5289	0.5368	0.5411	0.5434	0.5280	0.5321
SS13	0.548	0.5005	0.5032	0.5069	0.5017	0.5040	0.5049	0.4953	0.4967
SS4	0.585	0.4408	0.4445	0.4454	0.4431	0.4464	0.4495	0.4337	0.4357
SS14	0.622	0.3819	0.3830	0.3856	0.3877	0.3880	0.3926	0.3683	0.3722
SS5	0.660	0.3634	0.3667	0.3619	0.3642	0.3665	0.3806	0.3293	0.3394
SS15	0.695	0.3360	0.3394	0.3419	0.3671	0.3703	0.3980	0.3232	0.3425
SS6	0.730	0.3474	0.3614	0.3283	0.3831	0.3744	0.4114	0.2998	0.3281
SS16	0.765	0.3746	0.3874	0.3780	0.4404	0.4365	0.4570	0.3594	0.3952
SS17	0.825	0.4576	0.4633	0.4597	0.4637	0.4688	0.4683	0.4112	0.4323
SS8	0.850	0.4575	0.4589	0.4726	0.4635	0.4740	0.4664	0.4137	0.4372
SS18	0.876	0.4605	0.4637	0.4652	0.4521	0.4596	0.4546	0.4178	0.4321
SS9	0.900	0.4468	0.4463	0.4623	0.4507	0.4594	0.4530	0.4283	0.4417

Table D.6b: Pressure readings (bar) at individual tapping points for steam dosed with 12 ppm ammonia contd.

Tapping Point	X/chord	Test 210499y	Test 210499f	Test 210499h	Test 210499j	Test 210499l	Test 210499o	Test 210499q	Test 210499r
WMP2	-0.350	1.0183	1.0165	1.0171	1.0241	1.0172	1.0121	1.0138	1.0137
WMP3	-0.137	1.0181	1.0146	1.0154	1.0232	1.0154	1.0101	1.0125	1.0112
WMP7	0.300	0.9838	0.9844	0.9834	0.9905	0.9828	0.9775	0.9790	0.9791
WMP11	0.446	0.8949	0.8947	0.8958	0.9029	0.8954	0.8915	0.8926	0.8924
WMP14	0.570	0.7960	0.7917	0.7944	0.8007	0.7929	0.7902	0.7918	0.7921
WMP16	0.648	0.6724	0.6852	0.6844	0.7023	0.6976	0.6828	0.6925	0.6886
WMP17	0.761	0.5968	0.5952	0.5964	0.6014	0.5950	0.5923	0.5935	0.5931
WMP19	0.834	0.5200	0.5231	0.5289	0.5300	0.5259	0.5158	0.5174	0.5161
WMP21	0.908	0.3746	0.3597	0.3592	0.3605	0.3592	0.3585	0.3581	0.3575
WMP23	0.949	0.3335	0.2972	0.2937	0.2770	0.2761	0.2717	0.2737	0.2724
WMP25	0.990	0.2736	0.2573	0.2440	0.2386	0.2218	0.2046	0.2026	0.2000
WMP27	1.058	0.3262	0.2423	0.2367	0.2175	0.2260	0.2196	0.2170	0.2159
WDS1	3.842	0.2509	0.2231	0.2127	0.2137	0.2043	0.1971	0.1968	0.1943
WDS2	-0.319	0.3697	0.2216	0.2149	0.1969	0.2191	0.1917	0.1914	0.1902
WDS4	-8.466	0.4513	0.3941	0.3944	0.3746	0.3772	0.3764	0.3647	0.3651
WDS5	-12.635	0.4773	0.3917	0.3898	0.3576	0.3662	0.3631	0.3403	0.3442
WDS6	-16.804	0.4635	0.3685	0.3679	0.3355	0.3471	0.3449	0.3240	0.3286
WDS7	-20.781	0.4264	0.3275	0.3289	0.2974	0.3118	0.3075	0.2951	0.2991
WDS8	-24.854	0.2967	0.2324	0.2311	0.2162	0.2200	0.2151	0.2143	0.2171
WDS9	-28.975	0.4072	0.2808	0.2807	0.2308	0.2375	0.2371	0.2328	0.2389
WDS10	-33.096	0.5097	0.2727	0.2681	0.2193	0.2671	0.2628	0.2493	0.2815
WDS11	-37.313	0.5469	0.3553	0.3589	0.2682	0.3486	0.3543	0.3420	0.3623
WDS12	-41.290	0.5681	0.4125	0.4248	0.3586	0.3906	0.3973	0.3863	0.4050
WDS13	-45.507	0.5776	0.4445	0.4578	0.4083	0.4440	0.4515	0.4390	0.4503

Tapping Point	X/chord	Test 210499y	Test 210499f	Test 210499h	Test 210499j	Test 210499l	Test 210499o	Test 210499q	Test 210499r
WDS14	-49.533	0.5688	0.4619	0.4760	0.4050	0.4670	0.4720	0.4540	0.4616
PS10	0.128	1.0739	1.0758	1.0769	1.0835	1.0743	1.0636	1.0653	1.0652
PS1	0.180	1.0679	1.0693	1.0698	1.0770	1.0683	1.0573	1.0589	1.0590
PS11	0.233	1.0679	1.0671	1.0667	1.0741	1.0653	1.0551	1.0570	1.0572
PS2	0.283	1.0565	1.0598	1.0600	1.0660	1.0579	1.0467	1.0483	1.0481
PS12	0.333	1.0544	1.0601	1.0588	1.0659	1.0564	1.0459	1.0473	1.0473
PS3	0.378	1.0505	1.0526	1.0521	1.0591	1.0502	1.0403	1.0424	1.0425
PS13	0.421	1.0413	1.0445	1.0442	1.0502	1.0419	1.0309	1.0325	1.0322
PS4	0.465	1.0383	1.0394	1.0409	1.0475	1.0394	1.0296	1.0303	1.0303
PS5	0.550	1.0188	1.0228	1.0214	1.0283	1.0197	1.0095	1.0107	1.0107
PS15	0.590	1.0066	1.0052	1.0057	1.0127	1.0045	0.9948	0.9968	0.9970
PS6	0.633	0.9898	0.9913	0.9903	0.9975	0.9891	0.9794	0.9808	0.9809
PS16	0.673	0.9703	0.9707	0.9707	0.9770	0.9695	0.9609	0.9612	0.9615
PS7	0.715	0.9485	0.9483	0.9475	0.9530	0.9458	0.9385	0.9405	0.9398
PS17	0.745	0.9270	0.9284	0.9282	0.9337	0.9261	0.9177	0.9190	0.9192
PS8	0.778	0.8924	0.8981	0.8952	0.9001	0.8921	0.8837	0.8854	0.8855
PS18	0.808	0.8740	0.8391	0.8771	0.8823	0.8739	0.8663	0.8689	0.8693
PS9	0.838	0.8417	0.8430	0.8421	0.8477	0.8404	0.8334	0.8346	0.8309
SSLE	0.000	1.0305	1.0314	1.0300	1.0384	1.0295	1.0192	1.0214	1.0224
SS10	0.245	0.7177	0.7217	0.7225	0.7229	0.7221	0.7098	0.7111	0.7109
SS1	0.318	-0.0908	0.3411	0.2505	0.4378	0.4483	0.3832	0.0311	-0.1208
SS11	0.381	0.5407	0.5450	0.5444	0.5480	0.5439	0.5380	0.5382	0.5388
SS2	0.433	0.4874	0.4932	0.4892	0.5003	0.4908	0.4857	0.4863	0.4858
SS12	0.475	0.5172	0.5214	0.5200	0.5268	0.5205	0.5145	0.5154	0.5152
SS3	0.510	0.5271	0.5103	0.5081	0.5208	0.5110	0.5096	0.5110	0.5109
SS13	0.548	0.4920	0.4923	0.4925	0.4951	0.4909	0.4831	0.4835	0.4834
SS4	0.585	0.4310	0.4298	0.4312	0.4324	0.4296	0.4224	0.4235	0.4236
SS14	0.622	0.3610	0.3608	0.3615	0.3633	0.3589	0.3525	0.3523	0.3523
SS5	0.660	0.3230	0.3145	0.3142	0.3163	0.3136	0.3084	0.3093	0.3091
SS15	0.695	0.3128	0.2697	0.2696	0.2706	0.2682	0.2655	0.2663	0.2660
SS6	0.730	0.2848	0.2282	0.2272	0.2303	0.2264	0.2242	0.2246	0.2239
SS16	0.765	0.3365	0.2015	0.2020	0.2028	0.2010	0.2196	0.2224	0.2251
SS17	0.825	0.3924	0.1588	0.1627	0.1611	0.1731	0.2461	0.2502	0.2524
SS8	0.850	0.3934	0.1494	0.1551	0.1512	0.1597	0.2460	0.2510	0.2540
SS18	0.876	0.4090	0.1548	0.1846	0.1564	0.2087	0.2541	0.2580	0.2594
SS9	0.900	0.4220	0.1557	0.1848	0.1578	0.1993	0.2536	0.2555	0.2569

Table D.6c: Pressure readings (bar) at individual tapping points for steam dosed with 12 ppm ammonia contd.

Tapping Point	X/chord	Test 210499ac	Test 210499af
WMP2	-0.350	1.0214	1.0200
WMP3	-0.137	1.0213	1.0206
WMP7	0.300	0.9868	0.9866
WMP11	0.446	0.8974	0.8944
WMP14	0.570	0.8007	0.7997
WMP16	0.648	0.6726	0.6676
WMP17	0.761	0.5993	0.5992
WMP19	0.834	0.5195	0.5186
WMP21	0.908	0.3650	0.3655
WMP23	0.949	0.2857	0.2896

Tapping Point	X/chord	Test 210499ac	Test 210499af
WMP25	0.990	0.2038	0.2050
WMP27	1.058	0.2419	0.2464
WDS1	3.842	0.2088	0.2110
WDS2	-0.319	0.2092	0.2150
WDS4	-8.466	0.3999	0.4008
WDS5	-12.635	0.3931	0.3932
WDS6	-16.804	0.3756	0.3746
WDS7	-20.781	0.3454	0.3444
WDS8	-24.854	0.2447	0.2419
WDS9	-28.975	0.3172	0.2993
WDS10	-33.096	0.4070	0.3687
WDS11	-37.313	0.4593	0.4414
WDS12	-41.290	0.4922	0.4757
WDS13	-45.507	0.5186	0.5063
WDS14	-49.533	0.5197	0.5178
PS10	0.128	1.0755	1.0757
PS1	0.180	1.0714	1.0706
PS11	0.233	1.0693	1.0689
PS2	0.283	1.0602	1.0588
PS12	0.333	1.0560	1.0549
PS3	0.378	1.0535	1.0530
PS13	0.421	1.0439	1.0431
PS4	0.465	1.0414	1.0410
PS5	0.550	1.0220	1.0214
PS15	0.590	1.0089	1.0083
PS6	0.633	0.9926	0.9923
PS16	0.673	0.9734	0.9727
PS7	0.715	0.9513	0.9516
PS17	0.745	0.9301	0.9299
PS8	0.778	0.8947	0.8957
PS18	0.808	0.8780	0.8789
PS9	0.838	0.8445	0.8447
SSLE	0.000	1.0337	1.0316
SS10	0.245	0.7170	0.7168
SS1	0.318	-0.0786	0.6452
SS11	0.381	0.5430	0.5421
SS2	0.433	0.4904	0.4903
SS12	0.475	0.5172	0.5174
SS3	0.510	0.5171	0.5174
SS13	0.548	0.4870	0.4854
SS4	0.585	0.4284	0.4276
SS14	0.622	0.3511	0.3505
SS5	0.660	0.3106	0.3092
SS15	0.695	0.2692	0.2669
SS6	0.730	0.2289	0.2266
SS16	0.765	0.2307	0.2001
SS17	0.825	0.2512	0.1729
SS8	0.850	0.2495	0.1781
SS18	0.876	0.2810	0.1746
SS9	0.900	0.2750	0.1744

Appendix E:

Data Acquisition Source Code

The data acquisition source code is attached on a CD-ROM. The source code is written in C++ and uses the wxWindows 2.2 (www.wxwindows.org) and NI-GPIB (www.ni.com) libraries. The source code can be compiled with either the Borland C++ 5.5 compiler or the Microsoft Visual C++ 6 compiler, but must be linked against the appropriate NI-GPIB library.

Borland make files, the wxWindows 2.2 source code and NI-GPIB libraries are included on the CD-ROM along with the free version of Borlands C++ compiler which was used to compile the project by the author.

Note that in order to function the code must be run on a PC which has a GPIB card installed and must be attached to an MDAS 7000 data acquisition unit.

References

Abbas, K. [1987]
"An Investigation of Viscous 2-D, 2-Phase Flows in Cascades of Steam Turbine Blading by the Time Marching Method"
Ph.D. Thesis, University of Birmingham

Abraham, F. F. [1974]
"Homogeneous Nucleation Theory"
Adv. Theor. Chem., Suppl. 1, Academic Press, New York

Adam, S and Schnurr G. H. [1997]
"Instabilities and Birfurcation in Non-Equilibrium in Two-Phase Flows"
J. Fluid Mech., vol. 348, pp 1-28

Aitken, J. [1881]
"On Dusts, Fog and Clouds"
Trans. Royal Society (Edinburgh), 30:337-368

Alty, T. and Mackay, C. A. [1935]
"The Accommodation and Evaporation of Coeffiecients of Water"
Proc. Royal Soc. (London), A 149: 104

Alubaidy, A. K. [1982]
"On the Supersonic Blade to Blade Two Phase Flow of Steam"
Ph.D. Thesis, University of Birmingham

Amelyushkin, V. N. [1989]
"Erosion on the Leading Edges of Steam Turbine Moving Blades"
Sov. Energy Tech. n3 pp 1-5

Andrews [1869]
"On the Continuity of the Gaseous and Liquid States of Matter"
Phil. Trans. Royal Society (London), no. 159, pg. 575

Araki, Ryoichiro, Kishimoto, Masaru, Yoshida and Koichi [1990]
"Behaviour of Titanium Blade to Erosion Phenomena caused by Water Droplets in Wet Steam"
Nippon Kikai, Gakhai Ronbun Shu, v56, n527

Armstrong, W. G. [1840]
"On the Electricity of a Jet of Steam Issuing from a Boiler"
Letters to M. Faraday, Phil. Mag. XVII, pp 370-374

Bakhtar, F., Ryley, D. J., Tubman, K. and Young, J. B. [1975]
"Nucleation studies in flowing high pressure expanding steam."
Proc. Instn. Mech. Engrs. 185

Bakhtar, F., Ghoneim, Z and Young, J. B. [1976]
"A Study of Nucleating and Wet Steam Flows in Turbines"
Proc. Inst. Mech. Engrs., 190:545-559

Bakhtar, F. and Young, J. B. [1978]
"A Study of Choking Conditions in the Flow of Wet Steam"
Proc. Institute of Mech. Engrs. Vol. 192, No. 21, pp. 237-242

Bakhtar, F. and Ghassemi, B. [1979)
"A Study of Nucleating and Wet Steam Flows in High Pressure Steam Turbines"
Inst. Mech. Engrs., Steam Turbines for the 1980's, Conf. Publ., C191/179, pp. 327-336

Bakhtar, F. and Piran, M. [1979]
"Thermodynamic Properties of Supercooled Steam"
Int. J. Heat & Fluid Flow, 1 (2):53-62

Bakhtar, F. and Tochai, M. T. M. [1980]
"An Investigation of Two-Dimensional Rows of Nucleating and Wet Steam by the Time-Marching Method"
Int. J. Heat & Fluid Flow, 2 (1):5-18

Bakhtar, F. and Heaton, A. V. [1981]
"A Theoretical Comparative Study of Wetness Problems in a Model and Full-Scale Turbine"
Aerothermodynamics of Steam Turbines, The Winter Annual Meeting, ASME, Washington D.C.

Bakhtar, F., Mouhandes, M. A. and Winterton, R. H. S., [1982]
"Corona Discharge in Steam"
J. of Electrostatics, Vol. 13, pp. 355-361

Bakhtar, F. and Alubaidy, A. K. [1984]
"On the Solution of Supersonic Blade-to-Blade Flows of Nucleating Steam by the Time Marching Method"
Inst. Mech. Engrs., Conf. on Comp. Methods in Turbomach., C82/84, pp. 101-111

Bakhtar, F. and Heaton, A. V. [1988]
"On the Dissimilarities in Wet Steam Behaviour in Model and Full-Scale Turbines"
Technology of Turbine Plant Operating with Wet Steam, BNES, London

Bakhtar, F. and Bamkole, R. O. [1989]
"An Examination of the Throughflow of Nucleating Steam in a Turbine Stage by a Time-Marching Method"
Proc. Inst. Mech. Engrs., 203: 233-243

Bakhtar, F. and Zidi, K. [1989]
"Nucleation Phenomena in Flowing High-Pressure Steam: Experimental Results"
Proc. Inst. Mech. Engrs., 203:195-200

Bakhtar, F. and Zidi, K. [1990]
"Nucleation Phenomena in Flowing High-Pressure Steam: Theoretical Analysis"
Proc. Inst. Mech. Engrs., 204:233-242

Bakhtar, F. and So, K. S. [1991]
"A Study of Nucleating Flow of Steam in a Cascade of Supersonic Blading by the Time Marching Method"
Int. J. Heat and Fluid Flow, 12 (1): 54-62

Bakhtar, F., Webb, R. A., Shojaee-Fard, M. H. and Siraj, M. A. [1991]
"An experimental facility for studies of nucleating and wet steam flows in turbine blading"
Proc. ImechE conf. on Turbomachinery, vol. 3, paper C423/003, pp. 191-199

Bakhtar, F., Ebrahimi, M. and Webb, R. A. [1995]
"On the Performance of a Cascade of Turbine Rotor Tip Section Blading in Nucleating Steam. Part 1: Surface Pressure Distributions"
Proc. Instn. Mech. Engrs. 209 Part C 115-124.

Bakhtar, F., Mashmoushy, M. and Buckley, J. R. [1997a]
"On the Performance of a Cascade of Turbine Rotor Tip Section Blading in Wet Steam. Part 1: Generation of Wet Steam of Prescribed Droplet Sizes"
Proc. Instn. Mech. Engrs. 211 Part C 519-529.

Bakhtar, F., Mashmoushy, M. and Jadayel, O. C. [1997b]
"On the Performance of a Cascade of Turbine Rotor Tip Section Blading in Wet Steam. Part 2: Surface Pressure Distributions"
Proc. Instn. Mech. Engrs. 211 Part C 531-540.

Bakhtar, F., Mashmoushy, M. and Jadayel, O. C. [1997c]
"On the Performance of a Cascade of Turbine Rotor Tip Section Blading in Wet Steam. Part 3: Wake Traverses"
Proc. Instn. Mech. Engrs. 211 Part C 639-648

Bakhar, F. and Henson, R. J. K. [1999]
"A Re-examination of the Effect of Impurities on Condensing Flows of Steam"
Proc. of Third International VGB/EPRI Conference, June 22-25, 1999, Freiburg

Bamkole, B. O. [1987]
"A Study of the Throughflow of Nucleating Steam by the Time-Marching Method"
Ph.D. Thesis, University of Birmingham

Band, W. [1939]
"Dissociation Treatment of Condensation of Water Vapour"
J. Chem. Phys., 7:324

Baumann, K. [1912]
"Some Recent Developments in Large Steam Turbine Practice"
J. Inst. Elec. Engrs., 48:768-877

Becker, R. and Doring, W. [1935]
"Kinetische Behandlung der Keimbildung in Ubersettigten Dampfen"
Ann. d. Phys. (Leipzig), 24:719-752

Bendemann, F. [1907]
"On the Flow of Water Vapour and Measurement of Steam Mass Flow"
Mitteilungen über Forschungsarbeiten (Berlin), no. 37

Benson, G. C. and Shuttleworth, R. [1951]
"The Surface Energy of Small Nuclei"
J. Chem. Phys., 19:130-131

Bijl, A. [1938]
"Discontinuities in the Energy and Specific Heats"
Ph.D. Thesis, University of Leiden, Germany

Binnie, A. M. and Woods, M. W. [1938]
"The Pressure Distribution in a Convergent-Divergent Steam Nozzle"
Proc. Inst. Mech. Engrs, 138:229-266

Binnie, A. M. and Green, J. R. [1943]
"An Electrical Detector of Condensation in High-Velocity Steam"
Proc. Royal Society (London), A 181:134-154

Bohn, D. and Holzenthal, K. [1997]
"Measurement of the Wetness Fraction and Droplet Size Distribution in a Condensation Turbine"
Proc. 2nd European Conference on Turbomachinery, Antwerp, Belgium, pp 55-63

Borenstein, S. W., Kelly, J. and Boone, D. [1990]
"Evaluation of Coatings to Reduce Erosion Related Problems"
ASME Power Div. Pub., Int. Joint Power Generation Conf. pp 15-21

Byers, H. R., [1965]
"Elements of Cloud Physics"
The University of Chicago Press

Cai, X. S., Wang, N. N. and Wei, J. M. [1994]
"The Development of an Optical Measurement Technique for Wet Steam Turbines"
Proc. of 3rd Int. Symposium on Multiphase Flow and Heat Transfer, Xian, China, p 432

Callender, H. L. [1915]
"On the Steady Flow of Steam through a Nozzle or Throttle"
Proc. Inst. Mech. Engrs., pp. 53-77

Campbell, B. and Bakhtar, F. [1970]
"Condensation Phenomena in High Speed Flow of Steam."
Proc. Instn. Mech. Engrs. 185 (London).

Choi, H. Y. [1967]
"Electrohydrodynamic Condensation Heat Transfer"
ASME AIChE Heat Transfer Conf. and Exhibit, Seattle, Wash.

Clements, R. M. and Smy, P. R. [1969]
"Electrostatic Probe Studies in a Flame Plasma"
J. of Applied Physics, v. 40, n. 11, pp 4553 – 4558

Clements R.M. and Smy P. R. [1974]
"Comments on: The use of Electrostatic probes to measure the Temperature profiles of Welding Arcs"
J. Phys. D: Appl. Phys., vol. 7, pp L133-136

Clements, R. M. and Smy, P. R. [1994]
"Langmuir Probes Characteristics in a High-pressure Plasma in the presence of Convection and Ionization"
IEEE Trans. on Plasma. Sci., vol. 22, no. 4, pp 435-440

Courtney, W. G. [1961]
"Remarks on Homogeneous Nucleation"
J. Chem. Phys., 35:2249-2250

Crane, R.I. [1973]
"Deposition of Fog Drops on Low Pressure Steam Turbine Blades"
Int. J. Mech. Sci., Vol. 15, pp. 613-631.

Cross, J. A. [1987]
"Electrostatics: Principles, Problems and Applications"
Adam Hilger, IOP Publishing Limited, Techno House, Redcliffe Way, Bristol

Dawe J., Rizvi S.A.H. and Smy P.R. [1993]
"Electron current to a cylindrical probe in a moving high pressure plasma"
Plasma Science, IEEE Transactions, pp 202-208, vol 21, issue 1

Deich, M. E., Tsiklauri, G. V., Shanin, V. K. and Danilin, V. S. [1972]
"Investigation of Flows of Wet Steam in Nozzles"
Teplofizika Vysokikh Temperatur, 10 (1):122-129

Deich, M. E., Kurshakov, A. V., Tiahchenko, A. A., Leonov, V. M. and Emet, O. Z. [1987]
"Condensation Instability in Supersonic Turbine Cascades"
Translated fiom Teploenergetika (Thermal Engineering), 34:600-604

Denton, J. D. [1975]
"A Time Marching Method for Two and Three-Dimensional Blade to Blade Flows"
ARC R. & M. No. 3775

Denton, J. D. [1983]
"An Improved Time Marching Method for Turbomachinery Flow Calculation"
ASME Paper 82-GT-239

Dooley, R. B., Bursik, A. and Staudt, U. [1999]
"Steam and Chemistry"
Proc. VGB/EPRI Conference on Steam Chemistry, Freiburg, Germany

Dooley, R. B., Feldburg, L. A., Kashinsky, V. I., O. I. Martynova, Petrov, A. Yu., Petrova, T. I., Popov, S. A., Povarov, O. A., Semenov, V. N. and Troitsky, A. N. [1997]
"Turbine Steam, Chemistry and Corrosion: Experimental Turbine Tests"
Final Report, TR-108185, EPRI, Palo Alto, CA
Dufour, L. and Defay, R. [1963]
"Thermodynamics of Clouds"
Academic Press, p. 144

Dunning, W. J. [1965]
"Problems in the Application of Classical Nucleation Theory"
Abstr. Proc. Case Inst. Tech. Cleveland, Ohio, Int. Symp. Nucl. Phenom. (April 1965), pp. 1-3

Dunning, W. J. [1969]
"General and Theoretical Introduction"
Nucleation (A.C. Zettlemoyer, ed.), Marcel Dekker, New York, pp. 1-67

Ebrahimi, M. [1991]
"An Experimental Study of the Performance of Cascades of Turbine Blading in Nucleating Flows of Steam."
Ph.D. Thesis, University of Birmingham

Ederhof, A. and Dibelius, G. [1976]
"Determination of Droplet Size and Wetness Fraction in Two Phase Flows using a Light Scattering Technique"
Inst. Mech. Engrs., Sixth Thermo. and Fluid Mech. Conv., University of Durham

EPRI TR-113090 [1999]
"Turbine Steam, Chemistry and Corrosion Generation of Early Liquid Films in Turbines"
EPRI Palo Alto, CA, TR-113090

Faraday, M. [1865]
"Experimental Researches in Electricity"
Vol. II, pp 106-126

Farley, F. J. M [1952]
"The Theory of the Condensation of Supersaturated Ion-Free Vapour"
Proc. Roy. Soc. (London), A 212:530-542

Farkas, L. [1927]
"Keimbildungsgeschwindigkeit inUbersattigten Dampfen"
Z. Phys. Chem., 125:236-242

Felici, N. J. [1984]
"Conduction and Electrification in Dielectric Liquids"
J. Electrostatics vol. 15, pp. 291-297

Filippov, G. A., Saltanov, G. A. and Ignatevskii, E. A. [1970]
"Analysing the Condensation of Supersaturated Steam in Turbine Stages"
Thermal Eng., Vol. 17, No. 12, pp. 26

Filippov, G. A., Povarov, O. A. and Priahin, V. V. [1973]
"The Investigation and Analysis of Wet Steam Turbines"
Energiya, Moscow

Filippov, G. A. and Povarov, O. A. [1980]
"Moisture Separation in NPP Turbines"
Energiya, Moscow

Flageollet-Daniel, C., Garnier, J. P. and Mirabel, P. [1983]
"Microscopic surface tension and binary nucleation"
J. Chem. Phys., vol. 78, no. 5, p. 2600

Frenkel, J. [1946]
"Kinetic Theory of Liquids"
Oxford University Press, London

Gardner, F. W. [1932]
"The Erosion of Steam Turbine Blades"
Engineer (London), 153: 146, 174 and 202

Gardner, G. C. [1963]
"Event Leading to Erosion in the Steam Turbine"
Proc. Inst. Mech. Engrs., London, 168 (1963-1964), I, 23:593-623

Gerber, A. G. and Knill K. J. [1999]
"Nonequilibrium Phase Change in Steam Undergoing Rapid Expansion: Solution Method Including Viscous Effects"
Proc. 33rd National Heat Transfer Conference, Albuquerque, New Mexico

Gerber A. G. [2002]
"Two-Phase Eulerian/Lagrangian Model for Nucleating Steam Flow"
ASME J. Fluids Engineering, vol. 124, pp 465-475

Gick A., Quigley M. and Richards P. [1973]
"The use of Electrostatic Probes to measure the Temperature profiles of Welding Arcs"
J. Phys. D: Appl. Phys., vol. 6, pp 1941-1949

Gibbs, J. W. [1888]
"On the Equilibrium of Heterogeneous Surfaces"
Collected Papers (Thermodynamics), Longmans, London, p.55

Ghassemi, B. [1977]
"A Study of Nucleation in High Pressure Steam Turbines"
Ph.D Thesis, University of Birmingham

Ghoneim, Z. [1975]
"A Study of Nucleating and Wet Steam Flows in Turbines"
Ph.D Thesis, University of Birmingham

Golvin, M. N. and Putnam, A. A. [1962]
"Inertial Impaction on Single Element"
Ind. Eng. Chem. Fluid, 1 (1):264-273

Guha, A. and Young, J. B. [1991]
"Time Marching Prediction of Unsteady Condensation Phenomena due to Supercritical Heat Addition"
European Conf. IMechE, "Turbomachinery, Latest Developments in a Changing Scene", paper C423/057, pp 167 – 173

Guha, A. and Young, J. B. [1994]
"The Effects of Flow Unsteadyness on the Homogeneous Nucleation of Water Droplets in Steam Turbines"
Phil. Trans. Royal Soc., Series A, vol. 349, pp 445-472

Gyarmathy, G. [1962]
"Grundlagen einer Theorie der Nassdampfturbine"
Dissertation ETH, Zürich, Juris-Verlag. (English Translation: CEGB (London) Rept. T-781, 1963)

Gyarmathy, G. and Meyer, H. [1965]
"Spontane Kondensation"
VDI Forschungsheft 508, VDI-Verlag, Düsseldorf

Gyarmathy, G. and Lesch, F. [1969-1970]
"Fog Droplet Observations in Laval Nozzles and in an Experimental Turbine"
Proc. Inst. Mech. Engrs., 184 (3G(III)): 29-36

Hamitt, F. G., Linh, D. O., Ernst, G. C., Hamitt, F. G. (Jr), Huang, Y. C., Hwang, J. B., KeUer, Y. C., Timme, E. [1976]
"Liquid-induced Erosion Research"
Trans. of Inst. of Fluid Flow Machinery, Poland, 70-72, 203-220

Haydon, D. A. [1974]
"The Electric Double –Layer and Electrokinetic Phenomena"
Recent Progress in Surface Science, Vol. 1, NY Academic Publishers, pp. 94-153

Heaton, A.V. [1978]
"A Study of Modelling in Wet Steam Turbines"
Ph.D. Thesis, University of Birmingham

Helmholtz, R. [1886]
"Untersuchungen über Dämpfe und Nebal, besonders über solche von losungen"
Ann. d. Phys., 27:508

Helmholtz, R. [1887]
Ann. d. Phys. N.F., 32:1

Henderson, J. B. [1913]
"Theory and Experiment in the Flow of Steam through Nozzles"
Proc. Inst. Mech. Engrs., parts 1-2:253-314

Henson, R. J. K. [1995]
"The Theoretical Investigation of the Flow of Wet Steam in a Cascade Rotor Tip Section Blading."
Ph.D. Thesis, University of Birmingham

Hermann, R. [1942]
"Condensation Shock Waves in Supersonic Wind Tunnel Nozzles"
Luftfahrtforschung, 19 (6):201. RTP Translation 1581

Hesler, S. and Maurer, R. [1998]
"Electrostatic Charge Measurement un the Turbine-Condenser Connection of Salf River Project's Navajo Generating Station Unit 3"
EPRI Project Report RP-3849-01

Hesler, S. and Herzog, J. [2000]
"Preliminary Results for Charge Test in Turbine Exhaust Conesville Unit"
EPRI Project WO8309-06

Heymann, F. J., [1970]
"Toward Quantitive Prediction of Liquid Impact Erosion and Erosion Resistance"
ASTM STP 474, Amer. Soc. For Testing and Materials, pp. 212-248

Hickman, K. C. [1954]
"Maximum Evaporation Coeffiecient of Water"
Ind. Engng. Chem., 46: 1442

Hill, P. G., Witting, H. and Demetri, E. P. [1963]
"Condensation of Metal Vapours During Rapid Expansions"
Trans. ASME, J. Heat Transfer, 85:303-317

Honneger, E. [1924]
"Corrosion and Erosion of Steam Turbine Blading"
Brown Boveri Review, 11:263
Honneger, E. [1927]
"Tests on Erosion Caused by Jets"
Brown Boveri Review, 14:95

Houghton, E.L. and Carpenter, P.W. [1993]
"Aerodynamics for Engineering Students"
Edward Arnold, pp 343-348.

Jameson, A., Schmidt, W. and Turkel, E. [1981]
"Numerical Solutions of the Euler Equations by Finite Volume Methods using Runge-Kutta Time Stepping Schemes"
AIAA Paper No. 81-1259

Jameson, A. [1982]
"Transonic Aerofoil Calculations"
MAE Report No. 1651, University of Princeton

Jamieson, D. T. [1965]
"The Condensation Coefficient of Water"
ASME Third Symposium on Thermodynamic Properties, Purdue University

Jonas, O. et. al. [1998]
"Steam, Chemistry, and Corrosion in the Phase Transition Zone of Steam Turbines: Volume 1: Key Results, Summary, and Interpretation; Volume 2: Individual Contributions of Participants"
EPRI Palo Alto, CA, AP-108184

Kantrowitz, A. [1951]
"Nucleation in Very Rapid Vapour Expansions"
J. Chem. Phys., 19 (9):1097-1100

Kaschiev, D. [1969]
"Solution of the Non-Steady State Problem in Nucleation Kinetics"
Surface Science, 14:209-220

Kirkwood, J. G. and Buff, E. P. [1949]
"The Statistical Mechanical Theory of Surface Tension"
J. Chem. Phys., Vol 17

Kleitz, A., Laali, A. R., Courant, J. J. [1988]
"Fog Droplet Size Measurement and Calculation in Wet Steam Turbines"
Tech. of Turbine Plant Operating with Wet Steam Int. Conf., MNES, IME, ENS, London, pp 177-182

Komarov, N. F. and Yurkov E. V. [1991]
"Corrosion Damage to the Blading and Dics of Steam Turbines"
Thermal Engineering, v. 38, n. 2, pp 66-70

Kosolapov Yu. S., Liberson, A. S., [1997]
"An Implicit Relaxation Method for Computation of Three Dimensional Steady Flows of Spontaneously Condensing Steam"
Computational Mathematics and Mathematical Physics, vol. 37, no.6, pp.739-747

Krzeczkowski, S. [1968]
"Motion of Drops in Flow Ahead of a Cylinderical Object"
Trans. Inst. Fluid-Flow Machinery (Poland), 40 (U):3-22

Krol, T. [1971]
"Results of Optical Measurements of Diameters of Drops Formed Due to Condensation of Steam in a Laval Nozzle"
Trans. Inst. Fluid Flow Mach. (Poland), 57:19-30

Laali, A. R. [1991]
"A New Approach for Assessment of the Wetness Losses in Steam Turbines"
Turbomachinery: Latest Developments in a Changing Scene, IMechE

Liberson A. S., Hesler S., McCloskey T. [1998]
"Inviscid and Viscous Numerical Simulation for Non-Equilibrium Spontaneously Condensing Flows in Steam Turbine Blade Passages"
IJPGC Conference Proc. August 23-26, Baltimore, MD, vol. 2, pp. 97-105

Liberson A. S., McCloskey, T. H., [1999]
"A Unified CFD Based Approach to a Variety of Condensation Processess in Low Pressure Steam Turbines"
Proc. of Third International VGB/EPRI Conference, June 22-25, 1999, Freiburg

Loschge, A. [1913]
"Flow of Steam through Nozzles"
Mitteilungen über Forschungsarbeiten (Berlin), no. 144

Lothe, J., Pound, G. M. [1962]
"Reconsiderations of Nucleation Theory"
J. Chem. Phys. 36 (8): 2080-2085

Maa, J. R. [1970]
"Rates of Evaporation and Condensation Between Pure Liquid and Their Own Vapours"
Ind. Eng. Chem. Fundam., Vol. 9, pp. 283

Mahpeykar, M. R. [1991]
"On the Theoretical Treatment of Two-dimensional Flows of Steam and Comparison with Measurements"
Ph.D. Thesis, University of Birmingham

Mamat, Z. A. [1996]
"The Performance of a Cascade of Nozzle Turbine Blading in Nucleating Steam"
Ph.D. Thesis, University of Birmingham

Martin, H. M. [1913]
"Undercooled Steam"
Engineering, 16th May, pp. 673-674

Martin, H. M. [1918]
"A New Theory of the Steam Turbine"
Engineering, 106:1-3, 53-55, 107-108, 161-162, 189-191, 245-246

Martin, H. M. [1923]
"The Supersaturation Limit"
Engineering, 115:607

Mashmoushy, H. A. [1994]
"On the Performance of Rotor Blades in Wet Steam."
Ph.D. Thesis, University of Birmingham

MacDonald, J. E. [1962 & 1963]
"Homogeneous nucleation of vapour condensation"
American J. Phys. 1962, 30, p870 and 1963, 31, p31

McDonald, P. W. [1971]
"The Computation of Transonic Flow Through 2D Gas Turbine Cascades"
ASME Paper No. 71-GT-89

Mills, A. F. and Seban, R. A. [1967]
"The Condensation Coefficient of Water"
Int. J. Heat and Mass Transfer, 10: 1815

Mirabel, P. and Katz, J. L. [1974]
"Binary homogeneous nucleation as a mechanism for the formation of aerosols"
J. Chem. Phys., vol. 60, no. 3, p. 1138

Moheban, M. and Young, J. B. [1984]
"A Time Marching Method for the Calculation of Blade-Blade Non-Equilibrium Wet Steam Flows in Turbine Cascades"
Inst. Mech. Engrs., Conf. on Comp. Methods inTurbomach., C76/84, pp. 89

Mohsin, R. [1999]
"A Theoretical Investigation of the Throughflow of Nucleating Steam in a Low Pressure Steam Turbine"
Ph.D. Thesis, University of Birmingham

Moore, M. J. and Sieverding, C. H. [1976]
"Two-Phase Steam Flow in Turbines and Separators"
McGraw-Hill, NY

Moses, C. A. and Stein, G. D. [1978]
"On the Growth of Steam Droplets Formed in a Laval Nozzle using both Static Pressure and Light Scattering Measurements"
J. Fluid Eng., 100:311-322

Mott-Smith, H. M., and Langmuir, I. [1926]
"The Theory of Collectors in Gaseous Discharges"
Phys. Review vol. 28 pp 727-763

Napari I., Noppel M., Vehkamäki H. and Kulmala M. [2002]
"An Improved Model for Ternary Nucleation of Sulfuric Acid–Ammonia–Water"
J. Chem. Phys. vol. 116(10) pp. 4221-4227

Noppel, M. [1998]
"Binary Nnucleation of Water–Sulfuric Acid System: A Reexamination of the Classical Hydrates Interaction Model"
J. Chem. Phys. vol 109(20) pp. 9052-9056

Oriani, R. A. and Sundquist, B. E. [1963]
"Emendations to Nucleation Theory and the Homogeneous Nucleation of Water from Vapour"
J. Chem. Phys., Vol. 38, pp. 2082-2089

Oswatitsch, K. L [1942]
"Condensation Phenomena in Supersonic Nozzles"
Z. Angew. Math. Mech., 22 (1):1-14. (RTP Translation No. 1905)

Oxtoby, D. W. and Kashchiev, D. [1994]
"A General Relation Between the Nucleation Work and the Size of the Nucleus in Multicomponent Nucleation"
J. Chem. Phys. vol. 100(10) pp. 7665-7671

Pauthenier, M. M. and Moreau-Hanot, M. [1932]
"La Charge des Particules Spheriques dans un Champ Ionise"
J. de Physique et le Radium, Series 7, Vol. 3

Petr, V. [1969]
"Measurement of an Average Size and Number of Droplets during Spontaneous Condensation of Supersaturated Steam"
Proc. IMechE, 184 (3G III), pp 22-28

Petr, V., Kolovratnik, M., Jiricek, I. and Jonas, O. [1995]
"Experimental Investigation into the Effects of Steam Chemistry on Droplet Nucleation"
EPRI State of the Art workshop on moisture nucleation in steam turbines, Rochester, USA

Petr, V. and Kolovratnik, M., [1997]
"Contribution to the Wet Steam Flow Problems in LP Steam Turbines"
Proc. 2nd European Conf. on Turbomachinery, Antwerp, Belgium, pp 65-72

Petr, V. and Kolovratnik, M., [1999]
"Modelling of the Droplet Size Distribution in LP Steam Turbine"
Proc. 3rd European Conf. on Turbomachinery, London, IMechE conf. trans., pp 771 – 782

Petr, V. and Kolovratnik, M., [2001]
"Heterogeneous Effects in the Droplet Nucleation Process in LP Steam Turbines"
Proc. 4th European Conf. on Turbomachinery, Firenze, Italy, pp 783 - 792

Petr, V. and Kolovratnik, M. [2003]
"Diagnostics of Wet Steam in LP Steam Turbines"
Conf. Proceedings. 5th European Conference on Turbomachinery, Fluid Dynamics and Thermodynamics, 17-22 March, Prague

Piran, M. [1975]
"Thermodynamic Properties of Supercooled Steam"
Ph.D. Thesis, University of Birmingham

Plummer, P. L. M. and Hale, B. N. [1972]
"Molecular Model for Pre-Nucleation Water Clusters"
J. Chem. Phys., 56 (9): 4329-4334

Preneger, W. [1940]
"Die Verdampfungsgeschwindingkeit der Flussingkeiten"
Z. Physik., Vol. 115

Pouring, A. A. [1965]
"Thermal Choking and Condensation in Nozzles"
Phys. Fluids, 8 (10): 1802-1810

Prandtl, L. [1935]
"General Considerations on the Flow of Compressible Fluids"
Proc. Volta High Speed Congress, Rome. RTP Translation 1872

Probstein, R. F. [1951]
"Time Lag in the Self-Nucleation of a Supersaturated Vapour"
J. Chem. Phys., 19 (5):616-626

Raleigh, J. W. S., [1882]
"On the Equilibrium of Liquid Conducting Masses Charged with Electricity"
Phil. Magazine, Vol. 14, Series 5, pp. 184-186

Rassam, S. Y. [1995]
"A Study of Wet Steam F1ows in a Cascade of Turbine Blading - Optical Observations"
M.Phil. Thesis, University of Birmingham

Rateau, A. M. [1905]
"Experimental Research on the Flow of Steam through Nozzles and Orifices"
A. Constable & Co. Ltd., London

Rieger, N. F. and Dooley, R. B. (eds) [1997]
"Moisture Nucelation in Turbines"
Proc. EPRI State of Art Workshop, EPRI, TR-108942, Rochester, N.Y.
Rieger, N. F. [1999]
"Nucleation and Condensation within an Electrostatic Field"
Proceedings VGB-EPRI International Conference on Steam Chemistry, June 22-25, 1999, Freiburg, Germany

Rieger, N. F. and Dooley, R. B. [2001]
"Electrostatic Charge and its influence on the Condensation of Steam in a Turbine"
EPRI, Palo Alto, CA, 1001332

Reiss, H. [1950]
"The Kinetics of Phase Transition in Binary Systems"
J. Chem. Phys., Vol. 18, no. 6, p.840

Reiss, H. and Katz, J. L. [1967]
"Resolution of the Translation-Rotation Paradox in the Theory of Irreversible Condensation"
J. Chem. Phys. 46 (7): 2496-2499

Rettalaita, J. T. [1938]
"Undercooling in Steam Nozzles"
Trans. ASME, 58:599-605

Rodriguez, J.M. [1992]
"A Runge -Kutta Time Marching Method for Two-Dimensional Nucleating Flows of Steam and Comparison with Measurements"
Ph.D. Thesis, University of Birmingham

Ryley, D. J. and Parker G. J. [1967]
"The Removal of Water from LP Steam Turbine Blades by Trailing Edge Suction Slots"
Proc. IMechE, 182, 94

Ryley, D. J., Ralph, W. J., Tubman, K. A. [1970]
"The Collision Behaviour of Water Drops Within a Low-Pressure Steam Turbine"
Inst. J. Mech. Sci., 12:589-596

Sakamoto T., Nagao S. and Tanuma T. [1992]
"Investigation of Wet Steam Flow for Steam Turbine Repowering"
ASME Power Div. Pub., Int. Joint Power Generation Conf., Atlanta NY, pp 33-40

Savage, R. A. [1989]
"A Study of Wetness Coefficients in Steam Turbine Blading."
Ph.D. Thesis, School of Man. and Mech. Eng., University of Birmingham

Schnurr, G. H. [1989]
"Two-dimensional Transonic Flow with Energy Supplied by Homogeneous Condensation: Onset condition and Two-dimensional Structure of Steady Laval Nozzle Flow"
Experiments in Fluids, vol. 7, no. ¾, pp 145-156

Schnurr, G. H. and Dohrmann, U. [1990]
"Transonic Flow Round Airfoils with Relaxation and Energy Supply by Homogeneous Condensation"
AIAA Journal, vol. 28, no. 7, p. 1187

Schweizer, J. W. and Hanson, D. N., [1971]
"Stability Limit of Charged Drops"
J. of Colloid and Interface Science, Vol. 35, no. 3, pp. 417-423

Sejna, M. and Lain, J. [1994]
"Numerical Modelling of Wet Steam Flow with Homogeneous Condensation on Unstructured Triangular Meshes"
ZAMM 74, no. 5, p T375

Semenov, V. N. [1985]
"Determination of Basic Regularitites of the Effect of Corrosive Environments on Reliability of Steam Turbines"
PhD Thesis, MEI, Moscow

Servida A., Morbidelli M. and Sigon F. [1992]
"Models for assessing the behaviour of the chemical species in steam and nucleation"
EPRI Int. Conf. on Interaction of Iron Based Materials with Water and Steam, Heidelberg, June 3-5

Shojaee-Fard, M. H. [1987]
"A Study of Two-Dimensional Nucleating Flows of Steam in a Blow-Down Cascade"
Ph.D. Thesis, University of Birmingham

Sigon, F. [1993]
"Evaluation of Binary Nucleation Models"
IAPWS Certified Research Need, Sep, 1993

Singh, G., Hunt, R. and McCallum M. [1999]
"Wet Steam Analysis using Eulerian Method for Two-dimensional Droplet Growth and Nucleation Equations"
Proc. 3rd European Conf. on Turbomachinery, London, IMechE conf. trans.

Singh, U. [1999]
"Method for Nucleating Steam Flow in Low-Pressure Turbine Stages"
Proc. 3rd European Conf. on Turbomachinery, London, IMechE conf. trans.

Siraj, M. A. [1987]
"An Experimental Investigation of Nucleating Steam Flow in a Cascade of Blades"
PhD. Thesis, The University of Birmingham

Skillings, S. A. [1987]
"An Analysis of the Condensation Phenomena Occuring in Wet Steam Turbines"
Ph.D. Thesis, University of Birmingham

Smith, A. [1965]
"The Influence of Moisture on the Efficiencies of a One-third Scale Model Low-Pressure Steam Turbine"
Proc. Inst. Mech. Engrs., 180 (3J)

Smith, A. [1976]
"Wilson Point Experiment in Turbines"
Proc. Conf. 'Steam Turbines of Great Output'. Trans. Inst. Fluid Flow Machinery, Pol. Ac. Sci. 70-72, pp 327-350

Smy P. [1976]
"The Use of Langmuir Probes in the Study of High-pressure Plasmas"
Advances in Physics, vol. 25, no. 5 pp 517-553

Snoeck, J. [1983]
"Two Dimensional Condensing Flow in Tnansonic Turbine Cascades"
V.K.I. Lecture Series 6, Aerothermodynamics of Low Pressure Steam Turbines and Condensers

So, K. S. [1984]
"A Study of Supersonic Blade-to Blade Wet Steam Row by the Time Marching Method"
Ph.D. Thesis, University of Birmingham

Stastny, M. [1976]
"Structure of Secondary Phase Downstream of Moving Blades in LP Cylinder Stages of Steam Turbines"
Proc. I. Mech. E. Conference, Steam Turbines for the 1980s, 1979-12 London, pp. 371-384

Stastny, M., Sejna, M. and Jonas, O. [1997]
"Modelling the Flow with Condensation and Chemical Impurities in Steam Turbine Cascades"
Proc. 2nd European Conference on Turbomachinery, Antwerp, Belgium, pp 81 – 88

Stastny, M., Sejna, M. [2001]
"Two-population Numerical Model of Heterohomogeneous Condensation of the Steam Flowing in Turbine Cascades"
Proc. 4th European Conference on Turbomachinery, Firenze, Italy, pp 803 - 812

Stauffer, D. [1976]
"Kinectic theory of two-component ('heteromolecular') nucleation and condensation"
J. Aerosol Sci., 7, p319

Steltz, W. G., Lee, P. K. and Linsay, W. T. [1981]
"The Verification of Concentrated Impuritites in Low Pressure Steam Turbines"
in "Aerothermodynamics of steam turbines" ed. Steltz and Donaldson, Proc. ASME Winter Annual Meeting, Washington D.C., pp. 73-82

Stodola, A. [1915]
"Undercooling of Steam in Nozzles"
Engineering, 11th June, pp. 643-646

Svoboda, R., Sandmann, H., Romanelli, S. and Bodmer, M. [1992]
"Early Condensate in Steam Turbines"
"Interaction of Iron-Based Materials with Water and Steam", Proc. International Conf., Heidelburg, Germany, TR 102101, EPRI, Palo Alto, CA, pp 32-1 – 32-16

Tanuma T. and Sakamoto T. [1991]
"The Removal of Water from Steam Turbine Stationary Blades by Suction Slots"
Turbomachinery: Latest Developments in a Changing Scene, IMechE, pp 179-190

Tarelin, A. O., Skliarov, V. P., Serhienko, Yu. I. and Weres, O. [1996]
"Electrical Method to Increase Power Output by Improving Condensation and Flow of Steam within the Turbine Neck and Condenser of a Steam Turbine"
Proc. Amer. Power Conf., 58th Annual Meeting, Chicago, IL

Tarelin, A. O. and Skliarov, V. P. [1999]
"Investigation of Electrophysical Effects in the Turbine Exhaust Upon Flow and Power Output"
EPRI, Palo Alto, CA, TR 113091

Taylor, G. I. [1964]
"Disintegration of Water Drops in an Electric Field"
Proc. Royal Soc. Series A, Vol. 280, pp. 383-397

Thorton D. V. [1988]
"Materials for Turbine Plant Operating with Wet Steam"
Technology of Turbine Plant Operating with Wet Steam, BNES Conf.

Tochai, M.T.M. [1978]
"A Study of High Speed 2-D Flows of Steam with Phase Change"
Ph.D. Thesis, University of Birmingham

Tolman, R. C. [1949]
"The Effect of Droplet Size on Surface Tension"
J. Chem. Phys., 17 (3): 333-337

Tohmfor, G. and Volmer, M. [1938]
"Dir Keimbildung unter dem Einfluß elekrischer Ladungen"
Annalen der Physik, Series 5 (Leipzig), Vol 33, pp. 109-131

Tomarov, G. V. [1989]
"Erosion – Corrosion of the Structural Materials in Saturated Steam Turbines"
Them. Eng. Vol. 36 n. 7

Thomson, J. J. [1871]
"Considerations of the Abrupt Change at Boiling or Condensation in Reference to the Continuity of the Fluid State of Matter"
Proc. Royal Society (London), 20:1-8

Thomson W. [1870]
"On the Equilibrium of Vapour at a Curved Surface of a Liquid"
Proc. Royal Society (Edinburgh), 7:63-68

Umeda, T. and Tatsuno, K. [1988]
"Particle Sizer using a Side Scattering Method"
Japan Joint Automatic Control Conf., Osaka, Japan, p617

Valha, J. [1970]
"Liquid Phase Movement in Large Condensing Steam Turbines"
Trans. of the Thermo. and Fluid Mech. Conv. IME, Glasgow

Velkof, H. R. [1962]
"Electrofluidmechanics: A Study of Electrokinetic Actions in Fluids"
ASD-R-61-642, Aeronautical Sys. Div., Air Force Systems Command, WPAFB, Ohio

Velkof, H. R. and Millar, J. H. [1964]
"The Effect of an Electrostatic Field on the Condensation of Vapour"
RTD-TDR-63-4008, Aeronautical Sys. Div., Air Force Systems Command, WPAFB, Ohio

Volmer, M. and Weber, A. [1926]
"Keimbildung in Ubersettigten Gebilden"
Z. Phys. Chem. 119:227-301

von Freuderich, J. [1927]
"The Injurious Influence of Wet Steam in Steam Turbines"
Brown Boveri Review, 14:119

Vukalovich, M. P. [1958]
"Thermodynamic Properties of Water and Steam"
6th edition (Mashgis, Moscow)

Wakeshima, H. [1954]
"Time Lag in the Self-Nucleation Process"
J. Chem. Phys., 22: 1614-1615

Wang, N. N., Wei, J. M., Cai, X. S., Zhansy, Z. W., Zheng, G. and Yu, X. H. [1998]
"Optical Measurement of Wet Steam in Turbines"
J. Eng. For Gas Turbines and Power, Vol. 120, n. 4, p 867

Walters, P. T. [1973]
"Optical Measurement of Water Droplets in Wet Steam and Gas Turbine Plant"
Inst. Mech. Engrs., Heat and Fluid Flow in Steam and Gas Turbine Plant, Conf. Publ.3

Walters, P. T. and Skingley, P. C. [1979]
"An Optical Instrument for Measuring the Wetness Fraction and Droplet Size of Wet Steam Flows in L.P. Turbines"
Inst. Mech. Engrs., Steam Turbines for the 1980's Conf. Publ.

Walters, P. T. [1985]
"Wetness and Efficiency Measurements in Low Pressure Turbines with an Optical Probe as an aid to Improving Performance"
ASME 85, JPGC-GT-9

Walters, P. T. [1988]
"Improving the Accuracy of Wetness Measurements in Generating Turbines by using a New Proceedure for Analysing Optical Transmission Data"
Tech. of Turbine Plant Operating with Wet Steam Int. Conf., MNES, IME, ENS, London, pp 183-191

Wegener, P. P. [1969]
"Gas Dynamics of Expansion Flows with Condensation and Homogeneous Nucleation of Water Vapour"
Non-Equilibrium Flows, Marcel Deckker, New York, 1: pp 163-243

Wegener, P. P. and Wu, B. J. C. [1976]
"Homogeneous and Binary Nucleation; New Experimental Results and Comparisons with Theory"
Faraday Discussions, 12th-14th April, Manchester, pp. 77-82

Wilemski, G. [1984]
"Composition of the Critical Nucleus in Multicomponent Vapor Nucleation"
J. Chem. Phys. vol. 80(3) pp. 1370-1372

Wilemski, G. [1987]
"Revised classical binary nucleation theory for aqueous alcohol and acetone vapours"
J. Chem. Phys., vol. 91, no. 10, p. 2492

Wilson, C. T. R. [1897]
"Condensation of Water Vapour in the Presence of Dust-free Air and other Gases"
Phil. Trans. Royal Society (London), A 189:265-307

Wilson, C. T. R. and Taylor, G. I. [1925]
"The Bursting of Soap Bubbles in a Uniform Electric Field"
Proc. of Cambridge Phil. Soc., Vol. 22, Pt 5, pp. 728-730

Whirlow, D. K., McCloskey, T. H., Davids, J., Chen, S., Kdambi, J. R. and Farn, C. L. [1984]
"Flow Instability in Low Pressure Turbine Blade Passages"
ASME Paper No. 84-JPGG-GT-15

Winkler, G. and Schnurr, G. H. [2001]
"Nucleating Unsteady Flows in Low Pressure Steam Turbine Stages"
Proc. 4th European Conf. on Turbomachinery, Fluid Dynamics and Thermodynamics, Firenze, Italy
pp. 793-802

Yellot, J. L. [1934]
"Supersaturated Steam"
Trans. ASME, 56:411-430

Yellot, J. L. and Holland, C. K. [1937]
"The Condensation of Flowing Steam. Part I – Condensation in Diverging Nozzles"
Trans. ASME, 59:171-183

Yeoh, C. C. and Young, J. B. [1982]
"Non-Equilibrium Stream Line Curvature Throughflow Calculations in Wet Steam Turbines"
Trans. ASME, J. Engineering for Power, 104:489-496

Yeoh, C. C. and Young, J. B. [1984]
"Non-Equilibrium Throughflow Analysis of Low Pressure Wet Steam Turbines"
Trans. ASME, J. Engineering for Power, 106:716

Young, J. B. [1973]
"Nucleation in High Pressure Steam and Flow in Turbines"
Ph.D. Thesis, University of Birmingham

Zamri, M. [1997]
"An Improved Treatment of Two-dimensional, Two-phase Flows of Steam by a Runge-Kutta Method."
Ph.D. Thesis, University of Birmingham.

Zeldovich, J. [1942]
"Theory of Nucleation and Condensation"
Sov. Phys. - JETP (Engl. Transl.) 12:525

Zeuner, G. [1907]
"Technical Thermodynamics"
Translated by J. F. Klein, A. Constable & Co. Ltd., London, vol II, pp. 83

Zidi, K. [1981]
"Spontaneous Condensation in Flowing High Pressure Steam"
Ph.D. Thesis, University of Birmingham